INVESTIGATION OF PHOTOSENSITISING BEHAVIOUR OF Ni, Pd AND Pt PHTHALOCYANINES TOWARDS PHENOLIC POLLUTANTS

A thesis submitted in fulfillment of the requirements for the degree of

Doctor of Philosophy

Of

Rhodes University

By

Taofeek Babatunde Ogunbayo

February 2011

Dedication

To my sojourn on the 'brink' (8th July 1999 to 10th Dec. 2004)

For the persistent description of who I am

To those who shared my faith in my style

For the stability that shamed the storm

To those who accept my conviction of my character

For the grace that will create reality out of celluloid fantasy

Acknowledgements

I give glory to the most high for his grace that ensured the completion of this project. My appreciation also goes to my supervisor, Prof. Tebello Nyokong for her guidance throughout the time of this programme.

I also thank my parents for their supports over the years. Some of my relatives and friends also deserve mentioning: Keji Ojudun, Sandra Clarke, Isiaq Ogunbayo, Dr. Idris Olasupo, Dr. Sheriff Salisu, Mrs. Yetunde Salisu, Segun Obilana, Toyin Odusanya, Tope Olomola, Dr. Humphery Atebe, Osedum Peter Igumbor, Dr. Eric Igbinigie, Ms. Modupe Akoro, Baba Olota, Bolanle Awosanya, Isiaq Akinola, Femi Sobowale, Mr. Tunde Rasheed Idowu, Mr. Kabir Adeoso, Isiaq Kazeem, Seun Afolabi, Yusuf Soyemi, Tunde Awosanya, Gbenga Awosanya, Prince Tai Onasegun, Alhaji Yusuf Ashiru, Hon. Tau Somide, Mr. O. Eleyoowo, Wasiu Akinola, Abdullahi Sobola, Dr. Sheriff, Alhaji Mahboob Adekilekun, Dr. Yususf Kazeem, Kunle Soluade and Tobi Soluade for their supports.

My appreciation also goes to the management of University of Lagos for study leave and to all staff and students of chemistry department, Rhodes University for their supports. My gratitude also goes to my funders African Laser Center (ALC) and Nanotechnology innovation center (NIC). I also commend every individual and organisation that was part of the conception and funding of the brilliant initiative called NIC for this opportunity and their foresight.

My final but unparalleled gratitude goes to all students and staff of S22: It is impossible to describe the feeling that the memory of our communion elicits. I can only say it's a distinct and everlasting one.

Abstract

Syntheses of various octasubstituted open-shell (Ni(II), Pd(II) and Pt(II)) metallophthalocyanines and their metal-free analogues have been carried out. Spectroscopic characterizations, photophysical and photochemical studies were carried out to determine the effects of these metals on the molecules using the metal-free phthalocyanine analogues as benchmark. Metal-binding studies of few thio-derivatised phthalocyanines were done to increase the number of palladium metal on the phthalocyanine ligands and determine the effect of increasing number of this metal on phthalocyanine properties. Palladium (PdPc) and platinum phthalocyanines (PtPc) gave good triplet and singlet oxygen quantum yields making them suitable for further investigation in application as photosensitisers.

Using 4-nitrophenol as model pollutant, photosensitization reactions were carried out under homogenous and heterogeneous conditions. The reactions were monitored using UV-vis spectroscopy. The MPcs were adsorbed on functionalized single wall carbon nanotube (SWCNT-COOH) to form heterogeneous photosensitizers with PtPc failing to adsorb on the SWCNT-COOH. Under the heterogeneous condition, all the PdPcs photosensitization kinetics was consistent with Langmuir-Hinshelwood reaction model. The best photosenstiser, β-palladium dodecylthio phthalocyanine was also deployed in sensitization of oxidation of 4-chlorophenol and pentachlorophenol under homogenous and heterogeneous conditions to establish the ability of the molecules to sensitize oxidation of wide range of phenolic pollutants. Identifications of the products of the reactions were conducted using gas chromatography and high pressure liquid chromatography (HPLC) hyphenated with mass analyzer (LC-MS). Mechanisms of all the reactions were investigated and all the complexes, in spite of reduced lifetime resulting from open-shell nature of the metals, sensitized the reactions through singlet oxygen mediated pathway. All the heterogeneous sensitisers were recyclable in the 4-nitrophenol oxidation but β-palladium dodecylthio phthalocyanine proved unrecyclable in the oxidation of pentachlorophenol.

Table of content

CHAPTER 2

2. EXPERIMENTAL

CHAPTER 3

CHAPTER 4

LIST OF SYMBOLS

A_{eq}	-	Equilibrium absorbance of Phthalocyanines-Pd complex
A_o,	-	Initial absorbance of phthalocyanines
A_∞,	-	Maximum attainable absorbance of the product
K	-	Binding constant
n	-	Number of bound Pd(II) ions to phthalocyanines
ΔA	-	Change in absorbance following laser pulse
I	-	Intensity of light
I_{abs}	-	Intensity of light absorbed
F	-	Fluorescence intensity
α	-	Non-peripheral position
β	-	Peripheral position
ε	-	Molar extinction coefficient
ε_T	-	Triplet state extinction coefficient
λ_{abs}	-	Wavelength of absorption spectrum maximum
λemi	-	Wavelength of emission spectrum maximum
λexci	-	Wavelength of excitation spectrum maximum
λmax	-	Wavelength maximum
η	-	Refractive index
Φ_Δ	-	Singlet oxygen quantum yield
Φ_F	-	Fluorescence quantum yield
Φ_{IC}	-	Internal conversion quantum yield
Φp	-	Photodegradation quantum yield
Φ_{Poll}	-	Quantum yield of degradation of pollutant
Φ_T	-	Triplet state quantum yield
τ_T	-	Triplet state lifetime
$^1O_2$ ($^1\Delta$g)	-	Excited long-lived singlet state oxygen

$^1O_2$ ($^1\Sigma g$)	-	Excited short-lived singlet state oxygen
O_2 ($^3\Sigma g$)	-	Ground state molecular oxygen
$\lambda_{Q(abs)}$	-	Q band absorption wavelength;
$\lambda_{Q(exc)}$	-	Q band excitation wavelength
$\lambda_{Q(emm)}$	-	Q band emission wavelength.
S_0	-	Ground singlet state
S_1	-	Excited singlet state
S_0	-	Ground singlet state
S_Δ	-	Efficiency of quenching of the triplet excited state by singlet oxygen
T_1	-	First excited triplet state
T_n	-	Excited triplet state (n = 1, 2,3…..)
k_d	-	Natural decay constant
k_q	-	Physical quenching constant
k_a	-	Rate of reaction between scavenger and singlet oxygen,.
N_A	-	Avogadro's constant.
e^-	-	Conduction electron
h^+	-	Positive hole
k_r	-	Rate constant for the adsorption of substrate
K_{ads}	-	Adsorption coefficient
k_{CP}	-	Pseudo first order kinetic constant of chlorophenol degradation

LIST OF ABBREVIATIONS

ADMA	-	Tetrasodium α,α-(anthracene-9,10-diyl) dimethylmalonate
AOD	-	Advanced oxidation processes
4-CP	-	4-Chlorophenol
1-CNP	-	1-Chloronaphthalene
CTMA	-	Cetyltrimethylammonium bromide
D_2O	-	Deuterated water
DBU	-	1,8-diazabicyclo[5.4.0]undec-7-ene
DCM	-	Dichloromethane
2,4-DCP	-	2,4-Dichlorophenol
DMF	-	*N*,*N*-dimethylformamide
DMSO	-	Dimethylsulphoxide
EPA	-	Environmental protection agency
HOMO	-	Highest occupied molecular orbital
IC	-	Internal conversion
IR	-	Infrared
ISC	-	Intersystem crossing
LUMO	-	Lowest unoccupied molecular orbital
4-NP	-	4-Nitrophenol
NiPc	-	Nickel phthalocyanine
P	-	Phosphorescence
PBS	-	Phosphate buffered solution
PCP	-	Pentachlorophenol
Pcs	-	Phthalocyanines
PDT	-	Photodynamic therapy
$^3PS^*$	-	Triplet state of the photosensitiser
$PS^{\cdot+}$	-	Radical specie of the photosensitiser
RO	-	Reverse osmosis
S	-	Scavenger

SWCNT-COOH	-	Functionalized single wall carbon nanotube
2,4,6-TCP	-	2,4,6-Trichlorophenol
TEM	-	Transmission electron microscopy
THF	-	Tetrahydrofuran
UV/Vis	-	Ultraviolet/visible
VR	-	Vibrational relaxation
XRD	-	X-ray diffraction technique

LIST OF FIGURES

LIST OF SCHEMES

LIST OF TABLES

Chapter 1

Introduction

1. INTRODUCTION

1.1. Phthalocyanines and their applications

Since phthalocyanines (Pcs) were serendipitously discovered and structurally elucidated **[1-10]**, they have been widely used as dyes and pigments. These molecules are being deployed in areas such as textile and printing. They have also being used as catalysts in many chemical reactions, photoconducting agents in photocopying devices, photosensitisers in photodynamic therapy (PDT) and in non-linear optical (NLO) applications. In addition, the use of these complexes is also growing in many other fields including chemical sensors development, electrochromism, liquid crystals, Langmuir-Blodgett films, functional polymers and semiconductors **[11-23]**. The driving force behind the versatility of this single molecular framework stems from its high degree aromaticity, chemical inertness, photo and thermal stabilities, intense colour, diverse coordination properties, architectural flexibility, unique electronic spectra and adaptability of molecular skeleton to meet various chemistry demands.

1.2. Structure-property relationship in phthalocyanines

Phthalocyanine, **Fig. 1.1**, is a planar 18 π-electron heterocyclic aromatic system consisting of four isoindole units linked together by aza nitrogen atoms. The more systematic name for this macrocycle is tetraazatetrabenzoporphyrin. The molecular architecture of Pcs can be adapted for various properties required to meet diverse application. The introduction of substituents to the peripheral (β) and non-peripheral (α) positions and the possibility of complexation of a variety of metals are ways of fine tuning phthalocyanines properties including their photophysical and photochemical behaviour.

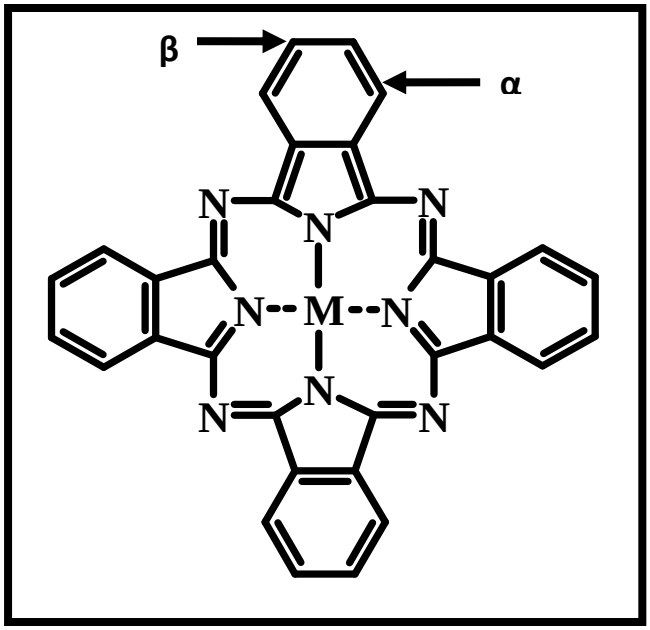

Figure 1.1: Structure of Metallophthalocyanines (MPc)

Manipulation of types of substituents and their positions can be used to adapt the solubility of Pcs in various solvents. Introducing quaternised and sulphonated groups as substituents promotes the solubility in aqueous media **[24,25]** while the introduction of organic functional groups like thio, aryloxo etc promotes solubility in organic solvents **[26,27]**. Closed shell diamagnetic metallophthalocyanines (MPcs) have been found to have robust photophysical and photochemical properties **[28-44]**, while transition metal phthalocyanines have been found to be effective in areas where electrochemically active species are required **[45-53]**.

1.3. Open-shell (Ni(II), Pd(II), Pt(II)) metallophthalocyanines as photosensitisers in oxidation reactions

One of the applications that exploit the photochemical properties of phthalocyanines (Pcs) is their use as photosensitisers in oxidation reactions. Closed shell diamagnetic metals have been investigated towards this end using nitrophenol and chlorophenols as model pollutants **[54-58]**. These processes led to a wide range of oxidation products such as fumaric acid, tetrachlorobenzoquinone, 4-nitrocatechol, benzoquinone and hydroquinone but the results were also marred by photobleaching of the

phthalocyanines during the oxidation processes. It was also observed in separate works that palladium phthalocyanines gave considerable triplet quantum yield **[39]** along with higher photostablility compared to most closed-shell metal phthalocyanines investigated **[59-61]**. In spite of this observation, open-shell metal phthalocyanines' ability to perform the function of photosensitization of oxidation reactions was never comprehensively and systematically investigated. The reason for this could be attributed to scanty number of these MPcs (including nickel and platinum) in existence. This is also due to the tendency of open-shell metals of which nickel, palladium and platinum are members to quench excited state of Pcs thereby reducing excited state lifetime and, by extension, the ability of their MPcs to initiate the photo-oxidation reactions. Unsubstituted Ni, Pd and Pt Pcs are known **[29,62-65]** however, they have low solubility and very few substituted derivatives exist **[39,66-68]**. **Table 1.1** shows some of the substituted Ni, Pd and Pt Pcs available before the commencement of this work and their photophysical and photochemical parameters.

Table 1.1: Open-shell substituted metal (Ni(II), Pd(II) and Pt(II)) phthalocyanines and their photophysical and photochemical parameters

Central metal	Substituents	$\Phi_F/10^{-4}$	Φ_T	τ /μs	Φ_Δ	Ref.
Ni	β,(18-crown-6-ether)$_4$	-	-	-	-	**66**
Pd	β,(t-butyl)$_4$	48	0.49	10.40	-	**28**
Pd	β,(OH)$_2$ (t-butyl)$_3$	69	0.23	8.30	-	**28**
Pd	α, (n-butoxyl)$_8$	-	0.77	3.50	0.64	**39**
Pd	$[SO_3]_4^-$	-	-	-	-	**67**
Pt	β, (biphenyl-malonic ester)$_4$	-	-	-	-	**68**

On few occasions **[60]** when these molecules were investigated for photosensitization, the work was not comprehensive enough to determine the pathways through which the reactions were initiated especially regarding how the shortened lifetime brought about by these metals affected the activities.

Due to these gaps in their studies, the intention of this work was to investigate how these metals (Ni(II), Pd(II) and Pt(II)) affect the phthalocyanine properties that contribute to their activities as photosenstisers. This was done by synthesizing novel substituted metallophthalocyanines and their corresponding metal-free analogues. Detailed studies of these molecules including spectral characterization, photophysical, photochemical and photosensitization properties were conducted. In addition, the promising phthalocyanines from the photochemical studies were investigated for their efficiencies as photosensitisers of oxidation reactions using three model pollutants as substrates.

1.4. Syntheses of phthalocyanines

Since the wide range of applications proposed for these molecules requires compounds with distinct and well defined physical, chemical and electronic properties, the synthetic methods must offer flexibility. This allows the integration of all components that advance the required features. This type of synthetic approach is made easy by commercial availability or ease of synthesis of basic precursors such as ortho-substituted aromatic dicarboxylic acid derivatives shown in **Fig. 1.2** which include phthalic anhydride (**1**), phthalic acid (**2**), phthalimide (**3**), diiminoisoindoline (**4**), o-cyanobenzamide (**5**) and phthalonitrile (**6**).

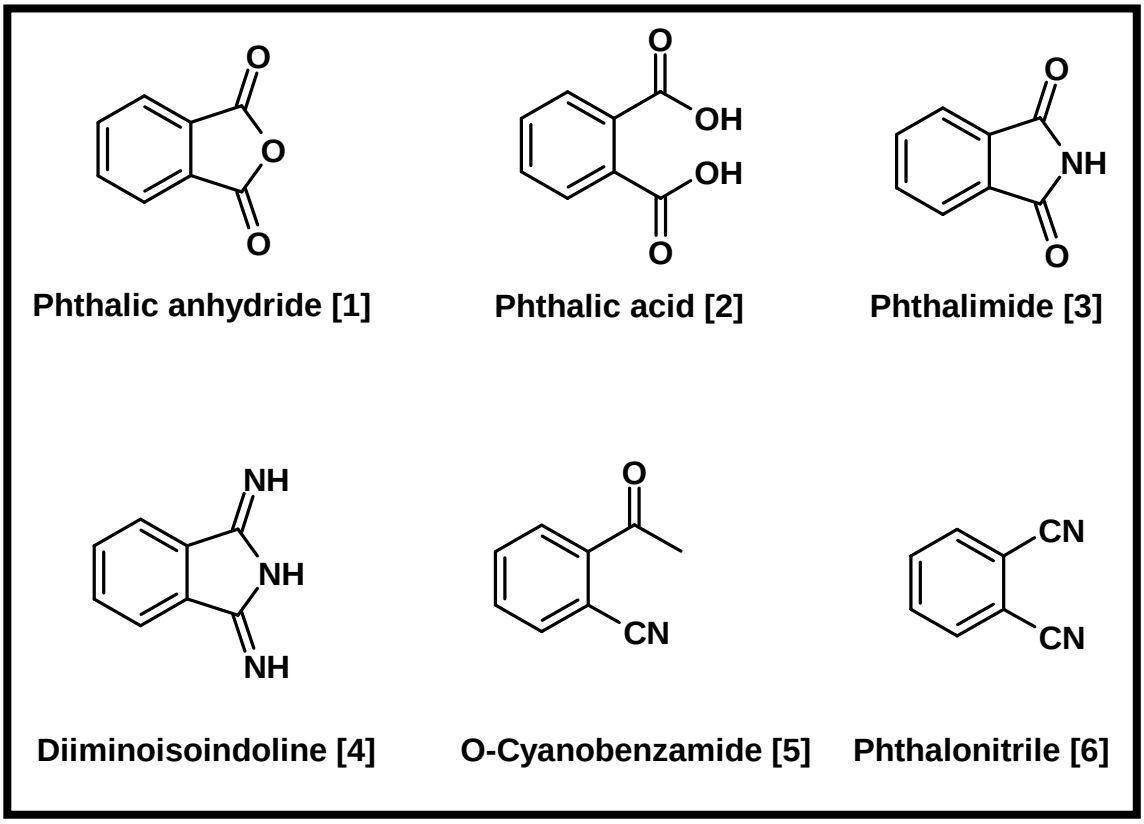

Figure 1.2: Basic Phthalocyanine Precursors

The insolubility of unsubstituted phthalocyanine derivatives requires that the synthetic pathways must involve incorporation of solubility promoters. Therefore the structural adaptability, in practice, requires regioselective synthetic approaches that provide access to assorted types of substituents.

Usually substituted MPc complexes are formed through catalysed cyclotetramerisation reactions of appropriately substituted precursors; hence the method used for achieving this in this work was the condensation of substituted derivatives of phthalonitrile. Phthalonitriles are favoured since they can be readily prepared through various synthetic pathways and their condensation reaction to form phthalocyanines gives improved yields compared to the other o-phthalic acid derivatives. Monosubstituted precursors lead to tetra substituted phthalocyanines and disubstituted precursors (disubstituted phthalonitrile) form octasubstituted phthalocyanine molecules. Another addition to the advantages of phthalonitrile as a precursor is that it readily gives good

yields of phthalocyanine complexes with most metals except mercury and silver **[69]** while other precursors like phthalimide and other phthalic acid derivatives give very unreliable results.

1.4.1. Synthesis of substituted phthalonitriles

In this work thio and aryloxo substituents were used as organic solvent solubility promoters. Substitutions at the α and β positions are possible, and phthalonitriles substituted at different positions may be used to achieve this. For octasusbtituted phthalocyanines, the precursors (disubstituted phthalonitrile) may be synthesized using established literature methods **[70-72]** starting with commercially available 2,3-dicyanohydroquinone (**7**) for α-substitution and 4,5-dichlorophthalic acid (**8**) for β-substitution, **Fig. 1.3**. 4,5-Dichlorophthalic acid (**8**) is used to synthesize 1,2-dichloro-4,5-dicyanobenzene (**9**) using established literature methods **[73]**.

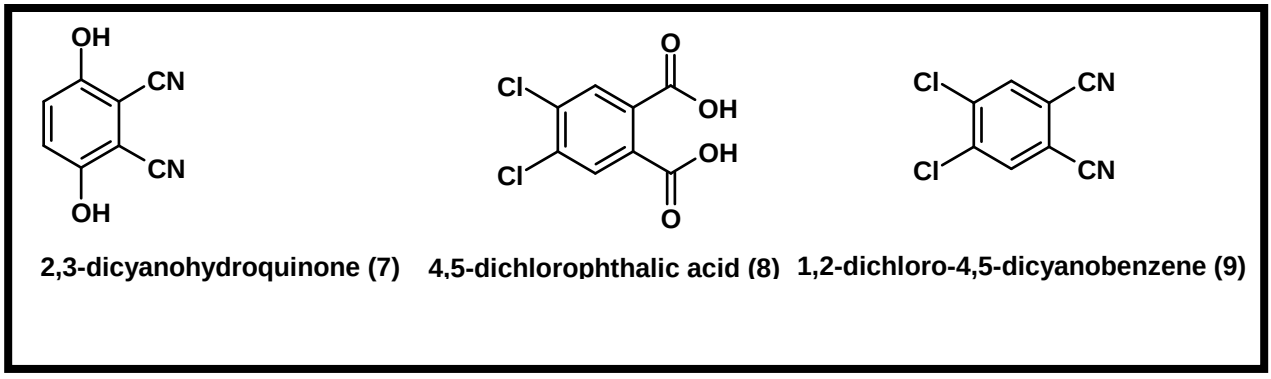

Figure 1.3: Substituted phthalocyanine precursors

The most employed reactions for the introduction of desired functionalities on phthalonitrile are nucleophilic aromatic substitution reactions. In spite of the bias of electron-rich aromatic system for electrophilic substitution, nucleophilic aromatic substitution becomes favourable when appropriate leaving groups such as nitro and halogen are present in the molecules. The electron-withdrawing dinitrile functionality in phthalonitriles makes them vulnerable to these nucleophilic attacks. Thiols **[74,75]**, alcohols **[76-79]**, amines **[80,81]** etc have been added successfully to phthalonitriles via

nucleophilic aromatic substitution. Schemes (1.1 and 1.2) show reaction pathways for the synthesis of precursors for α and β octasubstituted MPcs respectively.

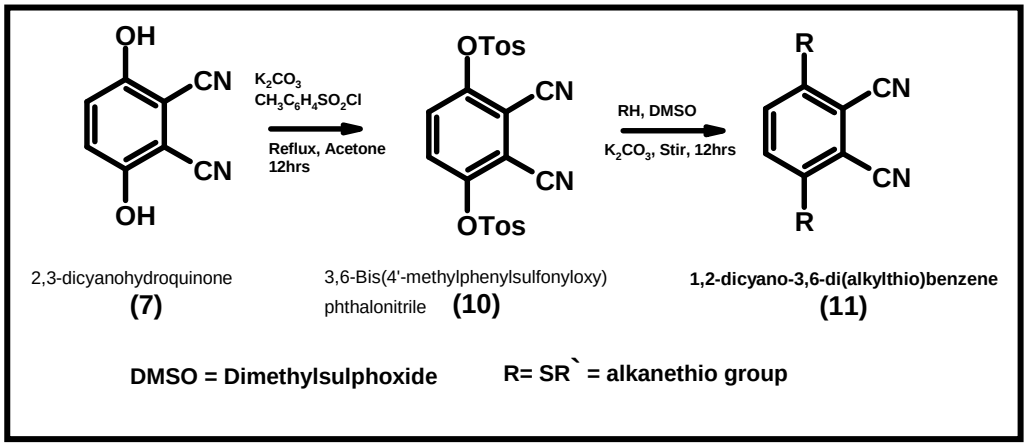

Scheme 1.1: Synthesis of precursors for α-substituted molecules

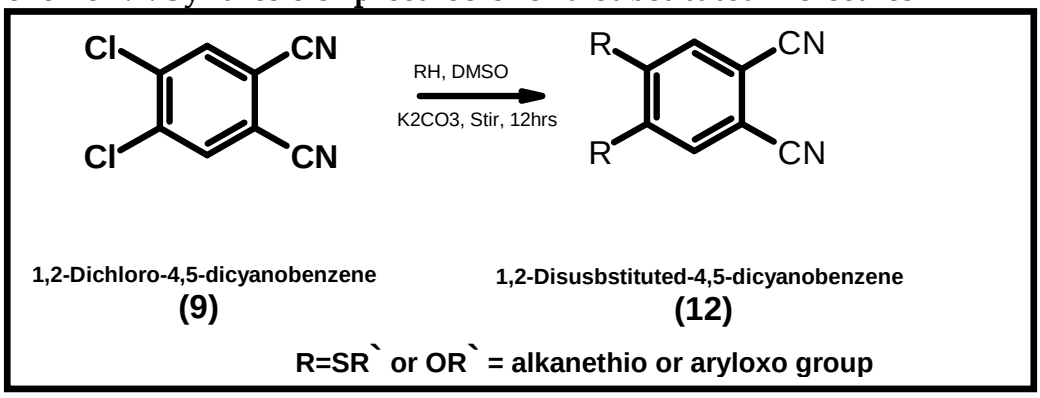

Scheme 1.2: Synthesis of precursors for β-substituted molecules

1.4.2. Synthesis of octasubstituted phthalocyanines

The mechanism of the condensation reactions of phthalonitriles to form phthalocyanines has been extensively examined. It likely involves a step-wise polymerization of precursors or reactive intermediates followed by coordination of central metal in case of metallophthalocyanines and ring closure to form the macrocycle **[69,82-86]**. This method proves effective in terms of purity of the final products when used for the synthesis of symmetrically octasubstituted MPcs since these phthalocyanine analogues do not produce constitutional isomers. In these reactions phthalonitriles are transformed into phthalocyanines via cyclotetramerization reaction at elevated temperature in either a melt of reagents or using a high boiling solvent such

as quinoline, 1-chloronaphthalene, chlorobenzene etc. The use of an organic base such as diaza(1,3)bicyclo[5.4.0]undecane (DBU), allows the reaction to proceed under milder conditions by promoting formation of alcholate. The alcholate adds to the cyano group of the phthalonitrile resulting in the formation of an alkoxy-isoindoline which in turn rapidly cyclises to phthalocyanines **[87-89]**. Other bases and solvents such as methanol, dimethyl formamide (DMF) among others have been used before **[90-95]** for phthalocyanines synthesis. The phthalocyanines employed in this work are octasubstituted and substitutents and central metals employed are shown in **Scheme 1.3**.

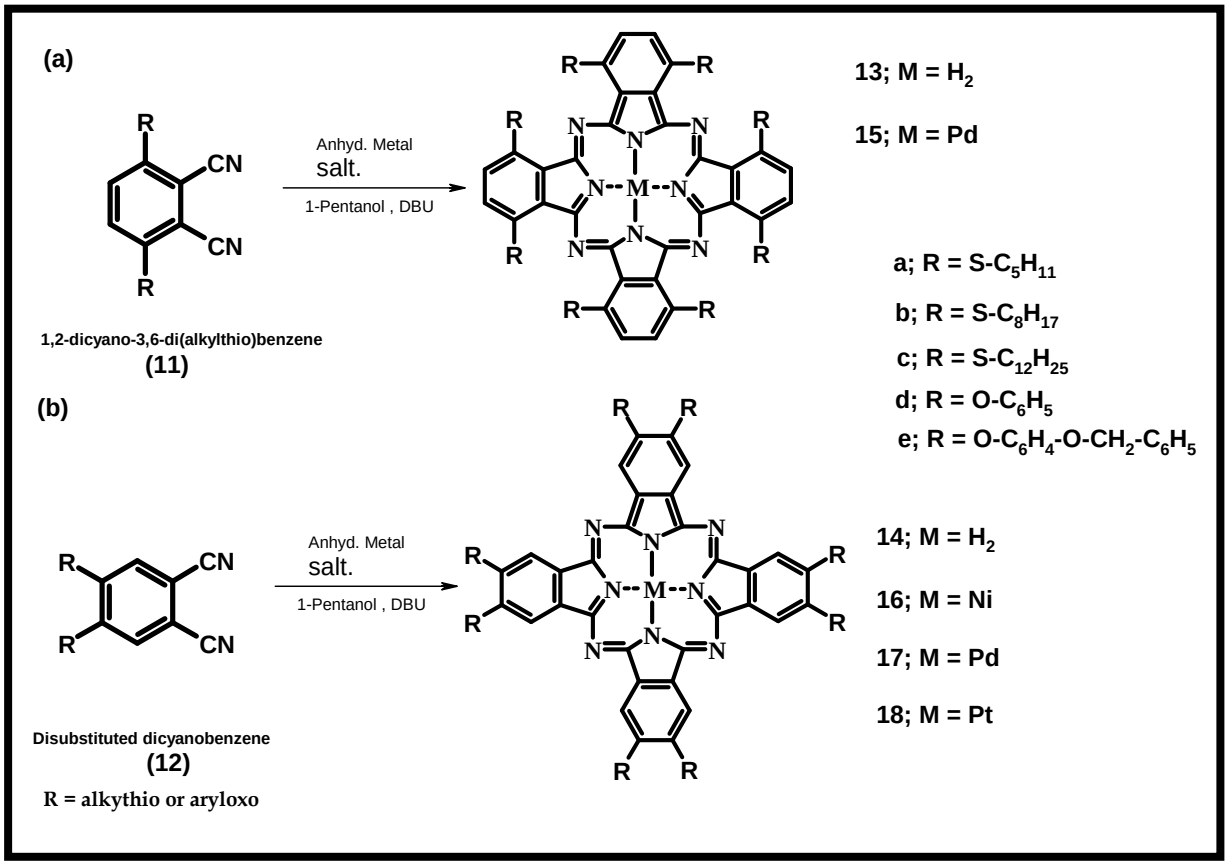

Scheme 1.3: Synthesis of (a) α-substituted phthalocyanine (b) β-substituted phthalocyanine from their precursors

1.4.3. Metal binding capacity of phthalocyanines and formation of Multinuclear complexes

Soft metal ion bindings (to the periphery of Pc ring) have been conducted using various MPcs, especially those bearing the thio functionality; and the chemical changes accompanying such binding were monitored spectrophotometrically. This is due to the optical sensitivity of thio substituted Pcs and MPcs to some metal ions **[96-98]**. The sulfur atoms in thio substituted MPcs can bind metals such as silver (I) and palladium (II). This theoretical basis offered opportunity in this work for attempted binding of palladium metal to the sulphur (S) groups attached to the phthalocyanine ring and, by extension, the synthesis of novel multinuclear complexes which could be useful in electrochemical and photochemical applications.

Since the broad intention of this project was to investigate the effect of open-shell metals which include Pd(II) on the singlet oxygen production and photosensitizing properties of phthalocyanine ligands, this metal coordination to the S groups attached to the Pc offers an opportunity for systematic study of the effect of increasing number of these metal ions on the relevant properties of the ligands. Thus, the ability of substituted phthalocyanines to chelate multiple palladium metal ions was explored in this work. Tetra substituted alkylthio-derivatised MPcs have been reported in literature in this respect, but these investigations were hampered by aggregation, which accompanied the metal binding **[96-98]**. Due to the negative effect of aggregation on photophysical and photochemical properties of tetrasubstituted phthalocyanines, octasubstituted (rather than tetrasubstituted) phthalocyanines were used for the metal coordination studies in this work.

The molecular architecture of the phthalocyanines might play a significant role in the binding processes. The point of attachment of the thio substituents to the ring (α or β) and their relative orientation in space should influence the ease of metal chelation because of the differences in intersubstituent distances. Hence both α and β substituted thio Pcs were explored in this work. The central metal in the Pc cavity could also have

an effect because of its influence on the Pcs symmetry and consequently intersubstituent distances. Since the effect of metallation on symmetry of the molecules was also expected to play a key role in the binding processes both metallated and unmetallated analogues of the molecule were investigated. The molecules used in these studies were unmetallated Pcs (**13**a, **14a**) and PdPc (complexes **15a** and **17a)** shown in **Scheme 1.3**.

1.5. Optical properties of phthalocyanines

Because of their structural relationship to porphyrins, the optical properties of phthlocyanines are explained using the models deployed in the explanation of porphyrin optical properties. Metallation of the Pc dianion, with a metal that maintains the planarity (i.e. that fits perfectly into the cavity) of the molecule increases symmetry from D_{2h} of H_2Pc to D_{4h} of MPc. Symmetry will drop to C_{4v} for metals that do not fit inside the ring. This was observed, for example, in tin phthalocyanine **[99,100]** where tin protruded out of the Pc cavity because of its ionic size. The diagonal N – N distance is smaller in phthalocyanines than in most porphyrins **[101]** which imply that in some cases, metals that form planar porphyrins complexes will form square pyramids in phthalocyanine complexes.

There have been several theoretical calculations for molecular orbitals to account for the spectral properties of Pcs. It is common to use the method proposed by Gouterman's group **[102-104]** which uses a four-orbital model to set up the states that account quite well for the first two allowed transitions in the UV-visible region of the spectrum. Gouterman's group proposed that the spectral properties of porphyrins analogues such as Pcs may be understood qualitatively by considering four frontiers orbitals: the HOMO-1, HOMO(a_{2u}, a_{1u}) (HOMO = Highest occupied molecular orbital) , LUMO and LUMO+1(e_g) orbitals (LUMO = Lowest unoccupied molecular orbital). The first two are occupied (and nearly degenerate in porphyrins) while the last two are unoccupied and degenerate when the macrocycle is perfectly square planar as in D_{4h} of MPc, **Fig 1.4**.

The accidental degeneracy of the top filled molecular orbitals, the a_{2u} and a_{1u} orbitals which is observed for porphyrins **[102,105,106]** no longer exists in MPc complexes. In Gouterman's four-orbital model, the first two bands arise from π-π*transitions. These first two allowed π-π* bands arise from transitions out of a_{1u} and a_{2u} HOMO orbitals into the doubly degenerate e_g (LUMO) orbital.

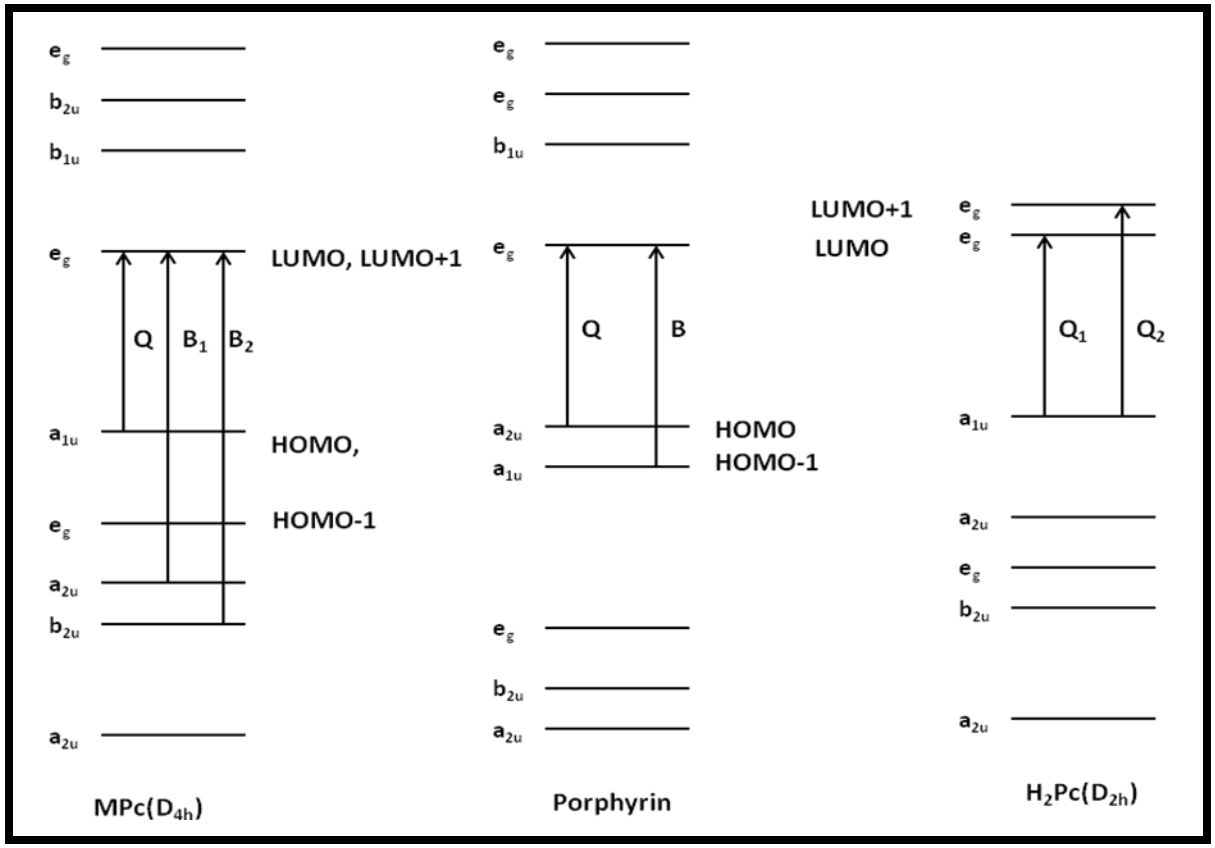

Figure 1.4: Origins of absorptions in the regions of the first two π-π* transitions, the Q and B bands, in MPcs and porphyrins and the split Q-bands in metal-free Pcs (H_2Pc).

For phthalocyanines, a_{1u} lies above a_{2u}, the bands arising from these levels are the Q and B (Soret) bands respectively. In MPc with D_{4h} symmetry (where the metal fit perfectly into the Pc cavity) the e_g is degenerate so only a single Q band is observed. Unmetallated Pcs have low symmetry (D_{2h}) hence the e_g, because of this low symmetry, appreciably looses its degeneracy and the single Q band of MPc becomes split in H_2Pc due to transitions from a_{1u} to the two nondegenerate e_g orbitals of the LUMO, **Fig. 1.5a**.

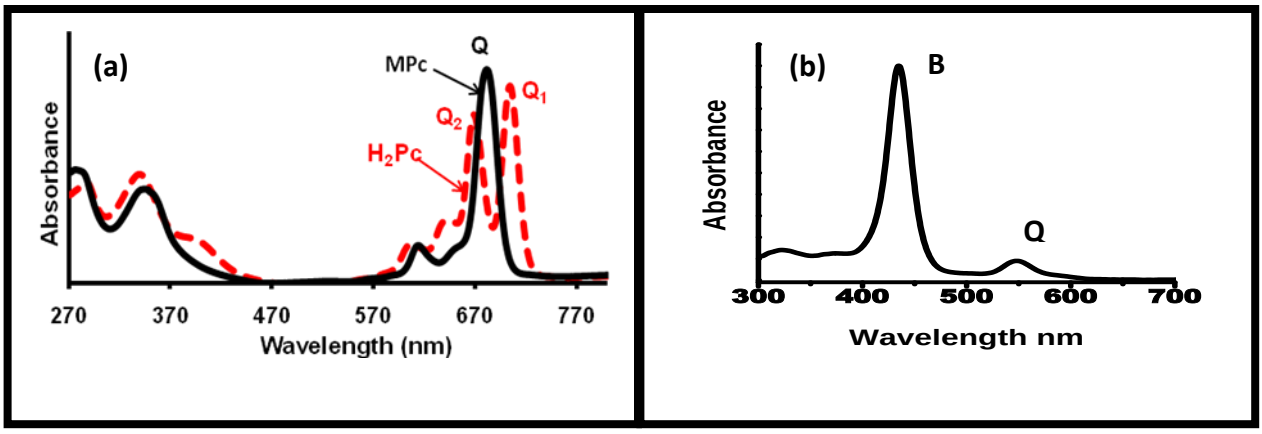

Figure 1.5: Spectra of (a) metal-free phthalocyanines (H_2Pc) and Metallated phthalocyanine (MPc) (b) Porphyrins

The accidental degeneracy of the a_{2u} and a_{1u} orbitals of porphyrins is expected to lead to almost coincident absorption bands due to $e_g \rightarrow a_{1u}$ and $e_g \rightarrow a_{2u}$ transitions, but in fact these two transition mix together by a process known as configurational interaction resulting in two bands with very different intensities and wavelengths, **Fig. 1.5b**.

Another situation observed in the optical spectra of MPcs, is due to the presence of non-bonding electrons on the azomethine nitrogens of the macrocycle. The non-bonding orbitals (n) are close in energy to the π orbitals (HOMO) and consequently, the $\pi^* \leftarrow$ n transition is expected to be coupled with $\pi^* \leftarrow \pi$ transition. It has been proposed that the band around 605 nm of MPcs could have partial contributions from the $\pi^* \leftarrow$ n transition **[107,108]**. This idea was supported by the clear observance of 605 nm band in the spectra of oxidized and reduced MPc ions, in which case the normal $\pi^* \leftarrow \pi$ transition probabilities are drastically weakened around the 605 nm and 670 nm regions **[109],** but the 605 nm band remains unchanged.

Substitution of the phthalocyanines also introduces another exciting trend to its spectra. Generally, electron-donating groups cause a red shift since they can donate electron density into the π-system increasing conjugation, hence lowering HOMO–LUMO gap resulting in red shift. The decrease in HOMO–LUMO gap is greater for non-peripherally substituted Pcs than for peripherally substituted ones. This difference has

been explained **[110,111]** to be due to linear combinations of the atomic orbitals (LCAO) coefficients at the non-peripheral positions of the HOMO being greater than those at the peripheral positions. As a result, the HOMO level is destabilized more at the non-peripheral position than it is at the peripheral position. Due to this, non-peripherally substituted MPcs are red shifted compared to peripherally substituted MPcs as shown in **Fig 1.6**.

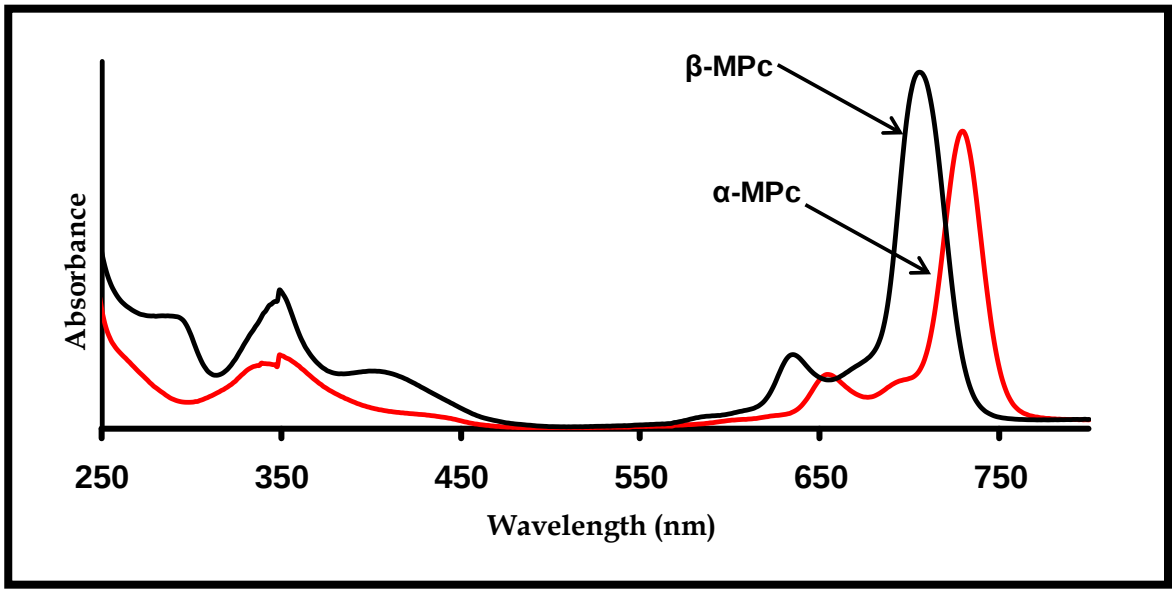

Figure 1.6: Spectra of α- and β-substituted metallophthalocyanines

It is known that the resolution of the split of the Q band of metal-free phthalocyanines (H_2Pc) decreases with increasing wavelength since e_g non-degeneracy diminishes as the wavelength of the Q-band increases leading to a Q band that appears unsplit **[112]**. The optical properties of MPcs also depend on the nature of the central metal **[101,113,114]** which also has an effect on the HOMO-LUMO gap of the phthalocyanines.

1.6. Photophysical properties of Pcs

1.6.1. Jablonski Diagram

Photophysical processes are processes that involve, on absorption of light, changes in the quantum states of a molecule with no effect on its chemical nature. In these processes, energy transfer may result in a variety of physical changes but the chemical integrity of the molecule is retained at the end of the process.

Absorption of electromagnetic radiation by molecules results in the excitation of an electron from a lower to a higher molecular quantum state. This state is energetically unstable with respect to the ground state, and therefore it finds a way of loosing the energy to return to the ground state as represented by the Jablonski diagram, **[Fig 1.7] [115-117]**. There are various physical deactivation pathways available and how favorable each of these pathways is depends on the types of molecules and nature of their electronic states.

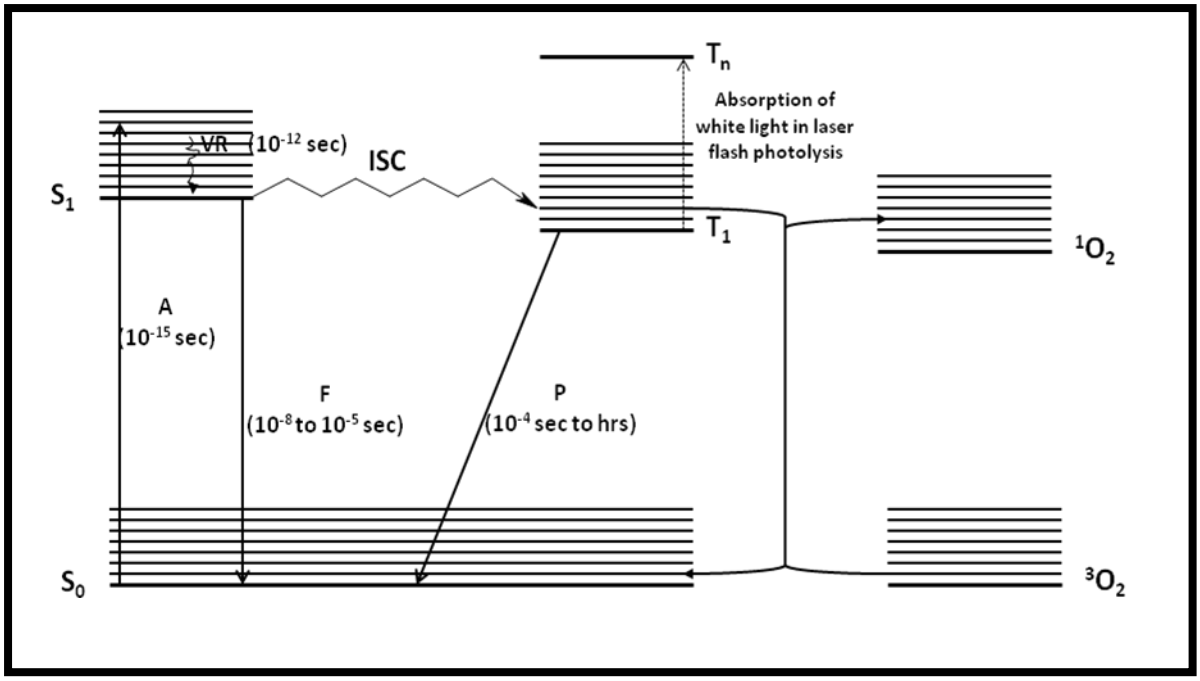

Figure 1.7: The jablonski Diagram showing transitions between the excited states and the ground state.

Absorption (A) occurs from vibrationless level of singlet ground state, S_0 to a vibrationally excited level of first singlet excited state, S_1. Through collisions with the solvent molecules, vibrational relaxation (VR) occurs and the excited molecules lose the vibrational energy and return to the first vibration level of S_1 from which there are many possibilities. These include fluorescence which is a radiative process, internal conversion (IC) and intersystem crossing (ISC) which are non-radiative processes. Because of the allowedness of the $S_1 \rightarrow S_0$ transition which leads to fluorescence (F) the time interval is very short (10^{-9} to 10^{-5} sec). When molecules move to T_1 through ISC, encouraged by the presence of a large central metal through heavy atom effect (spin-orbit coupling), the T_1 state may emit phosphorescence (P), but the state, among other things, can also undergo energy transfer to ground state molecular oxygen to generate singlet oxygen capable of initiating oxidation of substrate. Another possibility is that the T_1 state is capable of further absorption of radiation to produce the T_n states. It is on this last possibility that the technique of laser flash photolysis used to study the properties of excited state molecules important to their efficacy as photosensitisers depends.

In spite of massive reports on photophysical and photochemical properties of metallophthalocyanines **[118,119]** and the establishment of effect of diamagnetic closed shell metals on these properties **[120-134]**, this type of exhaustive investigation for open-shell metals has not been conducted. Thus, systematic investigation of the photophysical properties of MPcs containing open-shell metals, especially Ni(II), Pd(II) and Pt(II) is essential for proper understanding of the effects of these metals on corresponding applications of Pcs. Such studies are scarce in the literature for these MPc complexes.

1.6.2. Fluorescence quantum yields (Φ_F)

Quantum yields measure the efficiency of photophysical processes and fluorescence quantum yield (Φ_F) is a measure of the efficiency of the fluorescence process. It is the ratio of the number of fluorescing molecules to the number of absorbed photons. The

Φ_F values can be determined by comparative method using **Eqn 1.1** and ZnPc as standard **[135,136]**.

$$\Phi_F = \Phi_{F(Std)} \frac{F.A_{Std}.\eta^2}{F_{Std}.A.\eta^2_{Std}} \qquad 1.1$$

where F and F_{Std} are the areas under the fluorescence curves of the MPc derivatives and the reference respectively. A and A_{Std} are the absorbances of the sample and reference at the excitation wavelength, and η and η_{Std} are the refractive indices of solvents used for the sample and standard, respectively. A standard such as ZnPc which has fluorescence quantum yield, Φ_F = 0.20 in DMSO **[120]**, may be employed.

Though fluorescence studies were carried out in this work, low yields were expected because our major focus was the population of triplet excited states through intersystem crossing which was expected to be enhanced by heavy atom effect of the central metals as reported for zinc, cadmium and mercury phthalocyanines **[137,138]**.

1.6.3. Triplet quantum yields (Φ_T) and lifetime (τ_T)

Triplet quantum yield represents the proportion of the singlet excited state phthalocyanines that get to the triplet state. While the triplet lifetime is the amount of time it takes the triplet state to be completely depopulated. Triplet lifetime indicates the time window available for the triplet state molecules to transfer photons to the ground state molecular oxygen and/or the substrates.

Triplet quantum yields may be determined using a comparative method based on triplet decay, using **Eqn 1.2 [139]**

$$\Phi_{T(sample)} = \Phi_{T(std)} \frac{\Delta A_T^{Sample} \varepsilon_T^{Std}}{\Delta A_T^{Std} \varepsilon_T^{Sample}} \qquad 1.2$$

where ΔA_T^{Sample} and ΔA_T^{Std} are the changes in the triplet state absorbance of the MPc derivatives and the standard, respectively. ε_T^{Sample} and ε_T^{Std} are the triplet state extinction

coefficients for the MPc derivative and standard, respectively. $\Phi_{T(Std)}$ is the triplet state quantum yield for the standard, for example, for ZnPc in 1-chloronaphthalene (1-CNP) , Φ_T = 0.67 **[28]** . Triplet lifetimes are determined by exponential fitting of the kinetic curves using OriginPro 7.5 software.

These triplet state parameters are determined using a laser flash photolysis system. A typical triplet decay curve and transient absorption spectrum of an MPc are shown in **Fig. 1.8a** and **b** respectively.

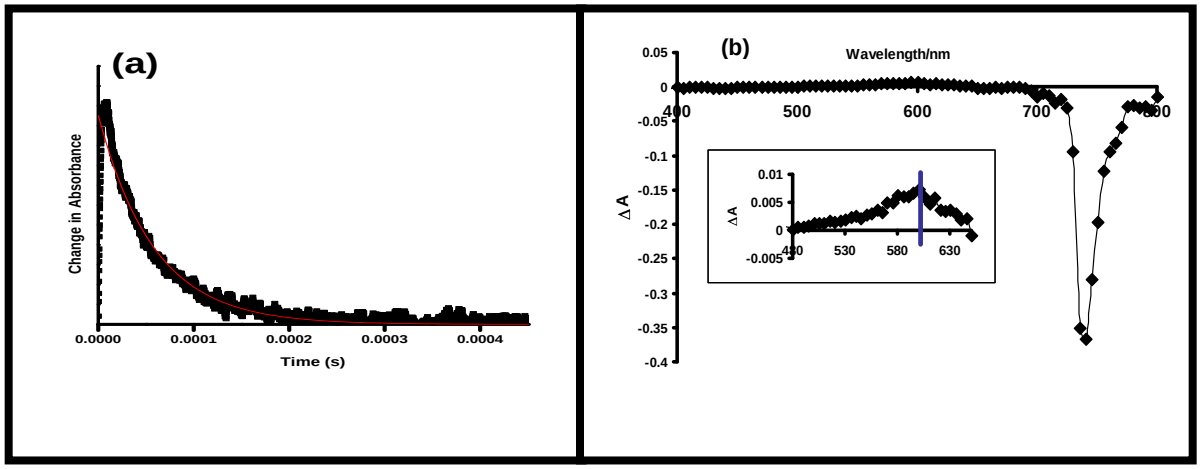

Figure 1.8: Typical (a) triplet decay curve (b) transient absorption spectrum of an MPcs (Insert: Wavelength of maximum $T_1 \rightarrow T_n$ absorption)

1.7. Photochemical Properties

1.7.1. Photosensitized singlet oxygen production by MPcs

Photosensitization is the process through which photophysical and photochemical alteration occurs in one molecular entity in contact with another entity at the excited state as a result of absorption of radiation. The molecular entity that initiates the reactions after absorption of light is called the photosensitiser. MPcs have proved to be potent photosensitisers because of their strong light absorption and long lifetime of their triplet excited state. One way through which excited molecules return to the ground state is by quenching and ground state molecular oxygen is an efficient quencher. During this quenching process the excited molecules transfer their excess

energy to the oxygen thereby generating excited states of oxygen known as singlet oxygen.

As shown in **Scheme 1.4** oxygen is unusual in that it has a triplet ground state. In the ground state, the outermost electrons are distributed according to Hund's rule in π_{2px^*} and π_{2py^*} antibonding orbitals **[140,141]**. The two electronically excited states above the ground state are singlet states, $^1\Sigma_g+$ and $^1\Delta_g$. $^1\Sigma_g+$ is more energetic but very short-lived and rapidly decays to lower energy singlet oxygen, $O_2(^1\Delta_g)$. The first singlet state $O_2(^1\Delta_g)$ possesses an energy of 94 KJ/mol and a radiative lifetime of 10^{-6} – 10^{-3} s while the second singlet state, $^1\Sigma_g+$, possesses an energy of 132 KJ/mol and radiative lifetime of 10^{-11} – 10^{-9} s. The difference in lifetime is attributed to the spin allowedness of the deactivation process **[142]**. Thus the threshold energy of the triplet state of MPcs to transfer energy to $^3O_2$ resulting in formation of singlet oxygen is 94 KJ mol^{-1} (0.98 eV).

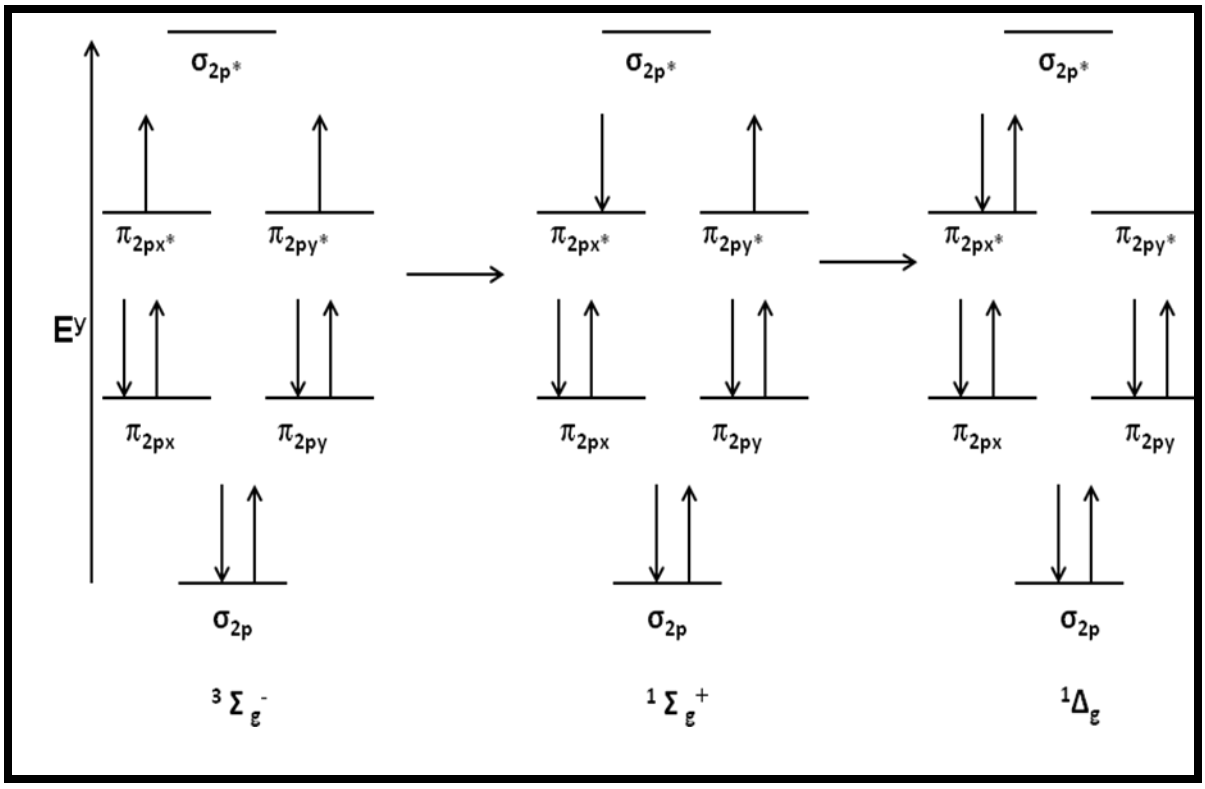

Scheme 1.4: Molecular orbital diagram showing the electron distribution in ground state molecular (triplet) oxygen and the two forms of singlet oxygen

For practical purpose, if $^1\Sigma_g+$ is formed in solution, it is immediately deactivated to $O_2(^1\Delta_g)$. As a result the singlet oxygen state which is considered to be involved in photosensitized reactions is $O_2(^1\Delta_g)$. Singlet oxygen has demonstrated its high reactivities through oxidative attacks in some systems such as cancer cells **[143,144]**. Once it is formed, singlet oxygen can be deactivated through physical quenching or chemical quenching. While physical quenching yields no useful results, chemical quenching of singlet oxygen leads to chemical transformation of the quenchers and it is this process that leads to the oxidation of substrates like phenolic compounds **[142],** which are of interest in this thesis. For a photosensitiser to effectively produce singlet oxygen it has to possess the following characteristics:

1) High absorption coefficient
2) High triplet quantum yield ($\Phi_T > 0.4$) and long triplet lifetime ($\tau_T > 1\mu s$)
3) Excited triplet state energy equal to or higher than that of singlet oxygen ($E_T \geq$ 94 KJ/mol)
4) High photostability

1.7.2. Singlet oxygen quantum yields (Φ_Δ)

The parameter that measures the efficacy of MPcs in the generation of singlet oxygen is the singlet oxygen quantum yield, Φ_Δ. The triplet quantum yield and lifetime of a photosensitiser are directly related to their efficiencies of singlet oxygen generation: a key component in the success of a photosensitiser **[123]**.

Φ_Δ value can be determined by photochemical and photophysical methods. In the photochemical method, which was used in this work, a solution containing oxygen, photosensitiser (MPc) and a singlet oxygen scavenger is irradiated and the decay of the scavenger is measured spectroscopically. Scavengers are sensitive compounds that react quickly with singlet oxygen as soon as it is produced. Some of good examples of this include 1,3-diphenylisobenzofuran (DPBF) and 9,10-anthracenediyl-bis(methylene)-

dimalonic acid (ADMA) used in this work. Other chemical quenchers compatible with organic solvents are guanine, furan and anthracene derivatives.

When singlet oxygen is produced by MPcs in the presence of a scavenger, S, there are many possible pathways for singlet oxygen quenching.

$$O_2(^1\Delta_g) \xrightarrow{k_d} O_2(^3\Sigma_g) \quad \text{(Natural decay)} \qquad 1.3$$

$$O_2(^1\Delta_g) + S \xrightarrow{k_a} \text{Oxidation Products (Chemical reaction)} \qquad 1.4$$

$$O_2(^1\Delta_g) + S \xrightarrow{k_q} O_2(^3\Sigma_g) + S \text{ (Physical quenching)} \qquad 1.5$$

$$O_2(^1\Delta_g) + MPc \longrightarrow O_2(^3\Sigma_g) + MPc \text{ (Physical quenching)} \qquad 1.6$$

$$O_2(^1\Delta_g) + MPc \longrightarrow \text{Oxidation Products (Chemical reaction)} \qquad 1.7$$

Eqn. 1.3 is the natural decay pathway of singlet oxygen and k_d is the natural decay constant. **Eqns. 1.5** and **1.6** represent the inconsequential physical interactions between singlet oxygen and scavenger or MPc respectively. These reactions do not lead to any chemical changes, except the return of singlet oxygen to ground state by transfer of energy, and k_q represent the physical quenching constant for the reaction between scavenger and singlet oxygen. **Eqns. 1.4** and **1.7** represent the chemical reactions between singlet oxygen with the scavenger or MPc, respectively. **Eqn 1.7** is the bleaching of the photosensitiser and must be negligible for the sensitizer to be effective, so the rate of this reaction is negligible compared to the rate of reaction between scavenger and singlet oxygen, k_a.

Φ_Δ may be determined by comparative method from **Eqn. 1.8 [134,145]**

$$\Phi_\Delta^{MPc} = \Phi_\Delta^{Std} \frac{R_S^{MPc} I^{Std}}{R_S^{Std} I^{MPc}} \qquad 1.8$$

where Φ_Δ^{MPc} and Φ_Δ^{Std} are singlet oxygen quantum yields of MPc and the standard respectively. R_S^{MPc} and R_S^{Std} represent the scavenger photobleaching rate in the presence

of MPc and standard respectively while I^{MPc} and I^{Std} are the rate of light absorption by the MPc and standard respectively.

If a standard is not involved in the determination, then singlet oxygen quantum yield can be calculated from **Eqn. 1.9 [146]**.

$$\frac{1}{\Phi_S} = \frac{1}{\Phi_\Delta} + \frac{1}{\Phi_\Delta}.\frac{k_d}{k_a}.\frac{1}{[S]} \qquad 1.9$$

where Φ_S is the quantum yield of the scavenger. The value $^1/_{\Phi_\Delta}$ is the intercept obtained from the plot ($^1/_{\Phi_S}$ versus 1/[S]). The quotient of $^{k_d}/_{k_a}$ is called the β-value;

Eqn. 1.10

$$\beta = \frac{k_d}{k_a} \qquad 1.10$$

where β is the constant for the scavenger decay in a certain solvent and can be calculated from the slope of the plot after Φ_Δ has been determined.

The quantum yield of the scavenger, Φ_S, can be obtained from **Eqn 1.11 [145]**

$$\Phi_S = \frac{[C_o - C_t]V}{I_{abs}t} \qquad 1.11$$

where C_o and C_t are the concentrations of the scavenger before and after irradiation respectively, V is the volume of the sample in the cell; t is the irradiation time. I_{abs} is given by **Eqn. 1.12**

$$I_{abs} = \frac{\propto AI}{N_A} \qquad 1.12$$

where $\propto$ is the fraction of light absorbed, A is the cell area irradiated, I is the light intensity from the lamp and N_A is the Avogadro's constant.

1.7.3. Photobleaching

While singlet oxygen is essential for the efficacy of phthalocyanines as photosenstisers, it also has a flip side of oxidizing the photosensitizers in the process thereby reducing their efficacies. Photobleaching is the process of photochemically induced oxidative fragmentation of the photosensitisers into low molecular weight compounds by singlet oxygen as represented in **Scheme 1.5**.

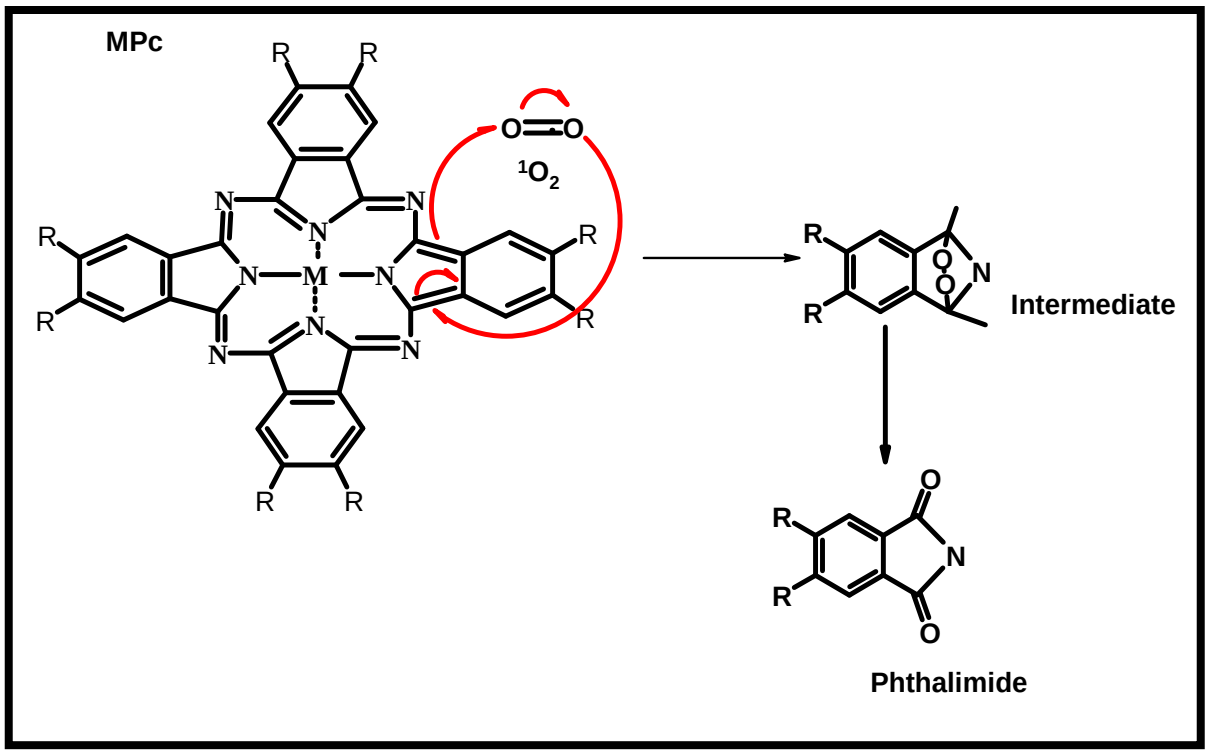

Scheme 1.5: Cycloaddition reaction of MPc with singlet oxygen

The ability of MPc photosensitisers to react with oxygen known as photobleaching has been extensively reported **[145,147,148]**. This singlet oxygen mediated process determines the photostability of MPc molecules and is experimentally identified by a collapse in the intensity of the Q-band of the molecules without the appearance of new peak in the visible region. The process takes place through Diels-Alder cycloaddition mechanism whereby the excited triplet state of MPc undergoes oxidative attack by

singlet oxygen species in the medium, forming phthalimide as a product **[145,147,149] (Scheme 1.5)**.

How stable a phthalocyanine is to this attack is partly a function of its structure with factors such as nature of central metals, aggregation and nature of substituents playing key role. Other factors such as solvent and light intensity are also important. It has been found that electron-withdrawing substituents reduces photobleaching tendency by making it difficult to oxidise the Pc ring while electron-donating group enhances probability of MPc to undergo ring photooxidative degradation **[150-152]**. MPcs substituted at the peripheral positions have been found to be less stable than ones substituted at the non-peripheral positions **[151]**. Chlorinated solvents such as chloroform and dichloromethane (DCM) have also been discovered to promote photobleaching because their low basicity leaves MPc molecules vulnerable to oxidative attack **[120,153,154],** while aqueous media have been found to slow down the process because of high aggregation of MPc **[155,156]**. This is probably due to the fact that in some cases, aggregated species may transform into monomers during photo-irradiation **[157]**. Strongly coordinating, highly solvating basic solvents, such as DMSO, permit axial coordination to the central metal atom thus partly shielding the MPc molecule from oxidative attack **[158]**.

Photobleaching quantum yield (Φ_P) is calculated using **Eqn 1.11** and it represents the fraction of the initial number of MPc molecules degraded per quanta of light absorbed.

1.8. Aggregation in phthalocyanines

Phthalocyanines aggregation is the coplanar association of rings in solution progressing from monomer to dimer and higher order complexes and is driven by non-bonded attractive interactions **[159-162]**. In the aggregated state, intermolecular interactions alter physical and chemical properties such as colour, photodynamic and catalytic activities of phthalocyanines compared to the monomers. Applications as dyes that are

dependent on photophysical properties of these molecules are more affected by aggregation.

The structure of the aggregates is of particular interest in phthalocyanine chemistry and H and J types of aggregates have been reported based on the geometry of the arrangement. Aggregation often result in broadening, splitting of the Q band and bathochromic or hypochromic shift of the aggregate peak depending on the type of aggregate **[163,164],** with H aggregation appearing to the blue and J type appearing to red of the Q band. The origin of this split of the Q band and position of the aggregate peak relative to the Q band is explained by exciton coupling model **[165,166]**.

The model, demonstrated by the qualitative energy picture in **Fig 1.9,** shows that interactions between two neighbouring phthalocyanines results in the formation of two new exciton states from the $^1E^m$ excited states of the MPc monomer. The transition moments of the molecules may be parallel (H aggregate) or in line (J aggregate).

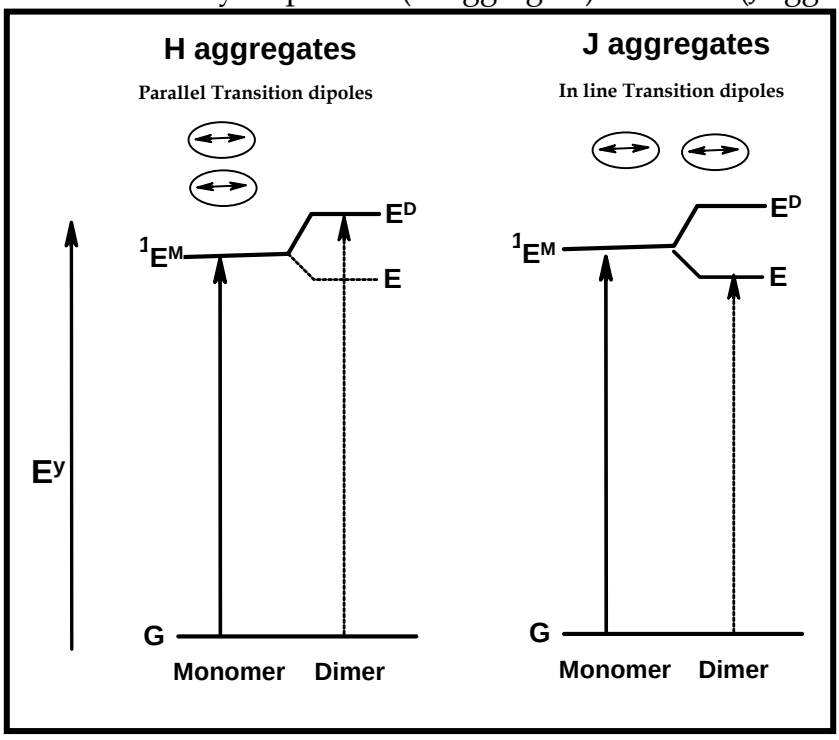

Figure 1.9: Energy diagram showing the split in energy levels of LUMO on aggregation (E^M = excited state of monomer, E^D = excited state of dimer)

In H-aggregation where the arrangement is cofacial, the dimer energy state is of parallel transition moments, making it a strongly allowed, with blue shifted absorption. For J-aggregation where the arrangement is co-planar the lower energy transition is the more strongly allowed hence J aggregates are red-shifted. H aggregation is observed in many organic dyes while J aggregation is rare for phthalocyanines.

Factors such as MPcs' central metals, type of substituents, position of substitutents as well solvents properties such as polarity **[162,167-169]** and coordinating ability **[112]** affect aggregation property of phthalocyanine molecules. Phthalocyanine aggregation is enhanced in polar solvent such as methanol and water **[160,170-174]** while introduction of bulky substituents especially at the non-peripheral position reduces aggregation by causing steric hindrance **[175,176]**. **Fig. 1.10** shows a typical H-type aggregation, and monomerisation of MPc on addition of surfactant.

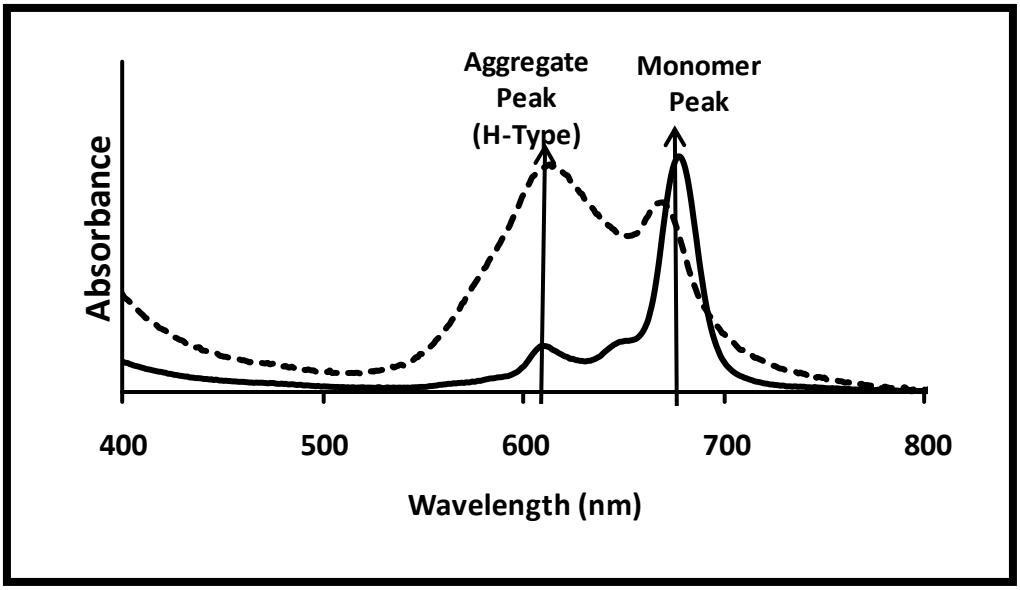

Figure 1.10: Absorption Spectra showing aggregation and monomerisation of phthalocyanines on addition of surfactant

Aggregation of phthalocyanines can be studied through electronic spectroscopy in the form of repetitive scans of the Q-band at varying Pc concentrations, temperature or by addition of surfactants.

1.9. Oxidation of Phenols

1.9.1. Phenols: Pollution and removal

Research on water purification has been growing in the last decades because of the new social and political concerns driven by renewed environmental and health consciousness among the people. These new concerns have given rise to stricter water quality control and regulations in many countries leading to more vigorous efforts in this research field. Phenols, listed by US environmental protection agency (EPA) in the Clean Water Act **[177-179]** constitute a group of priority toxic pollutants targeted by these efforts. Due to their diverse origins, they can be found in ground waters, wastewaters and soils **[180-184]**.

The need to restore sites contaminated by these pollutants has led to research into numerous methods that hold potential for their removals, degradation or transformation to less toxic forms. The conventional methods used for these include biological, thermal and chemical treatments **[185]**. The first requires a long residence time for microorganisms **[186]** to degrade the pollutant, thermal treatments present considerable emission of other hazardous compounds; and the chemical treatment, which include processes such as flocculation, precipitation, adsorption on granular activated carbon (GAC), air stripping or reverse osmosis (RO), require a post-treatment to remove the pollutant **[187,188]**.

Other methods involve the oxidation of these pollutants using various oxidants **[189-198]**. Electrochemical methods have also been used **[199-201]**. Among these techniques, the advanced oxidation processes (AOPs) **[202,203]** have shown promise for the near ambient degradation of soluble organic contaminants from waters and soils, because they can provide an almost total degradation **[204-215]**. Even though the techniques discussed above can provide the conversion of contaminants to less harmful compounds, usually oxygenated organic products and low molecular acids, processes that can bypass these oxidants, many of which act as pollutants themselves, are still

highly desirable to avoid re-pollution during decontamination. Photocatalysis shows the potential for this type of degradation.

1.9.2. Photocatalysis

Photocatalysis is the initiation of degradation or transformation reactions of molecules using a combination of light and photoactive materials as catalysts. This line of research has been of intense investigation for the conversion of pollutants into materials of less toxicity. Photodegradation of pollutants is gaining extensive attention in the quest for efficient and benign conversion processes in the area of environmental management because the employment of catalysts in the initiation of degradation makes the method fast, cheap, adaptable and applicable to deal with low concentration of pollutants even at parts per billion ranges.

Pollutants have been photodegraded or transformed directly with ultraviolet (UV) radiation **[193,195-198,216]**. Chemicals such as hydrogen peroxide **[193,195,216-218]** and ozone **[180,193,195-198]** have also been employed as oxidants in the presence of UV light. Due to the environmental problems associated with these methods, employing them becomes undesirable. Photocatalysis involving the use of photosensitisers can be categorized into two broad techniques based on the mechanism through which the sensitizer initiates the reaction. The two are semiconductor mediated photocatalysis and triplet-state mediated photocatalysis.

1.9.2.1. Semi-conductor mediated photocatalysis

In semi-conductor mediated photocatalysis, the sensitizers are semiconductors **[219-223]**. Photodegradation is preceded by conduction electron (e^-) and positive hole (h^+) formation, **Eqn. 1.13**, **Scheme 1.6**.

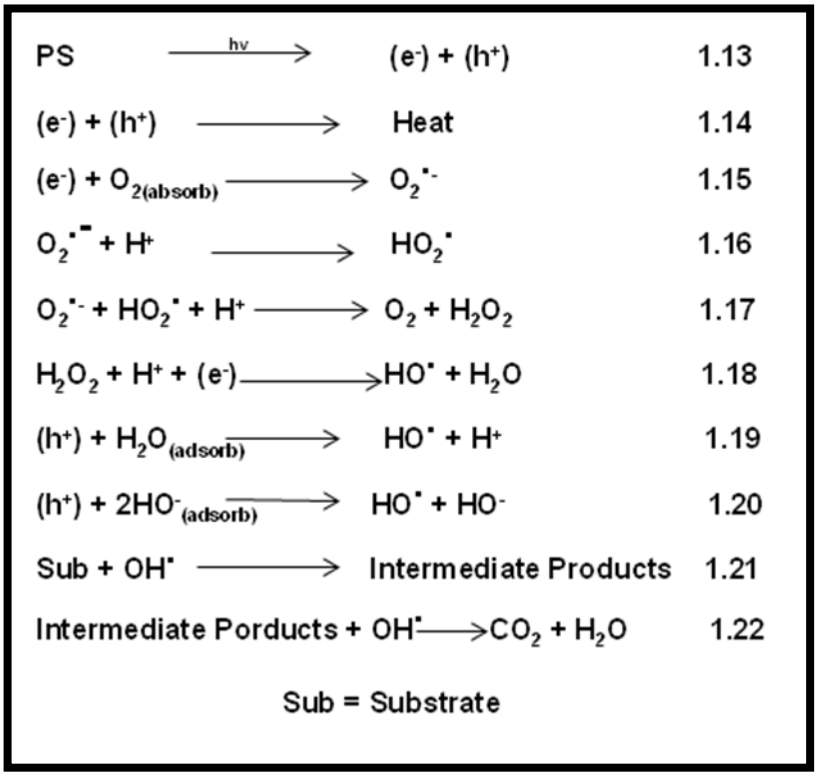

Scheme 1.6: Mechanism of degradation in semi-conductor mediated photocatalysis

A few of these high energy electron-hole pair (h^+/e^-) migrate to the surface of the catalyst where they initiate oxidation and reduction respectively on the substrate adsorbed on the catalyst surface leading to their degradation **(Eqns. 1.15-1.22)** and sometimes complete mineralization, while the remaining e^- and h^+ recombine in few nanoseconds and their energies dissipated as heat **(Eqn. 1.14) [224-226]**. TiO_2 is an example of semiconductor photocatalyst that operates through this pathway.

Table 1.2 gives the summary of the pollutants used in this work and literature results (pseudo-first order kinetic constants) obtained in the presence of various oxidants and semi-conductors.

Table 1.2: Previous methods used in degradation/transformation of substituted phenols and pseudo-first order kinetic constants

Phenols	Degradation agents/Reaction Type	k_{CP} (min^{-1})	Ref.
4-NP	Microbes		**186**
	Photocatalysis (semi conductor e.g. TiO_2)	1.5×10^{-1}	**227**
4-CP	UV	5.08×10^{-2}	**195**
	Fenton's reagents	7.00×10^{-3}	**216**
	Fenton's reagents/Fe powder	1.40×10^{-2}	**228**
	Fenton's reagents/Graphite-Fe	5.38×10^{-5}	**228**
	H_2O_2/UV	5.07×10^{-2}	**195**
	Ozone	1.70×10^{-2}	**180**
	Ozone/UV		**193**
	Ozone/Fe^{2+}/UV	6.42×10^{-2}	**197**
	Photocatalysis (semi conductor e.g. TiO_2)	2.70×10^{-4}	**219**
PCP	UV/Homogenous	5.39×10^{-2}	**195**
	Fenton's reagents	-	**229**
	H_2O_2/UV	0.458	**195**
	Ozone/UV	-	**230**
	Photocatalysis(semi conductor e.g. TiO_2)	2.96×10^{-6}	**185**

4-NP = 4-Nitrophenol; 4-CP = 4-Chlorophenol; PCP = Pentachlorophenol

Semi-conductor photocatalyst (TiO_2) shows the highest rate constant for 4-NP degradation while it gave moderate performance for 4-CP and PCP **[180,185,195,216,219,227-230]**. In spite of tremendous amount of work on the catalysts and degradation agents above, most of them pose drawbacks that make search for alternative agents desirable. TiO_2, a semi-conductor heterogeneous catalyst, has been found to be an inefficient photosensitiser, due to the band gap that falls in the near-UV region where only about 4 % of solar energy is effective while Fenton reagent has its drawback as the H_2O_2 which is part of the reagent is consumed in the process **[231-239]**.

1.9.2.2. Triplet state mediated photocatalysis

This type of catalysis involves the triplet state of the molecules and it has two reaction path possibilities namely Type I and Type II reactions **[240-243]**. Type I reaction, shown in **Scheme 1.7** is the mechanism that involves the transformation of the photogenerated triplet state of the photosensitiser ($^3PS^*$) into a radical specie ($PS^{\cdot+}$) via electron transfer interaction with ground state molecular oxygen ($^3O_2$) which also gets transformed to a radical specie ($O_2^{\cdot-}$) in the process **[Eqns 1.23, 1.24]**. This oxygen radical, in a chain of subsequent reactions, generates hydroxyl radicals ($OH^{\cdot}$), hydroxyl ions and other reactive species **[Eqn 1.25 – 1.27]** capable of initiating degradation or transformation reactions on the substrate. The photosensitiser radical also has the capacity to kick-start a reaction on the substrate **[Eqns. 1.28, 1.29]**.

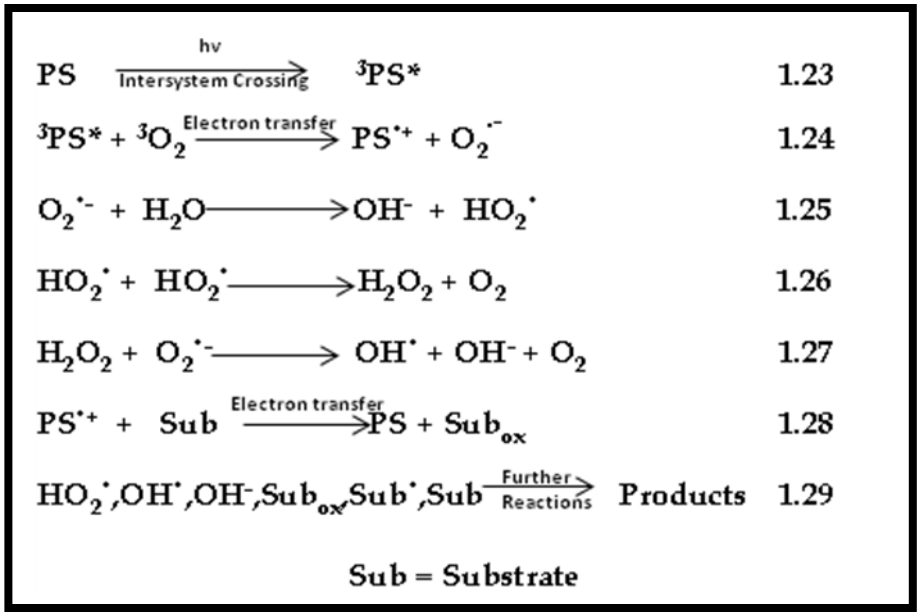

Scheme 1.7: Type I reaction mechanism in triplet state mediated photocatalysis.

The Type II **(Scheme 1.8)** reaction mechanism starts with the energy transfer interaction between triplet state of the photosensitisers ($^3PS^*$) and ground state molecular oxygen ($^3O_2$) to give energetic singlet oxygen ($^1O_2$) **(Eqn. 1.31)** which is capable of oxidizing the substrate **(Eqn. 1.32)**.

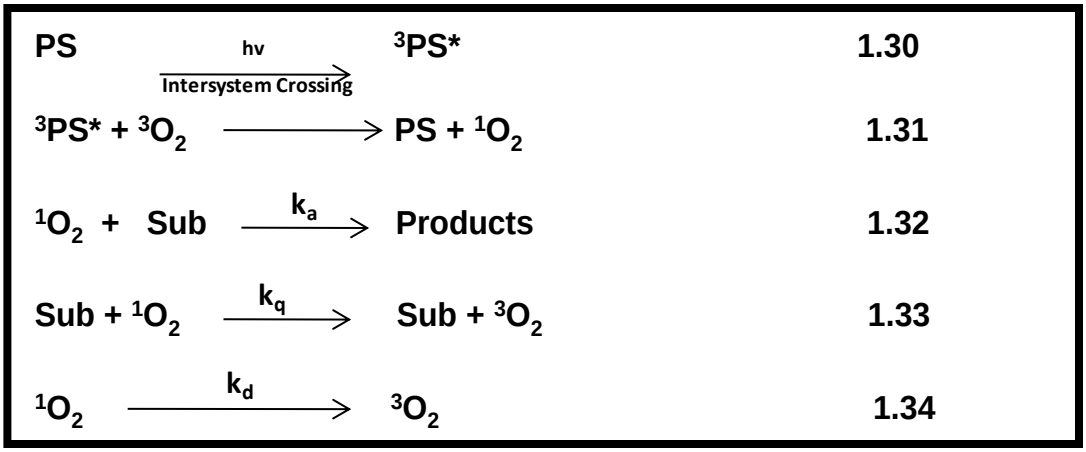

Scheme 1.8: Type II reaction mechanism in triplet state mediated catalysis.

If the reaction goes through Type II mechanism under homogenous conditions, the quantum yield of phototransformation (Φ_{Poll}) of pollutants is represented by **Eqn. 1.35**.

$$\Phi_{Poll} = \Phi_{\Delta} \frac{k_a[Poll]}{k_d+(k_a+k_q)[Poll]} \quad 1.35$$

where k_a is rate constant for the oxidation reaction, **Eqn. 1.32,** k_q represents the physical quenching constant for the reaction between pollutant and singlet oxygen, **Eqn. 1.33** and k_d is the natural decay constant, **Eqn. 1.34**.

Eqn 1.35 can be rewritten in a double reciprocal to give **Eqn 1.36**

$$\frac{1}{\Phi_{Poll}} = \frac{1}{\Phi_{\Delta}}\left\{\frac{k_a+k_q}{k_a} + \frac{k_d}{k_a[Poll]}\right\} \quad 1.36$$

The rate constants for the photodegradation of the pollutants by singlet oxygen (k_a) and physical quenching of singlet oxygen by the pollutant (k_q) can be obtained from the slope and intercept, respectively, **Eqn. 1.36**.

The quantum yield of the pollutant, Φ_{poll}, can be obtained by replacing scavenger (S) with pollutant (Poll) in **Eqn 1.11** to give **Eqn 1.37**

$$\Phi_{Poll} = \frac{[C_o - C_t]V}{I_{abs}t} \quad 1.37$$

where C_o and C_t are the concentrations of the pollutant before and after irradiation respectively, V is the volume of the sample in the cell; t is the irradiation time. I_{abs} is given by **Eqn. 1.12**

1.9.3. Langmuir-Hinshelwood Kinetics

While homogenous reactions for degradations of many phenols have been carried out, it is well known that heterogeneous systems could exhibit several advantages over corresponding homogenous systems. Long lifetime of catalyst, facile recovery and easy separation of catalyst are among the advantages. It is for this reason that heterogeneous reactions were also explored in this work.

Adsorption of reactants on the surface of the catalyst is the first step in every reaction under heterogeneous catalysis and Langmuir–Hinshelwood equation **(Eqn. 1.38)** has been used to describe the kinetics of the adsorption-desorption behavior of the reactants.

$$\frac{1}{\text{rate}} = \frac{1}{k_r} + \frac{1}{k_r K_{ads} C_o} \qquad 1.38$$

where k_r is the rate constant for the adsorption of substrate (e.g. substituted phenols), C_0 is the initial concentration of the substrate. K_{ads} is the adsorption coefficient and represents the equilibrium between the rates of adsorption and desorption **[244]**. In Langmuir–Hinshelwood kinetics it is assumed that all species are adsorbed on the surface of the catalyst before they take part in any reactions. Hence, species react in the chemisorbed state on the surface. It is important to understand the adsorption – desorption behavior of the model substrate on the catalyst. Langmuir-Hinshelwood (L-H) equation **(Eqn 1.38)** which has been used to describe the competitive adsorption of substrates, reaction intermediates and phenolic oxidation products **[245,246]** was deployed. The plots of reciprocal of initial rate of phototransformation vs. reciprocal of initial concentration of substrate gives k_r as the intercept, the adsorption coefficient (K_{ads}) can then be determined from the slope.

1.9.4. Catalyst Supports in heterogeneous catalysis

Some catalysts or sensitisers that have been used in homogenous catalysis have been effectively deployed in heterogeneous catalysis by finding a creative way to immobilize them onto a solid support. **Table 1.3** shows metallophthalocyanines that have been used under homogenous conditions and those that have been immobilized on solid support for degradation of various phenolic compounds. Supports such as silane gel, organobentonite, anionic clay, polydivinylbenzene, alumina and ambilite have been used for supporting MPcs in heterogeneous reactions for degradation of chlorophenols **[58,67,247-252]**.

Table 1.3: Metallophthalocyanines used in previous experiments on transformation of substituted phenols and materials as catalyst supports in heterogeneous media

Substrate	MPc	Rαn Type	Het. Catalyst support	Ref.
4-NP	MgPc, ClAlPc, ZnPc, $ZnPc(NO_2)_4$, $ZnPc(NH_2)_4$, $ZnPcF_{16}$, $ZnPcCl_{16}$,	Heterogeneous	No support (Suspension)	**55**
	$ZnPc(COOH)_8$, $ZnPcS_{mix}$, $ZnPcS_4$,	Homogenous		**54**
4-CP	AlPc	Heterogeneous	CTMA-modified bentonite	**251**
	$ZnPcS_4$, $ZnPcS_{mix}$, $AlPcS_{mix}$,Zn Pc$(COOH)_8$, $AlPc(COOH)_8$, $SiPcS_{mix}$, $SnPcS_{mix}$, $GePcS_{mix}$, $AlPcS_4$	Heterogeneous	Amberlite IR-900	**58**
	$ZnPcS_4$, $AlPcS_4$, $ZnPcS_{mix}$, $AlPcS_{mix}$, $ZnPc(COOH)_8$, $AlPc(COOH)_8$	Homogenous	_____	**56**

Table 1.3 (Contd.): Metallophthalocyanines used in previous experiments on transformation of substituted phenols and materials as catalyst supports in heterogeneous media

Substrate	MPc	Rαn Type	Het. Catalyst support	Ref.
2,4-DCP	AlPc	Heterogeneous	CTMA-modified bentonite	**251**
	ZnPc	Heterogeneous	Polydivinylbenzene	**249**
	$CoPcS_4$	Heterogeneous	MCM-41(mesoporous molecular sieve)	**252**
2,4,6-TCP	$PdPcS_4$	Heterogeneous	Anionic Clay	**67**
	$PdPcS_4$	Heterogeneous	Organobentonite	**248**
	AlPc	Heterogeneous	CTMA-modified bentonite	**251**
PCP	$ZnPcS_4$, $ZnPcS_{mix}$, $AlPcS_{mix}$, $ZnPc(COOH)_8$, $AlPc(COOH)_8$, $SiPcS_{mix}$, $SnPcS_{mix}$, $GePcS_{mix}$, $AlPcS_4$	Heterogeneous	Amberlite IRA-900	**58**
	$AlPcS_4$, $AlPcS_{mix}$, $ZnPcS_{mix}$, $SiPcS_{mix}$, $SnPcS_{mix}$,	Homogenous	————	**57**

4-NP = 4-Nitrophenol; 4-CP = 4-Chlorophenol; 2,4-DCP= 2,4-Dichlorophenol; 2,4,6-TCP = 2,4,6-Trichlorophenol; PCP = Pentachlorophenol; CTMA = Cetyltrimethylammonium bromide; S_4 = tetrasulphonated, S_{mix} = mixture of substituted sulphonated derivatives (mono,di,tri and tetra sulphonated)

However the immobilizations of catalyst onto some of these supports are time-consuming and difficult. Single walled carbon nanotube is used in this work for the first time to test the efficacy of our sensitisers under heterogeneous condition because of the ease of immobilization onto this support.

1.9.4.1. Single wall Carbon nanotubes as catalyst support

Nanoscale materials frequently show behavior which is intermediate between that of a macroscopic solid and that of an atomic or molecular system. Its properties will be different from those of a single atom. The number of atoms on the crystal's surface, for instance, is a significant fraction of the total number of atoms, and therefore will have a large influence on the overall properties of the crystal. The higher surface area of these nanomaterials give them a higher chemical reactivity than the corresponding bulk solid and assorted number of these type of nanomaterials available today are been deployed in varieties of applications.

After the discovery of a new form of elemental carbon, other extraordinary carbon forms **[253,254]** have been characterized one of which is the carbon nanotubes. These particularly fascinating and useful forms of carbon are graphite-like sheets wrapped in such a way that the carbon atoms on one edge of the sheet are covalently bound to the atoms on the opposite edge of the sheet **[255]**. Theses tubes can be single-walled (SWCNT) or multiwalled, and can be closed at one or both ends.

Carbon nanotubes are chemically stable because the valencies of all its carbon atoms are saturated, however the end of carbon nanotubes are more chemically active because of the strain on these ends. These terminal strains have been exploited for opening the ends through oxidative chemical methods and in the process making available large surface areas which possess excellent adsorbent properties for materials such as hydrogen gas, methane **[256,257]** and pollutants like phenol **[258,259]**. Moreover, carbon nanotubes can be good conductors because electrons can freely move along these tiny, wire-like structures and can also be a semiconductor depending on the diameter.

A wide range of roles are played by carbon nanotubes. They have been extensively studied both as model systems for one-dimensional confinement and for potential applications, such as electron emitters **[260-267]**. Their deployment in this study is based on their ability to easily adsorb the photosensitisers (MPcs) used in this work through π-π interactions thereby providing opportunity for investigating their efficiency as solid support for sensitisers for the purpose of heterogeneous photosensitization.

1.9.4.2. Preparation of Supported catalysts

There are in principle two ways to make supported catalysts:

(1) Coprecipitation: By coprecipitating the catalytically active component and the support from homogenous solution to give a mixture that is subsequently dried to yield a porous material with a high surface area. This procedure is used when materials are cheap and obtaining the optimum catalytic activity per unit volume of catalyst is the main consideration. This method is, however, very difficult to control.

(2) By loading pre-existing support materials with the catalytically active phase by means of impregnation or precipitation from solution. This is the preferred method when catalyst precursors are expensive and the aim is to deposit the catalytically active phase in the form of nanometer-sized particles on the support. Filling the pores or the surface of the support with a solution of the catalytically active element, after which the solvent is removed by decantation or drying or both, is a straightforward way to load a support with active material. In this process various interactions are possible between the dissolved catalyst precursor and the surface of the support, which can be used to obtain a good dispersion of the active component over the support **[268]**. This method was used in this work by taking the advantage of π-π interaction that is possible between the phthalocyanine molecules and functionalized single wall carbon nanotubes.

1.9.4.3. Characterization of Supported catalysts

Catalyst characterization is an important aspect of catalysis. Various methods such as spectroscopy and microscopy offer tools to investigate the nature of an active catalyst when it gets onto a support. Such knowledge gives good understanding of catalysts and offer opportunity for improvement and design of new ones **[268]**. X-ray diffraction is one of the oldest and most frequently applied techniques in supported catalyst characterization. It is used to identify crystalline phases inside catalysts by means of lattice structural parameters, and to obtain an indication of particle size **[268]**. Transmission electron microscopy is the electron microscopic techniques most often used for the characterization of supported catalysts. In general, detection of supported particles is possible, provided that there is sufficient contrast between particles and support, a limitation that may impede applications of transmission electron microscopic (TEM) technique on well-dispersed supported oxides. The determination of particle sizes or of distributions therein is now a routine matter, although it rests on the assumption that the size of the imaged particle is truly proportional to the size of the actual particle and that the detection probability is the same for all particles, independent of their dimensions **[269]**.

1.9.5. Phthalocyanines in Photocatalysis

In the search for ways to avoid problems posed by some of the earlier photocatalysts, metallophthalocyanines with their high absorptions in the visible region and non-destructive singlet to energetic triplet state transition, received attention. It has been shown that phthalocyanines catalyze reactions mainly through Type II reaction and generation of singlet oxygen is essential for the success of this pathway. Considerable singlet to triplet state transition and long life time of the triplet state are major factors influencing successful singlet oxygen generation of molecules. Large atomic size metals are the best choice for applications that are dependent on efficient singlet-triplet

transition because of their enhancement of intersystem crossing while closed shell diamagnetic metals improve triplet state lifetimes as opposed to open-shell metals.

The dependent of photocatalytic efficacy of phthalocyanines on long-lived triplet state and considerable singlet oxygen quantum yield has popularized the use of large atomic size closed-shell diamagnetic metals **[120,124,134,270,271]**. However a major problem of the use of these molecules is photobleaching. With open-shell metal phthalocyanines holding promises of high triplet quantum yields and high photostability along with triplet lifetime long enough to generate singlet oxygen, the broad aim of this work is to investigate what contribution these metals can make to photooxidation processes of substituted phenols.

1.10. Aims of Thesis

The aims of this thesis are summarized as follows

1. Syntheses and characterization of thio and aryloxo derivatised octasubstituted metal-free phthalocyanines and their open-shell-metallated (Ni(II), Pd(II) and Pt(II)) analogues, **Scheme 1.3**.
2. Investigation of Pd(II) binding abilities of thio derivatised phthalocyanines from (1) above with the aim of formation of novel self-assembled multinuclear complexes with these open-shell metal.
3. Isolation and characterizations of multinuclear complexes formed in (2) above
4. Study of the effects of these open-shell metals on the spectral, photophysical and photochemical properties of phthalocyanine ligands by comparing the properties of the metal-free and metallated derivatives with particular focus on singlet oxygen generating abilities of these molecules.
5. Study of the photophysical and photochemical properties of the multinuclear complexes formed in (2) above and comparison with the results from (4) to form an insight into the effects of multiple metals on the molecules.
6. Investigation of the photosensitizing abilities of promising phthalocyanines from (4) above in homogenous photo-oxidation reaction using phenolic pollutant as substrate.
7. Investigation of the photosensitizing abilities of promising phthalocyanines from (4) above supported on functionalized Single-walled carbon nanotubes in heterogeneous photo-oxidation reaction using phenolic pollutants (4-Nitrophenol, 4-chlorophenol and pentachlorophenol) as substrates.
8. Investigation of the mechanism of reactions in (6) and (7) to ascertain the reaction pathways and direct involvement of singlet oxygen of the molecules in the reactions.

Chapter 2

Experimental

2. EXPERIMENTAL

2.1. Equipment

The equipments used in the study are listed below

(i) ^{1}H-Nuclear magnetic resonance (^{1}H-NMR) spectra were obtained in deuterated solvents using Bruker AVANCE II 600 MHz spectrometer or Bruker EMX 400 NMR spectrometer

(ii) FT-IR spectra (KBr pellets) were obtained on a Perkin Elmer Spectrum 2000 FT-IR spectrometer or Bruker Vertex 70-Ram II spectrophotometer.

(iii) Elemental analyses were done using a Vario EL III MicroCube CHNS Analyzer

(iv) Mass spectra data were collected with a Bruker AutoFLEX III Smartbeam TOF/TOF Mass spectrometer. The instrument was operated in positive ion mode using an m/z range of 400 – 3000. The voltage of the ion sources were set at 19 and 16.7 kV for ion sources 1 and 2 respectively, while the lens was set at 8.50 kV. The voltages for reflectors 1 and 2 were set at 21 and 9.7 kV respectively. The spectra were acquired using dithranol as the MALDI matrix, using a 354 nm Nd:YAG laser.

(v) Varian Cary 500 Scan UV-Vis-NIR or Shimadzu UV-2550 UV-Vis-NIR Spectrophotometers were used to obtain ground state electronic absorption spectra.

(vi) Fluorescence emission and excitation spectra were recorded using Varian Cary Eclipse Fluorescence spectrometer

(vii) Triplet absorption and decay kinetics were recorded on a laser flash photolysis system **(Fig. 2.1)**; the excitation pulses were produced by a Nd: YAG laser (Quanta-Ray, 1.5 J / 9ns) pumping a dye laser (Lambda Physic FL 3002, Pyridine 1 in methanol). The analyzing beam source was from a Thermo Oriel xenon arc lamp, and a photomultiplier tube was used as detector. Signals were recorded

with a two-channel digital real-time oscilloscope (Tektronix TDS 360); the kinetic curves were averaged over 256 laser pulses. Triplet lifetimes were determined by exponential fitting of the kinetic curves using OriginPro 7.5 software.

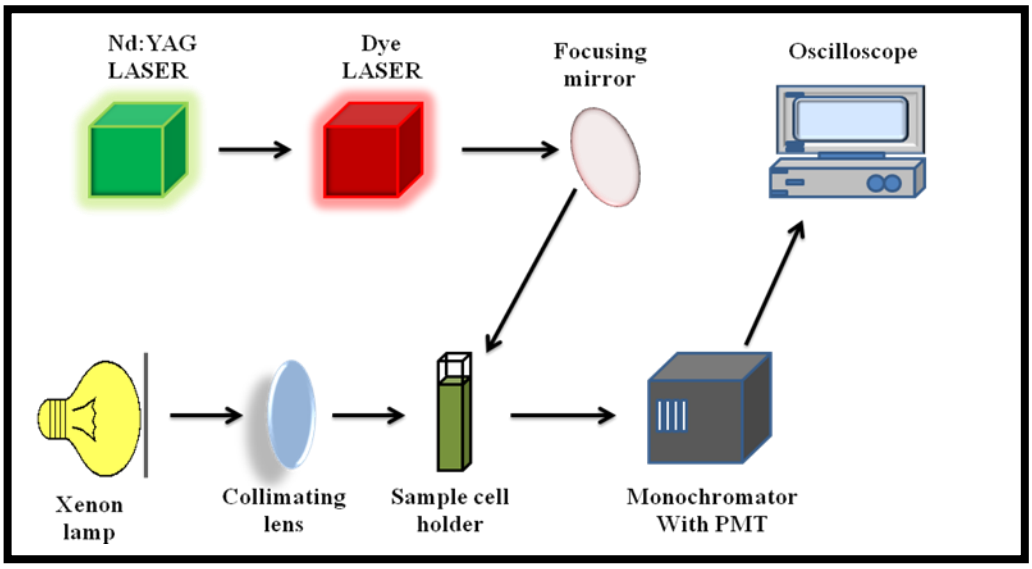

Figure 2.1: Schematic representation of a laser flash photolysis set-up

(viii) Raman spectra were obtained with a Bruker Vertex 70 – Ram II spectrometer (equipped with a 1064 nm Nd:YAG laser and a liquid nitrogen cooled germanium detector). Solid samples mixed with KBr were used.

(ix) X-ray powder diffraction patterns were recorded on a Bruker D8, Discover equipped with a proportional counter, using Cu-Kα radiation (λ = 1.5405 Å, nickel filter). Data were collected in the range from 2θ = 5° to 60°, scanning at 1° min^{-1} with a filter time-constant of 2.5 s per step and a slit width of 6.0 mm. Samples were placed on a silicon wafer slide. The X-ray diffraction data were treated using Eva (evaluation curve fitting) software. Baseline correction was performed on each diffraction pattern by subtracting a spline fitted to the curved background and the full-width at half-maximum values used in this study were obtained from the fitted curves.

(x) Transmission electron microscopy (TEM) images were obtained on JEOL JEM 1210 transmission electron microscope at 100 kV accelerating voltage

(xi) For the Gas chromatography (GC) analysis, an Agilent Technologies 6820 GC system (HP 5973, using an HP-1 column) was employed.

(xii) High performance liquid chromatography (HPLC) equipment connected in tandem to a mass spectrometer (LC/MS) was also used for identification of oxidation products. A dual wavelength UV detector was used for HPLC analyses and the wavelengths used were 254 nm and 318 nm. The HPLC conditions utilized included an Agilent Eclipse XDB-C18 column {150 x 4.6 (i.d.) mm} 5 μm particle size and a mobile phase with gradient elution starting at 10% MeOH:H_2O (pH 5.5 with formic acid) for 10 min and then ramping to 100% MeOH in 10 min. A Finnigan MAT LCQ ion trap mass spectrometer equipped with an electrospray ionization (ESI) source was used for mass analysis. Spectra were acquired in the negative ion mode, with the capillary temperature set at 200 ^oC and sheath gas set at 80 arbitrary units, with the capillary and tube lens voltages set at -20 and -5 V respectively.

(xiii) For photochemical studies, photo-irradiations were done using the set-up shown in **Fig. 2.2**. The lamp was general electric quartz line lamp (300W). Glass cut-off filters (Schott) of appropriate wavelengths and a water filter were used to filter off ultraviolet and infrared radiations respectively so that only the Q-band of phthalocyanines was irradiated. An interference filter was also placed between the light and the sample. The reaction vessel for the study was a 1 cm pathlength UV-vis spectrometric cell, fitted with a tight-fitting stopper.

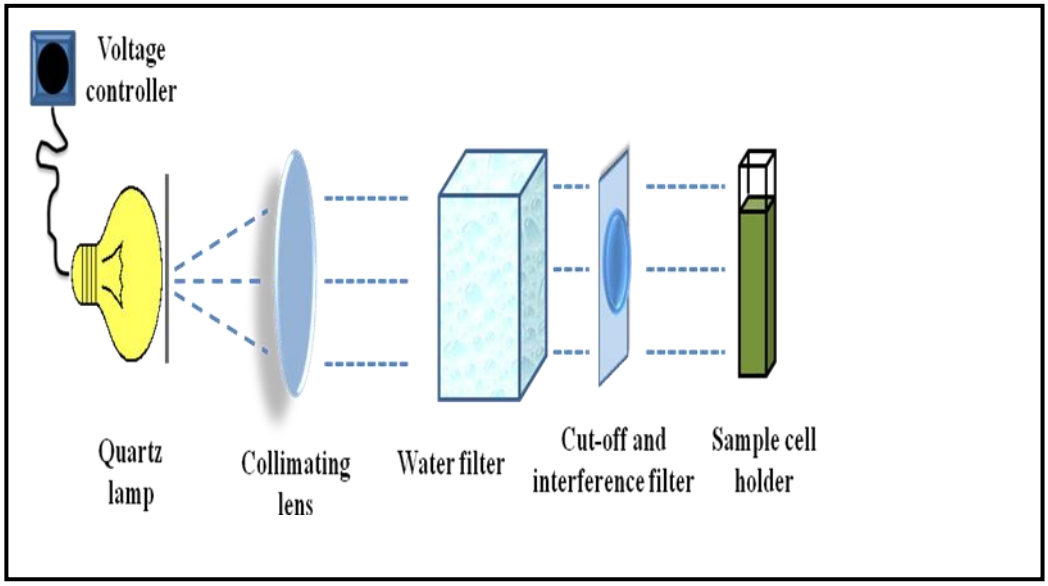

Figure 2.2: Schematic representation of a photochemical set-up

(xiv) The intensity of the light reaching the reaction vessel was measured with a POWER MAX 5100 power meter

(xv) The pH of the buffer solutions in photocatalysis was measured using a WTW pH 330/SET-1 pH meter.

2.2. Materials

2.2.1. Solvents

All solvents used in this work were purified before use according to reported method **[272]**. 1-Pentanol, dimethyl sulphoxide (DMSO), N, N'-Dimethyl formamide (DMF), methanol, ethanol, diethylamine sodium hydroxide (NaOH) and dichloromethane (DCM) were purchased from SAARCHEM. Chloroform ($CHCl_3$), deuterated chloroform ($CDCl_3$), deuterated pyridine, tetrahydrofuran (THF), 1-chloronaphthalene (1-CNP), D_2O and acetone were obtained from Merck. All solvent used for HPLC were HPLC grade.

2.2.2. ***Reagents.***

4-Nitrophenol (4-NP), fumaric acid, 4-nitrocatechol, 4-chlorophenol, pentachlorophenol, tetrachlorobenzoquinone, hydroquinone, benzoquinone, $NiCl_2.6H_2O$, $PtCl_2$, $PdCl_2$ and dicyanohydroquinone were purchased from SAARCHEM. Pentanethiol, octanethiol, dodecanethiol, Potassium carbonate (K_2CO_3), sodium carbonate (Na_2CO_3), 8-diazabicyclo{5.4.0}-undec-7-ene (DBU), diphenylisobenzofuran (DPBF), anthracene-9,10-bis-methylmalonate (ADMA) and single wall carbon nanotubes (SWCNTs, 0.7 – 1.2 nm in diameter and 2 – 20 μm in length) were purchased from Aldrich.

2.3. Photophysical and Photochemical studies

2.3.1. Fluorescence Quantum Yields (Φ_F)

The emission spectra of the complexes and standard were measured in different solvents, corrections for the differences in refractive indices were done and **Eqn. 1.1** employed. The standard used in the experiment was a zinc phthalocyanine in dimethyl sulphoxide (DMSO) (Φ_F= 0.20) **[120]**,

2.3.2. Triplet Quantum Yields and Lifetimes

Triplet absorption and decay kinetics of the complexes were recorded on a laser flash photolysis set-up **(Fig. 2.1)** described in **Section 2.1**. The solution of each of the complexes under investigation was adjusted to an absorbance of ~1.5 and introduced into a 1 cm pathlength spectrophotometric cell. Argon was bubbled through the solution for 30 minutes and the solution irradiated at the Q band maximum. The triplet quantum yields (Φ_T) were determined by triplet absorption method using **Eqn. 1.2** and ZnPc in 1-CNP as standard (Φ_T = 0.67) **[28]**. Triplet lifetimes were determined by exponential fitting of the kinetic curves using Origin Pro 7.5 software.

2.3.3. Singlet Oxygen Quantum Yields

The singlet oxygen quantum yields (Φ_Δ) determinations for phthalocyanines were recorded with the set-up shown in **Fig 2.2**. The studies were carried out using solutions

containing DPBF (90 μM) and the Pcs (absorbance~0.2 at the Q band wavelength). A solution of complex (2 ml) was introduced into a 1 cm quartz cuvette saturated with oxygen and irradiated using set-up described above. The irradiation and measurement were repeated until around 80% decay of DPBF was observed **[273].** The DPBF absorbance was corrected for the absorbance of sensitizer at the respective detection wavelength. The light intensity reaching the reaction vessel was calculated to be 8.92 x 10^{15} photons cm^{-2} s^{-1}.

The DPBF quantum yield Φ_{DPBF} was calculated using **Eqn. 1.11** and the determined extinction coefficient of DPBF in 1-chloronaphthalene (ε_{CNP} = 20287 M^{-1} cm^{-1}) and Φ_{Δ} values were calculated using the plots derived from **Eqn. 1.9**.

2.3.4. *Photodegradation*

Photodegradation (Φ_P) quantum yields were determined in the same way as Φ_{Δ} except no quencher was added. Q-band absorbance was ~ 1.0. The light intensity reaching the reaction vessel was found to be 5.2 x 10^{18} photons cm^{-2} s^{-1}.

The wavelength of the interference filter was chosen such that it was close to the Q-band of the MPc under investigation. The steady reduction in the Q-band absorption intensity with irradiation time was recorded and used for the calculation of Φ_P using **Eqn. 1.11**.

2.3.5. Photocatalysis procedure

The irradiation experiments were carried out with the set-up in **Fig. 2.2** The intensity of the light reaching the reaction vessel was measured with a power meter (POWER MAX 5100, Molelectron Detector Inc.) and was found to be 3.5 x 10^{15} photons cm^{-2} s^{-1}. The transformation of the analyte was monitored through the absorption peak of the analyte after each photolysis cycle. A 1 cm pathlength UV-vis spectrophotometric cell, fitted with a tight fitting stopper was used as the reaction vessel. The products were separated and analysed using both gas chromatography (GC) and high performance liquid

chromatography (HPLC) equipment, the latter connected in tandem to a mass spectrometer (LC/MS).

2.4. ***Purification and Functionalisation of SWCNTs***

SWCNTs were purified and oxidized to form SWCNT-COOH by adding raw SWCNTs (100 mg) to a mixture of HNO_3 and H_2SO_4 (3:1) **[274].** The resulting suspension was stirred at a temperature of 70°C for 2 h. The final mixture was cooled to room temperature and washed with excess Millipore water until a pH of 5 was obtained. The purified SWCNTs (SWCNT-COOH) were dried in an oven for 12 h.

2.5. Immobilisation of MPcs on SWCNTs

Each of the MPc derivatives selected for this study was dissolved in DCM to give an absorbance of approximately 2 and 50 mg purified SWCNTs was added and the mixture was stirred until there was no change in absorbance of the MPcs. The mixture was centrifuged and the supernatant was decanted, leaving the particles of MPcs adsorbed on SWCNT (represented as ads-MPc-SWCNT-COOH). The particles were washed with distilled deionised water, methanol and acetone and air-dried for 24 h. The concentrations of MPcs adsorbed were calculated from the differences in absorbances.

Singlet oxygen generation capacities of ads-MPc-SWCNT-COOH were investigated using ADMA as a singlet oxygen quencher. An aqueous solution of 6.0×10^{-5} mol dm^{-3} ADMA containing a suspension of each of the ads-MPc-SWCNT-COOH conjugates, was successively irradiated at the Q-band of MPc, centrifuged and decanted into UV-Vis cell and absorbance recorded. Quantum yields of ADMA (Φ_{ADMA}) were calculated using **Eqn. 1.11** and singlet oxygen quantum yields (Φ_{Δ}) were calculated from **Eqn. 1.9**.

2.6. Syntheses

2.6.1. *Syntheses of Substituted Phthalonitrile*

All the phthalonitriles used in this study are listed below

1. 1,2-dicyano-3,6-di(pentylthio)benzene**(11a)**
2. 1,2-dicyano-3,6-di(octylthio)benzene**(11b)**
3. 1,2-dicyano-3,6-di(dodecylthio)benzene**(11c)**
4. 1,2-dicyano-4,5-di(pentylthio)benzene (**12a**)
5. 1,2-dicyano-4,5-di(octylthio)benzene (**12b**)
6. 1,2-dicyano-4,5-di(dodecylthio)benzene (**12c**)
7. 1,2-dicyano-4,5-diphenoxy benzene (**12d**)
8. 1,2-di(benzyloxyphenoxy) -4,5-dicyanobenzene (**12e**)

The syntheses of **10** and phthalonitriles **11a, 12b, 12c, 12d** and **12e** have been reported **[70-72, 275].**

1,2-Dicyano-3,6-di(octylthio)benzene (*11b*) (Scheme 3.1)

Following literature methods for synthesis of substituted phthalonitriles **[72]**, **11b** was synthesized as follows: octanethiol (2.01 g, 20 mmol)] was dissolved in absolute dimethylsulfoxide (DMSO) (15 ml) under N_2 and **10** (2.00 g, 10 mmol) was added. After stirring for 15 min, finely ground anhydrous K_2CO_3 (6.00 g, 43.4 mmol) was added portionwise within 2 h with efficient stirring. The reaction mixture was stirred under N_2 at room temperature for 12 h. Then water (30 ml) was added and the aqueous phase extracted with chloroform (3 x 20 ml). The combined extracts were treated first with Na_2CO_3 solution (5%), then with water and the solvent was evaporated and the product was crystallized from ethanol. Yield: 2.40 g (78.9%). ^{1}H-NMR (400 mHz); δ ppm ($CDCl_3$) 7.52 (2H, s, Ar-H), 3.06–3.02 (4H, t, –CH_2), 1.74–1.68 (4H, m, –CH_2), 1.48–1.45 (4H, m, –

CH_2), 1.31–1.29, (16H, m, –$(CH_2)_4$), 0.93 –0.90 (6H, m, –CH_3). IR (KBr pellets) vmax / cm-1] : 3469,3094, 3021, 2934, 2871, 2574, 2232(C≡N), 1827, 1573, 1469, 1226, 1127, 916, 734(C–S), 687, 539.

1,2-Dicyano-3,6-di(dodecylthio)benzene (*11c*) (Scheme 3.1)

The same method used for the synthesis of **11b** was also used for **11c** except dodecanelthiol was employed instead of octanethiol. The amounts of reagents used were: dodecanethiol (3.01 g, 20 mmol), **10** (2.00 g, 10 mmol), K_2CO_3 (6.00 g, 43.4 mmol). Yield: 4.4 g (85%). ^{1}H-NMR (400 mHz); δ ppm ($CDCl_3$): 7.52 (2H, s, Ar-H), 3.04–3.01 (4H, t, –CH_2), 2.71–2.68 (4H, m, –CH_2), 1.70–1.66, (12H, m, –$(CH_2)_3$), 1.29–1.24, (12H, m, –$(CH_2)_3$), 0.93 –0.90 (18H, m, –$(CH_2)_3$-CH_3). IR (KBr pellets) vmax/cm- 1] : 3468,3090, 3024, 2931, 2868, 2577, 2231(C≡N), 1822, 1579, 1462, 1353, 1129, 921, 741(C–S), 683.

1,2-Dicyano-4,5-di(pentylthio)benzene (*12a*) (Scheme 3.2)

The same method used for the synthesis of **11b** was also used for **12a** except pentanethiol was employed instead of octanethiol and **9** used instead of **10**. The amounts of reagents used were: pentanelthiol (2.00 g, 20.0 mmol)], **9** (2.00 g, 7.6 mmol); anhydrous K_2CO_3 (6.00 g, 43.4 mmol). Yield:1.90g(79%); ^{1}H NMR (400 MHz, $CDCl_3$) δ_H /ppm: 7.72 (2H, s, Ar-H), 3.05 - 3.01 (4H, t, S-CH_2), 1.84 -1.75 (4H, m, -CH_2), 1.59 – 1.48 (4H, t, -CH_2), 1.42 – 1.38 (4H, m, -CH_2), 0.97 – 0.94 (6H, t, -CH_3), ; [IR (KBr pellets) v_{max}/ cm^{-1}]: 3467,3094, 3022, 2933, 2871, 2574, 2236(C≡N), 1825, 1573, 1469, 1352, 1226, 1127, 916, 738(C-S), 687, 531.

2.6.2. Phthalocyanines

The phthalocyanines complexes used in the study are listed below

Metal-free phthalocyanines (H_2Pc)

1. Metal-free-1,4,8,11,15,18,22,25-octakis(pentylthio)phthalocyanine (α-OPPc)(**13a**)
2. Metal-free-1,4,8,11,15,18,22,25,-octakis(octylthio)phthalocyanine (α-OOPc)(**13b**)
3. Metal-free-1,4,8,11,15,18,22,25-octakis(dodecylthio)phthalocyanine (α-ODPc)(**13c**)
4. metal-free-2,3,9,10,16,17,23,24-octakis(pentylthiophthalocyanine) (β-OPPc)(**14a**)
5. Metal-free-2, 3, 9, 10, 16, 17, 23, 24-octakis(octylthio)phthalocyanine (β-OOPc) **(14b)**
6. Metal-free-2, 3, 9, 10, 16, 17, 23, 24-octakis(dodecylthio)phthalocyanine (β-ODPc) **(14c)**
7. Metal-free-2,3, 9, 10, 16, 17, 23, 24-octakis(phenoxy)phthalocyanine (β-O(PhO)Pc) (**14d**)
8. Metal-free-2,3,9,10,16,17,23,24-octakis(benzyloxyphenoxy)phthalocyanine (β-O(BeOPhO)Pc) (**14e**)

Palladium phthalocyanine complexes (PdPc)

9. Palladium(II)-1,4,8,11,15,18,22,25-octakis(pentylthio)phthalocyanine (α-PdOPPc)(**15a**)
10. Palladium(II)-1,4,8,11,15,18,22,25-octakis(octylthio)phthalocyanine (α-PdOOPc)(**15b**)
11. Palladium(II)-1,4,8,11,15,18,22,25-octakis(dodecylthio)phthalocyanine (α-PdODPc)(**15c**)

12. Palladium(II)-2,3,9,10,16,17,23,24-octakis(pentylthio)phthalocyanine (β-PdOPPc) (**17a**),
13. Palladium(II)-2,3,9,10,16,17,23,24-octakis(octylthio)phthalocyanine (β-PdOOPc) (**17b**),
14. Palladium(II)-2,3,9,10,16,17,23,24-octakis(dodecylthio)phthalocyanine (β-PdODPc) (**17c**),
15. Palladium(II)- 2, 3, 9, 10, 16, 17, 23, 24-Octakis(phenoxy)phthalocyanine (β-PdO(PhO)Pc) (**17d**)
16. Palladium(II)- 2,3, 9,10,16,17,23,24-Octakis(benzyloxyphenoxy)phthalocyanine (β-PdO(BeOPhO)Pc) (**17e**)

Nickel phthalocyanine complexes (NiPc)

17. Nickel(II)-2,3,9,10,16,17,23,24-octakis(pentylthio)phthalocyanine (β-NiOPPc) (**16a**)
18. Nickel(II)-2,3,9,10,16,17,23,24-octakis(octylthio)phthalocyanine (β-NiOOPc) (**16b**)
19. Nickel(II)-2,3,9,10,16,17,23,24-octakis(dodecylthio)phthalocyanine (β-NiODPc) (**16c**)
20. Nickel(II)-2,3, 9, 10, 16, 17, 23, 24-octakis(phenoxy)phthalocyanine (β-NiO(PhO)Pc) (**16d**)
21. Nickel(II)-2,3,9,10,16,17,23,24-octakis(benzyloxyphenoxy)phthalocyanine (NiO(BeOPhO)Pc) (**16e**)

Platinum phthalocyanine complexes (PtPc)

22. Platinum(II)- 2,3, 9, 10, 16, 17, 23, 24-octakis(phenoxy)phthalocyanine (β-PtO(PhO)Pc) (**18d**)
23. Platinum(II)-2, 3, 9, 10, 16, 17, 23, 24-octakis(benzyloxyphenoxy)phthalocyanine (β-PtO(BeOPhO)Pc) (**18e**)

Metallophthalocyanines Syntheses

Syntheses of complex 16c, **[70]** has been reported in literature.

2.6.2.1. Metal-free phthalocyanines (H_2Pc)

α-OPPc (*13a*) (Scheme 3.1)

In refluxing pentanol (10 ml), 3,6-bis(pentylthio)-4,5-dicyanobenzene **(11a)** (0.50 g, 1.5 mmol) and DBU (1.66 ml, 1.0 mmol) were added. The solution was heated to reflux for 5 h. The solution was then allowed to cool and the solvent removed under reduced pressure. This was followed by titration with cold methanol to precipitate the product. The black precipitate was dissolved in DCM and passed through a silica column; DCM was used as the eluting solvent. Yield: 0.18 g (37%), UV/Vis [(1-CNP, λ_{max} /nm, (log ε)] 813 (5.05), 719 (3.5). $C_{72}H_{98}N_8S_8$ Calc: C, 64.80; H, 7.36 N, 8.42, S, 19.24. Found, C, 64.87; H, 7.47, N, 7.71, S, 20.44%. ^{1}H-NMR (400 mHz); δ ppm; ($CDCl_3$), 8.00 (8H, s, H_{arom}), 3.32-3.35 (16H, t, Ar –SCH_2-), 2.15-2.00 (16H, m, Ar-SCH_2-CH_2-), 1.65 -1.2 (32H, m, $H_{aliphatic}$), 1.00-0.80 (24H, t, CH_3); MS (ESI–MS) m/z: Calc. 1331.45; Found$[M-H]^+$: 1330.43. [IR (KBr pellets) υ_{max}/ cm^{-1}]; 3057 (N-H), 2953 (C - H), 2922 (C - H), 2358, 2336, 1865, 1791, 1730, 1652(C=N), 1556, 1538, 1505, 1456, 1320, 1278, 1217, 1186, 1142, 1077, 939, 808, 736, 668 (C – S - C), 577, 499, 418.

α-OOPc (*13b*) (Scheme 3.1)

Synthesis and purification was as described for **13a** using 3,6-bis(octylthio)-4,5-dicyanobenzene **(11b)** (0.53 g, 1.0 mmol) and DBU (1.66 ml, 1.0 mmol). Yield: 0.32 g (70%), UV/Vis [(1-CNP, λ_{max} /nm, (log ε)] 813 (5.06), 719 (3.60). $C_{96}H_{146}N_8S_8$ Cald.: C, 69.09; H, 8.82 N,6.71, S, 15.37. Found, C, 68.03; H, 8.53, N, 6.29, S, 14.02%. ^{1}H-NMR (400 mHz); δ ppm ($CDCl_3$) 7.76 (8H, s, H_{arom}), 3.29 (16H, t, SCH_2-), 1.97-1.95 (16H, m, CH_2-), 1.65 (16H, m, -CH_2), 1.97-1.40 (64H, m, -$(CH_2)_4$), 1.94 (24H, m, CH_3), 0.34 (2H, s, N-H). MS (ESI–MS) m/z: Calc. 1666.16; Found$[M]^+$: 1666.75. [IR (KBr pellets) υ_{max} /cm^{-1}]; 3051(N-H), 2950 (C-H), 2925 (C-H), 2356, 2334, 1862, 1784, 1654 (C=N), 1550, 1532, 1500, 1456, 1325, 1281, 1210, 1140, 930, 731, 662 (C-S-C), 577, 492.

α-ODPc (*13c*), (Scheme 3.1)

Synthesis and purification was as described for **13a** using 3,6-bis(dodecylthio)-4,5-dicyanobenzene **(11c)** (0.53 g, 1 mmol) and DBU (1.66 ml, 1 mmol). Yield: 0.30 g (59%), UV/Vis [(1-CNP, λ_{max} /nm, (log ε)] 813 (5.08), 719 (3.80). $C_{128}H_{210}N_8S_8$ Cald.: C, 72.60; H, 10.00 N,5.29, S, 12.11. Found, C, 72.39; H, 11.75, N, 5.18, S, 12.56 %. ^{1}H-NMR (400 mHz); δ ppm ($CDCl_3$) 7.79 (8H, s, H_{arom}), 3.32 (16H, t, SCH_2-), 2.01-1.96 (16H, m, CH_2-), 1.68-1.66 (16H, m, CH_2-), 1.46-1.31 (128H, m, $(CH_2)_8$), 0.92-0.84 (24H, m, CH_3), 0.37 (2H, s, N-H). MS (ESI–MS) m/z: Calc. 2116.93; Found[M]$^+$: 2116.70. [IR (KBr pellets) υ_{max} /cm^{-1}]; 3053(N-H), 2952 (C-H), 2923 (C-H), 2357, 2331, 1861, 1786, 1654 (C=N), 1552, 1534, 1501, 1459, 1327, 1279, 1215, 1142, 931, 734, 660 (C-S-C), 581, 497.

β-OPPc (*14a*), (Scheme 3.2)

Synthesis and purification was as described for **13a** except that the reflux was for 1h using 1,2-bis(pentylthio)-4,5-dicyanobenzene (**12a**) (0.50 g, 0.95 mmol) Yield: 0.37 g (74%), UV/Vis [(1-CNP, λ_{max} / nm, (log ε)] 736 (5.12), 707 (5.04), 673 (4.51), 640 (4.40), 457 (4.43). $C_{72}H_{98}N_8S_8$ Cald.: C, 64.80; H, 7.36 N, 8.42, S, 19.24. Found, C, 65.93; H, 7.75, N, 6.16, S,19.91 %. ^{1}H-NMR (400 mHz); δ ppm ($CDCl_3$) 8.37 (8H, s, H_{arom}), 3.44-3.40 (16H, s, Ar –SCH_2-), 2.14-2.09 (16H, q, Ar-SCH_2-CH_2-), 1.82-1.78 (16H, q, $H_{aliphatic}$), 1.66-1.60 (16H, q, $H_{aliphatic}$), 1.31-1.22 (24H, t, CH_3-); MS (ESI–MS) m/z: Calc. 1331.45; Found[M-H]$^+$: 1330.49. [IR (KBr pellets) υ_{max} / cm^{-1}]; 3049 (N-H), 2957, 2926, 2858 (C–H), 1648(C=N), 1592, 1507, 1461, 1400, 1325, 1325, 1073, 1026, 935, 868, 749, 681 (C–S-C).

β-OOPc (*14b*), (Scheme 3.2)

Synthesis and purification was as described for **13a** using 1,2-bis(octylthio)-4,5-dicyanobenzene (**12b**) (0.42 g, 1.0 mmol) and DBU (1.66 ml, 1.0 mmol). Yield: 0.37 g (74%), UV/Vis [(1-CNP, λ_{max} / nm, (log ε)] 737 (5.15), 710 (5.10), 673 (4.72), 638 (4.62), 452 (4.57). $C_{96}H_{146}N_8S_8$ Cald.: C, 69.09; H, 8.82 N,6.71. Found, C, 68.93; H, 8.75, N, 6.56%.

^{1}H-NMR (400 mHz); δ ppm ($CDCl_3$) 8.23 (8H, s, H_{arom}), 3.40-3.37 (16H, t, SCH_2-), 2.10-2.00 (16H, m, CH_2-), 1.79-1.75 (16H, m, -CH_2), 1.58-1.35 (88H, m, -CH_2, CH_3). MS (ESI-MS) m/z: Calc. 1666.16; Found[M]$^+$: 1666.46. [IR (KBr pellets) υ_{max}/cm^{-1}];: 3052 (N-H), 2949, 2935, 2855, 1669, 1597, 1511, 1469, 1409, 1329, 1331, 1079, 1021, 939, 871, 751, 682 (C–S-C).

β-ODPc (*14c*), (Scheme 3.2)

The same method used for **13a** was employed using **12c**. The amounts of reagents were: 1,2-bis(dodecylthio) -4,5-dicyanobenzen (**12c**) (0.53 g, 1.0 mmol) and DBU (1.66 ml, 1.0 mmol). Yield: 0.35 g (64%), UV/Vis [(1-CNP, λ_{max}/nm, (log ε)] 737 (5.18), 710 (5.11), 672 (4.72), 638 (4.62), 452 (4.57). $C_{128}H_{210}N_8S_8$ Cald.: C, 72.60; H, 10.00 N,5.29. Found, C, 71.93; H, 10.42, N, 5.16 %. ^{1}H-NMR (400 mHz); δ ppm ($CDCl_3$) 8.30 (8H, s, H_{arom}), 3.42-3.40 (16H, t, SCH_2-), 2.13-2.09 (16H, m, CH_2-), 1.80-1.69 (16H, m, CH_2-), 1.50-1.30 (152H, m, CH_2, CH_3). MS (ESI-MS) m/z: Calc. 2116.91; Found[M]$^+$: 2117.19. [IR (KBr pellets) υ_{max} /cm^{-1}]; 3049 (N-H), 2962, 2922, 2857, 1666, 1571, 1500, 1467, 1405, 1331, 1319, 1069, 1028, 937, 872, 748, 676 (C–S-C).

β-O(PhO)Pc (*14d*), (Scheme 3.2)

The same method used for **13a** was employed using **12d** but the time was 8 hr instead of 5 h. The amounts of reagents were: 1,2-diphenoxy-4,5-dicyanobenzene (**12d**) (2.00 g, 6.4 mmol) and DBU (6.20ml, 4.0 mmol). Yield: 0.14 g (78%). UV/Vis [(1-CNP, λ_{max} / nm, (log ε)] 706 (5.31), 672 (5.62), 642 (4.72), 610 (4.58). $C_{80}H_{50}N_8O_8.H_2O$. Calc.: C, 76.80; H, 4.00; N,8.96 %. Found, C, 74.72; H, 4.07, N, 9.02 %. ^{1}H NMR (400 mHz); δ ppm ($CDCl_3$) 8.53 (8H, s, Pc–H), 7.20–7.38 (40H, m, phenyl–H). MS (ESI-MS) m/z: Calc. 1250.30; Found[M]$^+$: 1250.29. [IR (KBr pellets) ν_{max}/cm^{-1}]; 3089 (N-H), 3061, 3042 , 1613 , 1270 (C–O–C), 989, 874, 743, 687.

β-O(BeOPhO)Pc (*14e*), (Scheme 3.2)

The same method used **13a** was employed but the time was 12 h instead of 5 h and **12e** was used. The amounts of reagents were: 1,2-bis(benzyloxyphenoxy) -4,5-dicyanobenzene (**12e**) (1.68 g, 3.2 mmol) and DBU (4.80ml, 3.0 mmol). Yield: 0.15 g (88%). UV/Vis [(1-CNP, λ_{max} / nm, (log ε)] 708 (5.31), 674 (5.24), 643 (4.76), 611 (4.62). Anal. Cald. For $C_{136}H_{98}N_8O_{16}.H_2O$: C, 77.78; H, 4.67; N,5.34 %. Found, C, 76.41; H, 5.24, N,5.79%.%. ^{1}H-NMR (400 mHz) , δ, ppm: ($CDCl_3$) 8.62 (8H, s, Pc–H), 7.60 - 7.00 (72H, m, phenyl–H), 5.10 (16H, s, CH_2). MS (ESI–MS) m/z: Calc. 2098.55; Found[M-H]$^+$: 2097.32. [IR (KBr pellets) ν_{max}/cm^{-1}]: 3053(N-H), 3063, 3033, 1602, 1222 (C–O–C), 945, 836, 737.

2.6.2.2. Palladium(II) *phthalocyanine derivatives (PdPc)*

α-PdOPPc (*15a*), (Scheme 3.3)

In refluxing pentanol (10 ml), 3,6-bis(pentanethio)-4,5-dicyanobenzene **(11a)** (0.50 g,1.5 mmol), $PdCl_2$ (0.12 g, 0.75 mmol) and DBU (1.70 ml, 1.0 mmol) were added. Reflux was continued for a further 18 h. The reaction was then cooled down and the solvent removed under reduced pressure, followed by titration with cold methanol to precipitate the product. The black precipitate was dissolved in DCM and passed through a silica column; DCM was used as the eluting solvent. Yield: 0.12 g (40%), UV/Vis [1-CNP, λ_{max} /nm, (log ε)] 750 (4.5), 679 (4.11), $C_{72}H_{96}N_8PdS_8$ Calc: C, 60.20; H, 6.74; N, 7.80%. Found: C, 59.63; H, 6.87; N, 7.51%. ^{1}H-NMR (400 MHz, $CDCl_3$) δ ppm: 8.71 (8H, s, Ar-H), 4.10 (16H, s, S-CH_2), 1.52 – 1.21 (48H, m, -$(CH_2)_3$), 1.21 – 0.92 (24H, m, -CH_3); MS (ESI–MS) m/z: Calc. 1435.86; Found[M-H]$^+$: 1434.72. [IR (KBr pellets) ν_{max}/cm^{-1}]: 2929, 2859, 1732, 1650(C=N), 1572, 1466, 1338, 1293, 1236, 1163, 941, 799, 750, 650(C-S-C).

α-PdOOPc (*15b*), (Scheme 3.3)

The same method used for **15a** was employed using **11b**. The amounts of reagents were: **11b** (0.42 g, 1.0 mmol) and $PdCl_2$ (0.08g, 0.45 mmol). Yield: 0.22g (56%). UV/Vis [(1-CNP, / λ_{max}/ nm, (log ε)] 756 (4.6), 679 (4.25). $C_{96}H_{144}N_8PdS_8$:Cald.: C, 65.07; H, 8.13; N,5.70%; Found, C, 65.11; H, 8.01; N,5.12%. ^{1}H NMR (400 MHz, $CDCl_3$) δ_H /ppm: 8.22 (8H, s, Ar-H), 3.40 (16H, m, S-CH_2), 1.61 – 1.31 (120H, m, -$(CH_2)_6$-CH_3)); MS (ESI–MS) m/z: Calc. 1773.16; Found[M-H]$^+$: 1772.22 [IR (KBr pellets) ν_{max}/ cm^{-1}]: 2962, 2930, 2858, 1466, 1414, 1381, 1264, 1143, 1078, 969, 874, 747(C-S). .

α-PdODPc (*15c*), (Scheme 3.3)

The same method used for **15a** was employed using **11c**. The amounts of reagents were: **11c** (0.53g, 1.0 mmol), DBU (1.66ml, 1 mmol) and $PdCl_2$ (0.08g, 0.45 mmol). Yield: 0.28g (53%). UV/Vis [(1-CNP/λ_{max}/nm, (log ε)] 756 (4.71), 679 (4.28). $C_{128}H_{208}N_8PdS_8$:Cald.: C, 69.23; H,9.37; N,5.04%. Found, C, 69.74; H,8.51; N,4.79%; ^{1}H NMR (400 MHz, $CDCl_3$) δ_H /ppm:8.32 (8H, s, Ar-H), 3.41 (16H, m, S-CH_2), 1.22 -0.77 (184H, m, -$(CH_2)_{10}$-CH_3)); Calc. MS (ESI–MS) m/z: Calc. 2221.07; Found [M-H]$^+$: 2220.12 [IR (KBr pellets) ν_{max}/ cm^{-1}]: 2929, 2858, 1729, 1472, 1377, 1269, 1108, 998, 818, 751(C-S), 647.

β-PdOPPc (*17a*), (Scheme 3.4)

The same method used for **15a** was employed but the reflux was for 1hr and **12a** was used. Amount of reagents: 1,2-bis(pentylthio)-4,5-dicyanobenzene (**12a**) (0.361 g, .01 mmol), $PdCl_2$ (0.08g, 0.45 mmol) and DBU (1.66ml, 1 mmol). Yield: 0.19g (50%), UV/Vis [(1-CNP, / λ_{max}/ nm, (log ε)] 744 (4.13), 698 (5.14), 683 (4.6),425 (4.55). $C_{72}H_{96}N_8PdS_8$:Cald.: C, 60.20; H, 6.74; N,7.80%; Found, C, 59.42; H, 7.11; N,7.01%; ^{1}H NMR (400 MHz, $CDCl_3$) δ_H /ppm: 8.19 (8H, s, Ar-H), 3.40 (16H, m, S-CH_2), 1.14 – 1.09 (48H, m, -$(CH_2)_3$), 0.91 – 0.88 (24H, m, -CH_3); MS (ESI–MS) m/z: Calc. 1435.86; Found [M-H]$^+$: 1434.76 [IR (KBr pellets) υ_{max}/cm^{-1}]: 2595, 2928, 2858, 1737, 1642, 1603, 1510, 1465, 1413, 1379, 1265, 1142, 1075, 968, 747(C-S).

β-PdOOPc (*17b*), (Scheme 3.4)

The same method used for **15a** was employed for the synthesis of **17b** using **12b.** The reflux was for 1 h instead of 18 h. The amounts of reagents were: 1,2-bis(octylthio)-4,5-dicyanobenzen (**12b**) (0.42 g, 1.0 mmol) and $PdCl_2$ (0.08g, 0.45 mmol). Yield: 0.26g (60%). UV/Vis [(1-CNP, / λ_{max}/ nm, (log ε)] 698 (4.88), 673 (4.25), 625 (4.31), 412 (4.50) $C_{96}H_{144}N_8PdS_8$:Cald.: C, 65.07; H, 8.13; N,5.70%; Found, C, 65.02; H, 8.06; N,4.02%. ^1H NMR (400 MHz, $CDCl_3$) δ_H /ppm: 8.21 (8H, s, Ar-H), 3.41 (16H, m, S-CH_2), 1.60 – 1.32 (120H, m, -$(CH_2)_6$-CH_3)); Calc. MS (ESI–MS) m/z: Calc. 1773.16; Found $[M-H]^+$: 1772.14. [IR (KBr pellets) ν_{max}/ cm^{-1}]: 2962, 2930, 2858, 1649, 1466, 1414, 1381, 1264, 1143, 1078, 969, 874, 747(C-S).

β-PdODPc (*17c*), (Scheme 3.4)

The same method used for **15a** was employed using **12c** and the reflux was for 1 hr instead of 18 h. The amounts of reagents used were: 1,2-bis(dodecylthio)-4,5-dicyanobenzen (**12c**) (0.53g, 1 mmol) and $PdCl_2$ (0.08g, 0.45 mmol). Yield: 0.30g (55%). UV/Vis [(1-CNP, / λ_{max}/ nm, (log ε)] 698 (4.92), 673 (4.25), 625 (4.29), 412 (4.50). $C_{128}H_{208}N_8PdS_8$:Cald.: C, 69.23; H,9.37; N,5.60%. Found, C, 69.25; H,9.37; N,5.04%; ^1H NMR (400 MHz, $CDCl_3$) δ_H /ppm: 8.35 (8H, s, Ar-H), 3.40 (16H, m, S-CH_2), 1.25 -0.75 (184H, m, -$(CH_2)_{10}$-CH_3)); Calc. MS (ESI–MS) m/z: Calc. 2218.07; Found $[M-H]^+$: 2217.19. [IR (KBr pellets) ν_{max}/ cm^{-1}]: 2926, 2856, 1731, 1652,1468, 1379, 1266, 1108, 998, 818, 749(C-S), 649.

β-PdO(PhO)Pc (*17d*), (Scheme 3.4)

Synthesis and purification was as outlined for **15a** using **12d** and 14 hr reflux instead of 18 hr. The amount of reagent employed were: 1,2-diphenoxy-4,5-dicyanobenzene (**12d**) (1.00 g, 3.2 mmol), $PdCl_2$ (0.27g, 1.50 mmol) and DBU (3.20ml, 2.0 mmol) . Yield: 0.07 g (65%). UV/Vis [(1-CNP, λ_{max}/nm, (log ε)] 668 (5.11), 640 (4.41), 602 (4.44). . $C_{80}H_{48}N_8O_8Pd.H_2O$ Calc.: C, 69.94; H, 3.50, N,8.16. Found, C, 68.92; H, 4.12, N,8.69%. ^1H NMR (600 mHz); δ ppm (Pyr-d_5) 8.43 (8H, s, Pc–H), 7.25–7.42 (40H, m, phenyl–H). MS

(ESI-MS) m/z: Calc. 1354.14; Found $[M]^+$: 1354.20. [IR (KBr pellets) ν_{max}/cm^{-1}]: 3072, 3039, 1589),1269 (C–O–C), 988, 882, 746, 688.

β-PdO(BeOPhO)Pc (*17e*), (Scheme 3.4)

Synthesis and purification was as outlined for **15a** using **12e** and 24 h reflux instead 18 h. The amount of reagents employed were: 1-pentanol (8ml), 1,2-bis(benzyloxyphenoxy)-4,5-dicyanobenzene (**12e**) (1.68 ml, 3.2 mmol), $PdCl_2$ (0.27g, 1.50 mmol) and DBU (4.80ml, 3.0 mmol). Yield: 0.11 g (62%). UV/Vis [(1-CNP, λ_{max} / nm, (log ε)] 670 (5.25), 603 (4.58). $C_{136}H_{96}N_8O_{16}Pd$ Cald.: C, 74.09; H, 4.39; N,5.08;. Found, C, 73.64; H, 5.90, N,5.89 %. ^{1}H-NMR ($CDCl_3$) δ, ppm 8.62 (8H, s, Pc–H), 7.60 - 7.00 (72H, m, phenyl–H, phenyl-H), 5.10 (16H, s, S-CH_2). MS (ESI–MS) m/z: Calc. 2202.95; Found $[M-H]^+$: 2201.59. [IR (KBr pellets) ν_{max}/cm^{-1}]; 3065(Ar-CH), 3035(Ar-CH), 1638, 1648(C=C), 1207 (C–O–C), 962, 827, 733, 693 (Pc skeletal).

2.6.2.3. Nickel(II) phthalocyanine derivatives (NiPc)

β-NiOPPc (*16a*), (Scheme 3.5)

The same method used for **15a** was employed but the reflux was for 1h and $NiCl_2$ was used instead of $PdCl_2$. The amounts of reagents were: 1,2-bis(pentylthio)-4,5-dicyanobenzene (**12a**) (0.361 g, 1 mmol), DBU (1.66ml, 1.0 mmol) and preheated $NiCl_2$. $6H_20$ (0.12g, 0.5mmol). Yield: 0.27g (80%). UV/Vis [(1-CNP, / λ_{max}/ nm, (log ε)] 725 (4.81), 697 (5.14), 665 (4.75), 628 (4.63, 424 (4.54) $C_{72}H_{96}N_8NiS_8$.DCM:Cald.: C,58.66; H,6.57; N,7.60%. Found**,** C,57.81; H,4.91; N,9.96%**.** ^{1}H NMR (400 MHz, $CDCl_3$) δ_H /ppm: 8.23 (8H, s, Ar-H), 3.32 (16H, m, S-CH_2), 1.48 – 1.31 (72H, m, -$(CH_2)_3$-CH_3)**;** MS (ESI–MS) m/z: Calc. 1388.15; Found$[M-H]^+$: 1387.11. [IR (KBr pellets) ν_{max}/ cm^{-1}]: 2930, 2860, 2235, 1604, 1465, 1421, 1411, 1350, 1200, 1077, 1023, 967, 956, 883, 788, 750(C-S), 658, 512.

β-NiOOPc (*16b*), (Scheme 3.5)

The same method used for **15a** was employed but the reflux was for 1h and $NiCl_2$ was used instead of $PdCl_2$ and **12b** was used. The amounts of reagents were: 1,2-bis(octylthio)-4,5-dicyanobenzen (**12b**) (0.42 g, 1 mmol), $NiCl_2$. $6H_2O$ (0.12g, 0.5 mmol) and DBU (1.66ml, 1.0 mmol). Yield:0.25g (60%). UV/Vis [(1-CNP, / λ_{max}/ nm, (log ε)] 707 (5.29), 679 (4.72), 634 (4.62), 424 (4.57)**.** $C_{96}H_{144}N_8NiS_8$:Cald.: C, 66.83; H, 8.41; N,6.49% .Found**,** C, 66.67; H, 8.23; N,6.65%**.** ^{1}H NMR (400 MHz, $CDCl_3$) δ_H /ppm: 8.17 (8H, s, Ar-H), 3.36 (16H, m, S-CH_2), 1.62 – 1.39 (120H, m, -$(CH_2)_6$-CH_3))**;** MS (ESI–MS) m/z: Calc. 1722.85; Found $[M-H]^+$: 1721.77. [IR (KBr pellets) υ_{max}/ cm^{-1}]: 2929, 2857, 1743, 1602, 1537, 1467, 1420, 1386, 1350, 1295, 1075, 970, 870, 787, 750(C-S), 691, 519.

NiO(PhO)Pc (*16d*), (Scheme 3.5)

The same method used for **15a** was employed but **12d** was used and $NiCl_2$ instead of $PdCl_2$. The time was 14 h instead of 18 h. The amounts of reagents were: 1,2-diphenoxy-4,5-dicyanobenzene (**12d**) (1.00 g, 3.2 mmol), $NiCl_2.6H_2O$ (0.36g, 1.5 mmol) and DBU (3.20ml, 2.0 mmol). Yield: 0.08 g (75%). UV/Vis [(1-CNP, λ_{max}/nm, (log ε)] 678 (5.29), 650 (4.65), 610 (4.59). $C_{80}H_{48}N_8O_8Ni.H_2O$. Calc.: C, 72.46; H, 3.62 N,8.45. Found, C, 71.92; H, 3.52, N,8.98 %**.** ^{1}H NMR (600 mHz); δ ppm (Pyr-d_5) 8.45 (8H, s, Pc–H), 7.20–7.36 (40H, m, phenyl–H). MS (ESI-MS) m/z: Calc. 1306.98; Found $[M]^+$: 1306.71. [IR (KBr pellets) ν_{max}/cm^{-1}]; 3061, 3032, 1599,1260 (C–O–C), 965, 801, 748, 687.

NiO(BeOPhO)Pc (*16e*), (Scheme 3.5)

The same method used for **15a** was employed but **12e** was used and $NiCl_2$ instead of $PdCl_2$. The time was 24 h instead of 18 h.. The amounts of reagents were: 1,2-bis(benzyloxyphenoxy)-4,5-dicyanobenzene (**12e**) (1.68 g, 3.2 mmol), $NiCl_2.6H_2O$ (0.36g, 1.50 mmol) and DBU (4.80ml, 3.00 mmol). THF was used as the eluting solvent for column chromatography. Yield: 0.13 g (74%). UV/Vis [(1-CNP, λ_{max} / nm, (log ε)] 680 (5.40), 648 (4.69), 610 (4.66). $C_{136}H_{96}N_8O_{16}Ni.2H_2O$ Cald.: C, 74.49; H, 4.60; N,5.11.

Found, C, 73.92; H, 5.18, N,5.12 %. ^{1}H-NMR ($CDCl_3$) δ, ppm: 8.72 (8H, s, Pc–H), 7.65 - 7.10 (72H, m, phenyl–H), 5.00 (16H, s,CH_2). MS (ESI–MS) m/z: Calc. 2155.24; Found $[M-H]^+$: 2154.92. [IR (KBr pellets) ν_{max} / cm^{-1}]; 3052(Ar-CH), 3031(Ar-CH), 1611(C=C), 1224 (C–O–C), 955, 820, 734, 694.

2.6.2.4. Platinum (II) phthalocyanine derivatives (PtPc)

β-PtO(PhO)Pc (*18d*), (Scheme 3.6)

Synthesis and purification was as outlined for **15a** using **12d** and 14 h reflux instead of 18 h. $PtCl_2$ was employed instead of $PdCl_2$. The amount of reagent employed were: 1-pentanol (8 ml), 1,2-diphenoxy-4,5-dicyanobenzene (**12d**) (1.00 g, 3.2 mmol), platinum chloride (0.40g, 1.50 mmol) and DBU (3.20 ml, 2.00 mmol). Yield: 0.07 g (61%). UV/Vis [(1-CNP, λ_{max} / nm, (log ε)] 658 (5.06), 636 (4.53), 593 (4.43). $C_{80}H_{48}N_8O_8Pt.H_2O$. Calc.: C, 65.70; H, 3.28; N,7.67. Found, C, 64.29; H, 4.13, N,8.11 %. ^{1}H NMR (600 mHz); δ ppm (Pyr-d_5) 8.63 (8H, s, Pc–H), 7.23–7.45 (40H, m, phenyl–H). MS (ESI-MS) m/z: Calc. 1443.36; Found Found $[M]^+$: 1443.60. [IR (KBr pellets) ν_{max}/cm^{-1}]; 3063, 3033, 1602 (C=C), 1251(C–O–C), 966, 852, 745, 688.

β-PtO(BeOPhO)Pc (*18e*), (Scheme 3.6)

Synthesis and purification of **18e** was as outlined for **15a** using **12e** and 24 hr reflux instead of 18 hr. $PtCl_2$ was employed instead of $PdCl_2$. The amounts of reagents employed were: 1- pentanol (8ml), 1,2-bis(benzyloxyphenoxy)-4,5-dicyanobenzene (**12e**) (1.68 g, 3.2 mmol), platinum chloride (0.40g, 1.50 mmol) and DBU (4.80ml, 3.0 mmol). Yield: 0.09 g (49%). UV/Vis [(1-CNP, λ_{max} / nm, (log ε)] 703 (4.13), 660 (5.22), 594 (4.54). $C_{136}H_{96}N_8O_{16}Pt.3H_2O$. Cald.: C, 69.93; H, 4.10 N,4.79. Found, C, 68.70; H, 4.55, N,5.11 %. ^{1}H-NMR ($CDCl_3$) δ, ppm 8.60 (8H, s, Pc–H), 7.70 - 6.96 (72H, m, phenyl–H), 4.95 (16H, s, CH_2), MS (ESI–MS) m/z: Calc. 2291.65; Found $[M]^+$: 2291.68. [IR (KBr pellets) ν_{max} /cm^{-1}]; 3052(Ar-CH), 3037(Ar-CH), 1634(C=C), 1261 (C–O–C), 949, 801, 741, 671 (Pc skeletal).

2.6.3. Metal-binding Synthesis of Palladium Phthalocyanine Complexes

Complexes **13a, 14a, 15a and 17a** were used for these studies because of sulphur donor and unmetallated cavity that is available for binding. For all binding studies, $PdCl_2$ was dissolved in ethanol and the Pc complexes in DCM. In order to minimize dilution effects, very small volumes (mL) of the $PdCl_2$ stock solution were added to 2 mL of the Pc solution, and changes were monitored spectroscopically. The complexes formed by the interaction between Pd(II) and the unmetallated phthalocyanines (**13a** and **14a**) were isolated by evaporating the solvents (ethanol/DCM) and recrystalyzing in ethanol.

Elemental analyses for the complex between Pd and **13a**:

Cald. for $C_{72}H_{98}N_8S_8(PdCl_2)_4$): C, 41.81; H, 4.80; N, 5.48. Found: C, 40.90; H, 4.92; N, 5.57.)

Elemental analyses for complex between Pd and **14a**:

Cald. for $C_{72}H_{98}N_8S_8(PdCl_2)_2$: C, 52.79; H, 5.86; N, 7.04. Found: C, 52.07; H, 5.94; N,6.93.

Results and Discussion

List of Publications

The results presented in these sections have been published in or submitted to peer-reviewed journals. The details of these articles are listed below and are not referenced in the sections.

1) Taofeek. B. Ogunbayo, A. Ogunsipe. T. Nyokong, ***The syntheses, characterization and fluorescence spectra of novel ocktakis(alkylthiophthalocyanato) nickel(II) and Pd(II) complexes,*** Dyes and pigments, 82 (2009) 422.

2) Taofeek. B. Ogunbayo, T. Nyokong, ***Synthesis and Pd(II) binding studies of octasubstituted alkylthio derivatised phthalocyanines***, *Polyhedron*, 28 (2009) 2710.

3) Taofeek. B. Ogunbayo, T. Nyokong, ***Photophysical and photochemical properties of Ni(II), Pd(II) and Pt(II) aryloxo and alkythio derivatised phthalocyanines***, *J. Mol. Structure*, 973 (2010) 96.

4) Taofeek. B. Ogunbayo, E. Antunnes, T. Nyokong, ***Investigation of homogenous photosensitised oxidation activities of palladium and platinum octasubstituted phthalocyanines: Oxidation of 4-nitrophenol***, J. Mol. Catal. A: Chem 334 (2011) 123.

5) Taofeek. B. Ogunbayo, T. Nyokong, ***Phototransformation of 4-nitrophenol using Pd phthalocyanines supported on single walled carbon nanotubes***, J. Mol. Catal. A: Chem. (2011), doi:10.1016/j.molcata.2011.01.016

6) Taofeek. B. Ogunbayo, T. Nyokong, ***Photocatalytic transformation of chlorophenols under homogeneous and heterogeneous conditions using palladium octadodecylthio phthalocyanine***, J. Mol. Catal. A: Chem., Submitted**.**

Chapter 3

Syntheses and Spectroscopic Characterization

3.1. Spectroscopic characterization of complexes

3.1.1. Metal-free phthalocyanine derivatives (13a-c and 14a-e)

The metal-free octasubstituted thio and aryloxo-derivatised phthalocyanines were synthesized following literature methods as described in experimental section. **Schemes 3.1** and **3.2** show the synthetic routes. The Pc derivatives were characterized by mass, IR and NMR spectroscopies, and elemental analyses.

The sharp peak for the C≡N vibrations in the IR spectra of phthalonitriles at ~2230 cm^{-1} disappeared after conversion into phthalocyanines. The metal-free phthalocyanines showed a band of C=N between 1652 and 1654 cm^{-1}. The Pcs also showed vibrations due to C–S–C group between 660 and 682 cm^{-1} and stretchings due to N-H appeared between 3051 and 3057 cm^{-1}. The vibrations due to C-O-C appeared at 1270 and 1222 cm^{-1} for **14d** and **14e** respectively

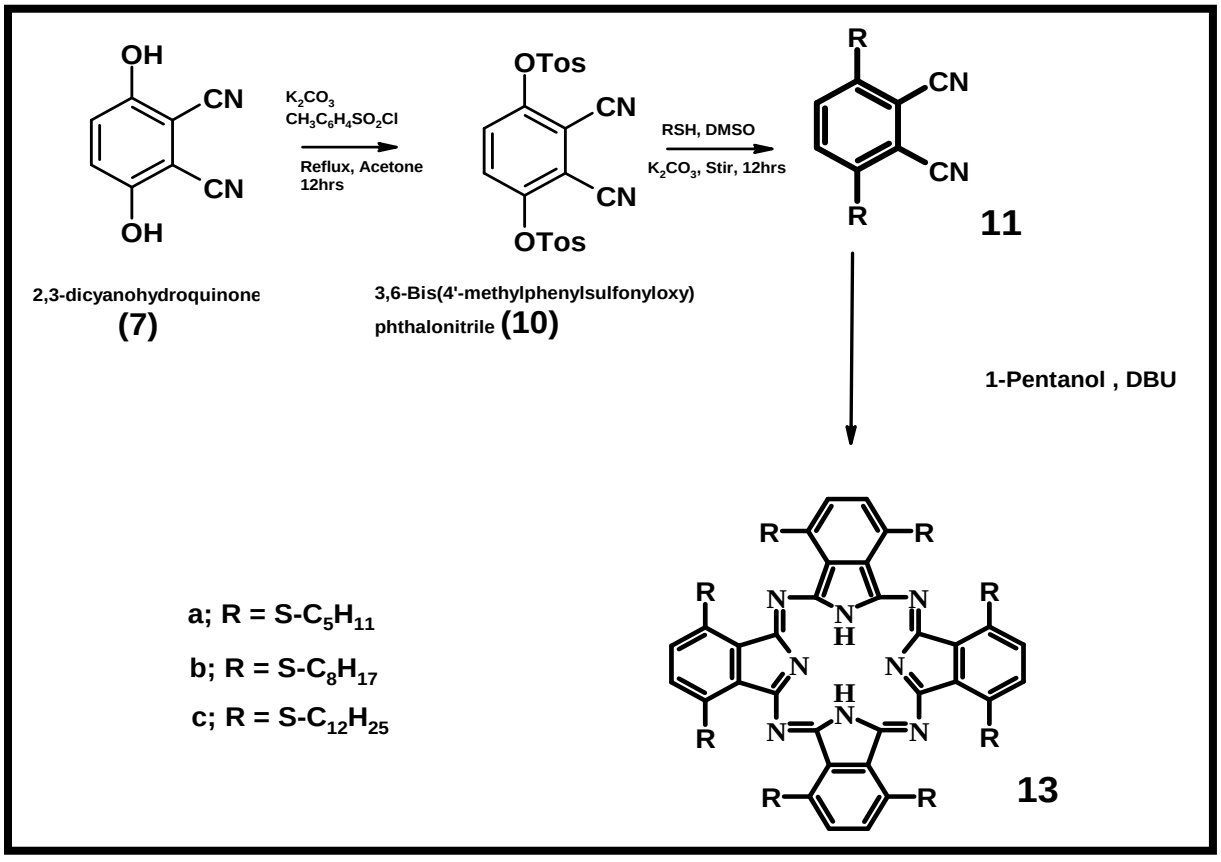

Scheme 3.1: Syntheses of metal-free α- thio-derivatised phthalocyanines

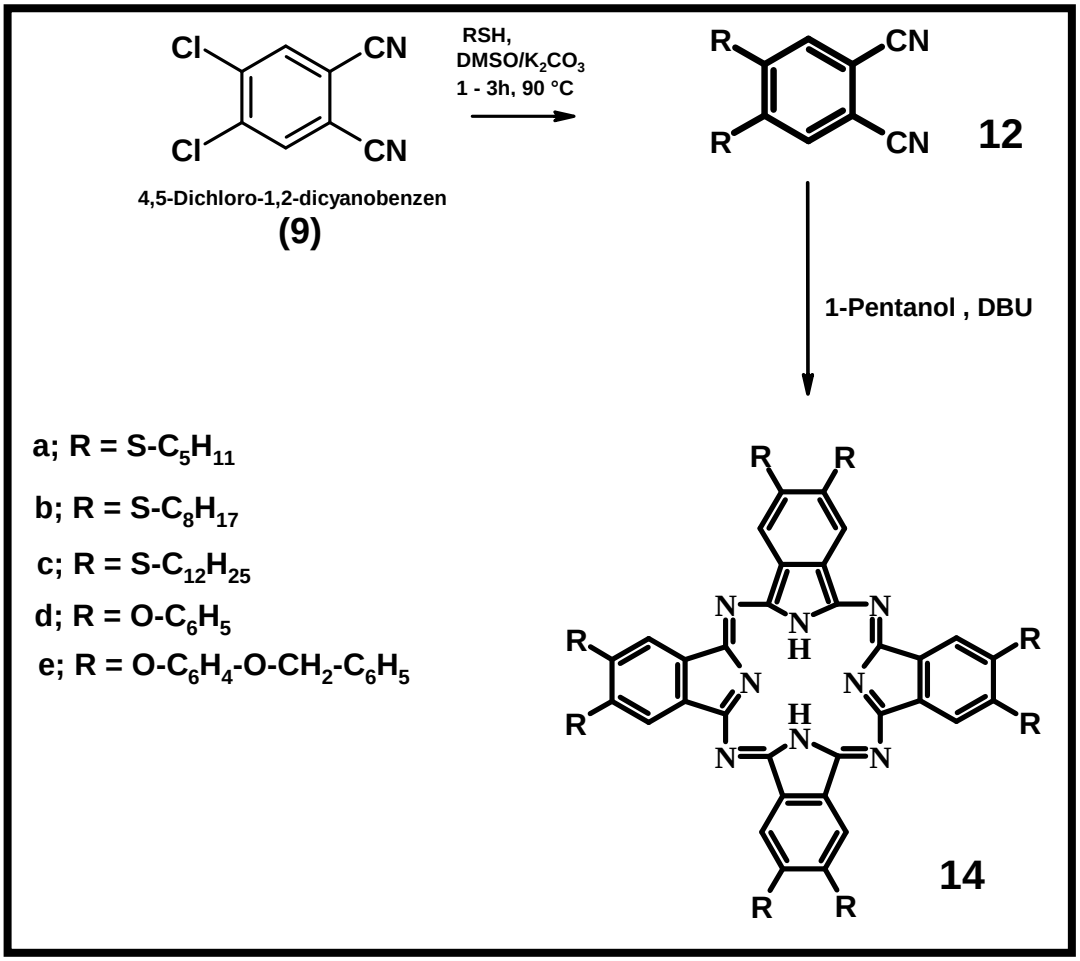

Scheme 3.2: Syntheses of metal-free β-octasubstituted phthalocyanines

^{1}H NMR for the molecules showed appropriate number of protons and at the right positions. The Pc ring protons appeared in the range of 7.76 ppm and 8.62 ppm integrating to 8 protons. **13b** and **13c** showed the cavity protons at 0.34 ppm and 0.37 ppm respectively integrating to 2 protons. **Figure 3.1** shows the ^{1}H NMR spectra of **14a** in $CHCl_3$. The cavity protons of other metal-free Pcs were not seen probably because of their high aggregation in chloroform, which was the solvent used for the ^{1}H NMR but additional analysis using IR, mass analysis and elemental analysis gave appropriate results as shown in the experimental section that confirmed the structure of the molecules. All the molecules exhibited excellent solubility in organic solvents such as DCM, chloroform, THF, and 1-CNP.

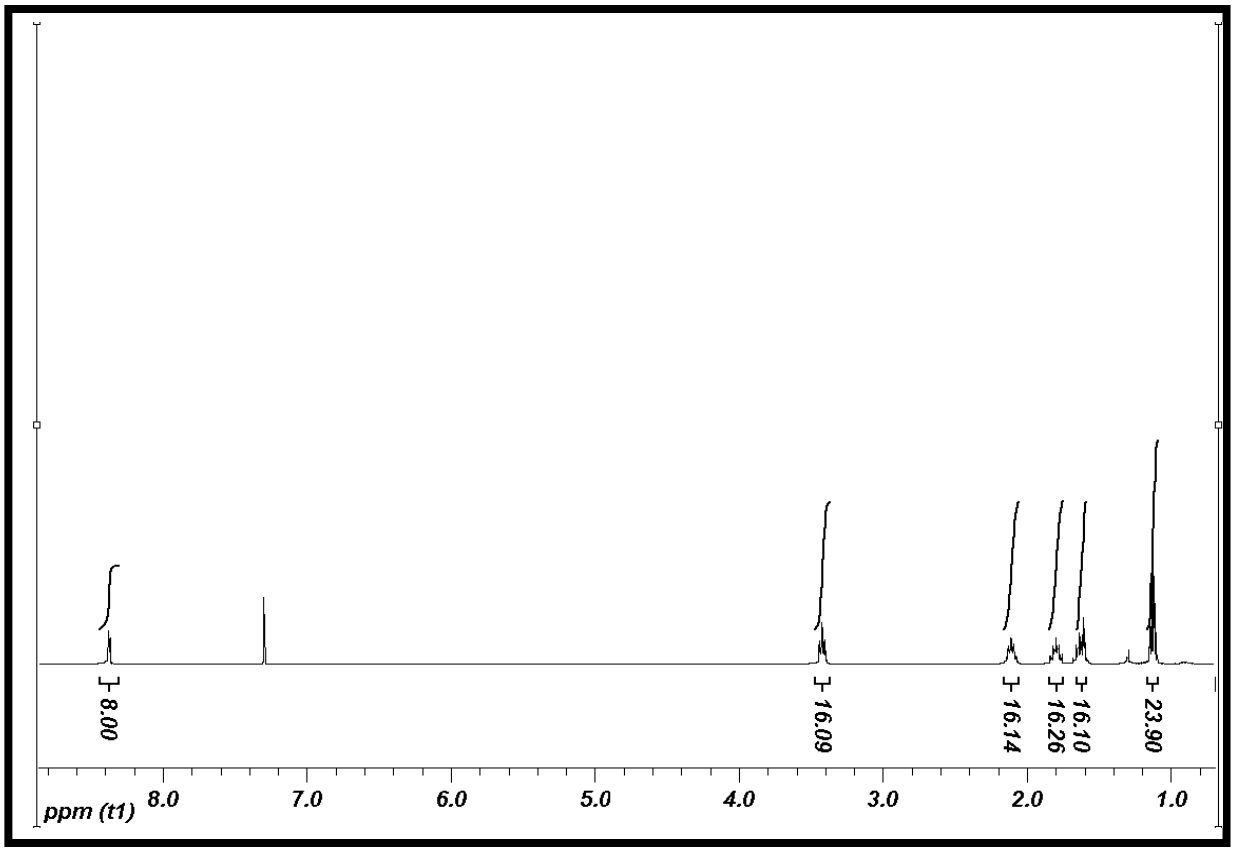

Figure 3.1: ^{1}H NMR spectrum of 14a in $CDCl_3$

Fig. 3.2 shows the UV/vis spectra of **13a-c** and **14a-e**. The spectra of metal-free β-substituted analogues showed a typical split Q-band. The aryloxo-derivatised showed their Q band at 706 nm and 672 nm for **14d** and 708 nm and 674 nm for **14e (Fig. 3.2b)**, **Table 3.1,** while thio-derivatives have their Q band at 707 nm and 736 nm for **14a**, **14b** and **14c**, **Fig. 3.2b**. The spectra of α-substituted analogues showed a red shift spectra compared to the peripheral analogues with their Q band at 813 nm, **Fig. 3.2a**.

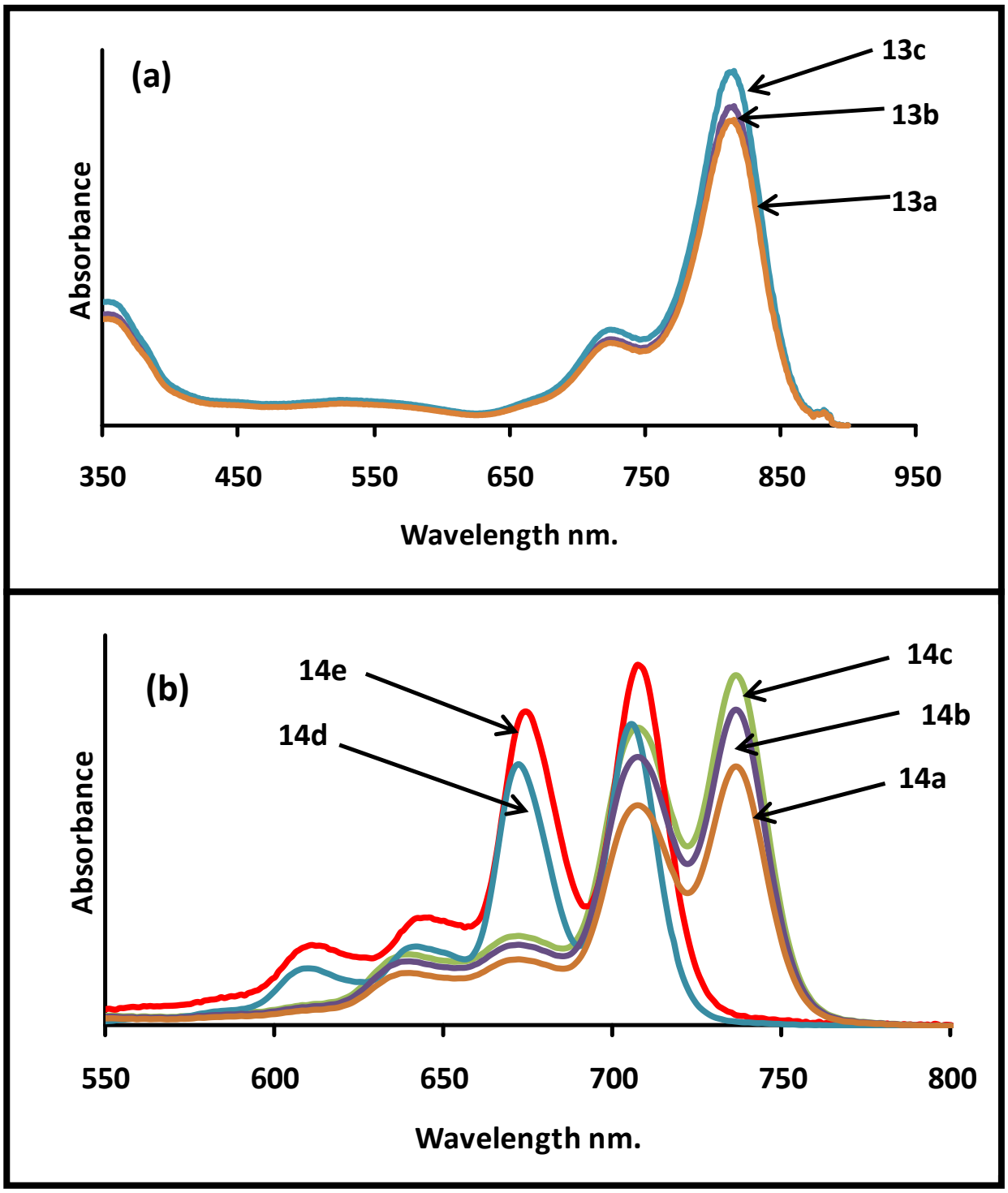

Figure 3.2: Absorption spectra of (a) 13a-c (b) complexes 14a-e in 1-chloronaphthalene (Concentration ~ 8 x 10^{-6} mol dm^{-3})

The α-substituted analogues did not show a typical split Q-band expected of unmetallated Pc; it is known that the resolution of split of the Q band decreases with

increasing wavelength **[112]**, hence for **13a-c**, the large red shift of the Q band must have resulted in unsplit Q band. The Q band is constant for all alkylthio-derivatised metal-free analogues (**13a-c**, **14a-c**) with increasing chain length showing that the chain length does not significantly affect the optical properties. The thio-derivatised molecules are red shifted compared to the aryloxo-derivatised because of higher electron-donating power of sulphur compared to oxygen.

.

Table 3.1: Spectral data for phthalocyanines (13 to 18) in 1-CNP

Pc	Central metal	substituents	Substituent position	Q band (nm)
13a	2H	-S-C_5H_{11}	α	813
13b	2H	-S-C_8H_{17}	α	813
13c	2H	-S-$C_{12}H_{25}$	α	813
14a	2H	-S-C_5H_{11}	β	736, 707
14b	2H	-S-C_8H_{17}	β	736, 707
14c	2H	-S-$C_{12}H_{25}$	β	736, 710
14d	2H	O-C_6H_5	β	706, 672
14e	2H	O-C_6H_4-O-CH_2-C_6H_5	β	708, 674
16a	Ni	-S-C_5H_{11}	β	696
16b	Ni	-S-C_8H_{17}	β	707
16c	Ni	-S-$C_{12}H_{25}$	β	709
16d	Ni	O-C_6H_5	β	678
16e	Ni	O-C_6H_4-O-CH_2-C_6H_5	β	680
15a	Pd	-S-C_5H_{11}	α	756
15b	Pd	-S-C_8H_{17}	α	756
15c	Pd	-S-$C_{12}H_{25}$	α	756
17a	Pd	-S-C_5H_{11}	β	698
17b	Pd	-S-C_8H_{17}	β	698
17c	Pd	-S-$C_{12}H_{25}$	β	698
17d	Pd	O-C_6H_5	β	668
17e	Pd	O-C_6H_4-O-CH_2-C_6H_5	β	670
18d	Pt	O-C_6H_5	β	658
18e	Pt	O-C_6H_4-O-CH_2-C_6H_5	β	660

3.1.2. Palladium(II) phthalocyanine derivatives (15a-c, 17a-e)

The palladium octasubstituted phthalocyanines were synthesized as described in experimental section. **Scheme 3.3** shows the synthetic route for the α-derivatised MPcs while **Scheme 3.4** shows the route for β-substituted. The non-peripherally octasubstituted thio-derivatised palladium phthalocyanines showed a band of C=N at 1650, 1645 and 1642 cm^{-1} for **15a**, **15b** and **15c** respectively The MPcs also showed vibrations due to C–S–C group between 751 and 747 cm^{-1}.

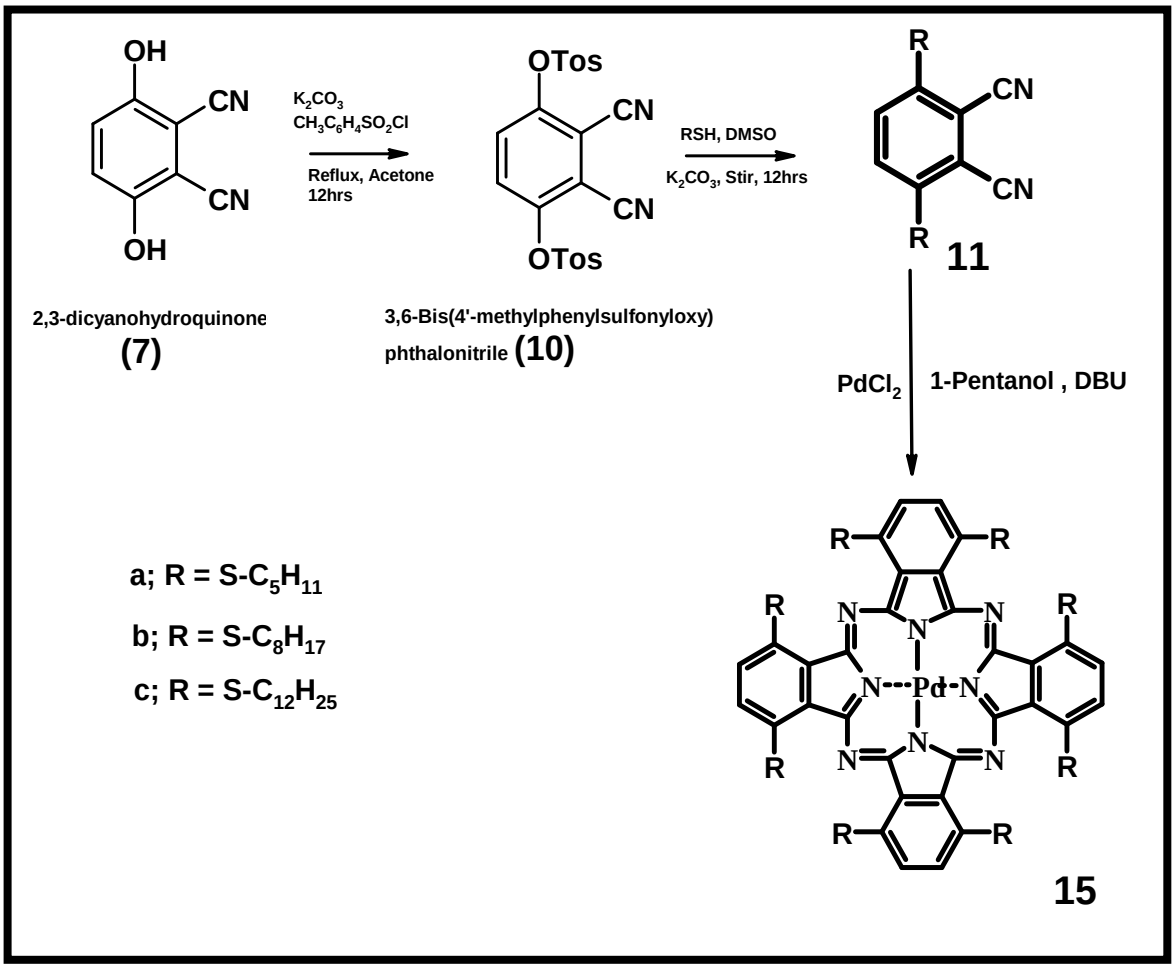

Scheme 3.3: Syntheses of α-thio-derivatised palladium (II) **phthalocyanines**

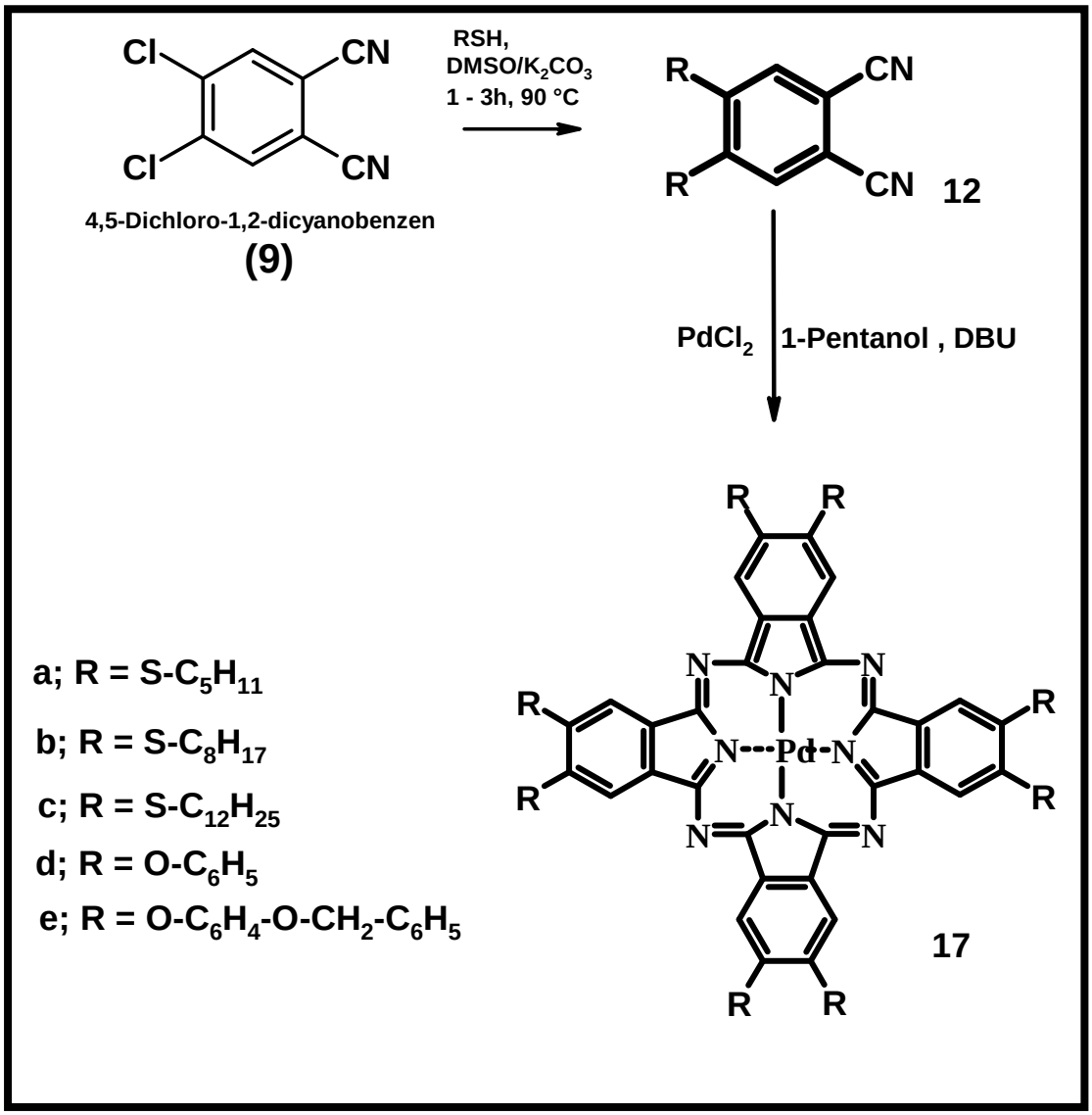

Scheme 3.4: Syntheses of β-thio-derivatised palladium (II) phthalocyanines

The peripherally substituted thio-derivatised palladium phthalocyanines **(**Complexes **17a-c)** showed a band of C=N between 1642 to 1652 cm^{-1}. They also showed vibrations due to C–S group between 747 and 749 cm^{-1} while the aryloxy derivatised MPcs **(**Complexes **17d** and **17e)** showed vibrations due to C-O-C at 1269 and 1207 cm^{-1} respectively.

^{1}H NMR of all the complexes were done in $CDCl_3$ except complex **17d** which was done in pyridine because it gave a poor spectrum in $CDCl_3$.The Pc ring protons appeared in the range of 8.19 ppm and 8.71 ppm integrating to 8 protons for the complexes.

Complexes **17d** and **17e** showed the aromatic protons of the substituents between 7.00 and 7.60 ppm. Mass and elemental analysis confirmed the formation of the complexes. All the molecules exhibited excellent solubility in organic solvents such as DCM, $CHCl_3$, THF, and 1-CNP.

Figure 3.3 shows the spectra of palladium phthalocyanines with the single Q band characteristics of MPcs. The three thio-derivatised α-derivatised PdPc (**15a-c**) have their Q band at 756 nm. The chain length has no affect whatsoever on the optical properties of the α-derivatised complexes, **Figure 3.3a**. In the case of β-substituted thio-derivatised MPcs (complexes **17a-c**), the chain length showed a little influence in the case of pentylthio-derivatised PdPc which showed an extra peak around 744 nm in addition to the Q band which is constant at 698 nm for the three complexes, **Figure 3.3b**. The origin of this peak is explained below for NiPc derivatives. The Q band of β-aryloxo derivatised PdPc complexes were blue shifted compared to the β-thio-derivatised analogues. This observation is consistent with what was observed for the metal-free analogues with Q band for complex **17e** and 17d appearing at 668 nm and 670 nm respectively in 1-CNP compared with 698 nm for complex **17a**, **17b** and **17c**. The 2 nm blue shift of phenoxy-derivatised compared with benzyloxy derivatised might be due to more electron donating ability of the former.

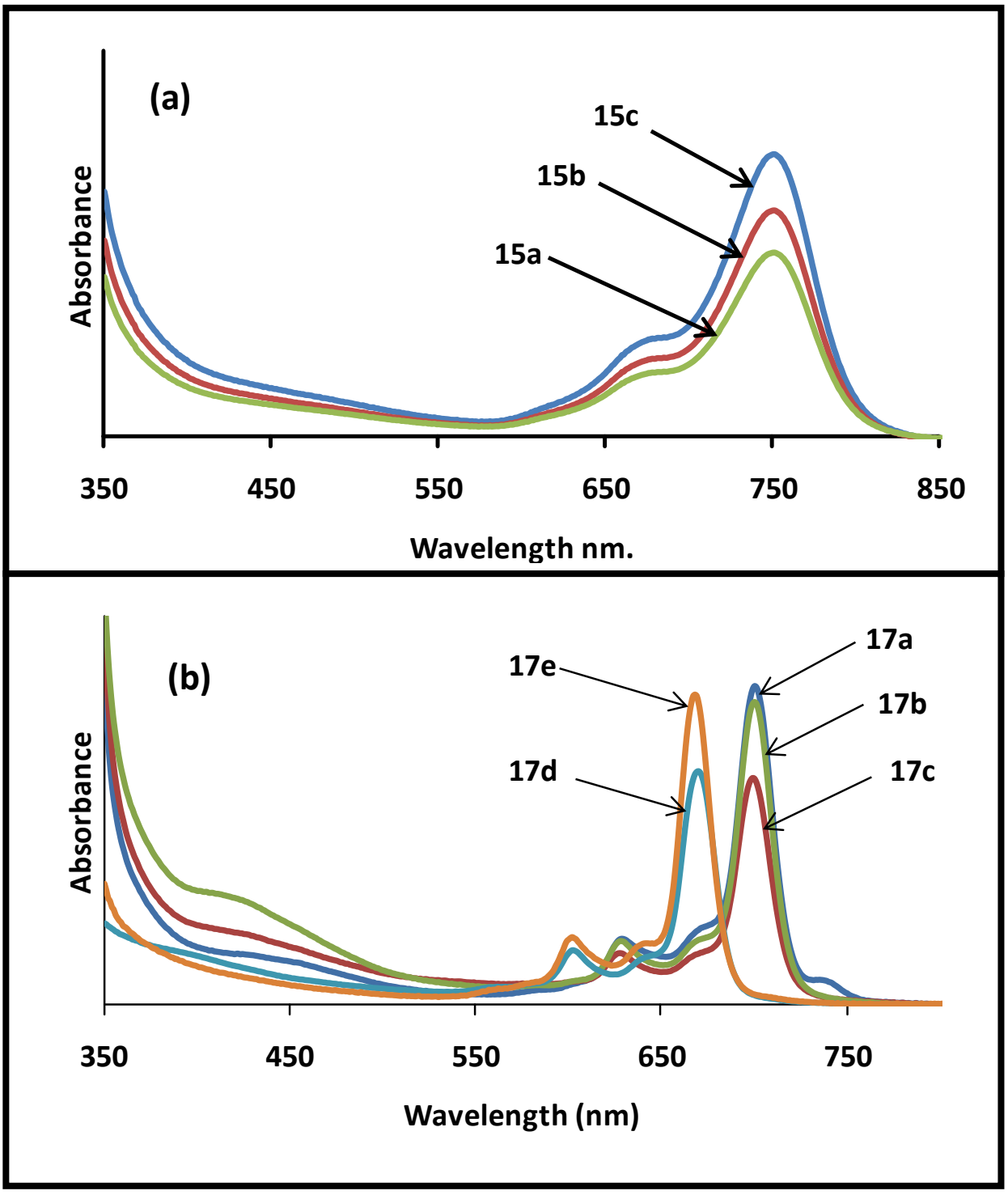

Figure 3.3: Absorption spectra of complexes (a) 15a-c (b) 17a-e in 1-CNP Concentration ~ 8 x 10^{-6} mol dm^{-3}.

As shown in **Fig. 3.4a** and **Fig. 3.4b** the Q band of PdPc complexes were blue shifted compared to their unmetallated analogues. The insertion of Pd into the cavity of the Pc led to a single Q band in the case of β-derivatised, **Figure 3.4b**, resulting from the transformation of low symmetry (D_{2h}) of metal-free analogues to D_{4h} symmetry of metallated analogues.

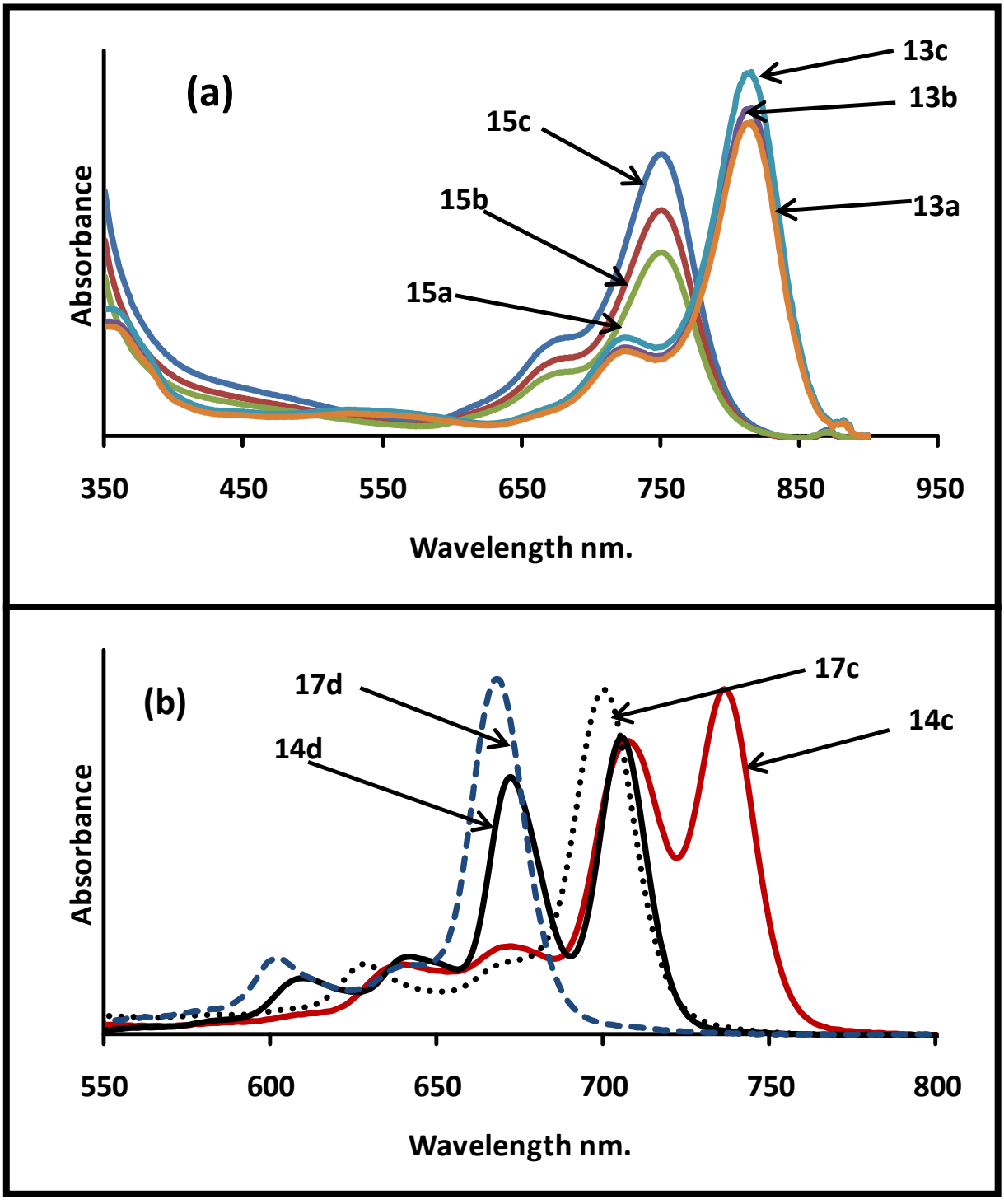

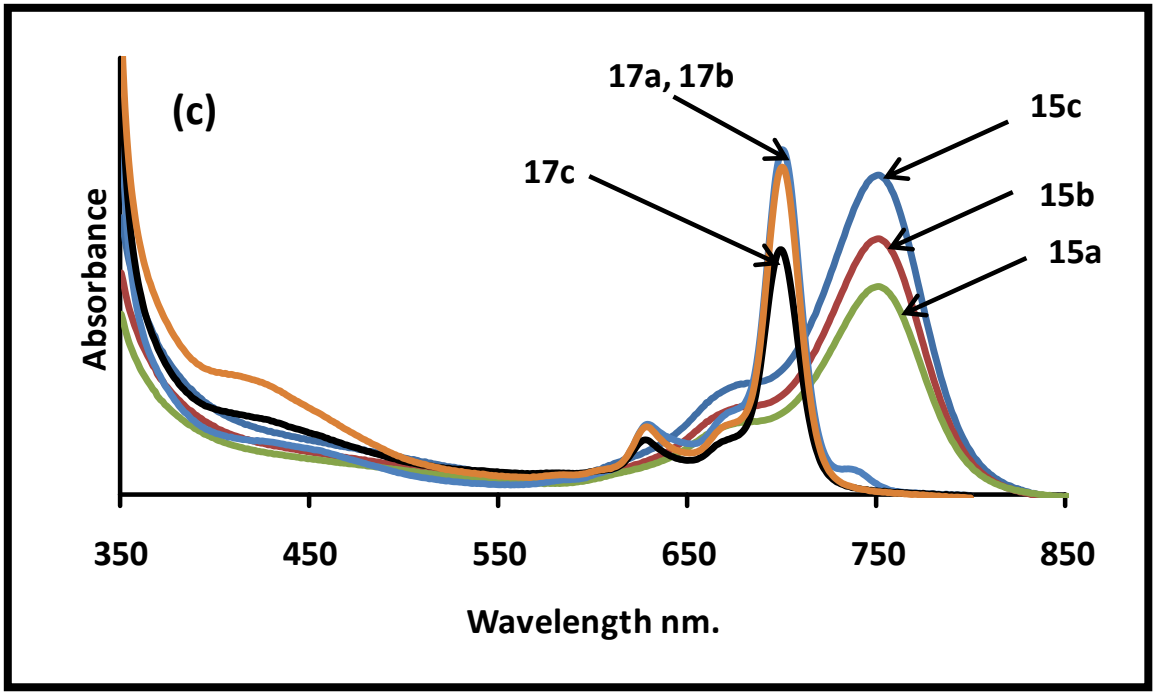

Figure 3.4: Absorption spectra of (a) α-PdPc complexes (15a-c) and α-metal-free analogues 13a-c (b) β-PdPc complexes (17c and 17d) and β-metal-free analogues (14c and 14d) (c) α-PdPc complexes (15a-c) and β-PdPc complexes 17a (blue), 17b (orange) and 17c (black). (Solvent : 1-CNP, Concentration ~ 8 x 10^{-6} mol dm^{-3}.)

Figure 3.4c shows the effect of substituent position on the position of the Q band of the PdPc complexes with non-peripherally substituted appearing at longer wavelengths than their peripherally substituted derivatives. The red shift of α-substituted derivative compared to β-substituted derivatives is attributed to greater electron density enhancement caused by the substitution at the non-peripheral position compared with the peripheral positions. This same effect was observed for the metal-free thio-derivatives.

*3.1.3. β-substituted nickel(II) phthalocyanine derivatives (***16a-e***)*

The peripherally octasubstituted thio and aryloxy derivatised nickel phthalocyanines, **16a-d** were synthesized as described in experimental section. The synthetic route is as shown in **Scheme 3.5**.

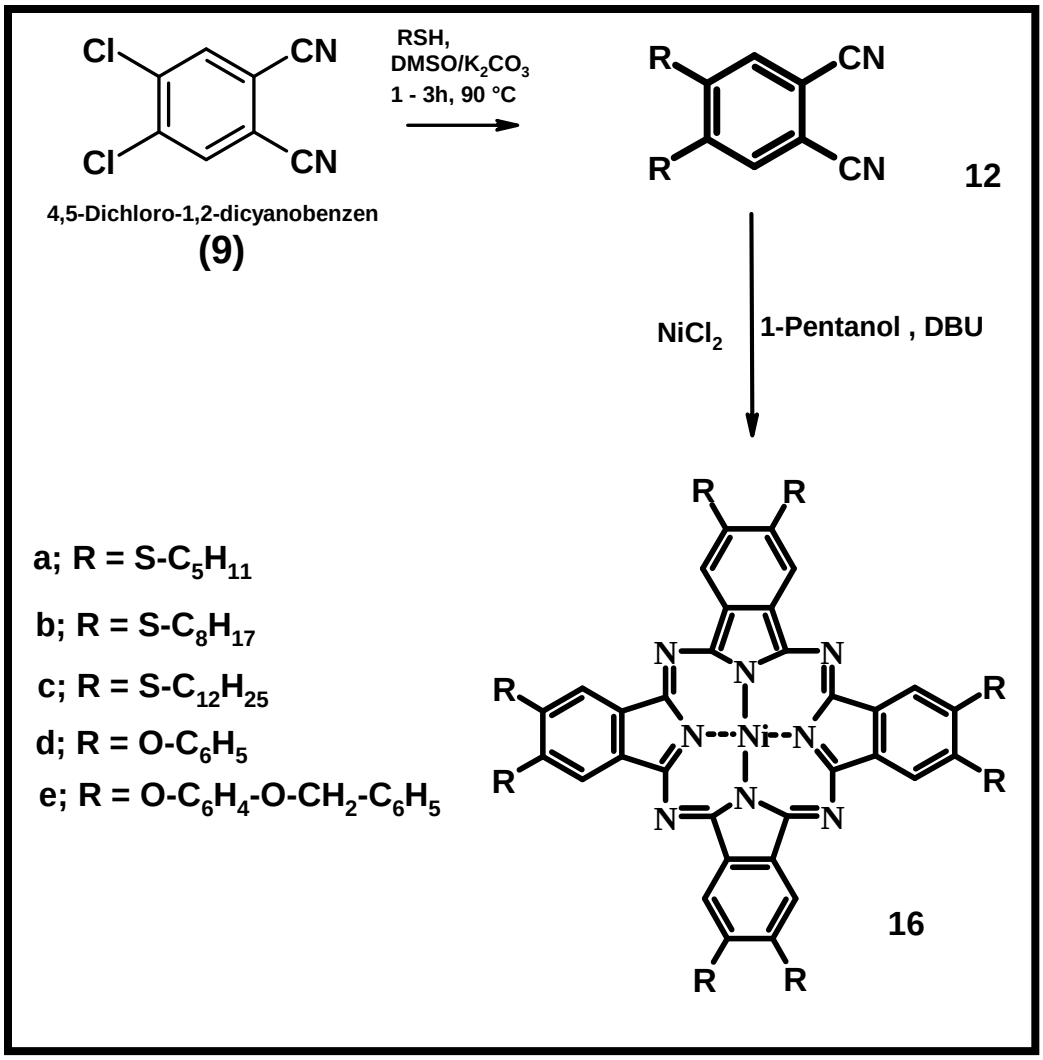

Scheme 3.5: Syntheses of peripherally octasubstituted nickel (II) phthalocyanines

The characterization of **16c** was as described in literature **[70]**. The β-substituted thio-derivatised nickel phthalocyanines showed a band of C=N at 1604 and 1602 cm^{-1} for **16a** and **16b** respectively The thio-derivatised MPcs showed vibrations due to C–S–C group between 658 and 691 cm^{-1}. Complexes **16d** and **16e** showed vibrations due to C-O-C at 1260 and 1224 cm^{-1} respectively. ^{1}H NMR of all the complexes were done in $CDCl_3$ except complex **16d** which was done in pyridine because the poor quality of its

spectra in $CDCl_3$. The Pc ring protons appeared in the range of 8.17 ppm and 8.72 ppm integrating to 8 protons for the complexes. Complexes **16d** and **16e** showed the aromatic protons of the substituents between 7.10 and 7.65 ppm. Mass and elemental analysis confirmed the purity of the complexes. All the molecules exhibited excellent solubility in organic solvents such as DCM, $CHCl_3$, THF, and 1-CNP.

Unlike β-substituted thio-derivatised PdPc whose spectra were relatively indifferent to increase in chain length, spectra of NiPc complexes showed a significant dependence on the chain length. For the NiPc derivatives, the Q-band positions for 1**6b** (707 nm) and 1**6c** (709 nm) are red-shifted relative to that of 1**6a** (696 nm), **Fig. 3.5**. On the average, the Q-band positions for the NiPc complexes are red-sifted relative to those of the PdPc complexes. The spectra of the pentylthio-substituted derivatives (**17a** and 1**6a**) exhibit extra peaks at ~ 740 nm, in addition to the normal Q-maxima.

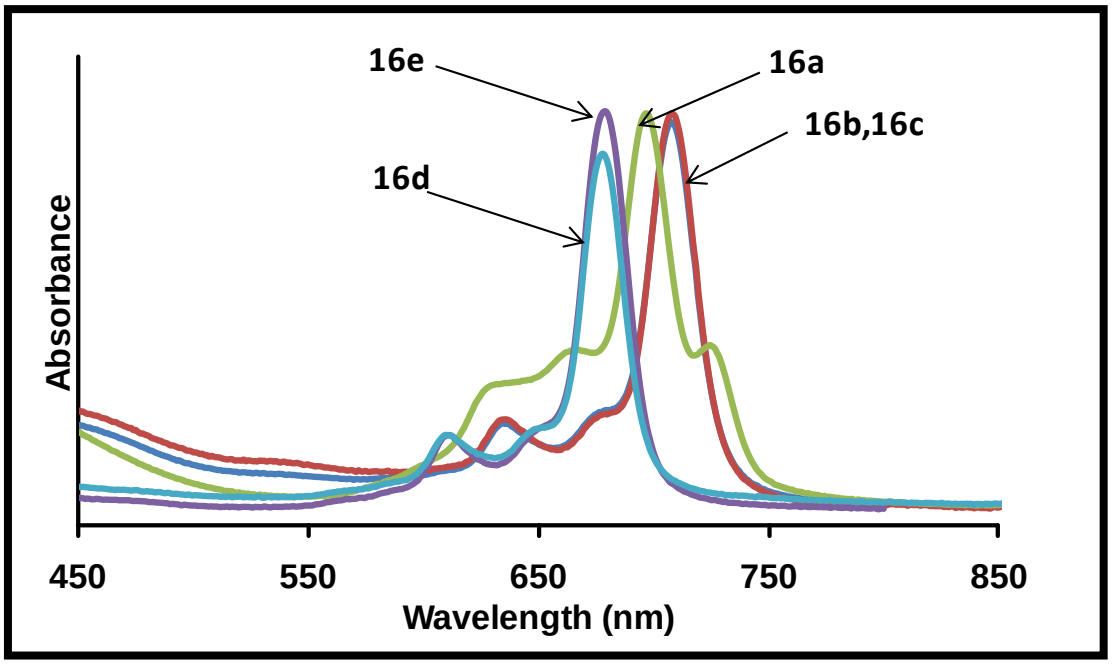

Figure 3.5: Absorption spectra of complexes 16a-e in 1-chloronaphthalene (16b (blue), 16c (red)). (Concentration ~ 8 x 10^{-6} mol dm^{-3})

The split in the Q band for alkylthio derivatives of CuPc and NiPc has been observed and could not be explained in terms of aggregation or demetalation since an extra band was also observed for unmetallated derivatives **[70]**. The split in the Q band was

explained in terms of intermolecular interaction between the central metal ion of one molecule with the thio group of another **[70]**. The extent of the split depended on the solvent **[70]**. It is proposed that the same type of interaction for the current complexes occurs, with the extent of the interaction resulting in differences in the extent of splitting of the Q bands of the complexes. Thus the splitting depends on the central metal and on the length of the chain. In the published work **[70]**, the dodecylthio NiPc derivative showed the splitting, but in different solvents. For 1**6a**, there is split in the Q band accompanied by a bluer shifted Q band compared to 1**6b** and 1**6c**. The Q band of spectra of alkyl MPc complexes are not known to shift with change in the chain length **[276-278]**. The observed spectra may suggest some demetalation, but refluxing the solution of 1**6a** in chloronaphthalane in the presence of a nickel chloride did not change the spectra in **Fig. 3.5.** Also the spectrum for **16a** in **Fig. 3.5** does not match that of the unmetalated derivative.

It is known that the degree of aggregation is increased by the presence of long alkyl chains **[279]**. While the complexes were highly aggregated in DCM, $CHCl_3$ and toluene they were not aggregated in 1-CNP at the concentrations used (hence this solvent was employed). Also, addition of surfactant, Triton X-100 brought about no observable spectral change. Again, the possibility of these complexes existing as mixtures of isomers is ruled out, as they all are octasubstituted. As a result, the observed band splitting will most likely have arisen from the intermolecular interactions discussed above. The scope of study on the complexes is limited by their aggregation in most solvents. **Fig. 3.6** shows the effect of the insertion of Ni into the cavity of the Pcs on their optical properties which was essentially the appearance of a blue shifted single Q band in place of a split Q band of metal-free derivatives due to the improvement in the symmetry of the MPcs.

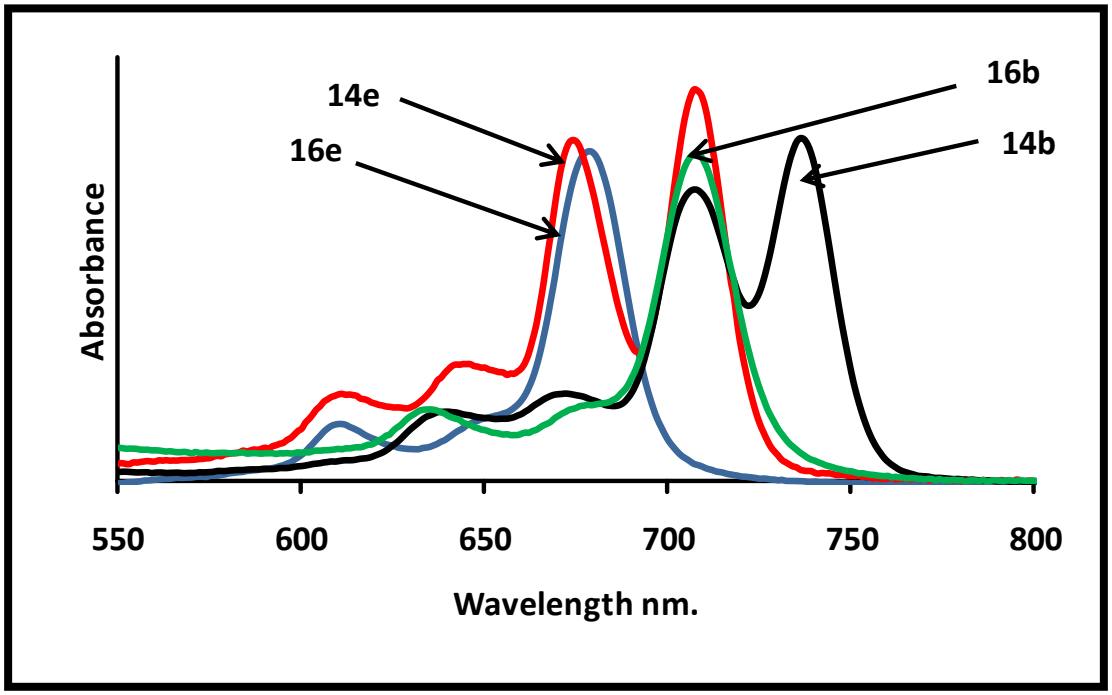

Figure 3.6: Absorption spectra of β-NiPc complexes (16e and 16b) and β-metal-free analogues (14b and 14e) in 1-CNP.

3.1.4. β-substituted platinum(II) phthalocyanine derivatives (18d and 18e)

The peripherally octasubstituted aryloxy derivatised platinum phthalocyanines, **18d** and **18e** were synthesized as described in experimental section. **Scheme 3.6** shows the synthetic route.

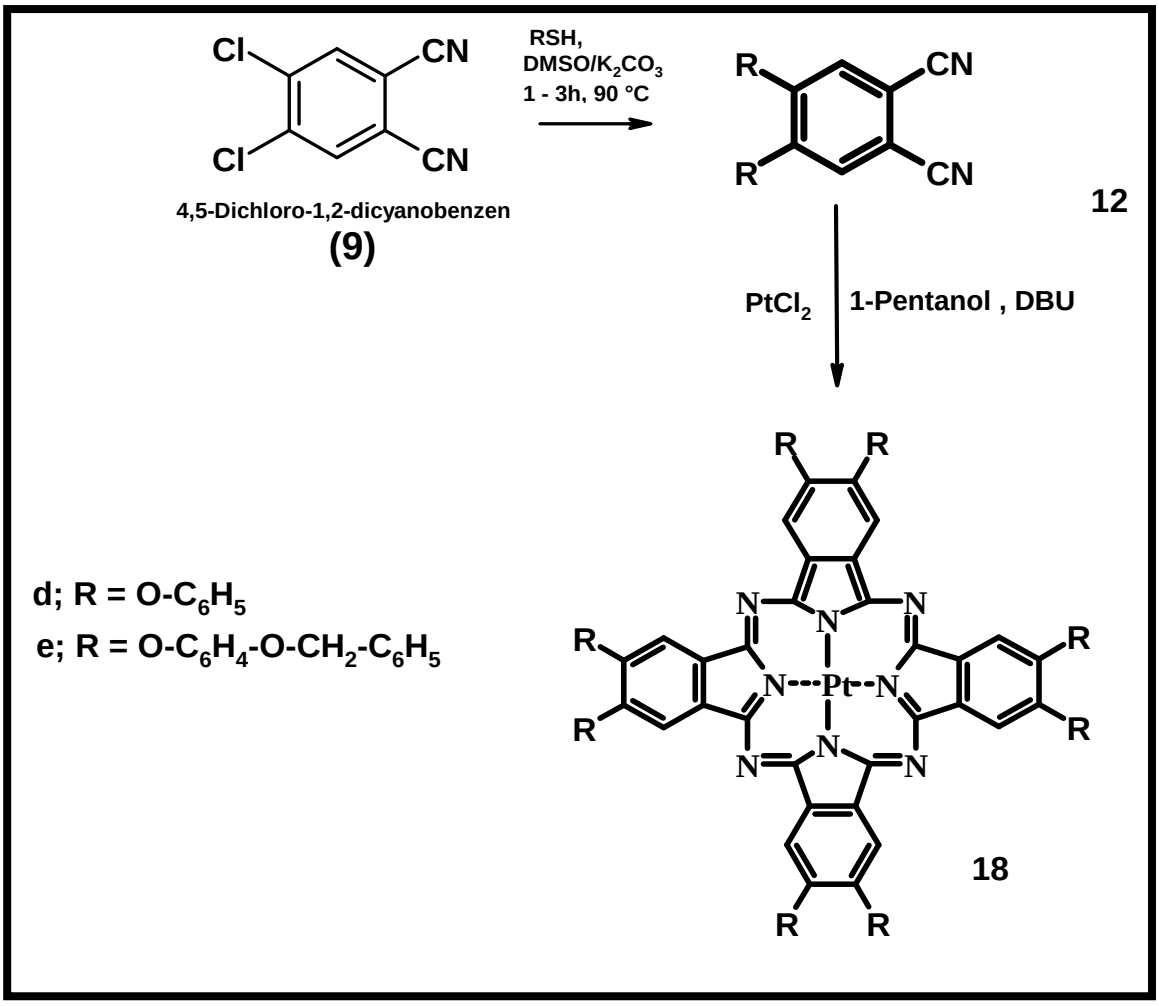

Scheme 3.6: Syntheses of peripherally octasubstituted platinum(II) phthalocyanines

All attempts at synthesis of thio-derivatised platinum phthalocyanines failed. The peripherally substituted aryloxy-derivatised platinum phthalocyanines, **18d** and **18e** showed a band of C=N at 1638 and 1642 cm^{-1} respectively. The MPcs showed vibrations due to C-O-C at 1251 and 1261 cm^{-1} respectively.

^1H NMR of complex **18d** was done in dueterated pyridine while $CDCl_3$ was used for complex **18e**. The Pc ring protons appeared at 8.63 ppm and 8.60 ppm for complex **18d**

and **18e** respectively integrating to 8 protons. Complexes **18d** and **18e** showed the aromatic protons of the substituents between 6.96 and 7.70 ppm. Mass and elemental analysis confirmed the formation and purity of the compounds. All the molecules exhibited excellent solubility in organic solvents such as DCM, $CHCl_3$, THF, and 1-CNP.

Fig. 3.7a shows the spectra of phenoxy-derivatised PtPc (**18d**) and benzyloxyphenoxy PtPc complex (**18e**). Complex **18d** has a single Q band at 658 nm while the benzyloxyphenoxy PtPc complex (**18e**), **Figs. 3.7a,** has its Q band at 660 nm. **18e** also showed an additional peak on the red side of the Q-band around 709 nm but this extra peak was not noticed in phenoxy derivative **(18d)**. This extra peak is associated with partial demetallation of the complex since Pt^{2+} central metal is unable to completely enter the central cavity of Pc ring due to its large ionic size. Demetallation was solvent dependent in that the extra peak was observed in chlorinated solvents as was reported before for CdPc complexes **[137]**. Studies have shown that, in chlorinated solvents, MPcs undergo oxidation with the formation of HCl as a by-product **[153]** which in certain cases reacts with the MPc to cause demetallation. **Fig. 3.7b** shows that the extra peak disappeared in pyridine. It is also possible that demetallation occurred during synthesis, this was evidenced by the presence of the extra peak during synthesis in 1-pentanol, and addition of Zn acetate resulted in the disappearance of the peak as a result of the coordination of the Zn to the centre of the ring. Attempts to eliminate the demetallated species using chromatography and eluting with several solvents and their mixtures were not successful. The extra peak might also be due to the formation of protonated specie. Basicity of aza nitrogen atoms in electron-rich Pcs is stronger than that of electron poor Pcs, hence protonated forms of this Pcs might sometime show extra peak on the red side of the Q band in chlorinated solvent and the dissaperance of the peak in pyridine. **Fig. 3.7c** shows the concentration dependence of complex **18e** in 1-CNP. As the concentration was increased, the intensity of the Q-band and the extra peak also increased and there were no new band due to the aggregated species for the

complex. The Beer–Lambert's law was obeyed for all of these compounds in 1-CNP for concentrations less than 1 x10^{-5} mol dm^{-3}.

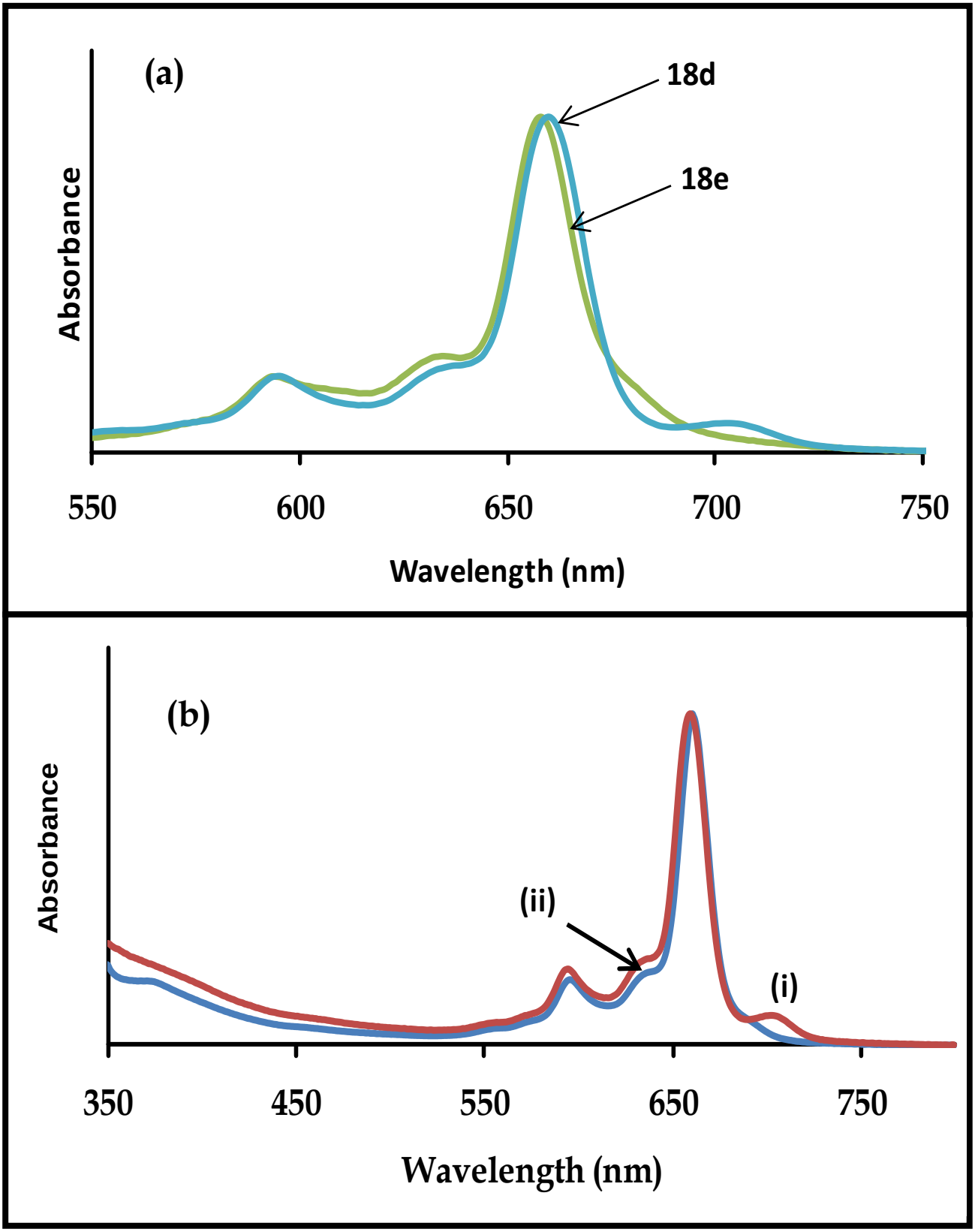

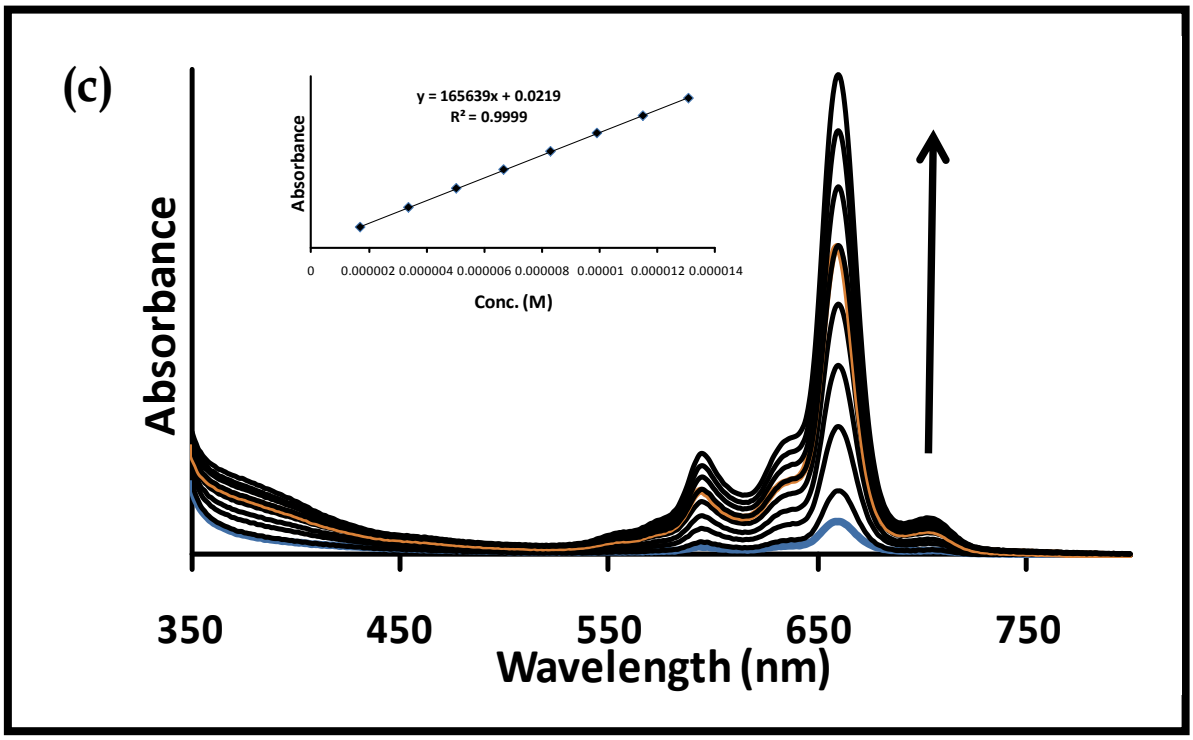

Figure 3.7: (a) Absorption spectra of β-PtPc complexes (b) Spectra of complex 18e in 1-CNP (i) and pyridine (ii) (c) UV-Vis spectral changes observed on increase in concentration of 18e in 1-CNP. Inset: Beer–Lambert's plot for 18e in 1-CNP. (Concentration range: 1.0 x10^{-6} mol dm^{-3} to 1.3 x 10^{-5} mol dm^{-3})

3.1.5. Effect of insertions of Ni, Pd and Pt on the Pcs spectra

The Q-bands of MPcs were observed in the range 658 – 756 nm in 1-CNP, **Table 3.1**. Their spectra in 1-CNP, showed monomeric behavior, evidenced by a single (narrow) Q-band typical of unaggregated MPcs. The Q-band of all the thio derivatised complexes (substituents **a**, **b**, and **c**), **Table 3.1**, are red shifted compared to the aryloxo substituted. Red shift is typical of all thio substituted phthalocyanine complexes **[280]**.

There is a clear red shift of the Q band as the size of the central metal decreases for the complexes. The Q band of NiPc (**16b**, **16c, 16d** and **16e**) is red shifted compared with that of PdPc analogues (**17b**, **17c, 17d** and **17e**) while the PtPc derivatives (**18d, 18e**) are blue shifted compared to PdPc (**17d**, **17e**) and NiPc (**16d**, **17e**) , **Figs. 3.8, 3.9 and 3.10, Table 3.1**. The wavelength of the Q band of NiPc>PdPc>PtPc for all the complexes except pentylthio-derivatised MPc. The effect of short chain on the Q band of complex **16a** (696 nm) make its comparison with Q band of complex **17a (698 nm)** an exception this trend. Red shift of the Q band in MPc complexes is due to the destabilization of the highest occupied molecular orbital (HOMO) **[281]**. There are some central metals such as Mn^{III}, Pb^{II} and Sn^{IV}, which show a large red shift compared to metals such as Ni^{II}, Zn^{II} **[92]**. The observed red shift of NiPc derivative (**16d, 16e**) compared to PdPc (**17d, 17e**) and PtPc **(18d, 18e**) derivatives, suggests that the former destabilizes the HOMO to a larger extent than the latter two complexes. The same reason holds for the thio-derivatised analogues. In DCM the MPcs displayed aggregation as evidenced by the presence of a blue shifted non-vibrational band in the visible region, **Figs. 3.8b, 3.9b and 3.10b.** The Q-bands of the monomers in DCM were observed at 669, 660 and 650 nm for **16d**, **17d** and **18d** respectively, **Fig. 3.5b** and 669, 662 and 652 for **16e**, **17e** and **18e** respectively, (**Table 3.1.**) **Fig. 3.6b,** showing a blue shift compared to the spectra in 1-CNP. The peaks due to the aggregates were observed at 613, 604, 599, 615, 597 and 590 nm respectively for **16d**, **17d**, **18d**, **16e**, **17e** and **18e**.

The red shift of the Q-band in 1-CNP compared to DCM might be due to aromatic nature of 1-CNP. Aromatic solvents have been known to bring about red-shift of Q-band relative to the non-aromatic ones **[282]**. Generally, aggregation is more

pronounced in non-coordinating solvents. Thus the observed extensive aggregation in DCM compared to 1-CNP could be because the polarity of DCM is higher than that of 1-CNP.

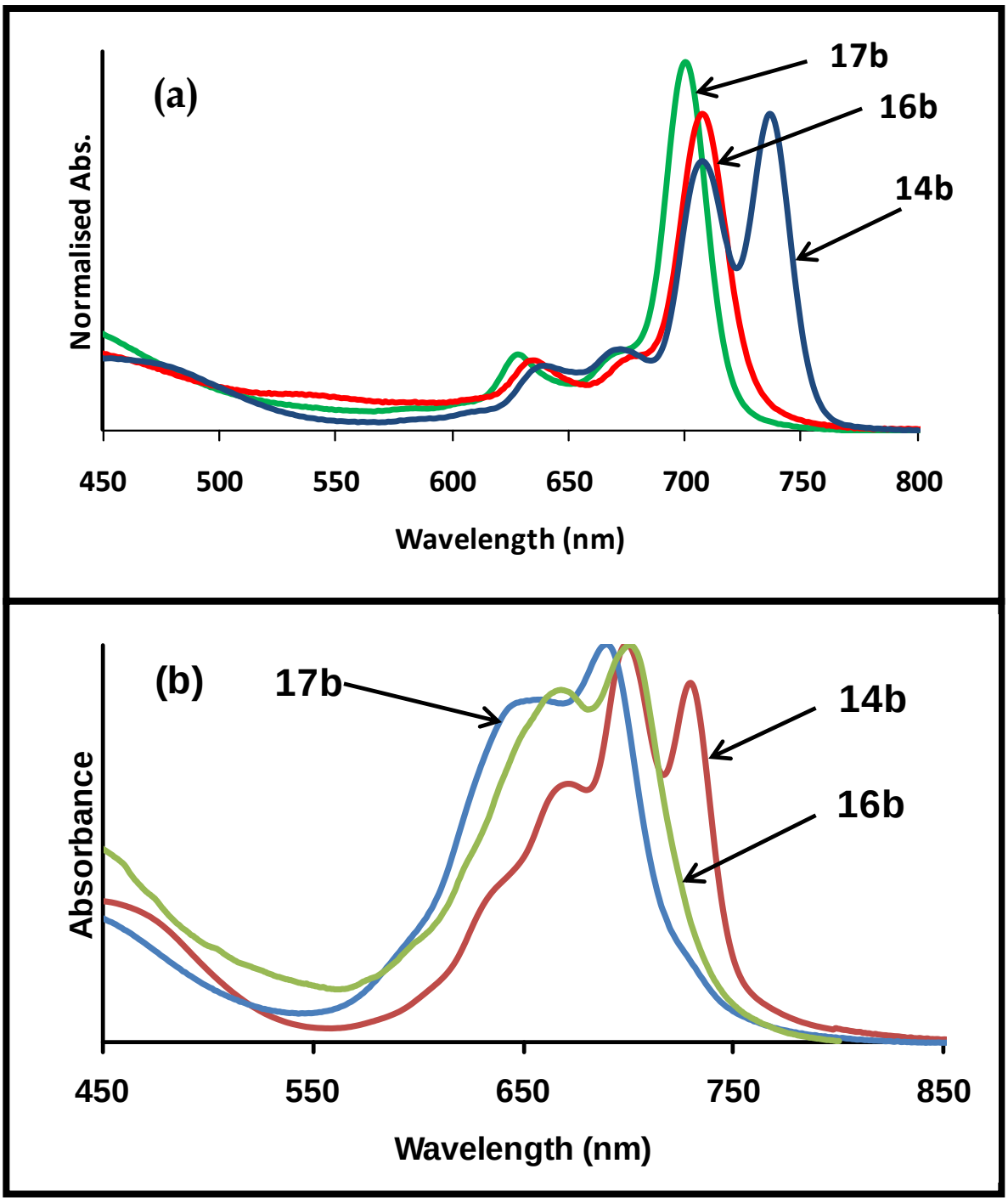

Figure 3.8: Absorption spectra of complexes 14b, 16b and 17b (a) in 1-CNP, and (b) in DCM. (Concentration ~ 1 x 10^{-6} mol dm^{-1})

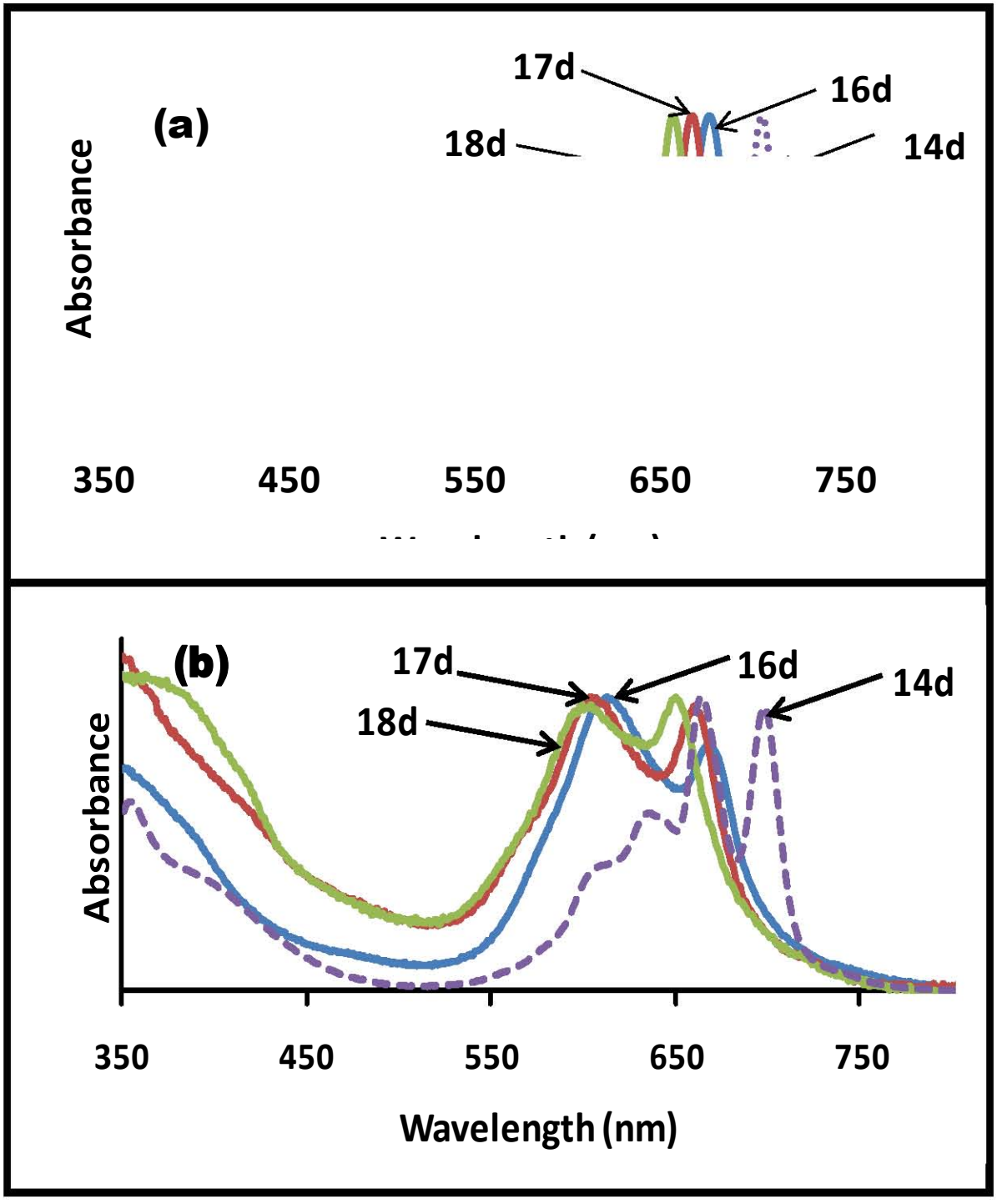

Figure 3.9: UV-Vis spectra of complexes 14d, 16d, 17d, and 18d (a) in 1-CNP and (b) in DCM. (Concentration ~ 1 x 10^{-6} mol dm^{-3})

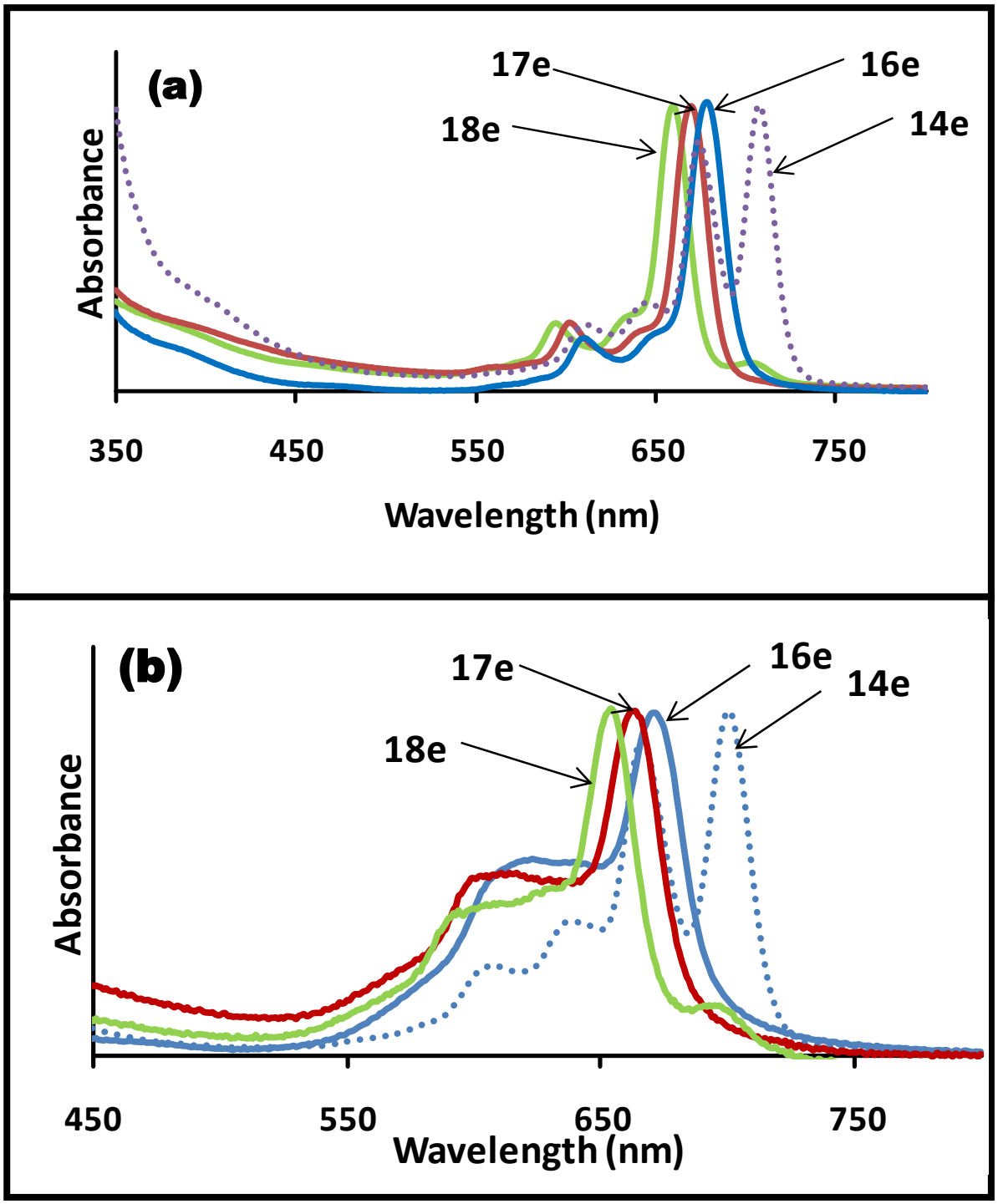

Figure 3.10: UV-Vis spectra of complexes 14e, 16e, 17e, and 18e (a) in 1-CNP and (b) in DCM. (Concentration ~ 1 x 10^{-6} mol dm^{-3})

3.2. Pd(II) binding to phthalocyanines and kinetic studies

3.2.1. Metal-free non-peripherally substituted octapentylthiophthalocyanine (13a).

It is possible that binding of Pd(II) to complex **13a** and **14a** will occur at the thio groups or at the central core of the Pc skeleton. On addition of Pd(II) to a solution of **13a**, spectral changes shown in **Fig. 3.11** were observed. The spectrum of the α-H_2Pc does not have the split Q band characteristic of metal-free Pcs due to the red shift discussed above. The first part shown in **Fig. 3.11a** consists of a decrease in the Q band intensity (at 801 nm in DCM) accompanied by broadening and the shift of the band to high energy (754 nm). These spectral changes are consistent with formation of aggregates observed on metal binding in thio substituted MPc complexes **[283]**. The lack of clear isosbestic points, suggests that there may be more than two species in solution. Higher aggregates could also be present in solution. Further addition of Pd(II) resulted in spectral changes shown in **Fig. 3.11b**, which consist of the decrease in the broad peak at 754 nm and the formation of a split peak with maxima at 708 and 732 nm with clear isobestic point at 680 nm and 743 m. The observed split in Q band suggests that a PdPc complex has not formed yet and the complex is still H_2Pc with Pd(II) ions coordinated to the pentylthio groups or the PdPc complex has formed with unsymmetrical substitution of Pd ions on the ring. Further addition of $PdCl_2$ resulted in the formation of a new band at 693 nm and the gradual disappearance of the split Q band **(Fig. 3.11c and d)**. Elemental analysis confirmed to binding of four Pd(II) ions at this stage, as reported in the experimental section. The ^{1}H NMR spectra of the complex isolated at this stage showed a change in chemical shift of the protons relative to what obtained in the original ligand (**13a**), the most conspicuous shift being the macrocyle protons indicating a change in electron distribution **[284-286]**. The singlet peak shifted downfield from 8.00 ppm to 8.30 ppm which indicated higher resonance of the ring protons due to desheilding effect that resulted from reduced mesomeric effect of the sulfur lone pairs of electrons on the ring when part of those lone pairs were used in coordination with Pd ions. The IR spectrum of this complex also showed a dramatic

change compared with that of **13a**. The bands between 1000 and 600 cm^{-1} showed conspicuous split, especially at 939, 808, and 736 cm^{-1}.

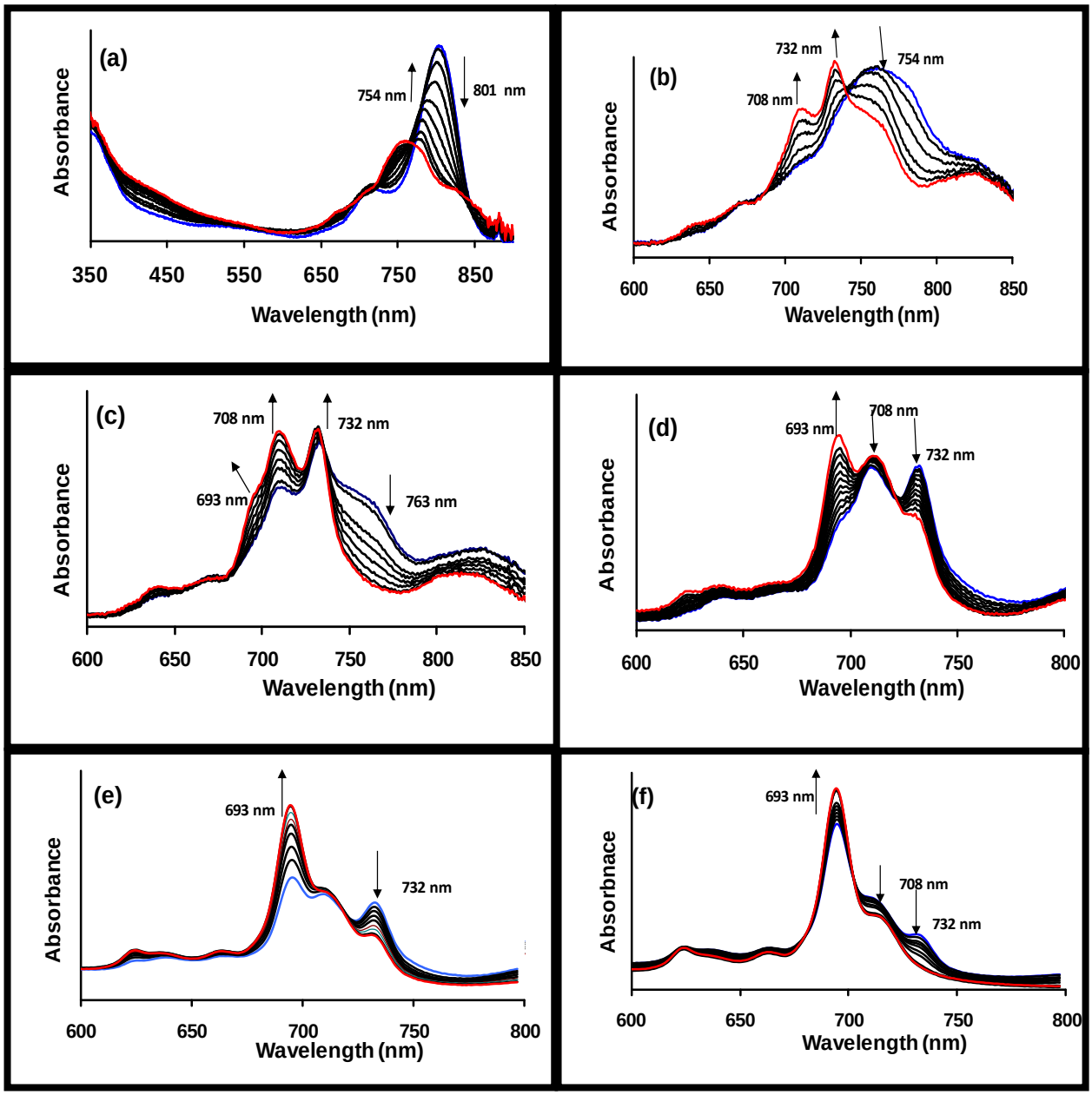

Figure 3.11: UV-Vis spectral changes observed on addition of $PdCl_2$ in ethanol to complex 13a (concentration = 5 x 10^{-6} M) in DCM. Concentration of $PdCl_2$ (a) 6.5 x 10^{-4} M to 3.05 x 10^{-3} M (b) 3.05 10^{-3} M to 7.20 x 10^{-3} M (c) 7.20 x 10^{-3} M to 1.0 x 10^{-2} M (d) 1.0 x 10^{-2} M to 1.18 x 10^{-2} M (e)1.18 x 10^{-2} M to 1.32 x 10^{-2} M (f) 1.32 x 10^{-2} M to 1.5 x 10^{-2} M . The first spectrum in (b) is the same as the last spectrum in (a), the first spectrum in (c) is the same as the last spectrum in (b), and so on.

A gradual disappearance of the split Q band and the appearance of a new single Q band that was blue shifted compared to the original split Q band were observed on further addition of Pd(II) ions with isobestic point around 710 nm, Fig. **3.11e**. The final spectrum in Fig. **3.11f** is typical of a metallated phthalocyanine complex **[101]**, and suggests the formation of a symmetrically substituted PdPc complex. No further spectral changes were observed on addition of more Pd ions. A blank test was conducted where a blank ethanol was titrated against the Pc solution, the only change observed was the reduction in absorbance of the Pc without the appearance of a new peak and the Pc started to crystallize out of solution. This might be due to insolubility of the Pc in ethanol.

For equilibrium studies, the steady increase in absorbance of the Q band of the Pc product formed with increase in Pd (II) ion concentration was noted and used in the determination of the binding constants as well as number of bound Pd (II) ions, according to equation 3.1:

$$\log\left[\frac{(A_{eq}-A_o)}{(A_\infty-A_{eq})}\right] = \log K + n\log[Pd^{2+}] \qquad 3.1$$

where A_{eq} is the equilibrium absorbance of the Pd-bound Pc (product); A_o, the initial absorbance before the addition of $PdCl_2$, and A_∞, the maximum attainable absorbance of the product. K is the binding constant, and n is the number of bound Pd(II) ions.

In the equilibrium studies for the binding of Pd(II) ions to complex **13a**, a plot $\log[(A_{eq} - A_o)/(A_\infty - A_{eq})]$ versus $\log[Pd^{II}]$ (**Fig. 3.12**), gave an equilibrium constant of $K = 1.2 \times 10^9$ $dm^3\ mol^{-1}$ and n of 5, thus showing that five Pd(II) ions are coordinated to the to the Pc at the end of the reaction.

The possible processes occurring during the addition of Pd ion to solutions of **13a** are shown by **Scheme 3.7**.

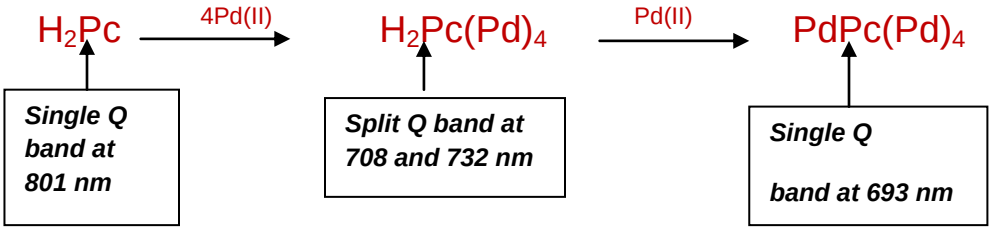

Scheme 3.7: Possible Processes involved in Pd(II) coordination to 13a.

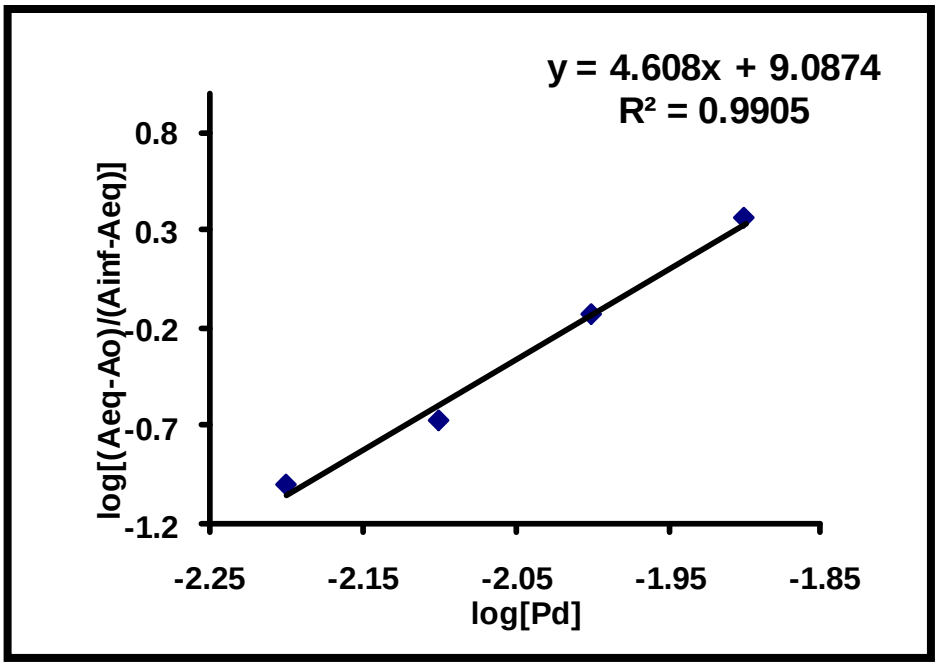

Figure 3.12: Plot of $\log[(A_{eq} - A_o)/(A_\infty - A_{eq})]$ versus $\log[Pd^{II}]$ for complex 13a in DCM.

When a large excess of $PdCl_2$ was added to **13a**, spectral changes shown in **Fig. 3.13** were observed, these consisted of direct formation of the final spectrum in **Fig. 3.11**. These changes occurred with time allowing for the calculation of rate constants assuming first order kinetics since Pd(II) is in excess. The rate constants were obtained by first plotting absorbance versus time for each concentration of Pd(II) (ranging from 1.5×10^{-3} to 5.0×10^{-3}) to obtain initial rates, the latter were then plotted against [Pd(II)] (**Fig. 3.13** inset) to get the rate constant from the slope using least square analysis. The value of the rate constant was 1.38×10^{-5} $dm^3\ mol^{-1}\ s^{-1}$. When low concentrations (< 1×10^{-4} M) of Pd(II) ions were employed for complex **13a**, changes with time observed in **Fig. 3.13** were not observed probably due to the slow nature of the spectral changes.

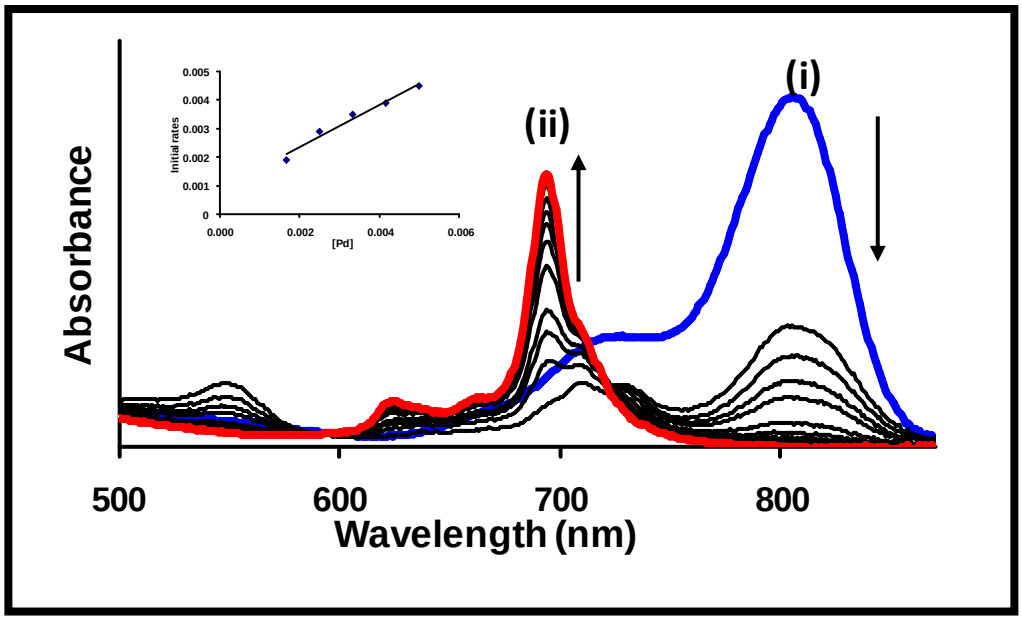

FIG.3.13: UV-Vis spectral changes observed on addition of excess $PdCl_2$ in ethanol concentration = 3 x 10^{-3} M) to a solution of 13a (1 x 10^{-5} M) in DCM. (i) Before and (ii) after addition of $PdCl_2$. Inset : Plot of initial rates versus the concentration Pd.

3.2.2. Metal-free peripherally substituted octapentylthiophthalocyanine (14a).

The spectra generated on the addition of Pd(II) ions to complex **14a** are shown in **Fig. 3.14**. For **14a**, The Q band is split since this complex is blue shifted compared to **13a**. Non-peripherally substituted MPc complexes show more red shift compared to peripherally substituted. The absorption spectrum of the Pc before the addition of Pd(II) ions is shown in **Fig 3.14a(i).** With the addition of Pd(II) ions the intensity of the peaks at 693 nm and 731 nm decreased and a new single peak appeared at 714 nm **(Fig. 3.14a(ii))**.

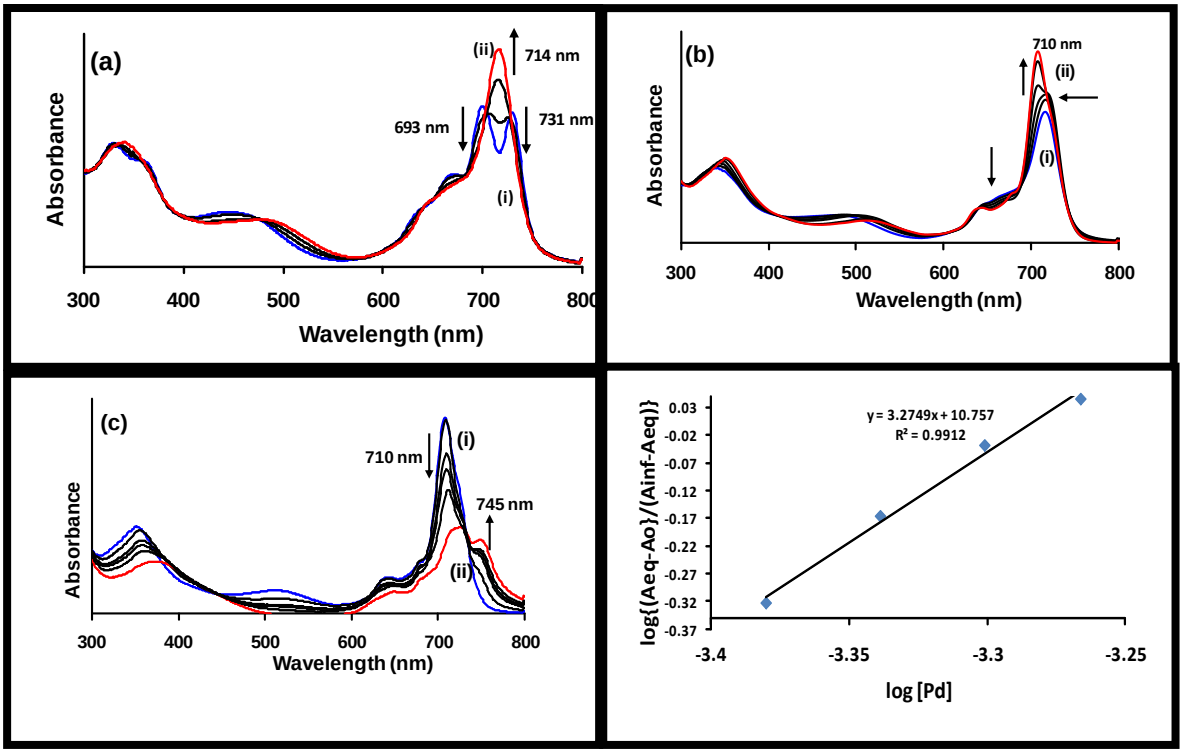

Figure 3.14: UV-Vis spectral changes observed on addition of $PdCl_2$ in ethanol to complex 14a (concentration = 5 x 10^{-6} M) in DCM. Concentration of $PdCl_2$ (a) 4.00 x 10^{-4} M to 4.61 x 10^{-4} M, (b) 4.61 x 10^{-4} M to 5.06 x 10^{-4} M, (c) 5.06 x 10^{-4} M to 5.5 x 10^{-4} M. The first spectrum in (b) is the same as the last spectrum in (a), the first spectrum in (c) is the same as the last spectrum in (b). (d) Plot of $\log[(A_{eq,} - A_o)/(A_\infty - A_{eq})]$ versus $\log[Pd^{II}]$ for complex 14a in DCM.

This spectrum resembles that of MPc suggesting the insertion of the metal into the centre of the Pc ring. The spectral changes could not be due to peripheral attachment of the Pd ions on the ring since a split Q band would still be observed due to loss of symmetry that would accompany such peripheral binding. The ^{1}H NMR spectra of the complex formed here also show change in chemical shift of some of the peaks due to change in electronic distribution of the complex on coordination with Pd ions. The aromatic and S-CH_2 protons did not show significant shift while the aliphatic and methyl protons were observed as mutiplets and triplets at 1.24 -1.19 ppm and 1.08 – 0.91 ppm integrating to 48 and 24 protons respectively. Elemental analysis of the complex at this stage confirmed the coordination of one Pd(II) ion, most probably into the center of

the ring hence no splitting in the Q band. The same type of split that was observed in the IR spectrum of **13a** was also noticed in the spectrum of **14a** at 935, 868 and 749 cm^{-1}.

Further addition of Pd(II) ions resulted in increase in the intensity accompanied by blue-shifting of the peak at 714 nm **(Fig. 3.14b)** to 710 nm with clear isobestic point at 680 nm. The blue shifting is as a result of the binding of Pd(II) ions to the peripheral sulphur, which engages the lone pair of electrons on sulphur and therefore cancels their mesomeric contribution to the ring electron density. As the addition of Pd(II) ions continued the broad peak around 710 nm started disappearing and a split band emerged at 720 and 745 nm as shown in **Fig. 3.14c.** This spectroscopic response might be due to unsymmetric substitution of Pd(II) ions. As was the case with complex **13a**, no further spectral changes were observed on addition of more Pd ions. The number of Pd(II) ions bound to the Pc and equilibrium constant was determined for complex **14a** using **Eqn.3.1** and **Fig. 3.14d**.

A plot $\log[(A_{eq}, - A_o)/(A_\infty - A_{eq})]$ versus $\log[Pd^{II}]$ **(Fig. 3,14d),** gave an equilibrium constant of $K = 5.7 \times 10^{10}$ dm^3 mol^{-1} and n of 3 for **14a**, thus showing that three Pd(II) ions are coordinated to the to the Pc at the end of the reaction. Probably the two at the periphery coordinated to adjacent sulphur instead of opposite ones giving rise to the loss of symmetry. The possible processes occurring during the addition of Pd ion to solutions of **14a** are shown by **Scheme 3.8**.

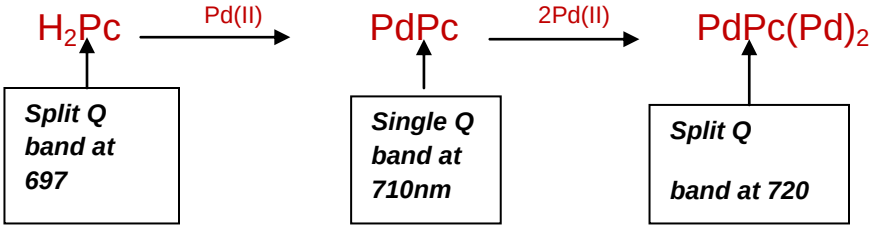

Scheme 3.8: Possible Processes involved in Pd(II) coordination to 14a.

The nature of Pd(II) binding differ between complexes **13a** and **14a** in that in **13a**, five Pd ions are coordinated, while for complex **14a** three Pd ions are coordinated. The differences in the binding abilities of the two compounds (**13a** and **14a**) could be due to

accessibility of binding sites. Also the modes of coordination of Pd(II) ions may be different for peripherally (**14a**) and non-peripherally (**13a**) substituted complexes since in the latter there is a possibility of coordination between pentylthio groups on adjacent benzene groups.

3.2.3. Palladium octapentylthiophthalocyanine complexes 15a and 17a.

Both **13a** and **15a** are non-peripherally substituted, however **15a** has a central Pd(II) ion unlike **13a** which is unmetalated. The same applies to **14a** and **17a**, which are both peripherally substituted, but the latter has a central Pd(II) ion and the former is unmetalated.

Fig. 3.15a(i) shows the spectra of **15a** before and after addition of Pd(II) ions. On addition of Pd(II) ions, reduction in intensity coupled with blue shifting from 750 nm to 718 nm of the Q band was observed **(Fig. 3.15a(ii)).**

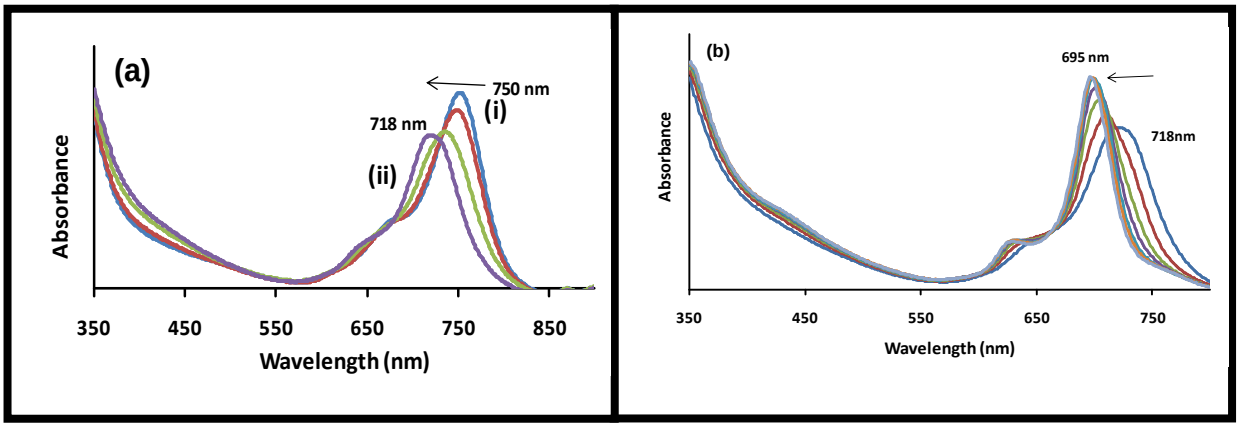

Figure 3.15: UV-Vis spectral changes observed on addition of $PdCl_2$ in ethanol to complex 15a (concentration = 5 x 10^{-6} M) in 1-chloronaphthalene. Concentration of $PdCl_2$ (a) 9.00 x 10^{-5} M to 4.00 x 10^{-4} M (b) 4.00 x 10^{-4} M to 1.5 x 10^{-3} M. The first spectrum in (b) is the same as the last spectrum in (a).

Effect of further addition of Pd(II) ions is depicted in **Fig. 3.15 (b),** and consists of continued blue shifting of the Q band from 718 nm to 695 nm and there is narrowing of the Q band and its increase in its intensity. The continuous shift towards the blue is consistent with the engagement of S lone pairs in the substituents, thereby reducing the

ring electron density and consequently causing the blue shift. The Q band maximum at 695 nm is similar to the final spectrum obtained for **13a** following addition of Pd(II) ions (Q band at 693 nm), suggesting that the final complexes are the same.

A plot $\log[(A_{eq,} - A_o)/(A_\infty - A_{eq})]$ versus $\log[Pd^{II}]$ for **15a (Fig. 3.16),** gave an equilibrium constant of K = 1.66 x 10^{13} dm^3 mol^{-1} and n of 4, thus showing that 4 Pd(II) ions are coordinated to the to the Pc at the end of the reaction, with the equilibrium favouring the formation of the complex with four Pd(II) ions coordinated all at the ring in a symmetrical fashion since the Q band of the final spectrum is not split.

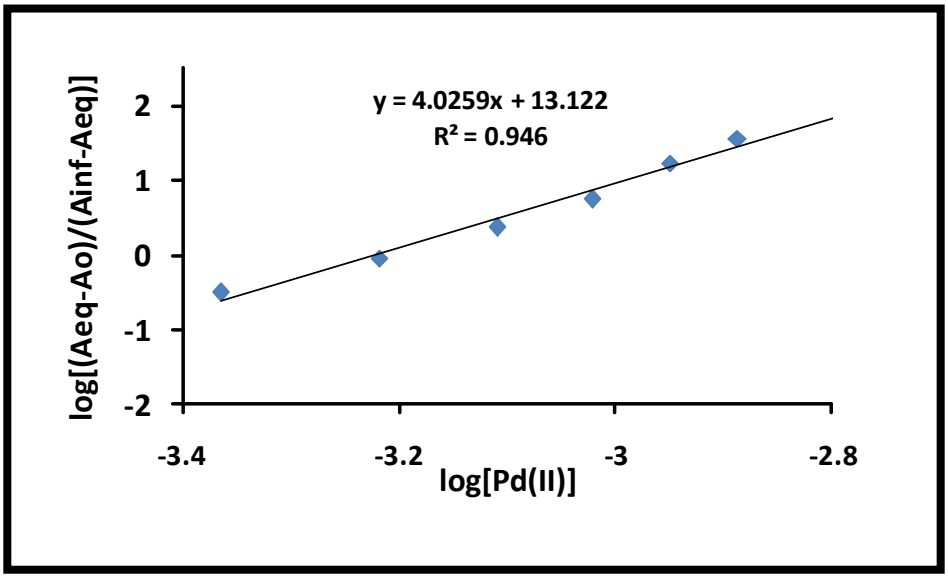

Figure 3.16: Plot of $\log[(A_{eq,} - A_o)/(A_\infty - A_{eq})]$ versus $\log[Pd^{II}]$ for complex 15ain DCM

For complex **17a** which is peripherally substituted, **Figs. 3.17a** and **3.17b** show that on titration with Pd(II) ions, the final spectrum shows a split Q band, suggesting unsymmetrical substitution by the Pd(II) ions as was the case with **14a**, which is also peripherally substituted. Thus the point of substitution (peripheral or non-peripheral) determines the nature of binding (symmetrical or non-symmetrical) of Pd(II) ions to the MPc complexes.

The possible processes occurring during the addition of Pd(II) ion to solutions of complex **15a** are shown by **Scheme 3.9**.

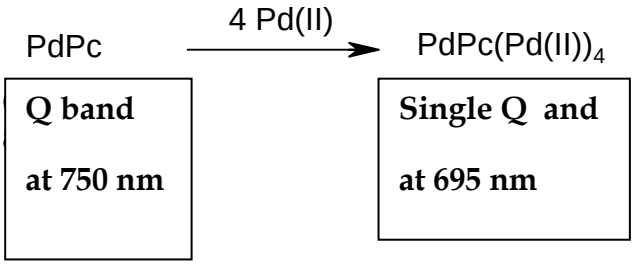

Scheme 3.9: Possible Processes involved in Pd(II) coordination to complex 15a

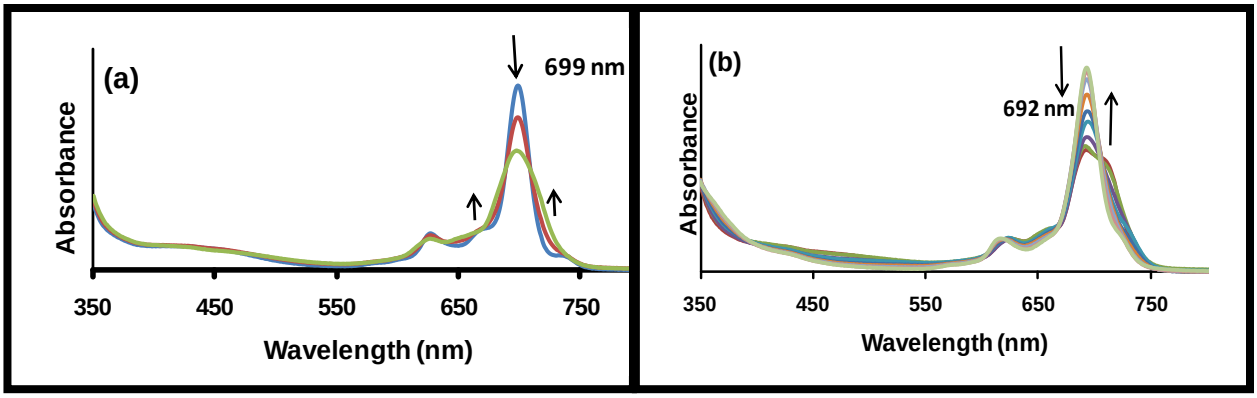

Figure 3.14:UV-Vis spectral changes observed on addition of $PdCl_2$ in ethanol to complex 17a (concentration = 8 x 10^{-6} M) in 1-chloronaphthalene. Concentration of $PdCl_2$ (a) 3.00 x 10^{-5} M to 2.50 x 10^{-4} M (b) 2.50 x 10^{-4} M to 1.5 x 10^{-3} M. The first spectrum in (b) is the same as the last spectrum in (a).

Chapter 4

Photophysical and Photochemical Studies

4.1. Photophysical Properties

4.1.1. Fluorescence spectra and quantum yield.

4.1.1.1. Metal-free phthalocyanines derivatives (H_2Pc)

The absorption and fluorescence excitation spectra of the β-substituted unmetallated derivatives (**14a**, **14b**, **14c**, **14d** and **14e**) are almost identical, using **14d (Fig. 4.1a)** and **14b (Fig. 4.1b)** as examples, implying that the absorbing species do not differ much from the fluorescing species.

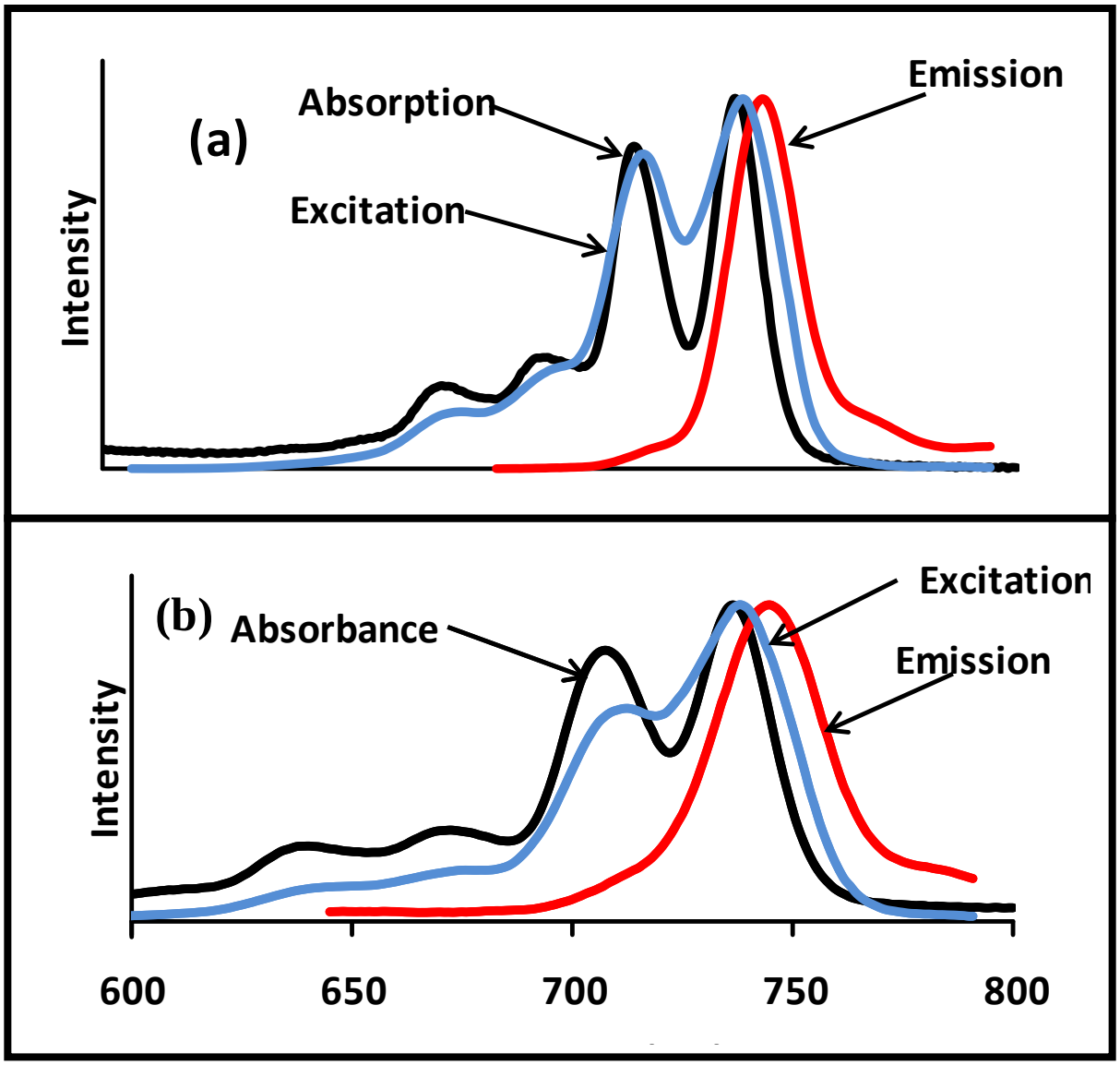

Figure 4.1: Absorption and fluorescence (excitation and emission) spectra of (a) 14d and (b) 14b in 1-CNP Excitation wavelength = 620 nm.

Metal free Pcs are known to fluoresce with only one main peak in non-aqueous media which has been assigned as the 0-0 transition of the fluorescence **[287]**, hence the observation of an unsplit fluorescence Q band in **Figs. 4.1a** and **b**. For complex **14b**, **Fig. 4.1b**, there is peak-to-peak matching between excitation and absorption spectra, but there is a decrease in intensity in the high energy band of the split pair. The excitation and emission of the non peripherally substituted thio derivatives (**13a-c**) were too weak to be analysed. The α substituted analogues on excitation probably undergo symmetry changes to complexes that are short lived compared to the β-substituted derivatives.

4.1.1.2. Palladium phthalocyanine derivatives (PdPc)

The absorption and fluorescence excitation spectra of thio-derivatised PdPc (**17b** and **17c)** are also almost identical **(Fig. 4.2)**, implying that the molecules absorbing species do not differ much from the fluorescing species; the fluorescence spectra are mirror images of the absorption spectra, **(Fig. 4.2)**. The fluorescence spectra are very weak compared to the metal-free derivatives due to the heavy atom effect of palladium.

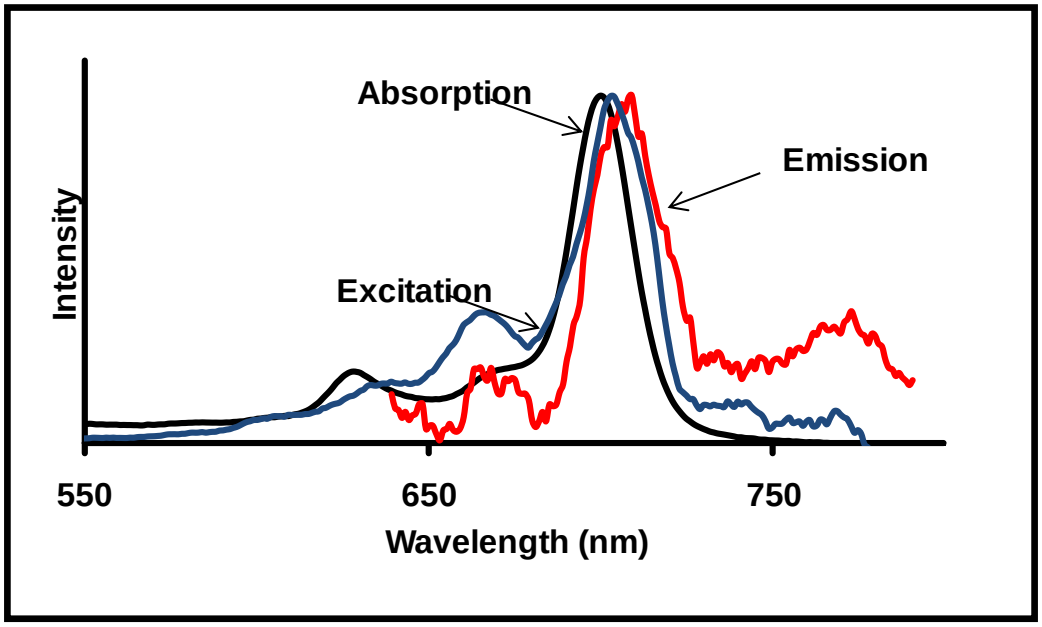

Figure 4.2: Absorption and fluorescence (excitation and emission) spectra of PdPc complex 17c in 1-CNP. Excitation wavelength = 630 nm

The fluorescence excitation spectra of the pentylthio and benzyloxyphenoxy derivative of PdPc **(17a and 17e)** are red shifted from their absorption spectra by 40 nm and 11 nm respectively **(Table 4.1),**

Table 4.1. Fluorescence data for the phthalocyanines (13 to 18) in 1-CNP

Complexes	Substituents	$\lambda_{Q(abs)}$ (nm)	$\lambda_{Q(exc)}$ (nm)	$\lambda_{Q(emm)}$ (nm)
13a(M = H_2)	S-C_5H_{11}	813	-	-
13b(M = H_2)	S-C_8H_{17}	813	-	-
13c(M = H_2)	S-$C_{12}H_{25}$	813	-	-
14a (M = H_2)	S-C_5H_{11}	707, 736	711, 738	745
14b (M = H_2)	S-C_8H_{17}	707, 736	711, 738	745
14c (M = H_2)	S-$C_{12}H_{25}$	707, 736	711, 738	745
14d (M = H_2)	-O-C_6H_5	672,706	677, 711	720
14e (M = H_2)	-O-C_6H_4-O-CH_2- C_6H_5	674,708	674,709	716
16a (M = Ni)	S-C_5H_{11}	696	695,725	730
16b (M = Ni)	S-C_8H_{17}	707	662,699	740
16c (M = Ni)	S-$C_{12}H_{25}$	709	727	730
16d (M = Ni)	-O-C_6H_5	678	-	-
16e (M = Ni)	-O-C_6H_4-O-CH_2- C_6H_5	680	-	-
15a(M = Pd)	S-C_5H_{11}	750	-	-
15b(M = Pd)	S-C_8H_{17}	756	-	-
15c(M = Pd)	S-$C_{12}H_{25}$	756	-	-
17a(M = Pd)	S-C_5H_{11}	698	738	745
17b(M = Pd)	S-C_8H_{17}	698	701	707
17c(M = Pd)	S-$C_{12}H_{25}$	698	703	709
17d (M = Pd)	-O-C_6H_5	668	-	-
17e(M = Pd)	-O-C_6H_4-O-CH_2- C_6H_5	670	681	682
18d (M = Pt)	-O-C_6H_5	658	-	-
18e (M = Pt)	-O-C_6H_4-O-CH_2- C_6H_5	660	709	713[c]

$\lambda_{Q(abs)}$ = Q band absorption wavelength; $\lambda_{Q(exc)}$ = Q band excitation wavelength; $\lambda_{Q(emm)}$ = Q band emission wavelength. [c] due to demetallated species.

This suggests a change in geometry upon excitation. The excitation and emission spectra of complexes **15a-c** and **17d** were too weak to be analysed. The excitation and emission spectra of complexes **15a-c** and the complexes formed from the Pd ion binding effort were also too weak to analyze. This could be due to high number of Pd(II) quenching the excited state of the multinuclear complex and structure of the non-peripherally substituted derivatives.

4.1.1.3. Nickel phthalocyanine derivatives (NiPc)

For the NiPc derivatives, the fluorescence excitation spectrum of **16c (Fig. 4.3a)** is red-shifted by about 20 nm relative to that of the absorption spectrum, suggesting a change in geometry upon excitation.

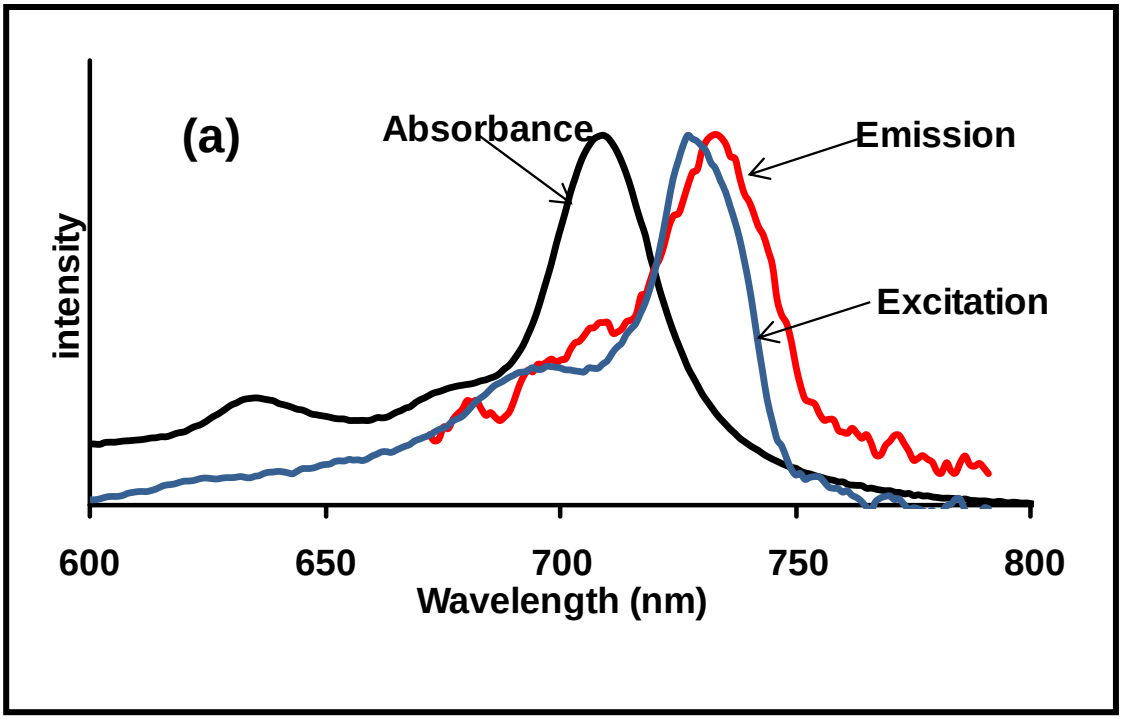

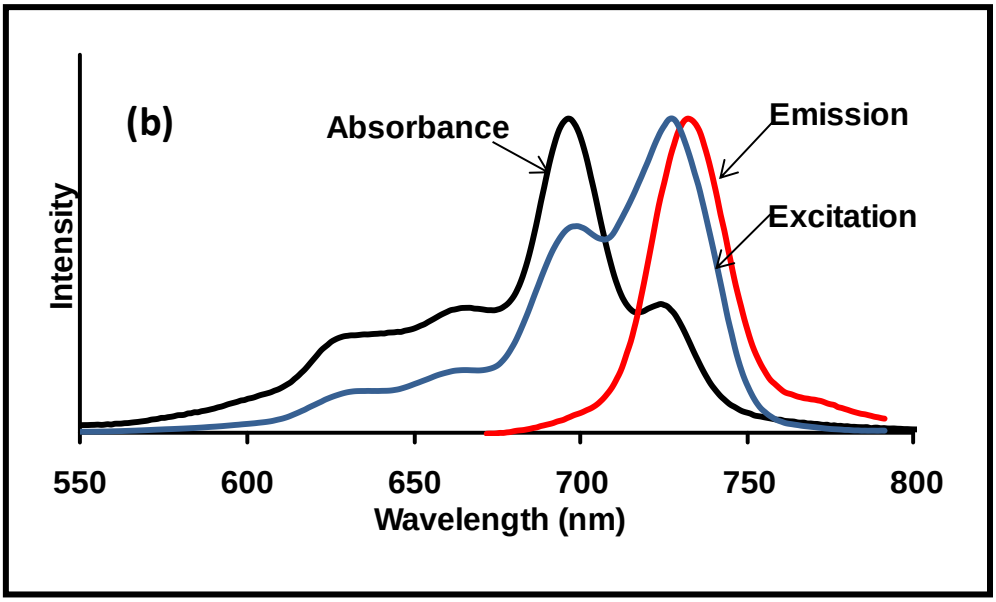

Figure 4.3: Absorption and fluorescence (excitation and emission) spectra of NiPc complexes (a) 16c and (b) 16a in 1-CNP. Excitation wavelength = 630 nm

In the case of **16a, 16b** and **16c,** the absorption and fluorescence excitation spectra are not similar; although there is almost a peak-to-peak matching, the intensities are reversed **(Fig. 4.3b),** which could be due to excitonic intensity borrowing and exchange between the two major transitions. The spectra of complexes **16d** and **16e** were too weak to be observed probably.

4.1.1.4. Platinum phthalocyanine derivatives (PtPc)

Since for the Pt analogue (**18e**), **Fig. 4.4,** the peak at 709 nm is due to partial demetallation discussed above, the excitation spectra is that of the unmetalated species which will fluoresce more efficiently than the metallated species. There will be more enhanced intersystem crossing in the metallated complex. The observed emission is that of the unmetallated species with emission Q band maximum of 713 nm which is not too different from that of unmetallated **14e** at 716 nm, **Table 4.1**. The enhanced intersystem crossing is responsible for lack of fluorescence for complex **18d** (**Table 4.1**), lending credence to the metal-free analogue as source of spectra in **Fig. 4.4**.

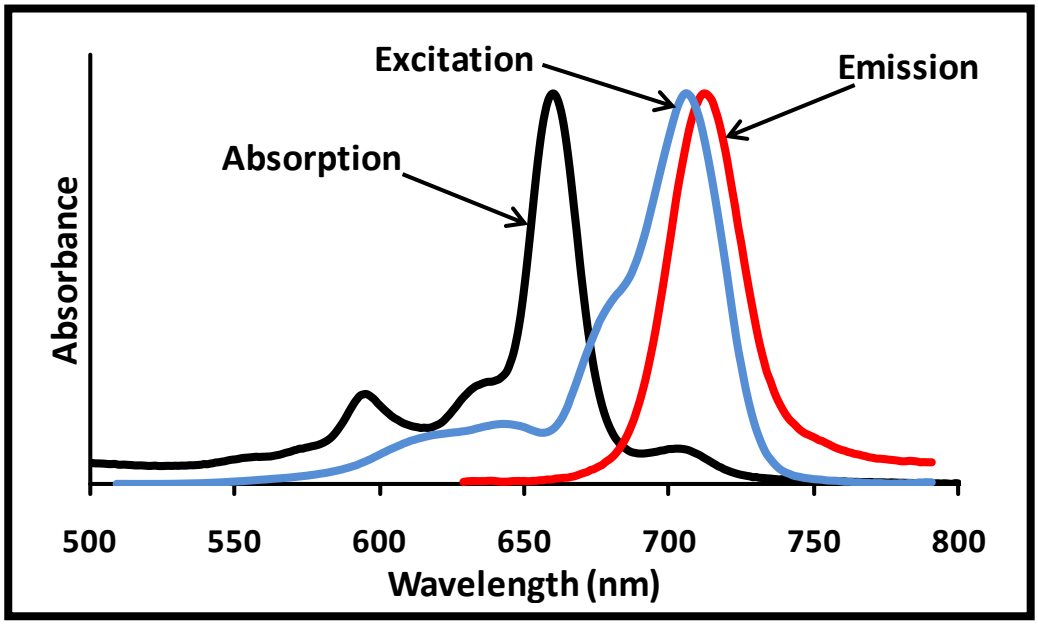

Figure 4.4: Absorption and fluorescence (excitation and emission) spectra of PtPc complex 18e in 1-CNP. Excitation wavelength = 620 nm

4.1.1.5. Aryloxo-derivatised MPcs Vs thio-derivatised MPcs

The excitation or emission spectra for **16d**, **16e** and **17d** were too weak to be analysed accurately while their thio-derivatised analogues (complex **16a-c** and **17a-c**) gave clear spectra. The implication of this is that excited states of phenoxy and benzyloxyphenoxy derivatised Ni, Pd and Pt phthalocyanines were quenched faster than alkylthio derivatised analogues (only for NiPc and PdPc complexes, attempts to synthesize PtPc alkylthio derivatives were not successful). This might be due to specific interactions between the central metals and phenoxy and benzyloxyphenoxy groups which quench the excited state faster than the alkylthio analogues. However, complex 18d did flouresce due to demetallation discussed above.

4.1.1.6. Fluorescence quantum yields

The fluorescence quantum yield (Φ_F) values of **14a**, **14b 14c,14d** and **14e**, in 1-CNP are, 0.10, 0.13, 0.15, 0.21 and 0.25 respectively, **Table 4.1** while those of the metallated derivatives are expectedly low (< 0.01 and 0.012), **18e** displayed a higher fluorescence quantum yield (Φ_F) which might be due to the demetalation discussed above, **Table 4.1**

The low fluorescence quantum yield observed for the PdPc and PtPc complexes is due to open-shell nature of the metals involved which promotes d-π interactions thereby quenching the singlet state of the complexes. Also the enhanced spin orbit coupling or low planarity might be responsible in lowering of fluorescence quantum yields **[288]**. It has also been reported that distortion in MPc complexes leads to low Φ_F values **[92]**. It is known that non-planar porphyrins have significantly lower Φ_F values than their planar counterparts **[288]**.

4.1.2. Triplet quantum yield and lifetime

4.1.2.1. Metal-free phthalocyanine derivatives (H_2Pc)

Both the triplet quantum yields and lifetimes were determined by laser flash photolysis. Transient spectrum **(Fig. 4.5)** of **14e** in 1-CNP showed a split Q band characteristic of unmetalated phthalocyanines. The triplet decay curve in **Fig. 4.6** obeyed first order kinetics suggesting minimum or absence of triplet–triplet recombination.

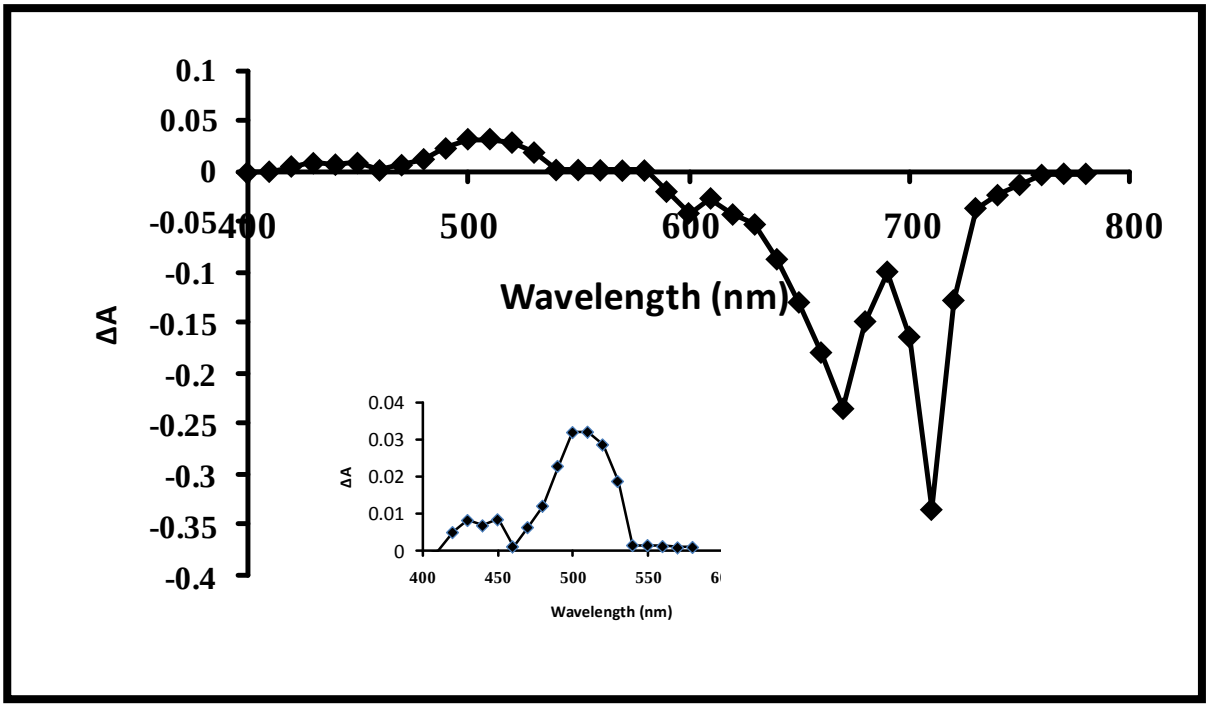

Figure 4.5: Transient absorption spectrum of 14e in 1-CNP at 520 nm. (Excitation wavelength = 707 nm). Insert: Transient absorption spectrum in the 500 nm region.

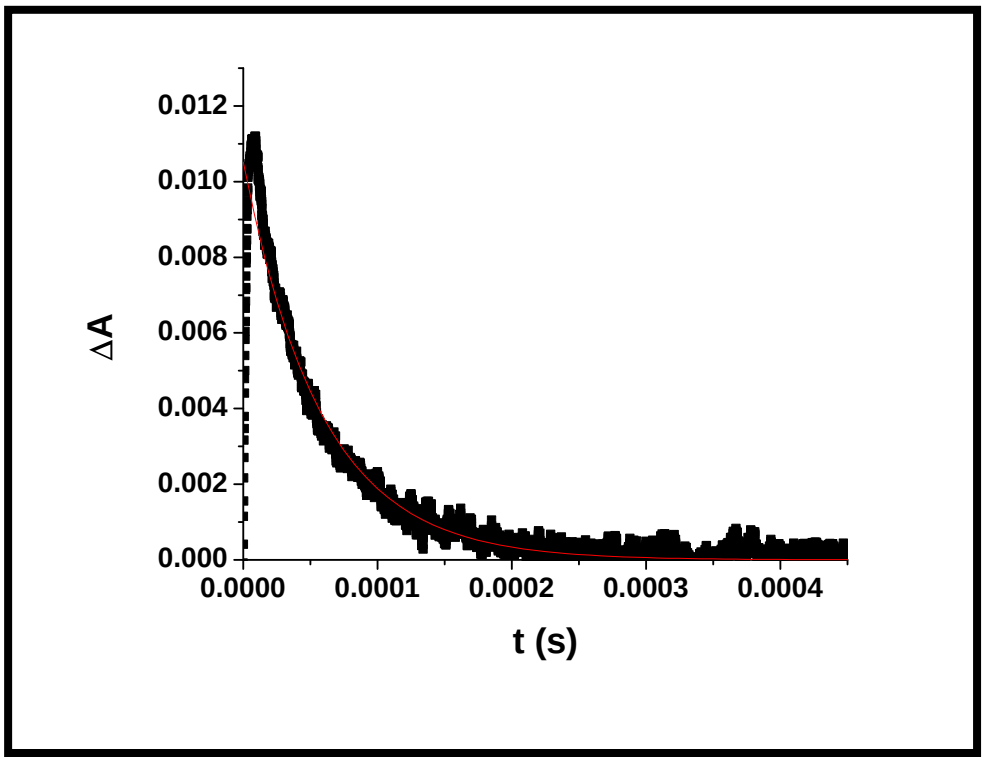

Figure 4.6: Triplet decay curve for 14d in 1-CNP. Excitation wavelength = 707 nm

The metal-free analogues (**13a, 13b, 13c, 14a**, **14b, 14c, 14d** and **14e**) gave Φ_T values of 0.33, 0.35, 0.31, 0.39, 0.40, 0.38, 0.40 and 0.47 with triplet lifetimes of 55, 49, 41, 62, 51, 44, 55 and 50 μs, respectively**, Table 4.2**.

Table 4.2: Photophysical and photochemical properties of aryloxo and thio-derivatised phthalocyanines. Solvent = 1-CNP. Bracket =Done in DCM

Compounds	Φ_F	Φ_T	τ_T(μs)	Φ_Δ	S_Δ	$\Phi_P(10^{-7})$
13a(M = H_2)	-	0.33	55	0.03	<0.1	131
13b(M = H_2)	-	0.35	49	0.03	<0.1	154
13c(M = H_2)	-	0.31	41	0.01	<0.1	149
14a (M = H_2)	0.10	0.39	62	0.04	0.1	155
14b (M = H_2)	0.13	0.40	51	0.04	0.1	159
14c (M = H_2)	0.15	0.38	44	0.04	0.11	173
14d (M = H_2)	0.21	0.40	55	0.05	0.13	99
14e (M = H_2)	0.25	0.47	50	0.01	0.02	10
16a (M = Ni)	< 0.01	0.09	6	<0.01	<0.1	187
16b (M = Ni)	<0.01	0.04	4	<0.01	0.25	192
16c (M = Ni)	<0.01	0.04	2	<0.01	0.25	19
16d (M = Ni)	-	-	-	<0.01	-	181
16e (M = Ni)	-	-	-	<0.01	-	198
15a(M = Pd)	-	0.42	13	0.39(0.34)	0.93	10
15b(M = Pd)	-	0.41	11	0.37(0.34)	0.90	9
15c(M = Pd)	-	0.39	08	0.37(0.36)	**0.95**	9
17a(M = Pd)	< 0.01	0.47	15	0.42(0.38)	0.89	10
17b(M = Pd)	<0.01	0.42	12	0.40(0.36)	0.95	11
17c(M = Pd)	<0.01	0.40	10	0.39(0.39)	0.98	13
17d (M = Pd)	-	0.51	23	0.49(0.30)	0.96	1
17e(M = Pd)	< 0.01	0.65	20	0.43(0.32)	0.66	2
18d (M = Pt)	-	0.62	17	0.42(0.29)	0.68	1
18e (M = Pt)	0.012	0.73	13	0.39(0.26)	0.53	1

4.1.2.2. Palladium and Platinum phthalocyanine derivatives (PdPc and PtPc)

Transient spectrum **(Fig. 4.7)** of complex **15a** in 1-CNP showed a single Q band characteristic of metallated phthalocyanines. The transient absorption spectrum is also similar to the its ground state absorption spectrum with Q band of both at 756 nm suggesting no change in symmetry at the excited state. The triplet decay curve of **15a** in **Fig. 4.8** also obeyed first order kinetics suggesting minimum or absence of triplet–triplet recombination.

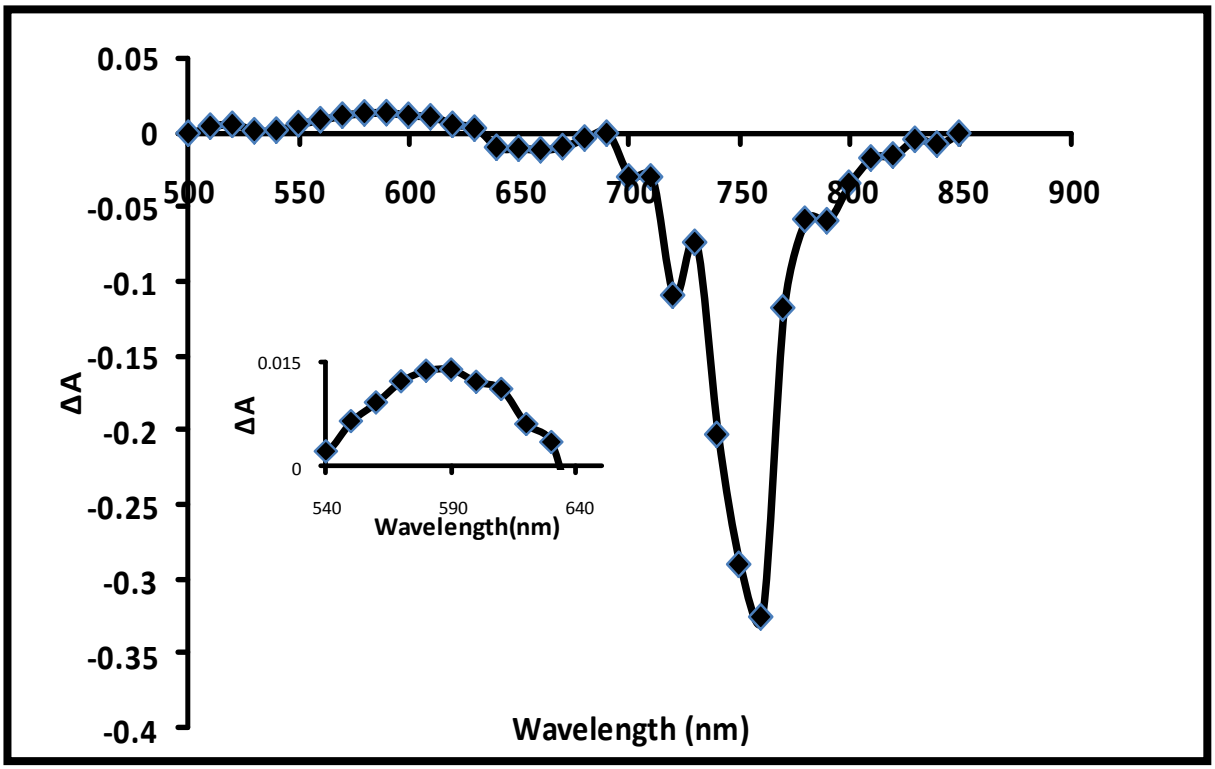

Figure 4.7: Transient absorption spectrum of PdPc complex 15a in 1-CNP (Excitation wavelength = 750 nm). Insert: Transient absorption spectrum in the 600 nm region.

While the metal-free octaphenoxy phthalocyanines, (**14d**) showed a triplet quantum yield (Φ_T) of 0.40, the MPc complexes **17d** (Pd) and **18d** (Pt) containing the same substituent, gave Φ_T = 0.51 and 0.62, respectively. The increase in the triplet quantum yield of the palladated and platinated octaphenoxy phthalocyanines (compared to unmetalated derivative, **14d**) is due to enhanced intersystem crossing. The triplet

lifetimes of the molecules reflect their open-shell nature. **14d** which was not metallated showed a lifetime of 55 μs while **17d** (Pd) and **18d** (Pt) showed lifetimes of 23 μs and 17 μs respectively, **Table 4.2**, demonstrating the effect of d-π interaction characteristics of open-shell metal phthalocyanines, this normally results in lower excited state lifetime.

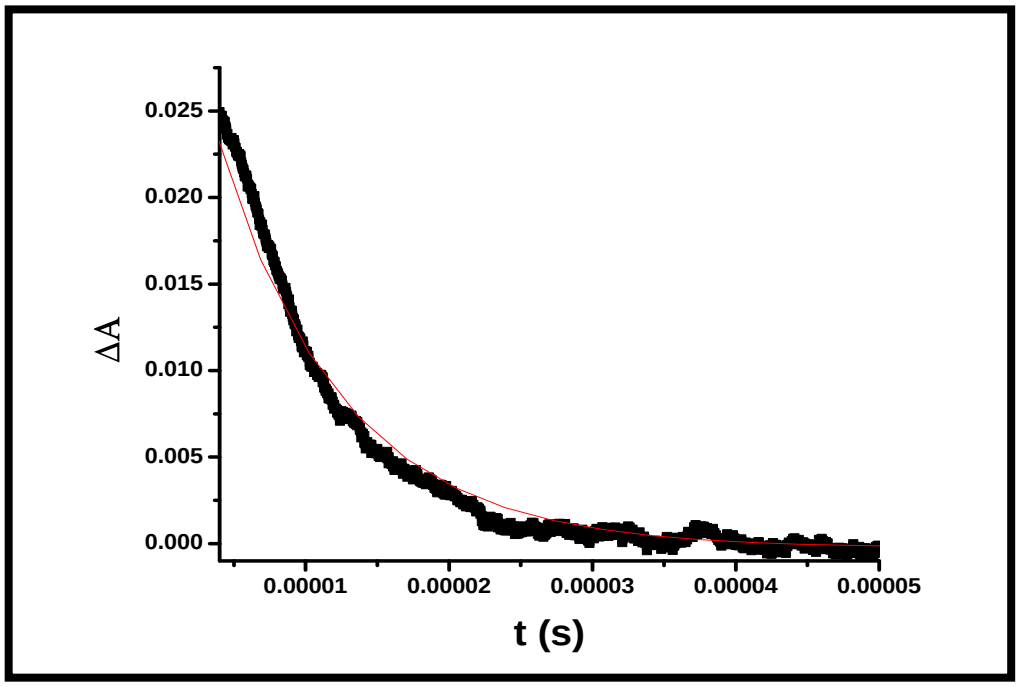

Figure 4.8: Triplet decay curve for PdPc complex 15a in 1-CNP (Excitation wavelength =750 nm)

The same trend was observed for octabenzyloxyphenoxy phthalocyanines, where the metal-free analogue (**14e**) has Φ_T = 0.47 but complexes **17e** (Pd) and **18e** (Pt) showed Φ_T = 0.65 and 0.73 respectively **(Table 4.2)** due to enhancement of intersystem crossing by the presence of Pd and Pt. The lifetime followed the same pattern as octaphenoxy derivatives with **14e**, **17e** and **18e,** showing lifetimes of 50 μs, 20 μs and 13 μs respectively. Due to the same reason discussed above, insertion of palladium metal into the thio-derivatised phthalocyanine ligands enhanced the triplet yields but also reduced the lifetime of the molecules compared to H_2Pc counterparts, with complexes **15a**, **15b**, **15c**, **17a**, **17b** and **17c** showing triplet quantum yields to 0.42, 0.41, 0.39, 0.47, 0.42 and 0.40 and triplet lifetimes to 13, 11, 8, 15, 12 and 10 μs, respectively, **Table 4.2**. The alkylthio derivatised phthlocyanines showed triplet quantum yields lower than their

oxy-derivatised counterparts while the effect of chain length did not give any consistent trend.

4.1.2.3. Nickel phthalocyanine derivatives (NiPc)

The Ni(II)Pc analogues (complexes **16d and 16e**) did not show any triplet absorption peak suggesting an extremely short triplet lifetime or yield. Insertion of nickel into the cavities of the rest of the Pc ligands caused drastic reduction in Φ_T values of these molecules with complexes **16a**, **16b** and **16c** having triplet quantum yields of 0.09, 0.04 and 0.04 and reduced of lifetimes of 6, 4 and 2 μs respectively. Thus nickel analogues of the alkylthio derivatised phthalocyanines were found to be slightly photoactive while that of oxy-derivatised showed no photoactivity. This is consistent with the observation in fluorescence studies where thio-derivatised NiPcs gave clearer emission and excitation spectra compared to their aryloxo-derivatised analogues. The non-display of photoactivity by nickel oxy-derivatised phthalocyanines is consistent with what was observed for nickel octabutoxyphthalocyanines and nickel octabutoxynaphthalocyanines **[289]** that made them good candidates for photothermal therapy (PTT). This suggests a specific interaction between aryloxy substituents and Ni(II) that efficiently quenches the excited states to a larger extent than the alkylthio substituents. The multinuclear complexes showed no triplet absorption peak probably because of low triplet lifetime.

4.2. Photochemical Studies

4.2.1. Singlet oxygen quantum yield

Singlet oxygen quantum yields were determined in 1-CNP using DPBF as a chemical quencher. The disappearance of DBPF was monitored using UV–Vis spectrometer **(Fig. 4.9)**. Many factors are responsible for the magnitude of the determined quantum yield of singlet oxygen including; triplet excited state energy, ability of substituents to quench the singlet oxygen, the triplet excited state lifetime and the efficiency of the energy

transfer between the triplet excited state and the ground state of oxygen. Based on the heavy atom effect, it would be expected that the PtPc complexes would give larger Φ_Δ values. However, the Φ_Δ value is slightly higher for PdPc **17e** compared to the corresponding PtPc complex **18e**. Complexes **17d** and **18d** show almost similar Φ_Δ values. The trend in the production of singlet oxygen quantum yields (Table 4.2) is as follows for the phenoxy and benzyloxyphenoxy complexes: Pd > Pt > H_2 > Ni. This trend shows the PdPc derivatives to have higher Φ_Δ values than the Pt complexes, yet the latter showed larger triplet quantum yields. This suggests that the PtPc complexes are less efficient in generating singlet oxygen than the corresponding PdPc derivatives, with low S_Δ values for the former complexes. The magnitude of S_Δ (= Φ_Δ/ Φ_T) represents the efficiency of quenching of the triplet excited state by singlet oxygen. Chain length and type of substituent did not show any consistent trend in Φ_Δ values. The variation in the Φ_Δ values for the alkylthio complexes was: Ni < Metal-free < Pd. The Φ_Δ values of all PtPc and PdPc complexes are however still sufficient for photosensitised transformation of 4-NP.

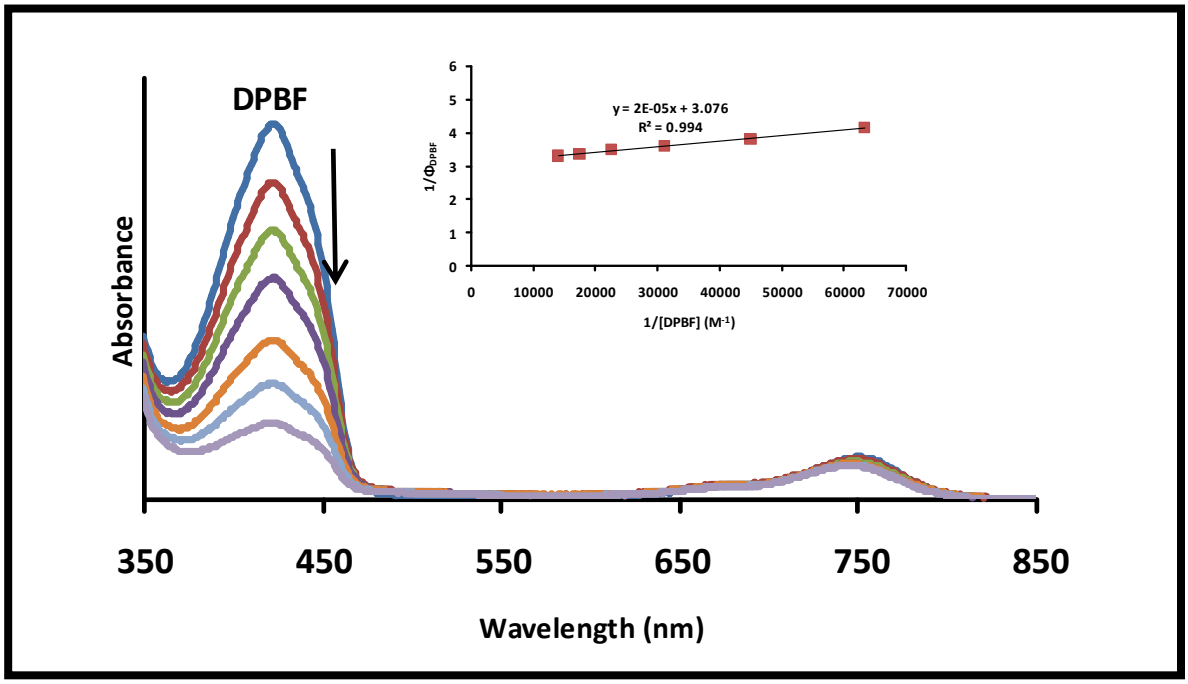

Figure 4.9: Typical spectrum for the determination of singlet oxygen quantum yield for PdPc complex 15a in 1-CNP.

Based on the all the photophysical and photochemical results, all the palladium and platinum phthalocyanines showed enough potential for application as photosensitisers while the metal-free and nickel analogues proved to be unsuitable for further study. Singlet oxygen quantum yields of PdPc and PtPc were also investigated in DCM since this solvent is more suitable than 1-CNP for UV-Vis monitoring of photosensitised oxidation reaction of phenolic pollutants. Due to the aggregation of these complexes in DCM, their quantum yields in DCM are slightly lower than in 1-CNP for PdPc. The values in DCM ranged between 0.32 and 0.39 while for PtPc the reduction is more significant, **Table 4.2**.

4.2.2. Photodegradation quantum yields (Φ_P)

Investigation of photodegradation of MPc complexes provides information on the stability of these derivatives under intense light. It is characterized by the decrease in absorption intensity, in the Q band region, without the appearance of new bands in the visible region on exposure of the MPc to intense light. The Φ_P values are especially important when considering complexes that may be applied as photocatalysts for the degradation and transformation of pollutants such as phenols and its derivatives. This investigation was undertaken here to determine the effect of Ni, Pd and Pt metals on the photostability of the phthalocyanine ligands. **Fig. 4.10** (complex **15a**) shows typical spectral changes that are observed during the photodegradation of MPcs.

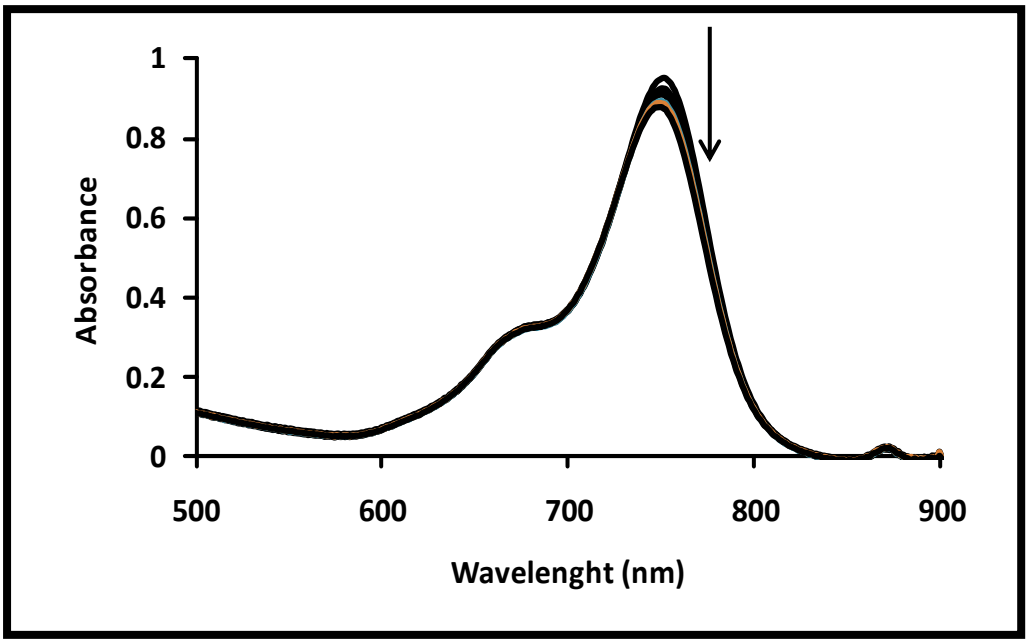

Figure 4.10: Photodegradation spectral changes of complex 15a in 1-CNP (Initial concentration = ~ 5.0 x 10^{-5} M).

As shown in **Table 4.2**, the insertion of Ni(II) into the cavity of the phthalocyanine ligands produced complexes with reduced photostability in **16a** and **16b**. **14a-e** showed quantum yield in the range from 9.9 x 10^{-6} and 1.7 x10^{-5} while the Ni(II) derivatives (complex **16a-e**) had yields in the range of 1.9 x $10^{-6}$and 1.98 x10^{-5}. Insertion of Pd(II) and Pt(II) into the Pcs cavity resulted in complexes with tremendously improved stability with Pt(II) giving a slightly better results than Pd(II), **Table 4.2**. The Φ_P of PdPc complexes ranged between 1 x 10^{-7} and 1.3 x 10^{-6} while PtPc complexes (**18d** and **18e)** had Φ_P of 1 x 10^{-7}. Phthalocyanines substituted at peripheral positions were also found to be less stable than those substituted at the non-peripheral positions.

Chapter 5

Photosensitised Oxidation Reactions

5.1. Homogenous photosensitized oxidation of 4-nitrophenol

Because of their high singlet oxygen quantum yields PdPc and PtPc were employed in this work while H_2Pc and NiPc were not used because of their low or non existent singlet oxygen quantum yields. The purpose of this study was to investigate the applicability of MPcs that gave promising photophysical and photochemical properties as photosensitisers of oxidation reactions using 4-nitrophenol(4-NP) as model pollutant. UV-vis spectroscopy is a very easy method of monitoring reactions. Because of the intense absorption of 1-CNP (in which MPcs are not aggregated) in the UV region, where 4-NP absorbs, DCM was chosen as the reaction solvent.

Aggregation in MPc affects their photosensitization behavior. Aggregation in MPc complexes is judged by a broadened and split Q band, with the blue shifted component being due to the aggregate. All the complexes were aggregated in DCM **(Figs. 3.8b, 3.9b and 3.10b)** but were not aggregated in 1-chloronaphthalene (which was employed above for photophysical studies). Singlet oxygen quantum yields of the chosen molecules were hence investigated in DCM and are shown in **Table 5.1** and discussed in chapter 4. The Φ_Δ values give an indication of the applicability of Pcs as photosensitisers. **Table 5.1** shows that all the complexes employed for photosensitization (PdPc and PtPc) gave reasonable Φ_Δ values and may be useful for phototransformation of phenols.

5.1.1. *UV/Vis Spectral changes*

These studies were carried out in DCM (in basic media using triethylamine as an organic buffer) since the phenolate ions, which are more oxidizable, are predominant in basic media (pKa 4-NP = 7.15) **[290]**. **Fig. 5.1** shows the spectral changes observed during homogenous photolysis of 4-NP in the presence of complex **17c** (as an example). There is a decrease in the absorbance (at 400 nm) of 4-NP during irradiation (with time) in the presence of complex **17c**. The absorbance of complex **17c** at 690 nm was relatively unchanged during the photolysis.

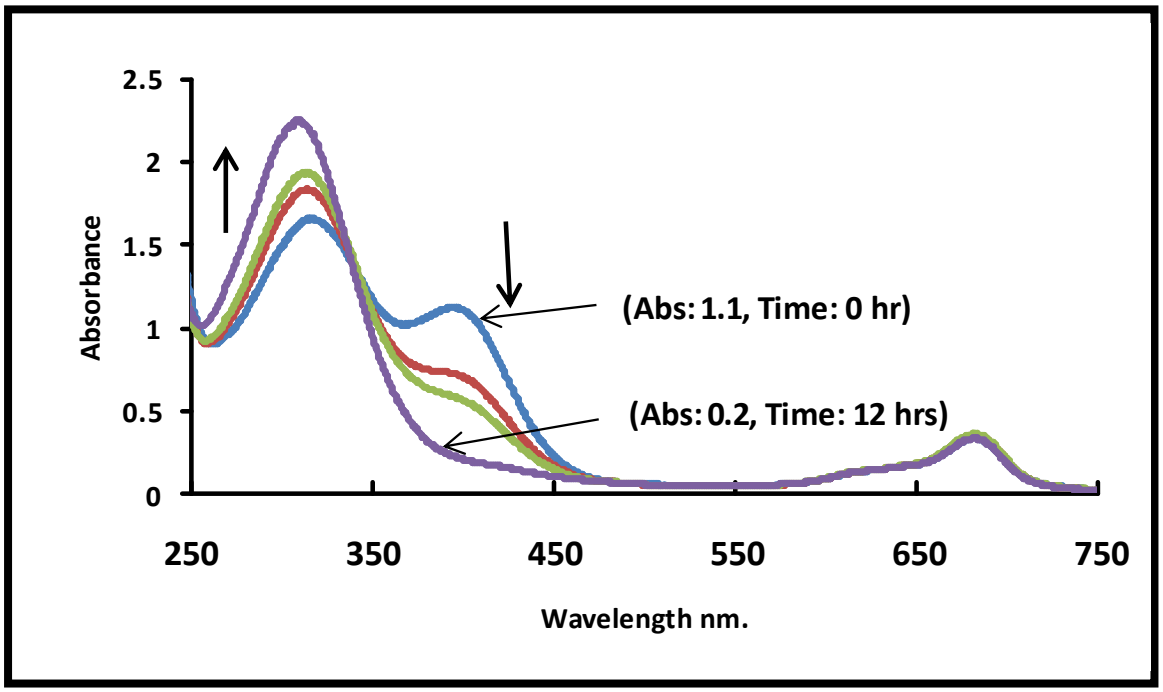

Figure 5.1: Electronic absorption spectral changes observed during the photolysis of 6.5×10^{-4} mol L^{-1} 4-NP in the presence of 350 mg L^{-1} of complex 17c in DCM.

The peak due to the phenolate ions at 400 nm started disappearing with simultaneous increase in the intensity of the peak at 260 nm due to the formation of the products. It has been reported before the peak near 300 nm is due to conversion of the phenolate ions to the protonated form **[290]**. However since we are working in basic media, the protonation reaction is not expected. The B band of phthalocyanines occurs in the 300 nm region hence complicating the spectra. Thus the disappearance of 4-NP rather than formation of products were employed for the studies in this work. The $\Phi_{4\text{-NP}}$ were calculated from the initial rate of disappearance of the 4-NP using **Eqn. 1.37 (**now **Eqn 5.1)** (where S (substrate) is replaced by 4-NP).

$$\Phi_{Poll} = \frac{[C_0 - C_t]V}{I_{abs}t} \qquad 5.1$$

Table 5.1 shows that the largest $\Phi_{4\text{-NP}}$ value was obtained for complex **17c**. Complexes **18e** and **18d** gave the lowest $\Phi_{4\text{-NP}}$ values. Low Φ_{Δ} values for Pt complexes would also give low $\Phi_{4\text{-NP}}$. Φ_{Δ} are also reduced by aggregated species which was more severe for **18e**.

The $\Phi_{4\text{-NP}}$ values obtained in the work are similar to those reported in aqueous media for the phototransformation of 4-NP using zinc tetrasulphonate phthalocyanines ($ZnPcS_4$), zinc octacarboxyphthalocyanines ($ZnPc(COOH)_8$) and a sulphonated ZnPc sample containing a mixture of differently substituted sulphonated derivatives ($ZnPcS_{mix}$) **[54]**. $ZnPc(COOH)_8$ showed the best catalytic behavior **[54]**, but degraded in solution, while the MPc complexes employed in this work do not show degradation.

The concentration of the catalyst will have an effect on phototransformation of the analyte. It is expected that the higher the catalyst concentration the higher the phototransformation of 4-NP. However as concentration of the photosensitisers increase, aggregation increases (which reduces catalytic activity of the photosensitizers). Experiments were conducted where Φ_{4-NP} values were calculated at different concentrations of the photosensitisers ranging, from 50 mg L^{-1} and 500 mg L^{-1}, **Fig. 5.2** (using **17c** as an example and [4-NP] = 3.5×10^{-4} mol L^{-1}).

Table 5.1: Complexes' photosensitisation parameters for phototransformation of 4-NP (3.5×10^{-4} M, DCM)

Complexes	Optimum photosensitiser concentration (mg L^{-1})	Φ_{4-NP} (10^{-4})	Φ_{Δ} (DCM)	$k_r = \frac{k_d}{\Phi_{\Delta} Slope}$ mol^{-1} L s^{-1}	$k_q + k_r$ mol^{-1} L s^{-1}
15a	200	12	0.34	1.71×10^5	1.7×10^9
15b	250	13	0.34	1.62×10^5	2.9×10^9
15c	300	15	0.36	1.97×10^5	4.2×10^9
17a	200	14	0.38	1.80×10^5	1.6×10^9
17b	300	15	0.36	1.70×10^5	2.7×10^8
17c	350	18	0.39	2.00×10^5	3.0×10^8
17d	250	9	0.30	1.40×10^5	3.1×10^8
17e	350	16	0.32	1.95×10^5	3.1×10^7
18d	200	0.3	0.29	2.30×10^5	4.0×10^8
18e	350	0.7	0.26	2.12×10^5	4.3×10^8

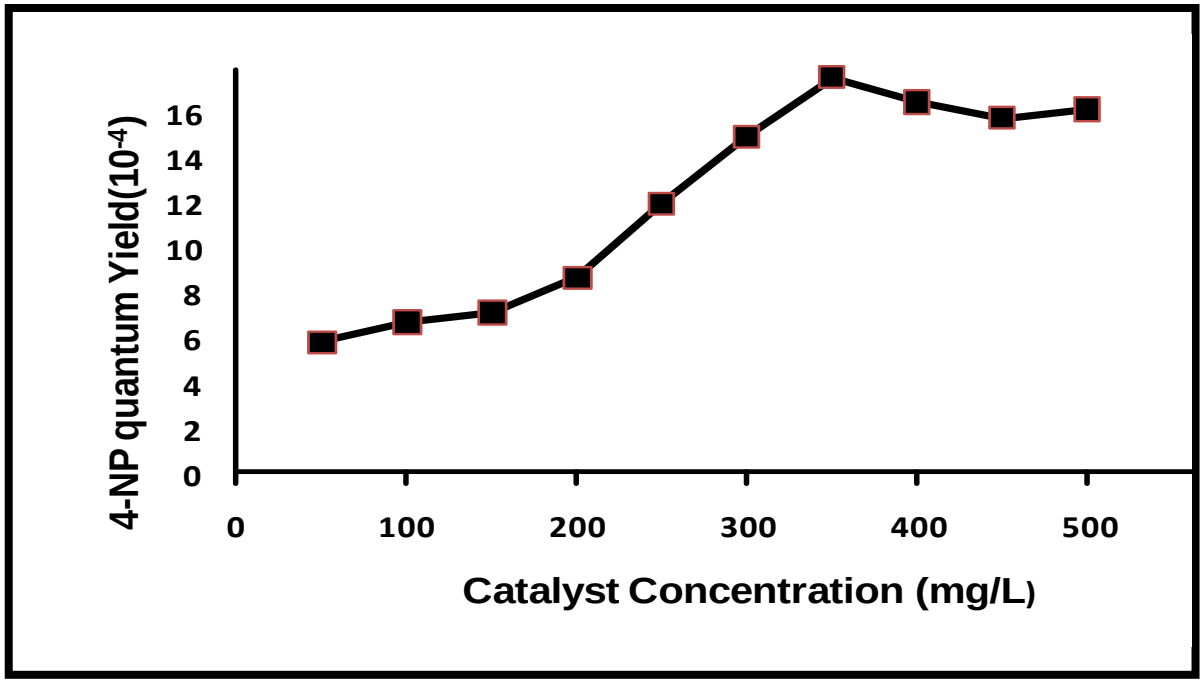

Figure 5.2: Plot of $\Phi_{4\text{-NP}}$ vs. concentration of photosensitisers to determine the optimum concentration of complex 17c for the phototransformation of 4-NP (3.5×10^{-4} mol L^{-1}) in DCM.

As the concentration of the MPc increased, the $\Phi_{4\text{-NP}}$ values increased until a maximum was reached and then there was slight decline, **Fig. 5.2.** The decrease in $\Phi_{4\text{-NP}}$ with increase in photosensitiser concentration could be due to extensive aggregation of the molecules at high concentrations. The optimum concentrations of the photosensitizers were 200 mg L^{-1} for **15a** and **17a** and **18d**, 250 mg L^{-1} for **15b** and **17d**, 300 mg L^{-1} for **15c** and **17b**, 350 mg L^{-1} for **17c**, **17e** and **18e** at 4-NP concentration of 3.5 x 10^{-5} mol L^{-1}, **Table 5.1**. A linearity $\Phi_{4\text{-NP}}$ versus 4-NP concentration, **Fig. 5.3**, was observed for concentrations less than 3.5 x 10^{-5} mol L^{-1}, hence below this concentration, $\Phi_{4\text{-NP}}$ may be accurately determined.

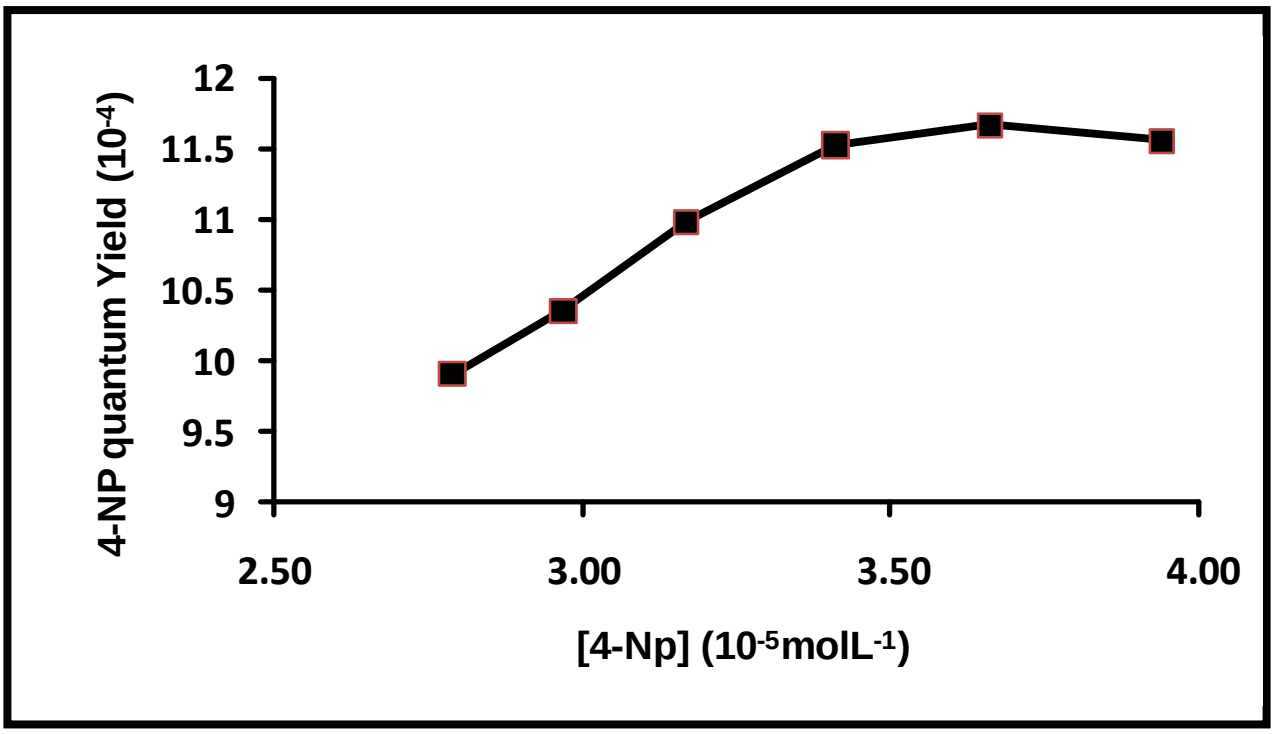

Figure 5.3: Plot of $\Phi_{4\text{-NP}}$ Vs concentration of 4-NP for phototransformation of 4-NP in the presence of complex 17b (300 mg L^{-1}) in DCM.

5.1.2. Kinetics of photosensitized reactions

The rate constant for photo-oxidation, k_r, was estimated from the slope of the plot of $1/\Phi_{4\text{-NP}}$ vs 1/[4-NP] [**Eqn 1.36** now **Eqn 5.2**]

$$\frac{1}{\Phi_{Poll}} = \frac{1}{\Phi_{\Delta}}\left\{\frac{k_a + k_q}{k_a} + \frac{k_d}{k_a[Poll]}\right\} \qquad 5.2$$

Employing **17a, 17c** and **17e** as examples, **Fig. 5.4,** k_r equals [k_d/Φ_{Δ} Slope] where k_d is the singlet oxygen decay constant in DCM (1.6×10^4 s^{-1} **[291]**), and Φ_{Δ} is the singlet oxygen quantum yield of the sensitizer in DCM.

Using k_r values as an indication of phototransformation efficiency, **Table 5.1** shows that photosensitized oxidation of 4-NP occurred faster when complexes **18d** and **18e** were used as sensitizers, with complex **17d s**howing the lowest rate towards the

photooxidation of 4-NP. The values k_r reported in this work for homogeneous phototransformation of 4-NP are much lower that the values obtained for sulfonated AlPc derivatives (order of 10^8 mol^{-1} L s^{-1}) **[57]** for the oxidation of chlorophenols.

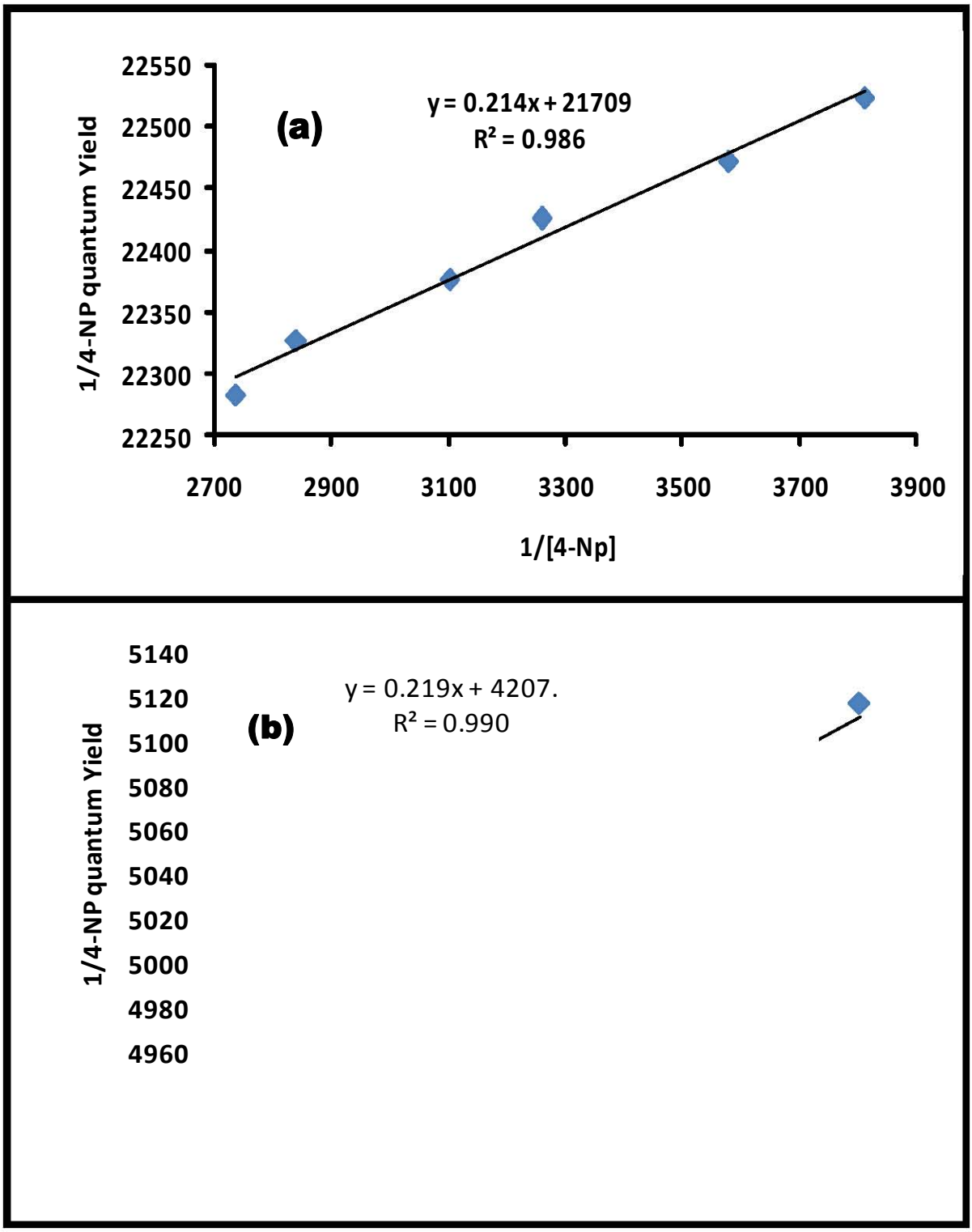

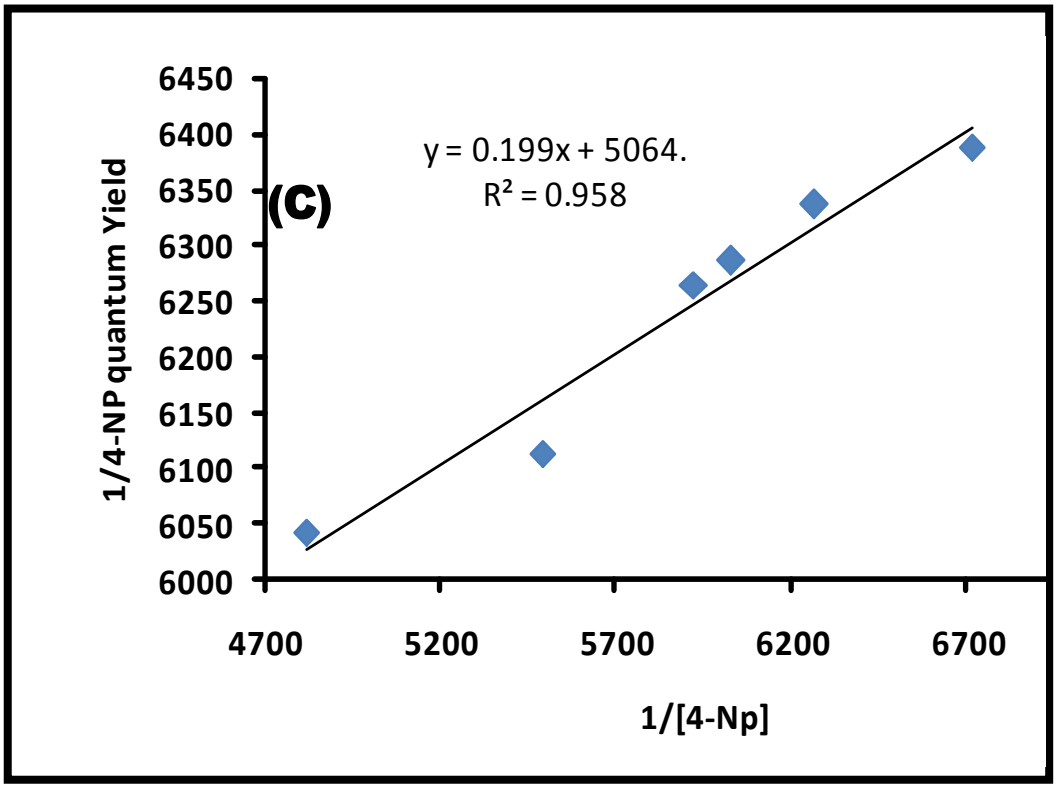

Figure 5.4: Plot of 1/ $\Phi_{4\text{-NP}}$ Vs 1/[4-NP] in the photo-oxidation of 4-nitrophenol for complexes (a) 17a (200 mg L^{-1}), (b) 17c (350 mg L^{-1}) and (c) 17e (350 mg L^{-1}) in DCM.

The quenching effect of the 4-NP on the singlet oxygen was estimated from (k_q + k_r) which is calculated from the intercept of the plot of $1/\Phi_{4\text{-NP}}$ vs 1/[4-NP]. Comparison of the (k_q + k_r) with k_r or estimation of k_q from the two gives the deactivation or quenching of singlet oxygen via other routes apart from oxidation reaction with 4-nitrophenol. The values of (k_q + k_r) for the sensitizers employed in this work ranged between 3.10 x 10^7 and 4.2 x 10^9 mol^{-1} dm^3 s^{-1} while k_r ranged between 1.4 x 10^5 and 2.3 x 10^5 $mol^{-1}dm^3s^{-1}$ **(Table 5.1)**. The implication of large (k_q + k_r) compared to k_r for all the sensitizers is that considerable amount of physical quenching of singlet oxygen took place during the reactions for all the complexes. The (k_q + k_r) values arrived at in this work are comparable with value of 2.8 x 10^8 $mol^{-1}dm^3s^{-1}$ obtained previously **[54]**.

5.1.3. Photosensitized transformationpProducts and mechanism of homogenous oxidation 4-NP.

GC and LC-MS were used to determine the products of phototransformation process by comparing the retention times of possible standards such as fumaric acid, 4-nitrocatechol, 1,4-benzoquinone and hydroquinone which are expected for the phototransformation of 4-nitrophenol. From comparison with the retention times of the standards, the two new peaks (hydroquinone at retention time of 5.4 min and 1,4-benzoquinone at retention time 2.9 min) were observed in the gas chromatogram traces, **Fig. 5.5**, after irradiation for 12 hr. The peak due to 4-NP (retention time = 2.3 min) was decreased in intensity. These peaks were all confirmed using GC analysis by spiking with the respective standards. **Fig. 5.6** also shows the formation of benzoquinone and hydroquinone with masses of 108.7 amu and 109.6 amu representing the molecular ions of benzoquinone and hydroquinone respectively. This, together with the GC and HPLC-UV detection analyses allows us to be confident about the products formed. According to the chromatograms, hydroquinone was the major product while benzoquinone, which was expected to be the final product, was present in small quantity. A blank test was conducted in which the substrate was photolysed in the presence of Pc-free SWCNT-COOH. The GC chromatogram of the resulting solution did not show any of the products peaks above suggesting that the SWCNT-COOH did not have any significant photochemical effect.

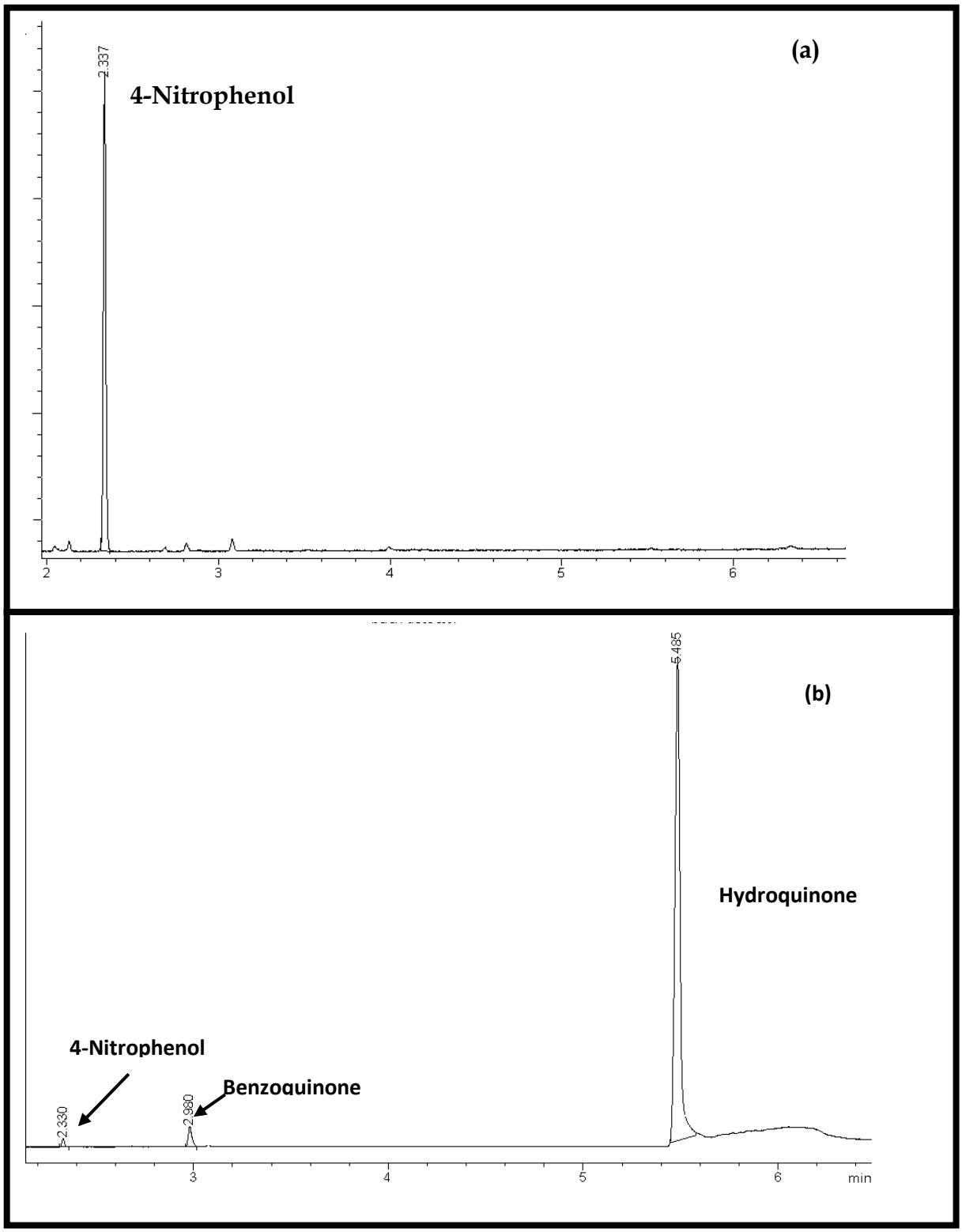

Figure 5.5: Gas Chromatogram for homogenous photosensitized oxidation products of 4-nitrophenol by complex 17c (a) before irradiation (b) after irradiation for 12 hrs. Concentrations of 17c = 350 mg $L^{-1}$and 4-nitrophenol = 3.5×10^{-4} mol L^{-1} in DCM.

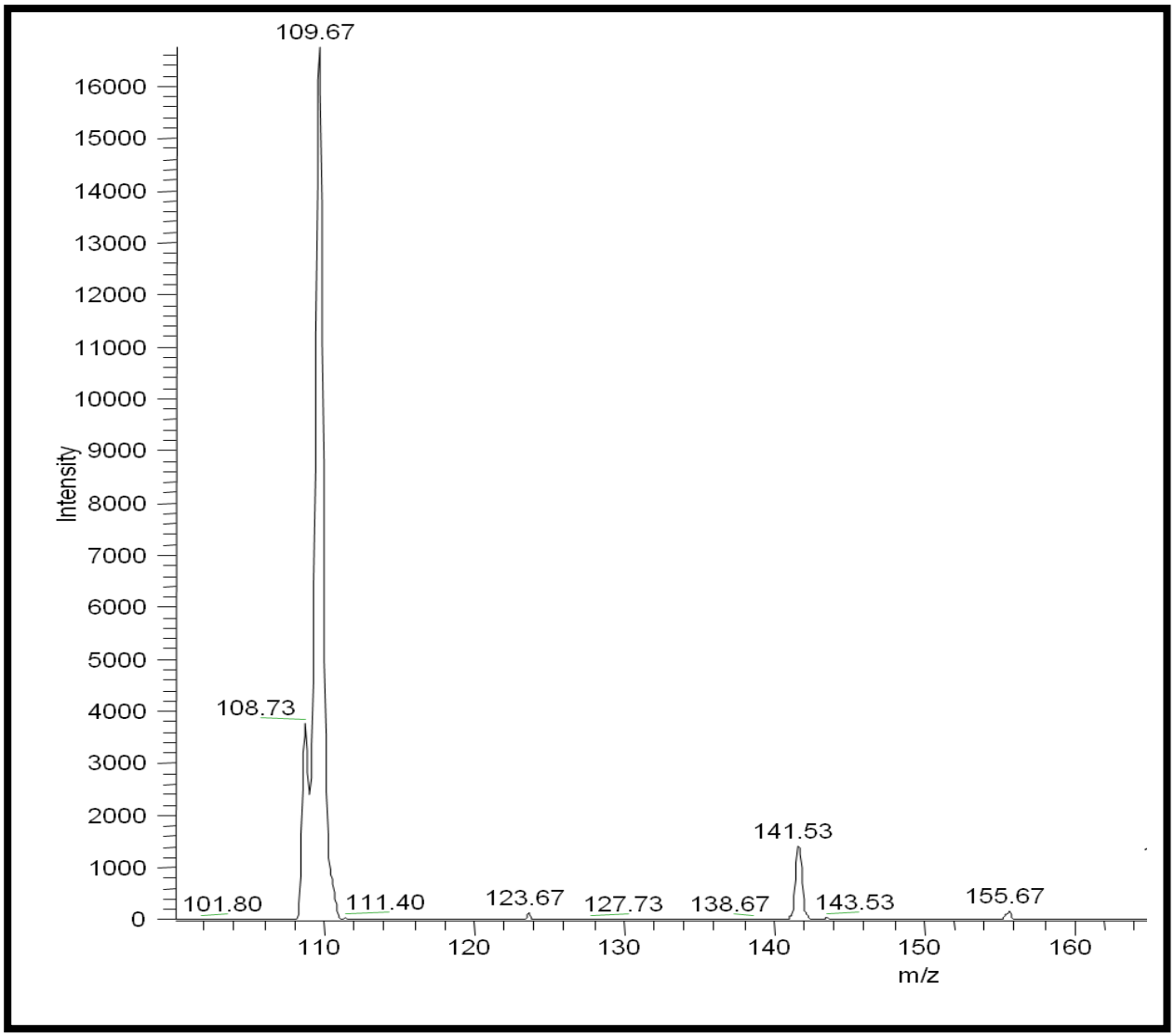

Figure 5.6: LC-MS spectrum of **photosensitized oxidation products of 4-nitrophenol by complex 17c after irradiation for 12 hrs. Concentrations of 17c = 350 mg $L^{-1}$and 4-nitrophenol = 3.5×10^{-4} mol L^{-1} in DCM.**

The mechanism for the phototransformation process was determined by using complex **17c** in the presence of sodium azide which is a singlet oxygen scavenger. While the rate of reaction was much faster in the absence of NaN_3 (whose concentration was in a ratio of 1:1 with the substrate) (presence of singlet oxygen), there was still 4-NP transformation happening in its presence (absence of singlet oxygen), **Fig. 5.7**, meaning that the reaction proceeded through both Type I and Type II mechanisms.

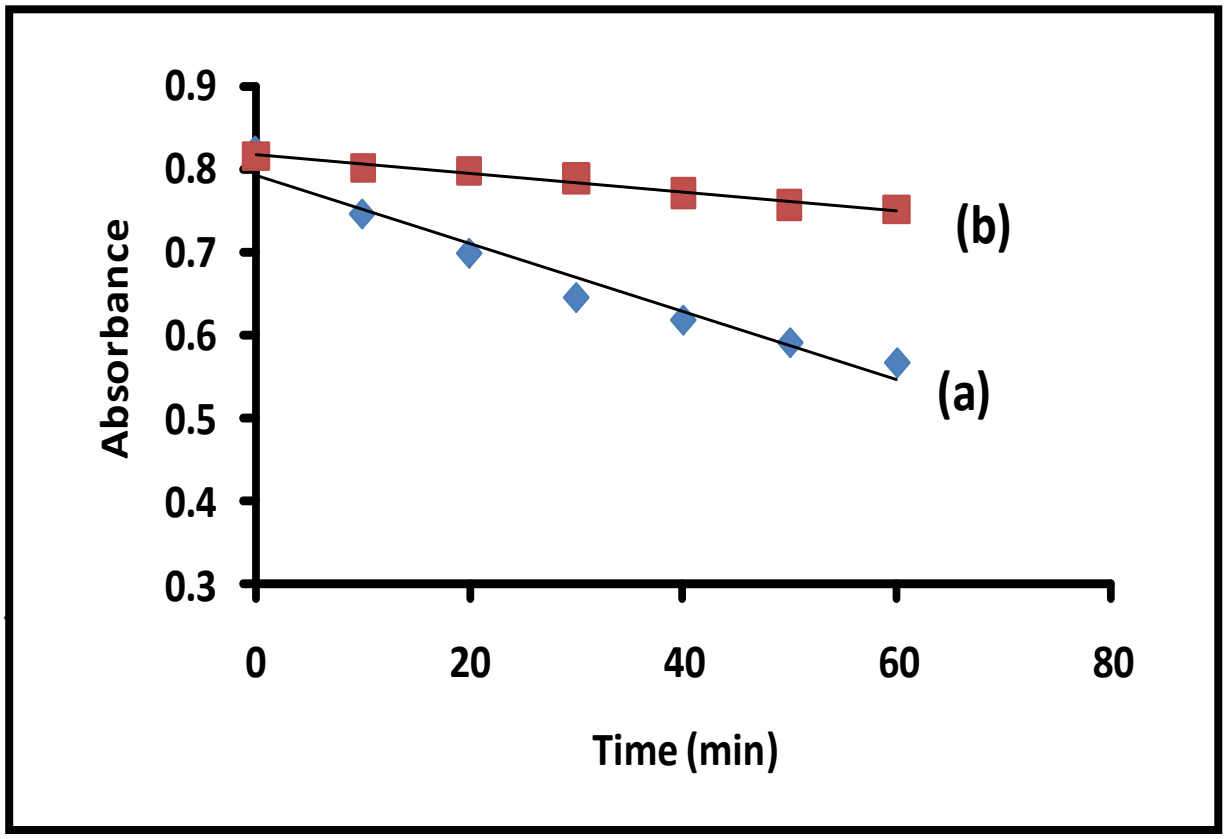

Figure 5.7: Absorption spectral changes observed for photosensitized transformation of 4-NP in the absence (a) and presence (b) of sodium azide. Concentrations of 17c = 350 mg $L^{-1}$and 4-nitrophenol = 3.5 × 10^{-4} mol L^{-1} in DCM.

The rate of reaction when the reaction medium was deareated by bubbling argon for 30 minutes was the similar to what was obtained in the presence of sodium azide and the only product noticed here was hydroquinone. The implication was that the two products might be produced through different path ways: Hydroquinone through Type I and benzoquinone through Type II reactions. Based on this result the proposed mechanism is shown in **Scheme 5.1**. The triplet state molecules interact with

deprotonated 4-nitrophenol (through Type I mechanism, **Scheme 1.7**) to generate a phenolate radical. The protons interacted with OH^- supplied by the basic media to give water which on reaction with triplet state molecules generated $OH^{\bullet}$ radical which in turn reacted with phenolate radicals to produce hydroquinone. The production of benzoquinone was likely from the direct oxidation of 4-Np by singlet oxygen as reported in the photo-oxidation of 4-chlorophenol **[292], Scheme 5.1**

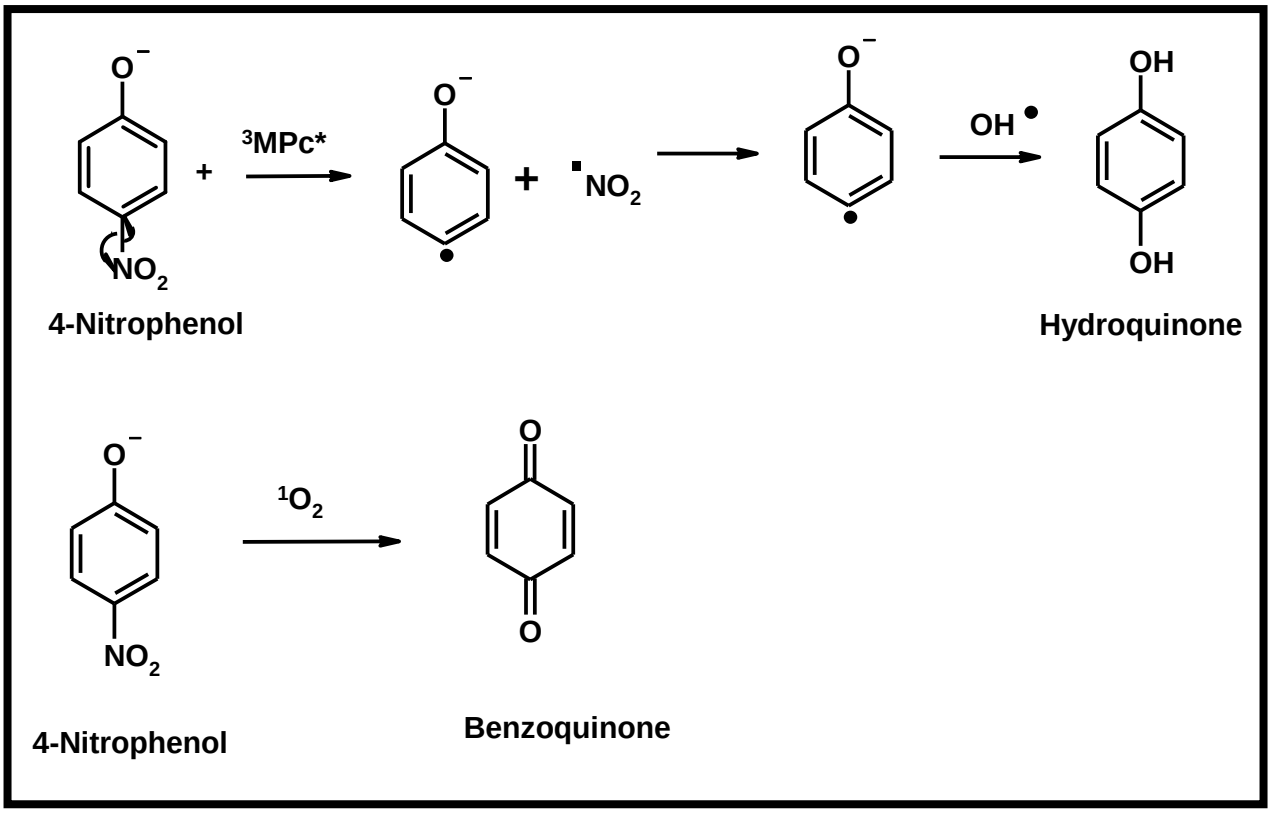

Scheme 5.1: Mechanism for oxidation of 4-nitrophenol.

5.2. Heterogeneous photosensitized oxidation of 4-nitrophenol

For these studies only PdPc derivatives were employed since they gave higher Φ_{Δ} and $\Phi_{4\text{-NP}}$ in DCM than PtPc derivatives **Table 5.1**.

5.2.1. UV-Vis spectral studies of the immobilisation of MPcs on SWCNTs to form ads-MPc-SWCNT.

Immobilization of PdPc complexes on SWCNTs was carried out by stirring DCM solutions of the PdPc derivatives in the presence of SWCNTs until there was no change in absorbance of the former, this was done over a period of 5 h or more depending on the PdPc derivative. The changes in absorbance of solution of complex **17a** in DCM during stirring in the presence of SWCNTs are shown in **Fig. 5.8a.**

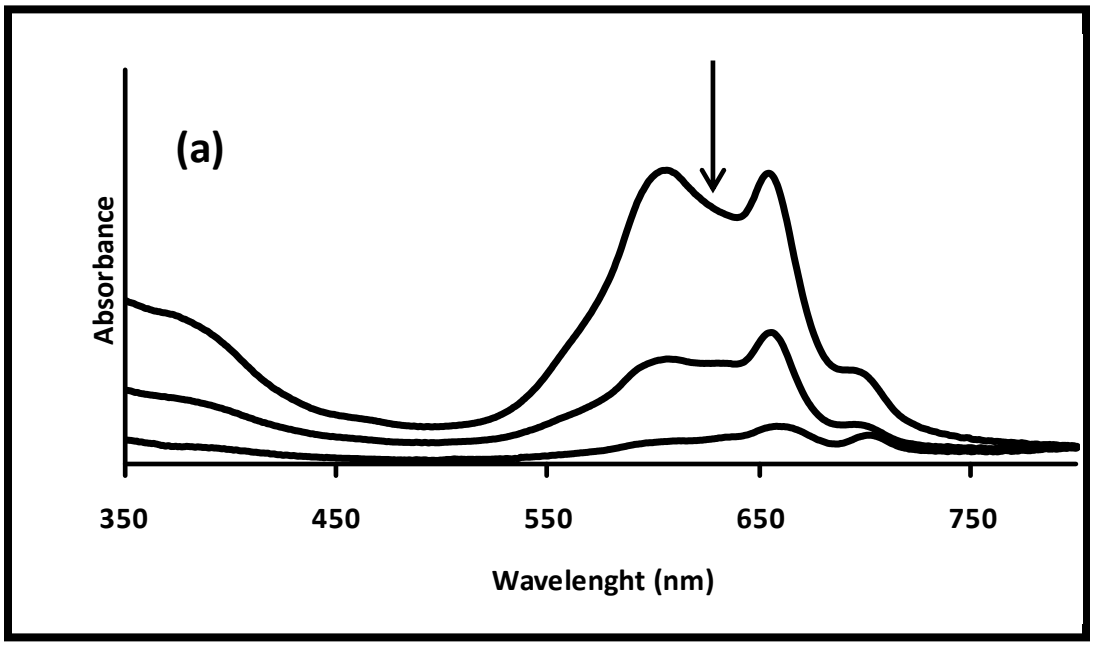

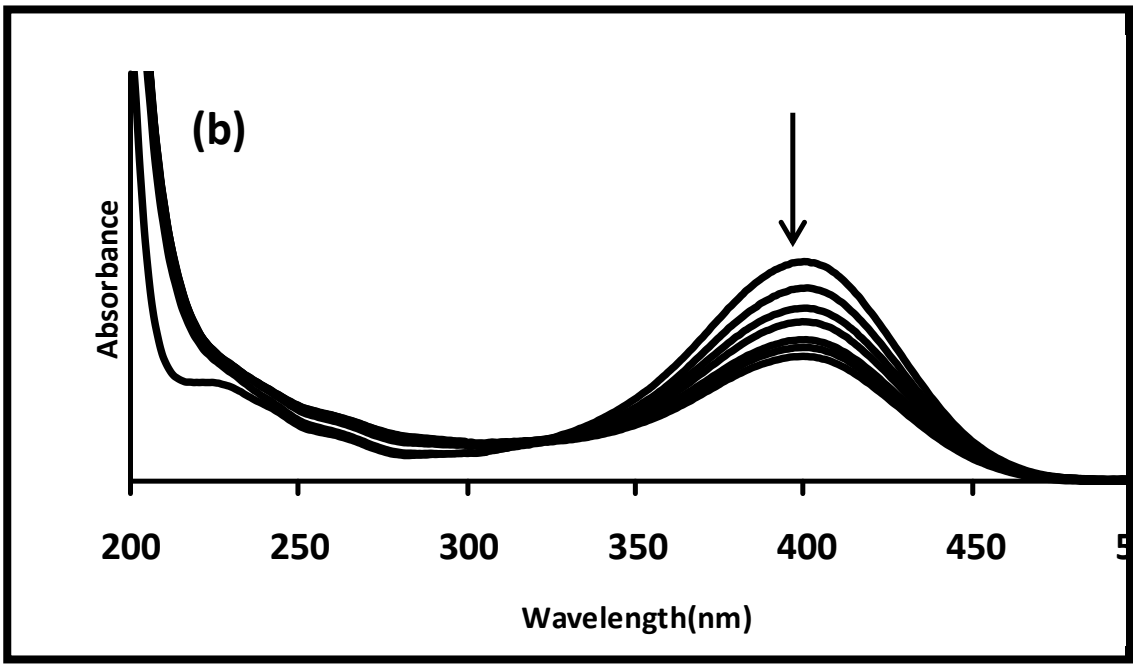

Figure 5.8: Spectral changes showing (a) the disappearance of complex 17a during its immobilization on SWCNT-COOH (200mg). Initial concentration of 17a = 1.2 ×10^{-5} mol dm^{-3}; time = 50 min) and (b) adsorption of 4-NP on SWCNTs (in the absence of MPc complexes).

The spectrum of complex **17a** shows extensive aggregation in DCM as stated above. Aggregation is judged by the presence of a broad band near 600 nm due to the aggregate and a sharper one at 650 nm, due to the monomer. Aggregation was displayed by all complexes in DCM. The small peak at 690 nm has been explained in chapter 3 as being due to intermolecular interaction between the central metal ion of one molecule with the thio group of another. On addition of SWCNTs to solution of **17a**, followed by stirring, there was a decrease in absorbance of complex **17a** as it adsorbs onto SWCNTs, **Fig. 5.8a**. The resulting conjugate is represented as ads-**MPc**-SWCNT-COOH. The peak at 690 nm however persists during immobilization suggesting that the interactions are still present.

SWCNTs are known to directly adsorb phenols **[258,259]** as shown by **Fig. 5.8b**. In order to check if following immobilization of PdPc derivatives onto SWCNTs, there were still parts of SWCNTs which were exposed, experiments were carried out where ads-MP**c**-SWCNT-COOH was immersed in a solution of 4-NP without photolysis. There was a

slight decrease in the absorbance of 4-NP (an average of 5%), showing that some empty sites were still left on SWCNTs where 4-NP could adsorb. The final spectrum following the adsorption of 4-NP (before photolysis) was used as the starting spectrum for all calculations done in this work. Experiments were also performed where PdPc derivatives were suspended in a solution of 4-NP without photolysis, and there were no changes in spectra confirming that the latter does not adsorb on the former. Experiments were also performed where SWCNTs following adsorption of 4-NP or PdPc derivatives was photolysed in pH 8.5 buffer only. There were no changes in absorbance which could be attributed to leaching of 4-NP (or its oxidation products) from the SWCNTs.

5.2.2. Characterization ads-MPc-SWCNT

5.2.2.1. XRD

X-ray diffraction technique was used to confirm the formation of SWCNT-MPc composites. Variations in nature and positions of peaks on XRD spectra are reflective of changes in structural features of the sample under consideration. **Fig. 5.9** shows the XRD spectra of SWCNT-COOH, complex **17c** alone and ads-**17c-**SWCNT-COOH. **Fig. 5.9a** (for SWCNT-COOH) shows sharp (2θ = 44.5° and 51.9°) and broad (2θ = 29.4° and 25.9°) peaks that are indicative of the crystalline and amorphous natures of the SWCNT-COOH, respectively. Using **international centre for diffraction data** (ICDD) database, the peak at 2θ = 25.9° is ascribed to (002) d-spacing of the SWCNT-COOH, **[293, 294]** while peaks at 2θ = 44.4° and 51.9° are characteristic of (100), **[293]** and (200) **[294]** reflections of carbon of the SWCNT-COOH, respectively. The only prominent peak in the XRD spectrum of complex **17c** was a broad one at 2θ = 24.1° **(Fig. 5.9b)**. Its broadness is an indication of the amorphous nature of complex **17c**. In the XRD spectrum ads-**17c**-SWCNT-COOH **(Fig. 5.9c),** the peak near 25° encompasses both **17c** and SWCNT-COOH. The differences in spectra indirectly suggest the adsorption of **17c** on SWCNT.

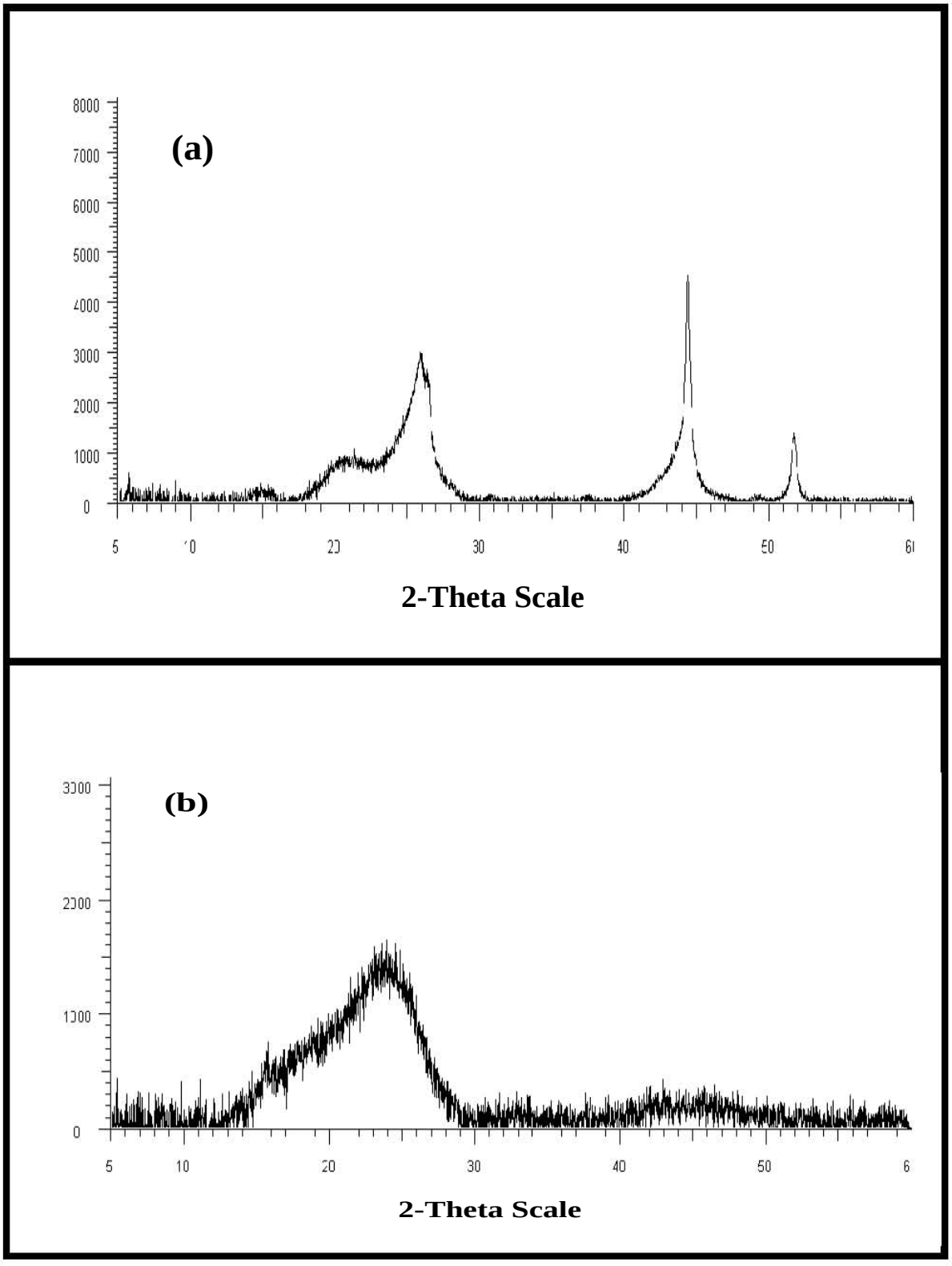
(a)
8000
7000
6000
5000
4000
3000
2000
1000
0
5
10
20
30
40
50
60
2-Theta Scale
(b)
3000
2000
1000
0
5
10
20
30
40
50
6
2-Theta Scale

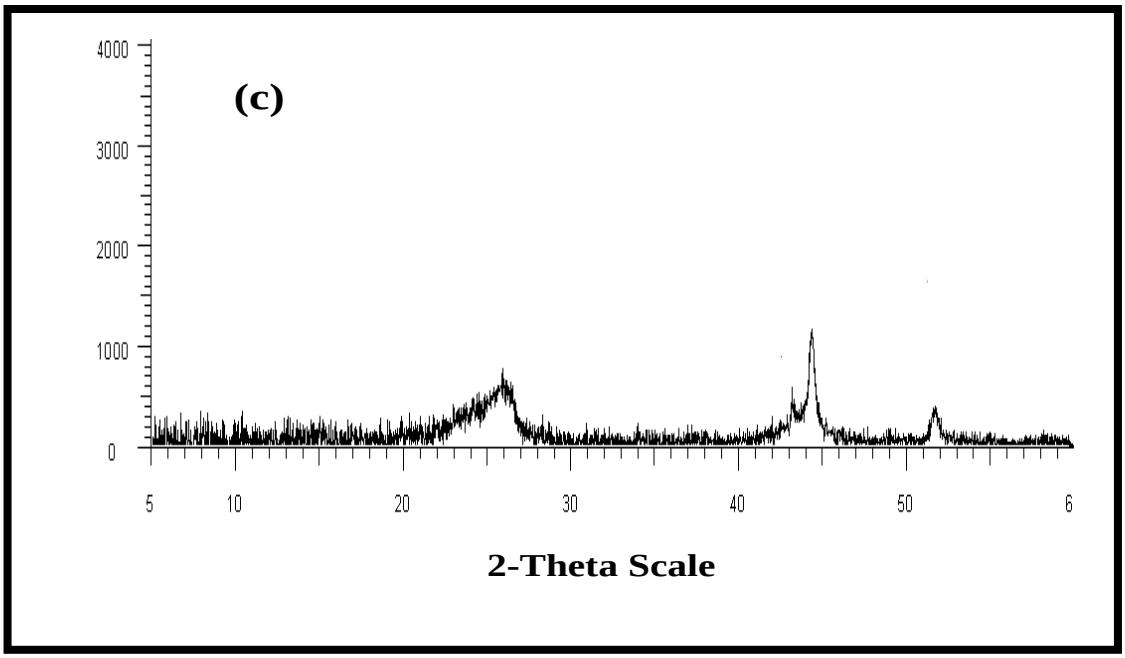

Figure 5.9: XRD spectra of (a) SWCNT-COOH, (b) Complex 17c and (c) ads-17c-SWCNT-COOH.

5.2.2.2. Raman spectroscopy

Raman spectroscopy is used for the characterization of disordered polycrystalline graphitic carbons. The Raman spectra of graphite show bands at about 1360 and at 1560 cm^{-1}. These two bands are the most diagnostic features, and are designated as D and G bands, respectively. Raman spectroscopy can be used to some extent to quantify changes in the SWCNTs using the ratio of D/G bands under fixed laser power intensity. Adsorption of MPc complexes may not cause extensive disruption to the carbon lattice due to the non-invasive π-π interactions i.e. preservation of the carbon nanotube structure, however small changes in the D/G ratio may indicate the presence of MPcs on the SWCNTs skeleton. We observed the G band at 1595 cm^{-1} for SWCNT-COOH and a weak D band near 1305 cm^{-1} as a broad peak **(Fig. 5.10)**. Functionalization of SWCNTs is known to enhance the D band **[295-297]** hence the increase in the D/G ratio from 0.023 for SWCNT-COOH to 0.72 for ads-MPc-SWCNT-COOH, indirectly confirms adsorption of PdPc derivatives on SWCNT-COOH.

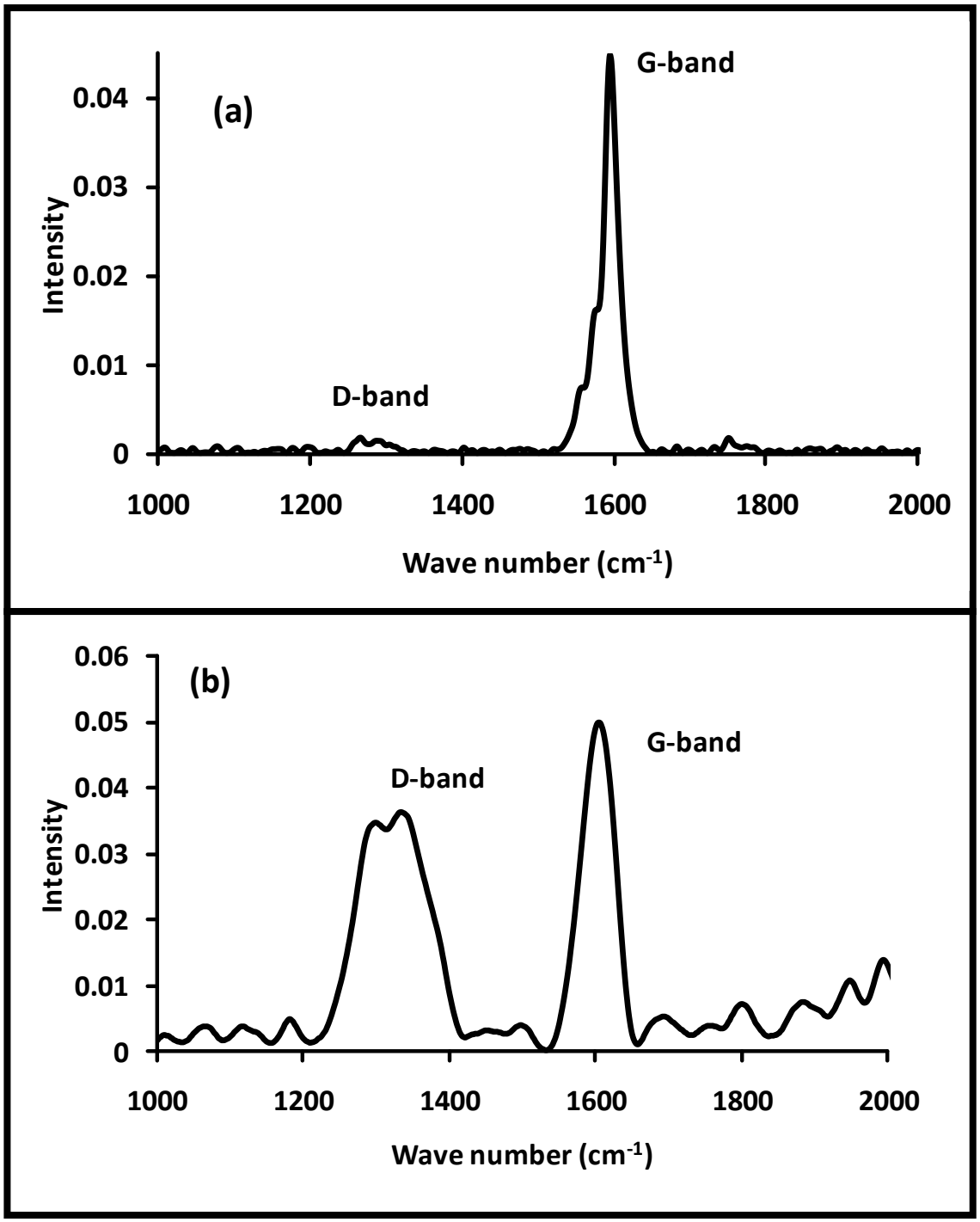

Figure 5.10: Raman spectra of (a) Functionalised single-wall carbon nanotube (SWCNT-COOH) (b) ads-15b-SWCNT-COOH

5.2.2.3. Transmission electron microscopic (TEM) characterization

TEM technique provided a microscopic view of the ads-MPc-SWCNT-COOH. **Fig. 5.11a** is the TEM image of SWCNT-COOH. The image obtained after the formation of the adsorbed species, ads-**17c**-SWCNT-COOH **(Fig. 5.11b)** was completely different showing coverage of the large portion of the surface of SWCNTs with PdPc derivatives.

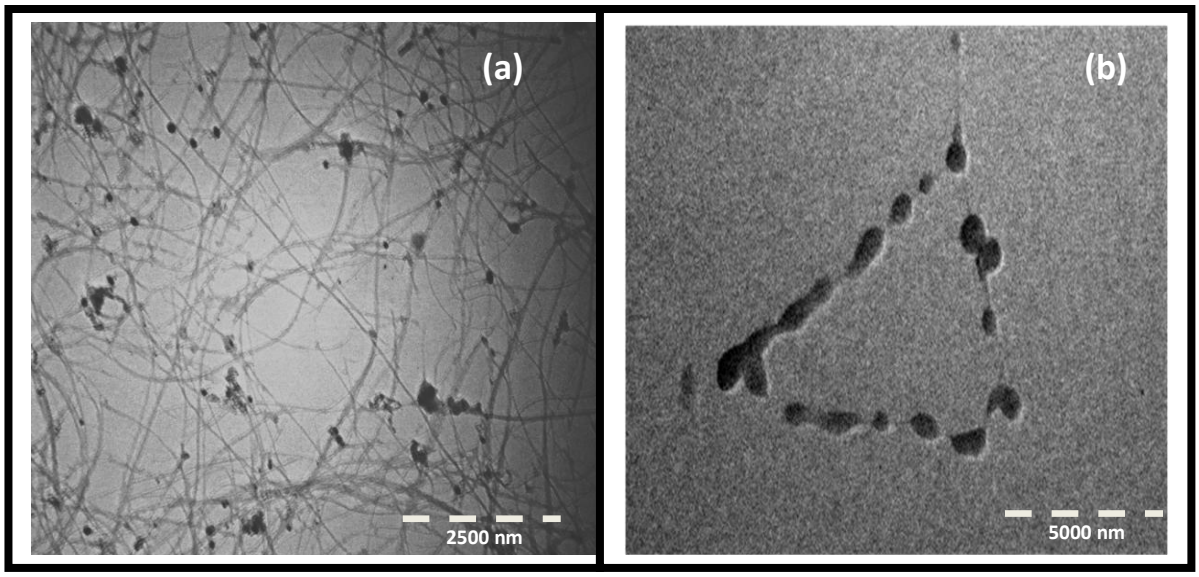

Figure 5.11: TEM images of (a) SWCNTs (magnification X 10000) and (b) ads-17c–SWCNT (magnification X 20000)

5.2.2.4. Singlet oxygen generation capacity of ads-MPc-SWCNT in pH 9 buffer

Since singlet oxygen is thought to be involved in the photocatalysis mechanism, its generation by ads-MPc-SWCNT-COOH was investigated. As stated in the experimental, interference filters were employed for peripheral (**17a-17e**) and non-peripheral (**15a-15c)** complexes, to ensure excitation of the low energy peak due to the monomer of the adsorbed Pc. This assumes that Q band maxima of the absorbed specie are about the same as that in solution with the expected broadening in the former. An aqueous solution of 6.0 x 10^{-5} mol dm^{-3} ADMA containing a suspension of each of the ads-MPc-SWCNT-COOH conjugates, was successively irradiated at the Q-band of MPc, centrifuged and decanted into UV-Vis cell and absorbance recorded. The decrease in absorbance of ADMA at 379 nm **(Fig. 5.12)** shows that singlet oxygen is formed on

photolysis of ads-MPc-SWCNT-COOH in the presence of ADMA. The spectra of the MPcs were not observed since they acted as heterogeneous catalysts in the reactions. The rather low Φ_{Δ} values of ads-MPc-SWCNT-COOH (0.19 to 0.27, **Table 5.2**) under heterogeneous condition compared with what was obtained in solution are ascribed to inefficient energy transfer to ground state oxygen or the solid nature of the molecules (in the former) which might encourage more aggregation.

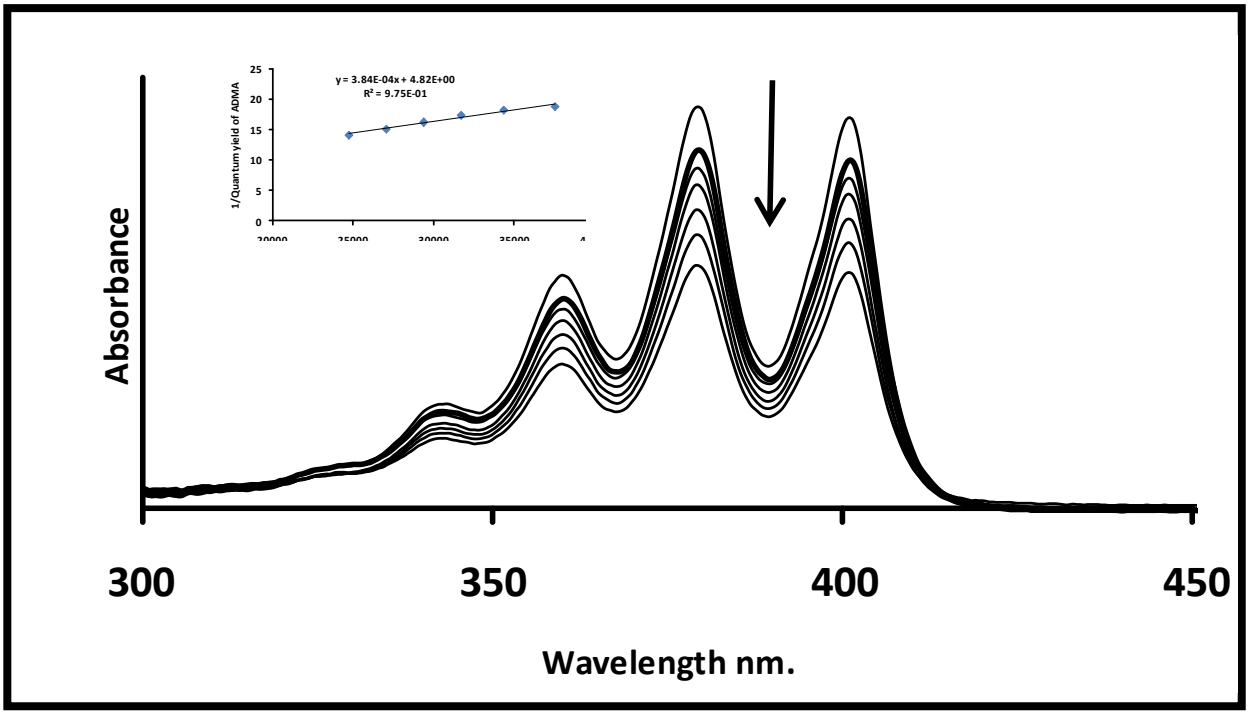

Figure 5.12: Electronic absorption spectral changes observed during the photolysis of ADMA to confirm singlet oxygen production by ads-15c-SWCNT-COOH. Initial ADMA concentration = 6.0 x 10^{-5} mol dm^{-3}; time = 60 min. Inset: Plot of $1/\Phi_{ADMA}$ versus 1/[ADMA] for the determination of singlet oxygen quantum yield using Eqn. 1.9.

Table 5. 2: Langmuir-Hinshelwood (L-H) parameters for the phototransformation of 4-NP on Ads-MPc-SWCNT-COOH and singlet quantum yields of the complexes (in the presence of SWCNTs) at pH 8.5.

Complex	4-NP (M)	$k_{obs}(min^{-1})(10^{-3})$	Φ_{Δ}	$k_r(Mmin^{-1})10^{-6}$	$K_{ads}(M^{-1})10^{3}$
Ads-15a-SWCNT	4.00×10^{-5}	3.19	0.23	1.40	0.33
	6.00×10^{-5}	2.27			
	8.00×10^{-5}	1.67			
	1.00×10^{-4}	0.63			
15b	4.00×10^{-5}	2.79	0.21	1.30	0.32
	6.00×10^{-5}	2.41			
	8.00×10^{-5}	1.33			
	1.00×10^{-4}	0.54			
15c	4.00×10^{-5}	3.29	0.20	1.90	2.8
	6.00×10^{-5}	2.67			
	8.00×10^{-5}	1.86			
	1.00×10^{-4}	0.98			
17a	4.00×10^{-5}	3.00	0.22	1.30	0.51
	6.00×10^{-5}	2.25			
	8.00×10^{-5}	1.52			
	1.00×10^{-4}	0.61			
17b	4.00×10^{-5}	2.7	0.22	1.10	0.42
	6.00×10^{-5}	2.1			
	8.00×10^{-5}	1.32			
	1.00×10^{-4}	0.42			
17c	4.00×10^{-5}	3.16	0.27	1.80	3.8
	6.00×10^{-5}	2.40			
	8.00×10^{-5}	1.74			
	1.00×10^{-4}	0.75			
17d	4.00×10^{-5}	2.22	0.19	0.70	0.19
	6.00×10^{-5}	1.64			
	8.00×10^{-5}	0.92			
	1.00×10^{-4}	0.11			
17e	4.00×10^{-5}	2.51	0.20	1.00	0.37
	6.00×10^{-5}	1.95			
	8.00×10^{-5}	1.27			
	1.00×10^{-4}	0.32			

5.2.3. Photocatalytic behavior of ads-MPc-SWCNT-COOH towards 4-NP

UV-vis spectroscopy was employed to monitor the transformation of 4-NP. Since the pKa of 4-nitrophenol is 7.15 these studies were carried out in aqueous solution at pH 8.5 because phenolate ions which are more oxidizable are predominant at these conditions as already stated. It is important to state that no change in spectra of 4-nitrophenol was observed when photolysis was done in the absence of ads-MPc-SWCNT-COOH. Also no transformation was observed when 4-nitrophenol was stirred in the presence of ads-MPc-SWCNT-COOH without photolysis. During photolysis at the Q band region of the PdPc derivatives, in the presence of suspended ads-MPc-SWCNT-COOH **(Fig. 5.13),** there was a gradual collapse of the 4-NP peaks at 250 and 400 nm.

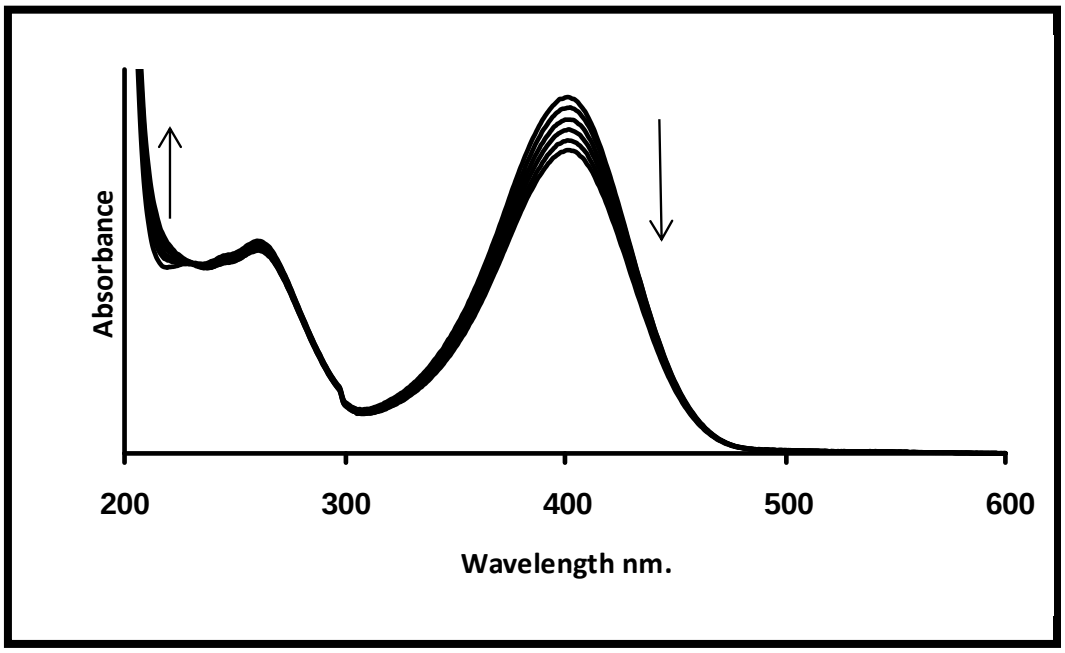

Figure 5.13: Spectral changes observed during photolysis of 4-NP using ads-17a-SWCNT-COOH. Initial 4-NP concentration = 1.00 ×10^{-4} mol dm^{-3}.

There was also an increase in the absorbance near 220 nm, possibly due to the photolysis products; however, absorption in this region will be affected by solvents. It is important to note that the spectra in **Fig. 5.13** were recorded after allowing the initial adsorption of small amounts of 4-NP onto SWCNTs (without photolysis), until no change in electronic absorption spectra of 4-NP was observed. The spectral changes

shown in **Fig. 5.13** were also observed for SWCNTs composite of complexes **15a, 15b, 15c, 17b**, **17c**, **17d** and **17e** though the rate of decrease in the 4-NP varied significantly.

5.2.4. Kinetic Studies for photolysis of 4-NP

As shown in **Fig. 5.14** the kinetics of transformation of 4-nitrophenol fitted into pseudo first order reaction kinetics. The apparent rate constant k_{obs} were obtained from the slopes in **Fig. 5.14** for all the MPcs composites for different concentrations of 4-nitrophenol ranging from 4×10^{-5} to 10×10^{-5} M.

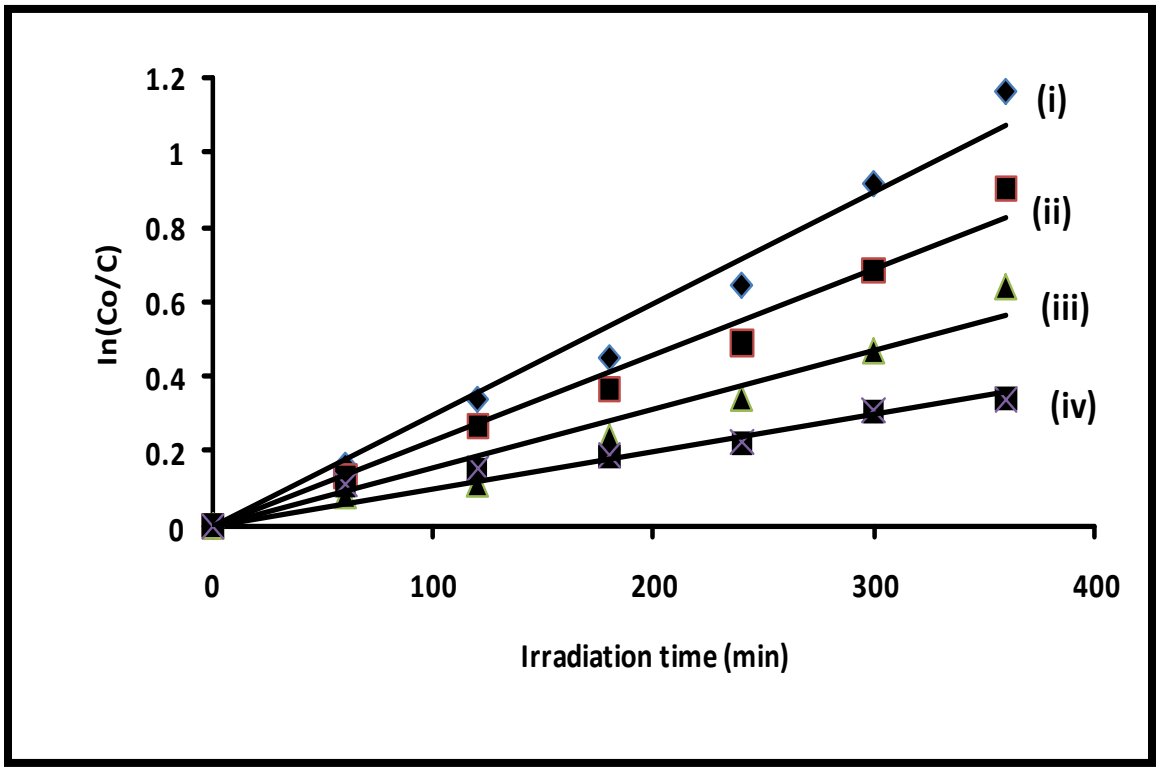

Figure 5.14: Langmuir-Hinshelwood kinetic plot for ads-15c-SWCNT-COOH in basic media.

The apparent rate of reaction (k_{obs}) were obtained from **Eqn. 5.3**

$$\ln(C_o/C_t) = k_{obs}t \qquad 5.3$$

Table 5.2 shows that for all ads-MPc-SWCNT-COOH the more dilute the 4-NP solution, the higher the apparent rate for transformation. The k_{obs} values for 4-NP concentrations of 4, 6, 8 and 10×10^{-5} M is stated in **Table 5.2**.

It is important to establish if the transformation reaction takes place following adsorption and to determine the adsorption coefficients. Langmuir-Hinshelwood model was employed for these studies.

Langmuir-Hinshelwood (L-H) equation (**Eqn 5.4**) has been used to describe the competitive adsorption of substrates, reaction intermediates and phenolic oxidant products **[223,246]**.

$$\frac{1}{\text{rate}} = \frac{1}{k_r} + \frac{1}{k_r K_{ads} C_o} \qquad 5.4$$

where k_r is the rate constant for the adsorption of 4-NP, C_0 is the initial concentration of the substrate (in this case 4-NP). K_{ads} is the adsorption coefficient and represents the equilibrium between the rates of adsorption and desorption **[244]**. The adsorption studies here are for 4-NP (or intermediates) on PdPc derivatives.

The plots of reciprocal of initial rate of phototransformation (after 60 min of irradiation) vs. reciprocal of initial concentration of 4-NP **(Fig. 5.15)** gives k_r as the intercept, the adsorption coefficient (K_{ads}) can now be determined from the slope. For the MPc-SWCNT composites of **15a-15c , 17a -17e** the plots were also found to be linear with a non-zero intercept.

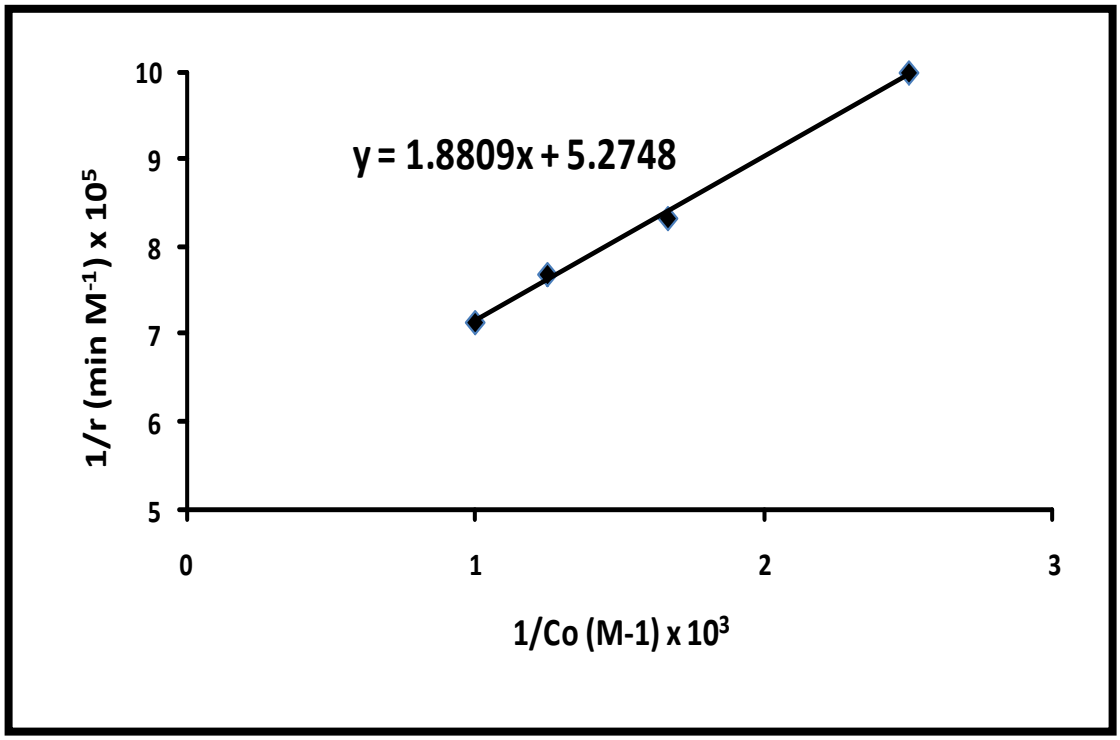

Figure 5.15: Plot of change in concentration with time during photolysis of 4-NP for different starting 4-NP concentrations using ads-17c-SWCNT-COOH as a photocatalyst ((i) 4× 10^{-5}, (ii) 6× 10^{-5}, (iii) 8 × 10^{-5} and (iv) =10 × 10^{-5} M.

The values of k_r and K_{ads} are shown in **Table 5.2.** According to **Table 5.2,** adsorption rate (k_r) was the lowest for ads-**17d**-SWCNT-COOH where **17d** is substituted with benzyl groups and ads-**17c**-SWCNT and ads-**15c**-SWCNT-COOH where complexes **17c and 15c** contain the longest alkyl chain, gave the largest k_r values, **Table 5.2**. Thus the adsorption rate of 4-NP is highest for long chain alkyl phthalocyanines on SWCNTs than for aryl group substituted phthalocyanines. Also for ads-**17c**-SWCNT-COOH and ads-**15c**-SWCNT adsorption of 4-NP (or its phototransformation products) is more favoured over desorption compared to the rest of the complexes as judged by the values of K_{ads}.

5.2.5. Catalyst stability

Following use for the photodegradation of 4-NP, the ads-**MPc**-SWCNT-COOH were cleaned by rinsing in water, dried and reused for the phototransformation of 4-NP. **Fig. 5.16** shows the plots of concentration versus time, for the first, second and third uses of ads-**1c-**SWCNT-COOH for the phototransformation of fresh solution of 4-NP. The rates changed from 1.21 x 10^{-6} M min^{-1} for the first use to 1.11 x 10^{-6} M min^{-1} for the second use and to 1.04 x 10^{-6} M min^{-1} for the third use. The rate decreased gradually by ~ 7% with each run beyond the three runs shown in **Fig. 5.16**.

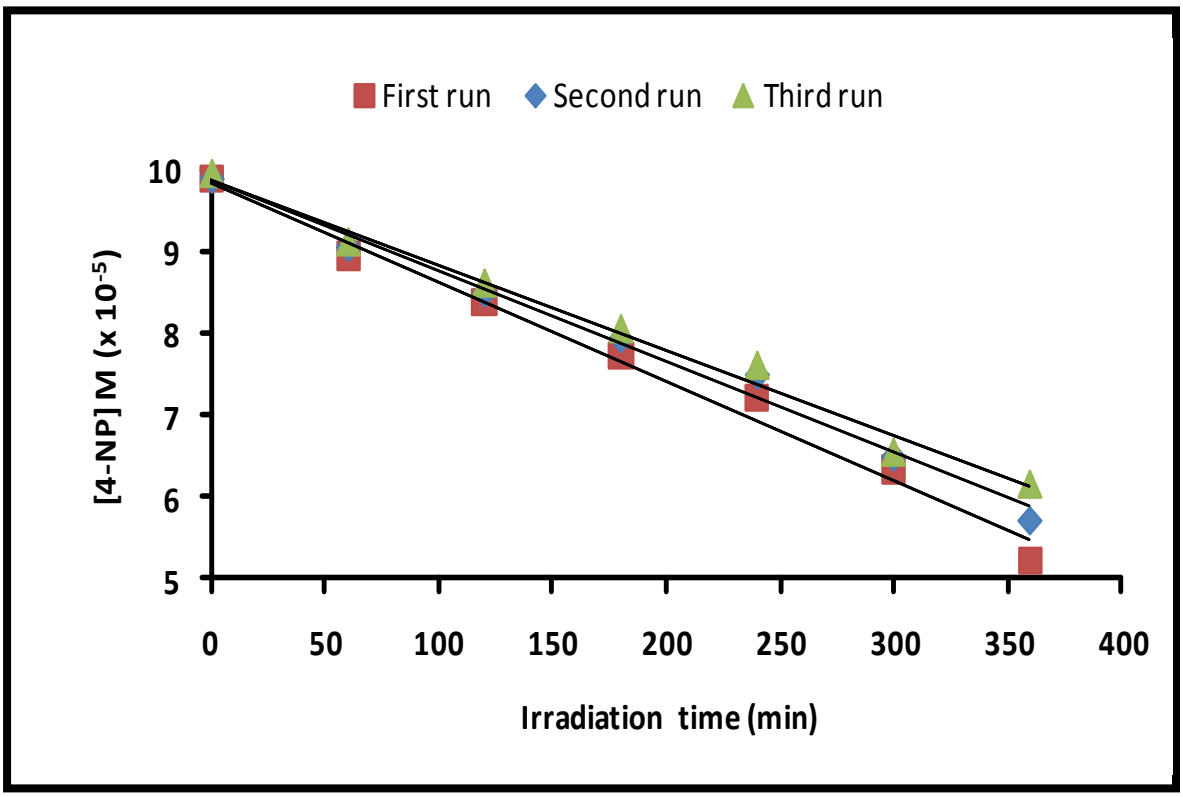

Figure 5.16: Plots of concentration versus time for the reuse of ads-17c-SWCNT-COOH for the phototransformation of 4-nitrophenol. pH 9 buffer.

The gradual reduction in rate might be due to permanent adsorption of intermediates on the surface of the catalysts thereby reducing their activities or due to degradation of the PdPc catalysts. TEM, XRD and Raman showed that the catalysts were still intact on the surface of the SWCNTs, since there were no changes in the images or spectra following the first uses. Compared to ZnPc derivatives where decreases in stabilities by 15 to 20 % have been reported **[54],** the present PdPc catalyst shows improved stability.

5.2.6. Products and Mechanism of heterogeneous oxidation of 4-nitrophenol

GC was used to determine the nature of the products of phototransformation reaction by comparing the retention times of expected standards for the catalyzed phototransformation of 4-nitrophenol. These include fumaric acid, 4-nitrocatechol, 1,4-benzoquinone and hydroquinone. Two new peaks were observed on the gas chromatogram traces similar to the transformation noticed in **Fig. 5.17**, after irradiation for 24 hr. These were identified (using spiking with standards) as hydroquinone and 1,4-benzoquinone. According to the chromatograms hydroquinone was present in a small quantity while the major product was benzoquinone, which was the final product,

The contribution of singlet oxygen in the phototransformation process was determined by using ads-**17c**-SWCNT-COOH in the presence of a singlet oxygen scavenger, sodium azide as was done for homogenous sensitisation. The rate of the reaction was much slower in the presence of NaN_3 (whose concentration was in a ratio of 1:1 with the substrate), meaning that the reaction proceeded through mainly Type II mechanisms, the same way as under homogenous condition **Scheme 5.1.** When the reaction medium was deareated the two products were still present but benzoquinone appeared to be in smaller quantities than in air, suggesting possible involvement of Type I (radical) mechanism, giving mainly hydroquinone while Type II (singlet oxygen) mechanism gives mainly benzoquinone. The production of benzoquinone is likely from the direct oxidation of 4-NP by singlet oxygen as observed for 4-chlorophenol **[55,292]** as discussed above under homogenous condition. The products obtained are similar to those obtained (as intermediates) in the past work for heterogeneous photo-oxidation of 4-nitrophenol **[55]**. Fumaric acid and 4-nitrocatechol were also observed as final products ZnPc derivatives suspended in solution **[55]**. However, the use of SWCNT as supports has advantages of ease of immobilization of MPcs and ease of removal from solution.

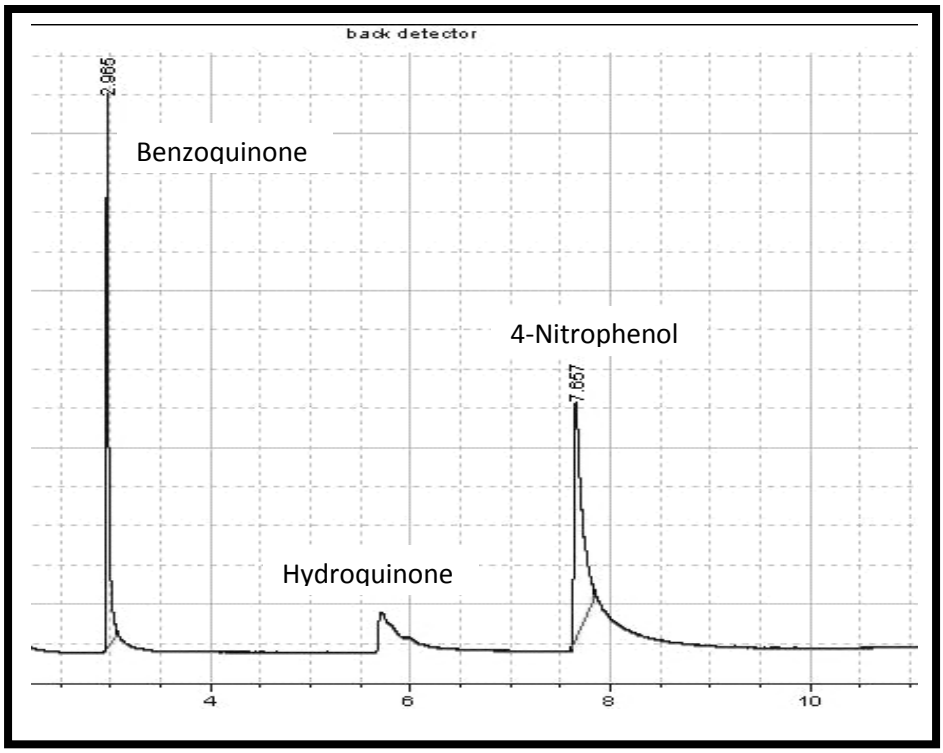

Figure 5.17: Gas Chromatogram of the photolysed 4-NP sample by ads-17c-SWCNT-COOH. Irradiation time =24 h, starting 4-NP concentration = 1 x 10^{-4} mol dm^{-3}.

5.3. Investigation of the photo-oxidation of chlorophenols using complex 17c as sensitizer

Of all the photosensitisers PdPc complex containing long alkyl chain (complex **17c**) was found to give best result for the phototransformation of 4-NP, hence it is employed in this work for the phototransformation of chlorophenols under homogeneous and heterogeneous conditions as a model of the photooxidation efficacy of the MPc complexes on other phenolic pollutants.

5.3.1. Spectroscopic characterization

The homogeneous photolysis of 4-CP and PCP were done in DCM. **Fig. 5.18** shows the spectral changes observed for pentachlorophenol (PCP) during homogeneous photolysis in the presence of the photosensitiser (complex **17c**) conducted in DCM. These studies were carried out in aqueous solution at pH 9 because phenolate ions which are more oxidizable are predominant at high pH.

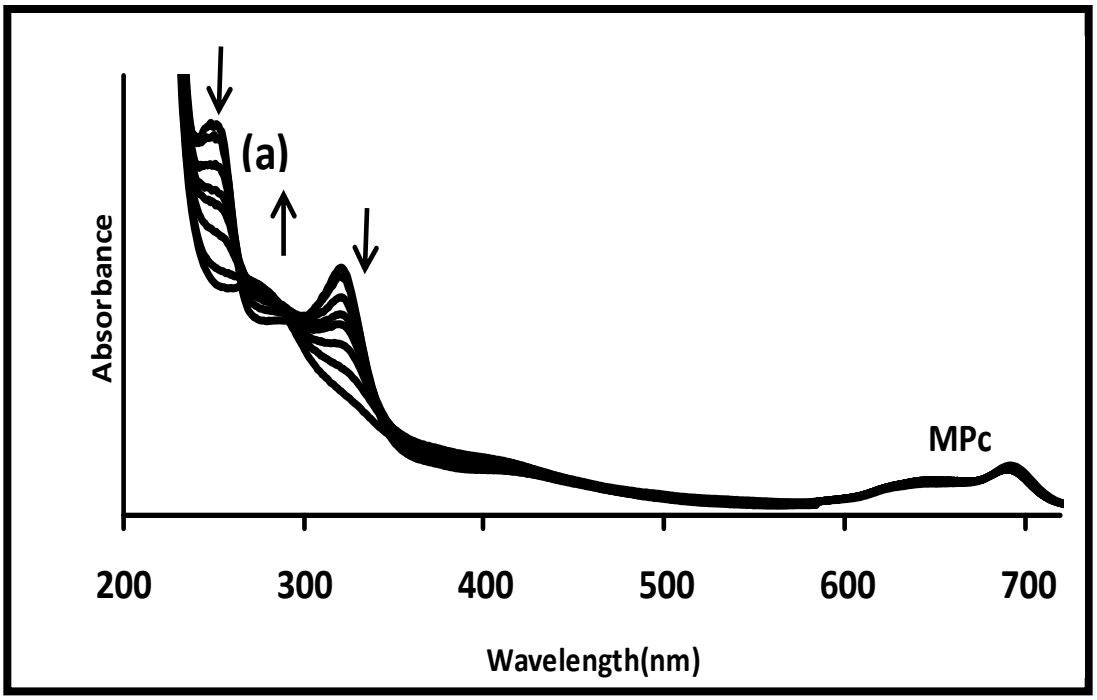

Figure 5.18: Spectral changes showing (a) the disappearance of PCP during homogeneous photolysis in the presence of complex 17c (300mg/L in DCM (basic media).

There was a decrease in the concentration of PCP during irradiation (with time) in the presence of **17c** while the concentration of **17c** remained relatively unchanged due to its high photostability as indicated by the lack of change in the absorbance of the Q-band of the complex at around 695 nm. The peaks due to PCP observed at 252 nm and 322 nm started disappearing with simultaneous appearance of a peak around 273 nm due to the formation of the product(s). The same trend was observed for 4-chlorophenol in the presence of photosensitisers with reduction in the absorbance of the peak at 280 nm, **Fig. 5.19**. The Φ_{CP} values were calculated from the initial rate of disappearance of the CP using **Eqn 5.1.** Effects of the complex absorption in the B band region were subtracted for all calculations. Φ_{CP} was found to be larger for 4-CP than PCP probably because the presence of more chlorine atoms on PCP made it more resistant to photodegradation than 4-CP.

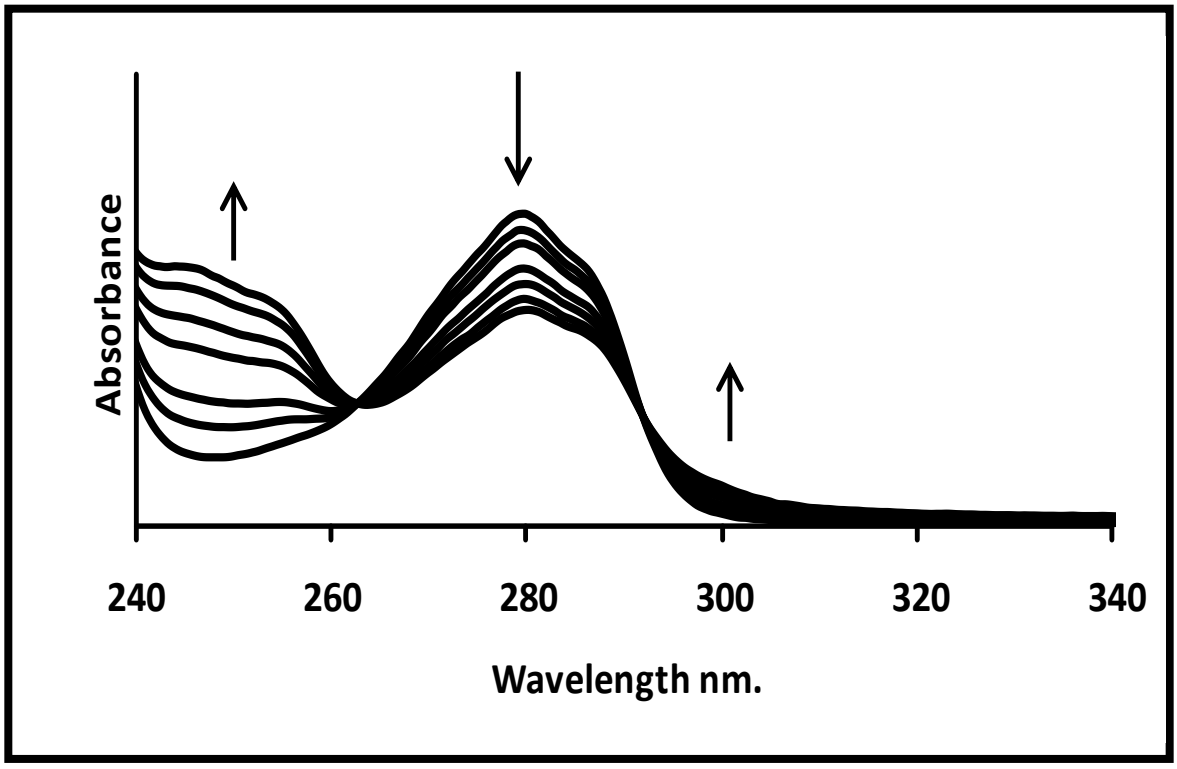

Figure 5.19: Spectral changes showing the disappearance of 4-CP during heterogeneous photolysis in the presence of ads-17c-SWCNT-COOH (500mg/L) basic aqueous media.

Because the concentration of the adsorbed catalyst might have an effect on the phototransformation of the analytes, experiments were conducted using various concentrations of the catalysts ranging from 50 mg L^{-1} and 600 mg L^{-1} and the initial rates of disappearance of CP were determined and Φ_{CP} were calculated.

As shown in **Fig. 5.20**, as the concentration of the sensitizer increased, the Φ_{CP} values increased until a maximum was reached around which the plot flattened and then there was a decline. The flattening could be due to inability of additional catalyst to bring commensurate increase in quantum yield as aggregation began to set in. The decrease in Φ_{CP} with increase in the concentration of **17c** could be due to extensive aggregation of the molecules at high concentrations. The optimum concentrations of the sensitiser were 350 mg L^{-1} for 4-CP and 300 mg L^{-1} for PCP**.** The percentage conversion of 4-CP was 91% and for PCP, the value was 70 %, **Table 5.3.**

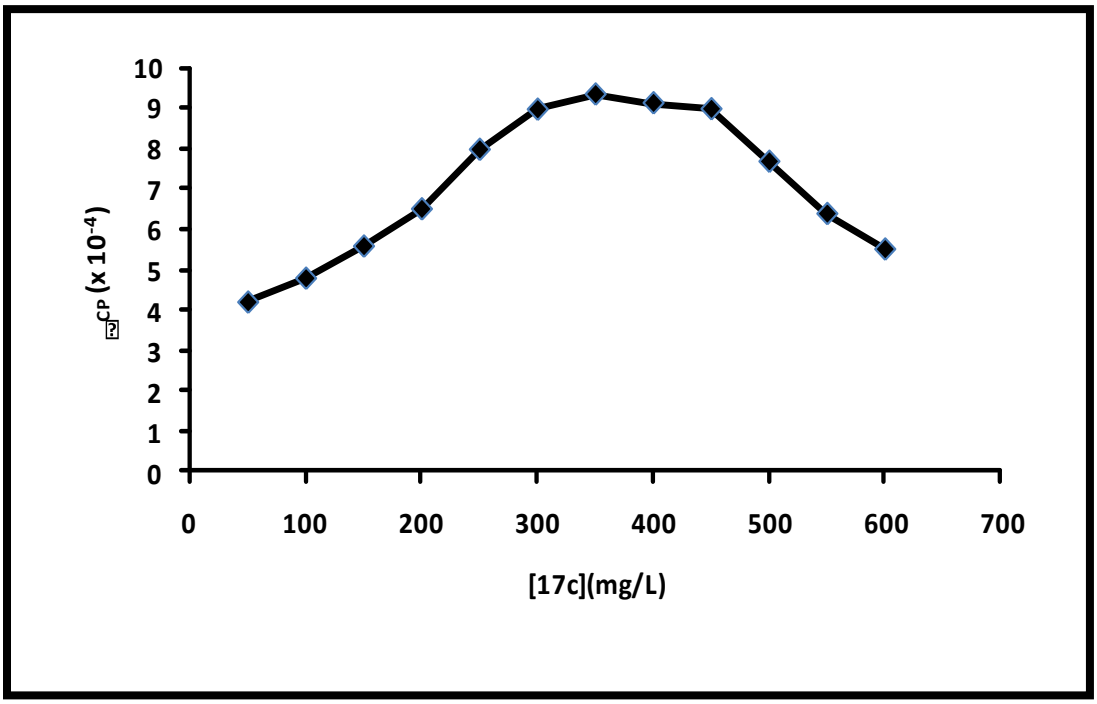

Figure 5.20: Plot of $\Phi_{4\text{-}CP}$ vs concentration of photosensitiser to determine the optimum sensitiser concentration for phototransfromation of 4-CP (Concentration = 1.00 x 10^{-4} M) in DCM.

Table 5.3: Photocatalytic parameters for phototransformation of 4-CP and PCP in basic media using 17c

Substrate	Optimum Catalyst Conc. (mg L^{-1})	Φ_{CP}	$k_a = \frac{k_d}{\Phi_\Delta Slope}$ (mol^{-1} L s^{-1})	$k_q + k_a$ (mol^{-1} L s^{-1})	Percentage conversion in 24 h (%)
4-CP	350	9×10^{-4}	3.4×10^4	5.2×10^4	91
PCP	300	2×10^{-5}	5.6×10^2	8.2×10^4	70

5.3.2. Kinetics of Photosensitisation

5.3.2.1. Homogenous reactions

The rate constant for homogeneous photo-oxidation, k_a, was estimated from the slope of the plot of $1/\Phi_{CP}$ vs 1/[CP] **(Figs. 5.21a and 5.21b), Eqn. 5.2**. k_a equals $k_d/\Phi_\Delta Slope$ where k_d is the singlet oxygen decay constant in DCM (1.6×10^4 **[291]**), and Φ_Δ is the singlet oxygen quantum yield of the sensitizer in DCM Φ_Δ=0.39.

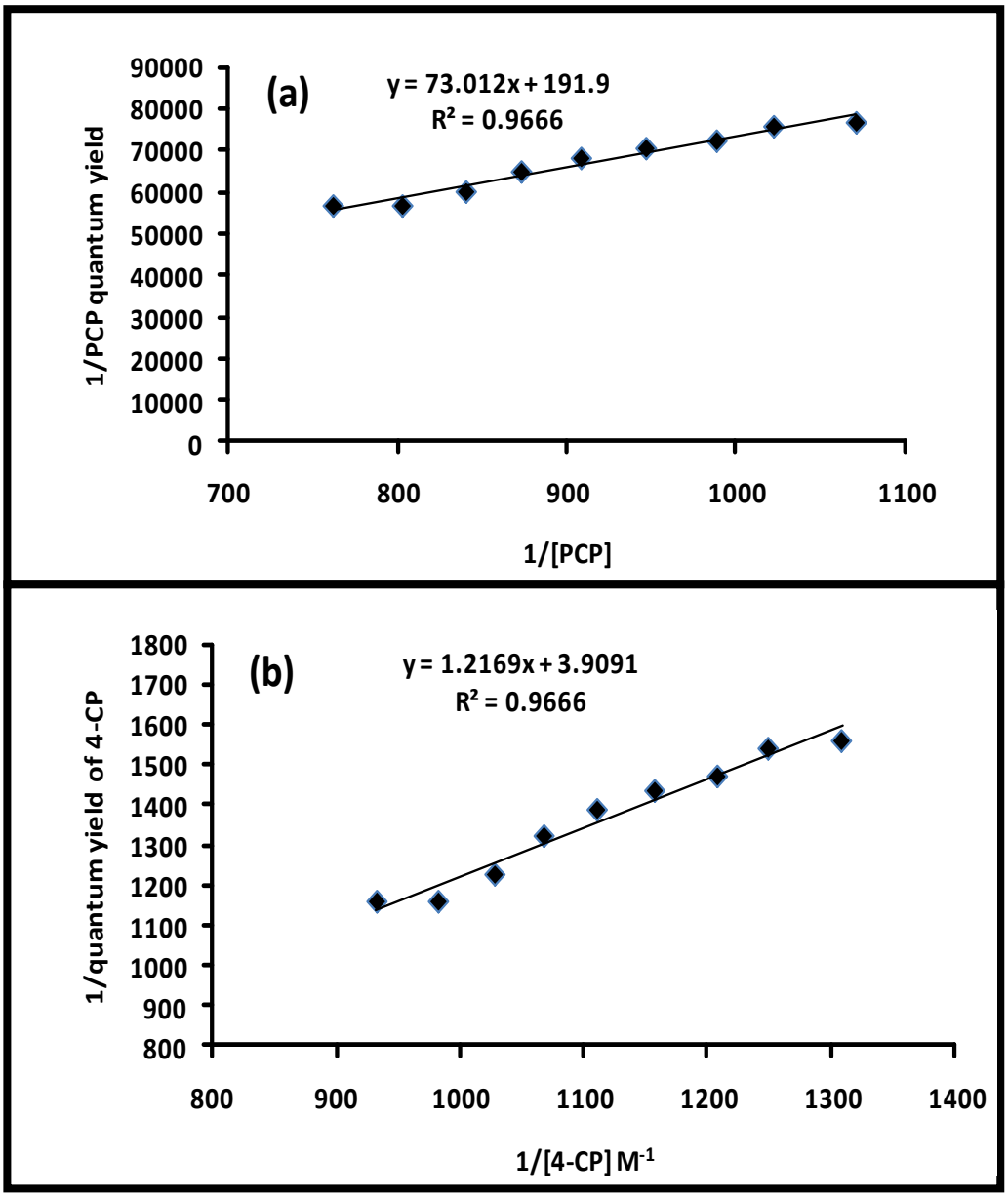

Figure 5.21: Plot of (a) $1/\Phi_{PCP}$ vs 1/[PCP] (catalyst (complex 17c) concentration = 300 mg/L (b) $1/\Phi_{4\text{-}CP}$ vs 1/[4-CP] (catalyst (Complex 17c) concentration = 350 mg/L)) in DCM.

Using k_a values as an indication of photodegradation efficiency, **Table 5.3** shows that photooxidation of 4-CP occurred faster than for PCP, due to plurality of the electron withdrawing chloride substituents which will make the ring difficult to oxidize. The breakdown of the aromatic ring has been reported to be slightly faster for 4-CP compared to PCP using semi-conductor particles **[298]**.

The quenching effects of the CPs on the singlet oxygen was estimated from (k_q + k_a) calculated from the intercept of **Figs. 5.21a** and **5.21b**. Comparison of the (k_q + k_a) with k_a or estimation of k_q from the two gives the deactivation or quenching of singlet oxygen via other routes apart from oxidation reaction with chlorophenols. The values of (k_q + k_a) for the sensitizer employed in this work were 8.2 x 10^4 and 5.2 x 10^4 mol^{-1} dm^3 s^{-1} for PCP and 4-CP respectively while k_a values were 5.6 x 10^2 and 3.4 x 10^4 mol^{-1} dm^3 s^{-1} for PCP and 4-CP, respectively **(Table 5.3)**. The implication of larger difference between (k_q + k_a) and k_a for PCP is that considerable amount of physical (chemically unproductive) quenching of singlet oxygen via **Eqn 1.33** took place during the reactions for PCP compared to 4-CP, hence the lower rate constant for PCP compared to 4-CP.

5.3.2.2. Heterogeneous reactions

For heterogeneous photosensitization, the optimum catalyst (as ads-**17c**-SWCNT-COOH) loading on SWCNT was determined using 1.00 x 10^{-4} M solution of 4-CP or PCP, while varying the catalyst concentration from 100 mg/L to 800mg/L and the initial rate of phototransfromation of 4-CP for each catalyst concentration determined, **Fig.5.22**. The removal of the CPs increased linearly with catalyst concentration until it reached 500 mg/L for both compounds after which there was a decrease probably due to shielding effect of the excess catalyst causing reduction in the penetration of light. The percentage conversion of 4-CP was 42% and for PCP, the values was 30 %, **Table 5.4**. This might be due to the difference in the chlorine atoms which make PCP more resistant to photo-oxidation. The percentage conversions of both pollutants were lower for heterogeneous reactions than for homogeneous reaction because of difference in singlet oxygen quantum yields for complex **17c** in DCM and ads-**17c**-SWCNT. The higher yield in the DCM gave rise to higher percentage conversion.

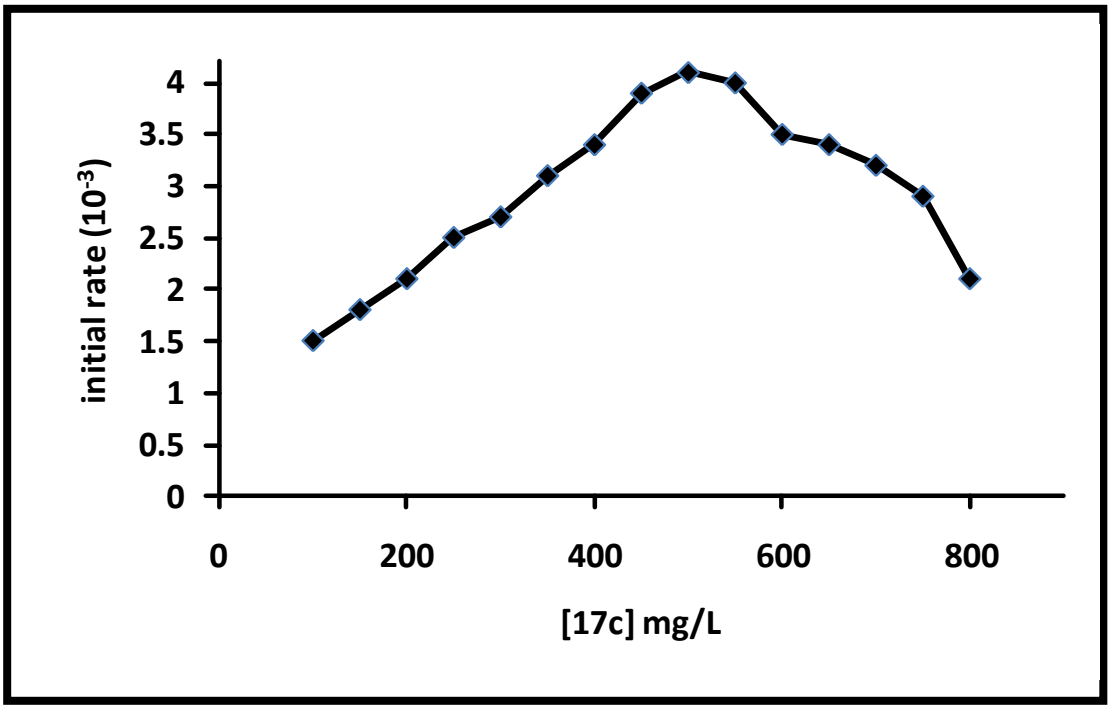

Figure 5.22: Plot of initial rate vs concentration of photosensitiser (ads-**17c**-SWCNT) **to determine the optimum sensitiser concentration for phototransfromation of 4-CP (Concentration = 1.00 x 10^{-4} M) .**

The kinetics of heterogeneous transformation of both 4-CP and PCP fitted into pseudo first order reaction kinetics. The apparent rate constant (k_{obs}) **Eqn. 5.3** was obtained from the slopes in **Fig. 5.23** (for PCP) for the two substrates at different concentration ranging from 4 x 10^{-5} to 10 x 10^{-5} M. The apparent rate of reaction k_{obs} for ads-PdODPc-SWCNT-COOH, **Table 5.4**, shows that the more dilute the CP solutions, the higher the apparent rate of transformation. The k_{obs} values ranged 1.21 x 10^{-3} min^{-1} and 3.12 x 10^{-3} min^{-1} for 4-CP and 1.80 x 10^{-3} min^{-1} and 4.00 x 10^{-3} min^{-1} for PCP for concentrations of 4, 6, 8 and 10 x 10^{-5} M. Thus the values are slightly higher for PCP.

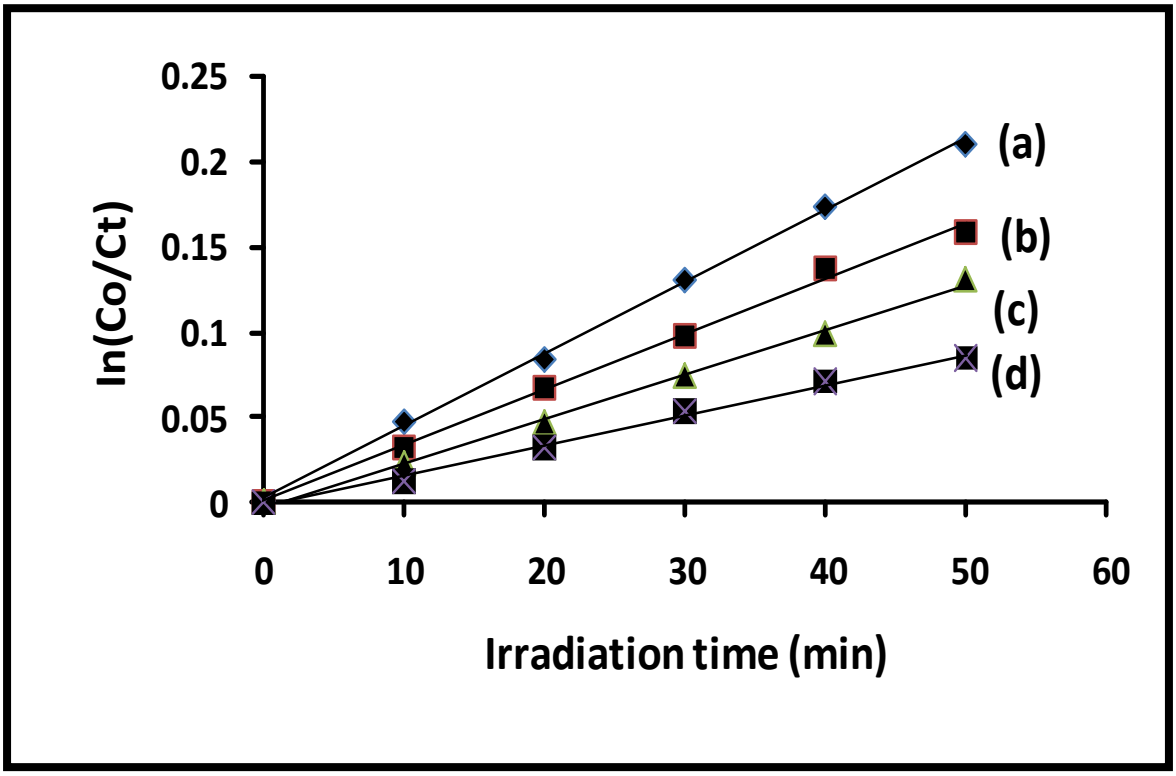

Figure 5.23: Langmuir-Hinshelwood kinetic plot for ads-17c-SWCNT-COOH in photooxidation of PCP. Starting concentrations are (a) 4 × 10^{-5} M, (b) 6 × 10^{-5} M (c) 8 × 10^{-5} M and (d) 10 × 10^{-5} M in water.

Langmuir-Hinshelwood model **(Eqn 5.4)** was employed for these studies.

The plots of reciprocal of initial rate of phototransformation vs. reciprocal of initial concentration of CPs **(Fig. 5.24)** gives k_r as the intercept, the adsorption coefficient (K_{ads}) was determined from slope. The plots were found to be linear with a non-zero intercept for both 4-CP and PCP. The values of k_r and K_{ads} are shown in **Table 5.4**. According to **Table 5.4**, adsorption rate (k_r) was lower for 4-CP with a value of 6.06 x 10^{-7} M min^{-1} compared to PCP 1.02 x 10^{-6} M min^{-1}. The values of adsorption coefficient (K_{ads} >>> 1) suggest that adsorption was more favoured than desorption for both substrate with adsorption of 4-CP being the more favoured because of its higher ratio.

Table 5.4: Langmuir-Hinshelwood (L-H) parameters for the phototransformation of 4-CP and PCP on Ads-PdODPc-SWCNT-COOH in basic media.

Substrate	Conc. (M)	k_{obs} (min^{-1}) (10^{-3})	k_r (M min^{-1})	K_{ads} (M^{-1})	Percentage conversion in 24 h (%)
4-CP	4.00×10^{-5}	3.12	6.06×10^{-7}	2.7×10^{3}	42
	6.00×10^{-5}	2.27			
	8.00×10^{-5}	1.92			
	1.00×10^{-4}	1.21			
PCP	4.00×10^{-5}	4.00	1.02×10^{-6}	5.56×10^{2}	30
	6.00×10^{-5}	3.30			
	8.00×10^{-5}	2.60			
	1.00×10^{-4}	1.80			

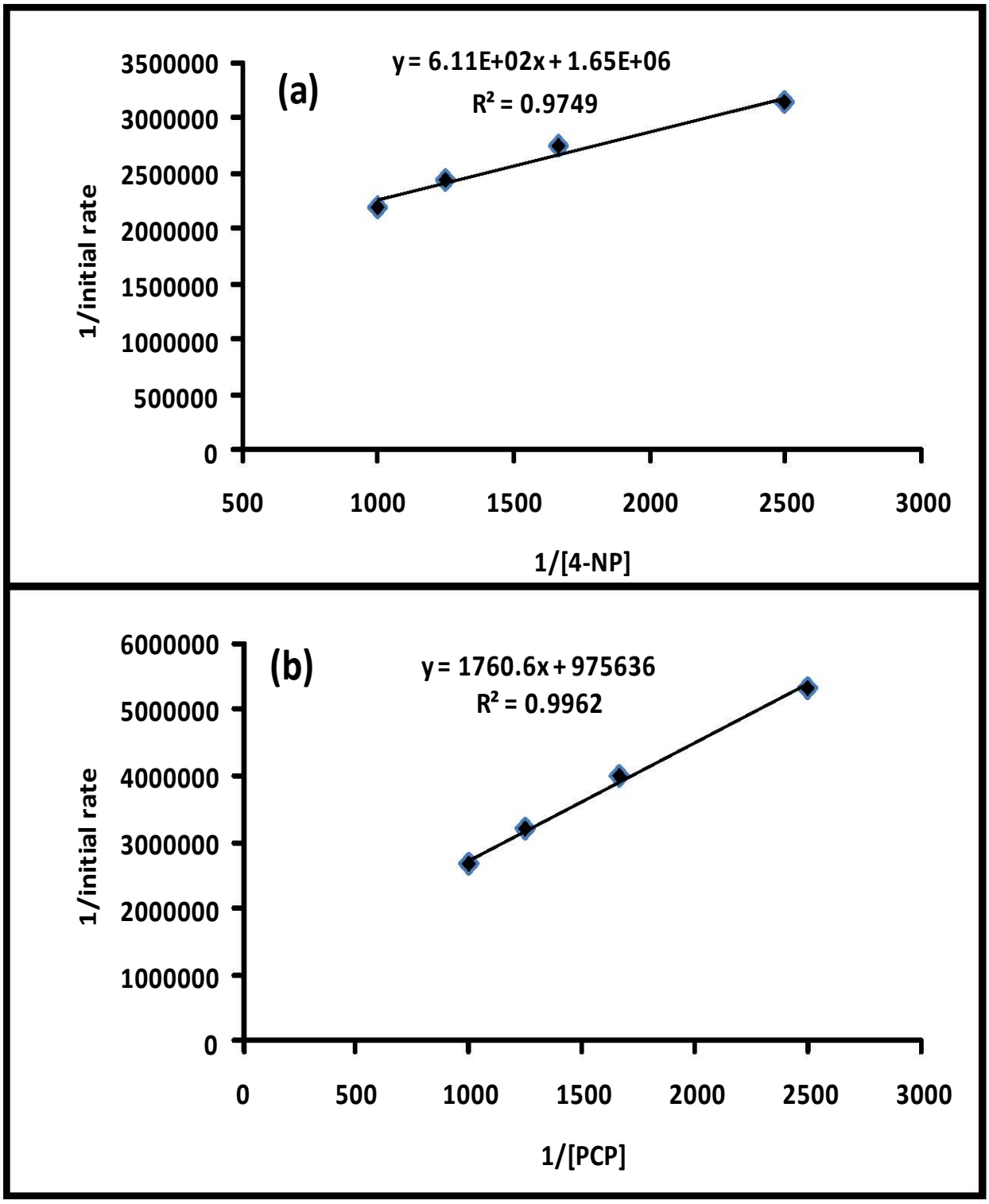

Figure 5.24: The plots of reciprocal of initial rate of phototransformation vs. reciprocal of initial concentration (a) 4-CP and (b) PCP using ads-17c-SWCNT-COOH as a sensitizer: (i) 4×10^{-5}, (ii) 6×10^{-5}, (iii) 8×10^{-5} and (iv) = 10×10^{-5} M in water.

5.3.3. Catalyst stability

Following use in the transformation of chlorophenols, the ads-**17c**-SWCNT-COOH were cleaned by rinsing in water, dried and reused for the phototransformation. **Fig. 5.25** shows the plots of concentration versus time, for the first, second and third uses of ads-**17c-**SWCNT-COOH for the phototransformation of fresh solution of PCP.

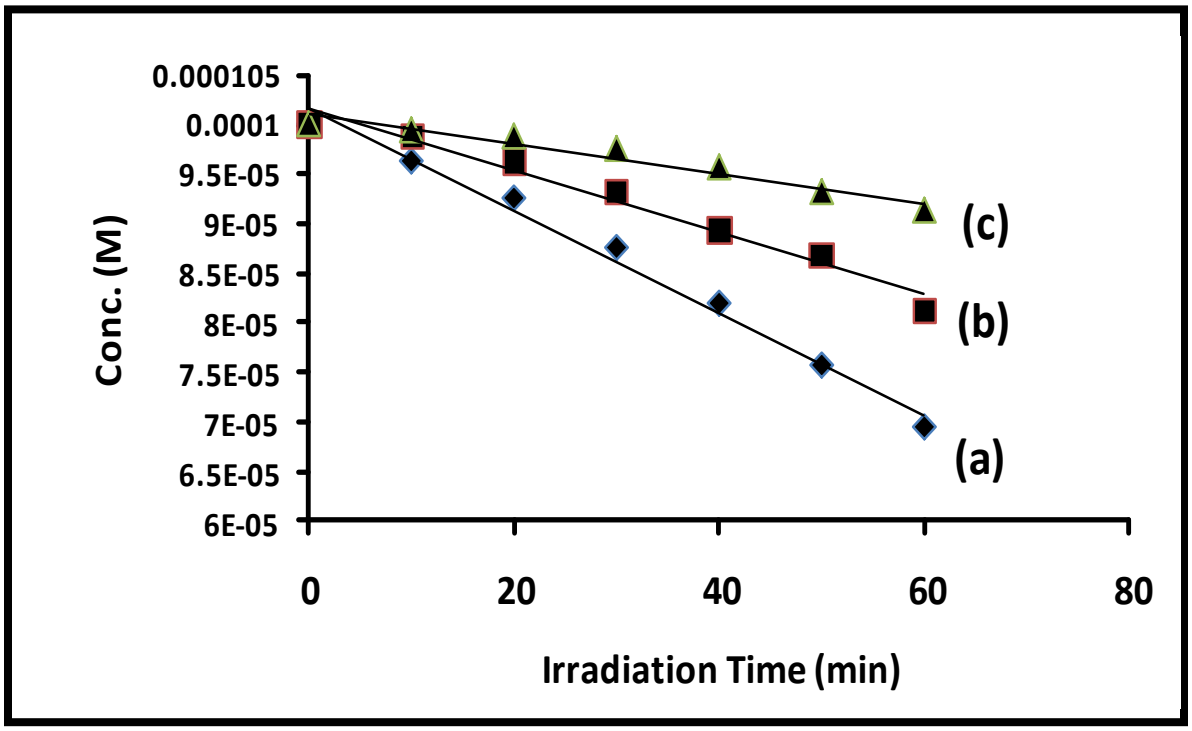

Figure 5.25: Plots of concentration versus time for the reuse of ads-17c-SWCNT-COOH for the photoransformation of PCP. (a) 1st use, (b) 2nd (re-use) and (c) 3rd (re-use) in water.

The rate changes remained approximately the same between 7.85 x 10^{-7} $Mmin^{-1}$ and 7.82 x 10^{-7} $Mmin^{-1}$ from the first to the third use in the case of 4-CP (figure not shown). But for PCP, **Fig. 5.25,** the story was completely different as the rate dropped drastically from 5.00 x 10^{-7} $Mmin^{-1}$ for the first use to 3.00 x 10^{-7} $Mmin^{-1}$ for the second use and 1.00 x 10^{-7} $Mmin^{-1}$ for the third use. The drastic reduction might be due to permanent adsorption of intermediates or even products on the surface of the catalyst thereby reducing its adsorption activities. This was confirmed by repeating the kinetics of the reactions for the reuse (second use) in the transformation of each of the substrate. While

both adsorption coefficient (K_{ads}) and adsorption rate (k_r) for 4-CP remained the same, both drastically went down in the case of PCP from 1.02 x 10^{-5} M min^{-1} and 556 M^{-1} to 5 x 10^{-6} Mmin^{-1} and 132 M^{-1} for k_r and K_{ads}, respectively implying that in the case of PCP the number of binding sites reduced significantly after use.

5.3.4. Photodegradation Products and Mechanism

GC was used to determine the products of homogeneous and heterogeneous phototransformation processes for the two substrate by comparing the retention times of standards of likely products like fumaric acid, 1,4-benzoquinone and hydroquinone, tetrachlorobenzoquinone. Two peaks due to the products were observed in the gas chromatogram traces for homogeneous photosensitization of 4-CP, **Fig. 5.26a**. These are: hydroquinone at 5.53 min which appeared in minute quantity (~5% of products) and 1,4-benzoquinone **(Scheme 5.2)** the major product which appeared at 3.00 min, under homogeneous catalysis.

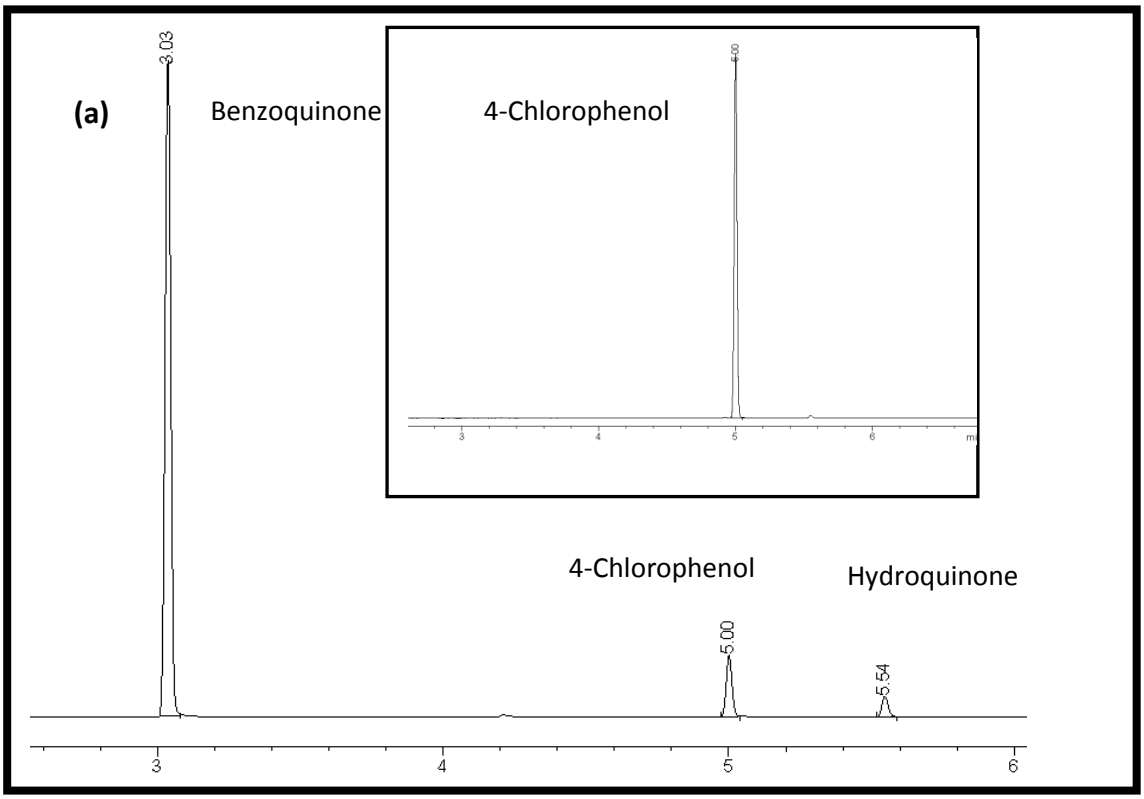

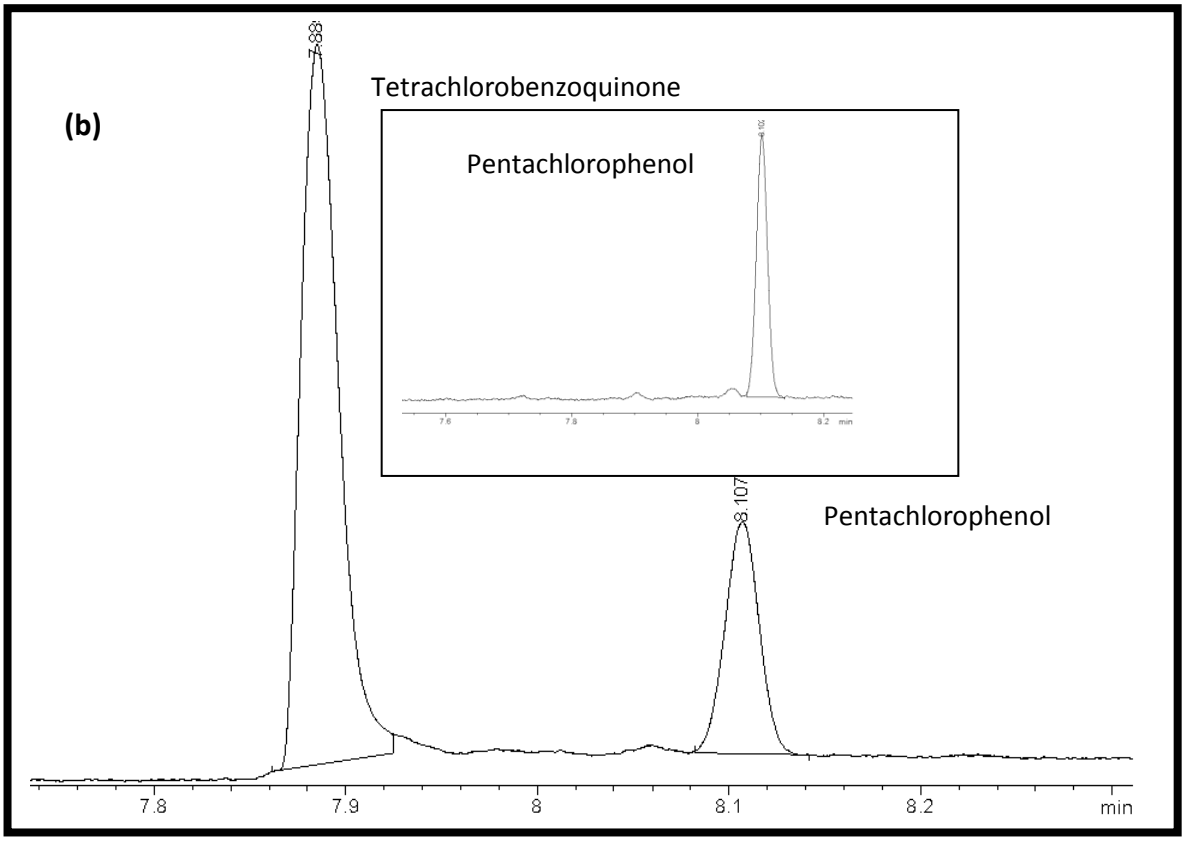

Figure 5.26: Gas chromatogram of the photolysed (a) 4-CP sample by complex 17c in DCM (b) PCP (in water) sample ads-17c-SWCNT-COOH. (Irradiation time =24 h, starting CP concentration = 1 x 10^{-4} mol dm^{-3}

These peaks were all confirmed during GC analysis by spiking with the respective standards. During heterogeneous catalysis the GC traces showed that the same products were formed but with higher proportion of hydroquinone (~20% of products). It is also important to mention that when oxygen was bubbled for longer period of time the proportion of hydroquinone in the products decreased while that of benzoquinone increased suggesting that singlet oxygen might be directly responsible for the production of benzoquinone while hydroquinone might be produced through Type I pathway (but in small amounts) as observed above for 4-NP. This was also confirmed by bubbling argon through a reaction medium before photolysis. In the presence of argon, hydroquinone was 70% of products though rate of reaction (4.00 x 10^{-7} M min^{-1}) was slower than when oxygen was bubbled (8.00 x 10^{-7} M min^{-1}) **(Fig 5.27)**.

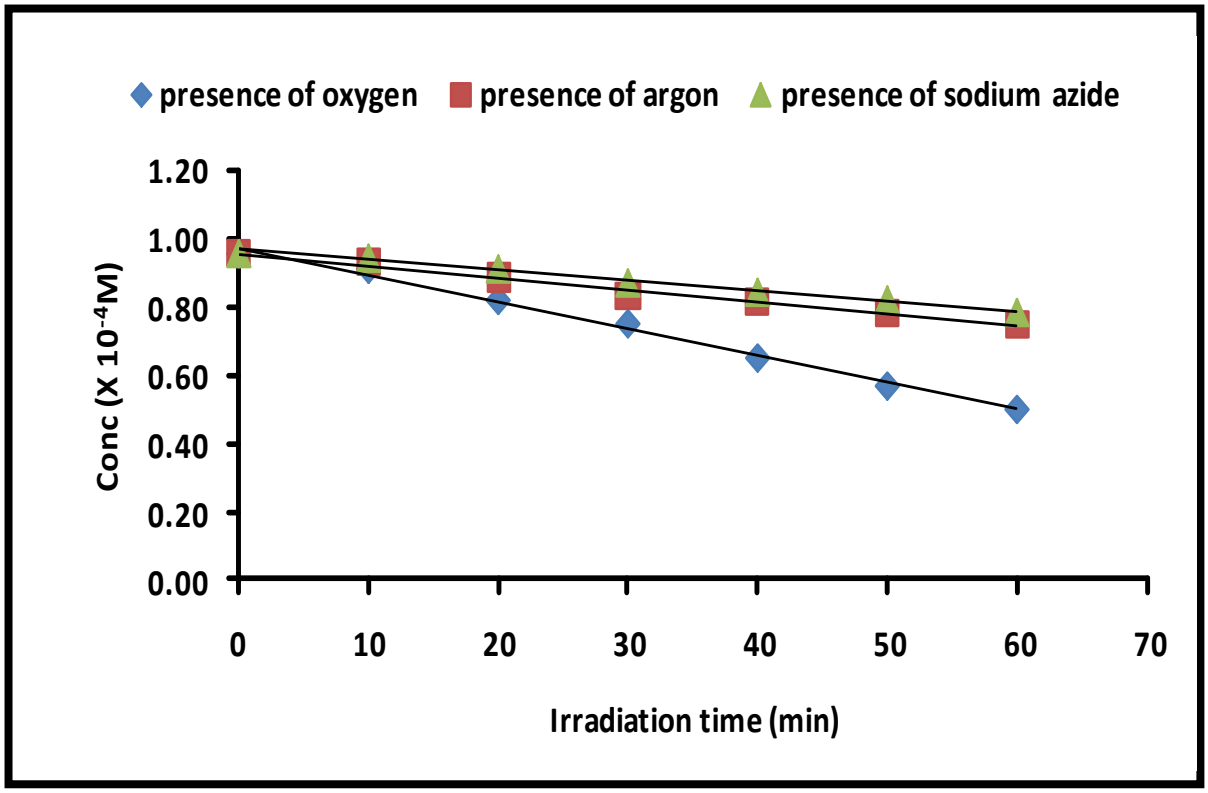

Figure 5.27: Demonstration of the effect of sodium azide and argon on 4-CP photo transformation rate using ads-17c-SWCNT-COOH.

Photolysis was also performed in the presence of a singlet oxygen scavenger, NaN_3(whose concentration was in a ratio of 1:1 with the substrate), the reaction rate was similar to when argon was bubbled with a rate of 3.00 x 10^{-7} M min^{-1}. The mechanism for 4-CP conversion is similar to that of 4-NP shown in **Scheme 5.1**. Homogeneous and heterogeneous **(Fig. 5.26b)** photosensitization of pentachlorophenol gave 2,3,5,6-tetrachloro-1,4-benzoquinone **(Scheme 5.2)** with homogeneous reaction giving 70% conversion as compared with 30% for heterogeneous reaction. Introduction of singlet oxygen scavenger halted the reaction suggesting that the only pathway available for this transformation is the Type II pathway.

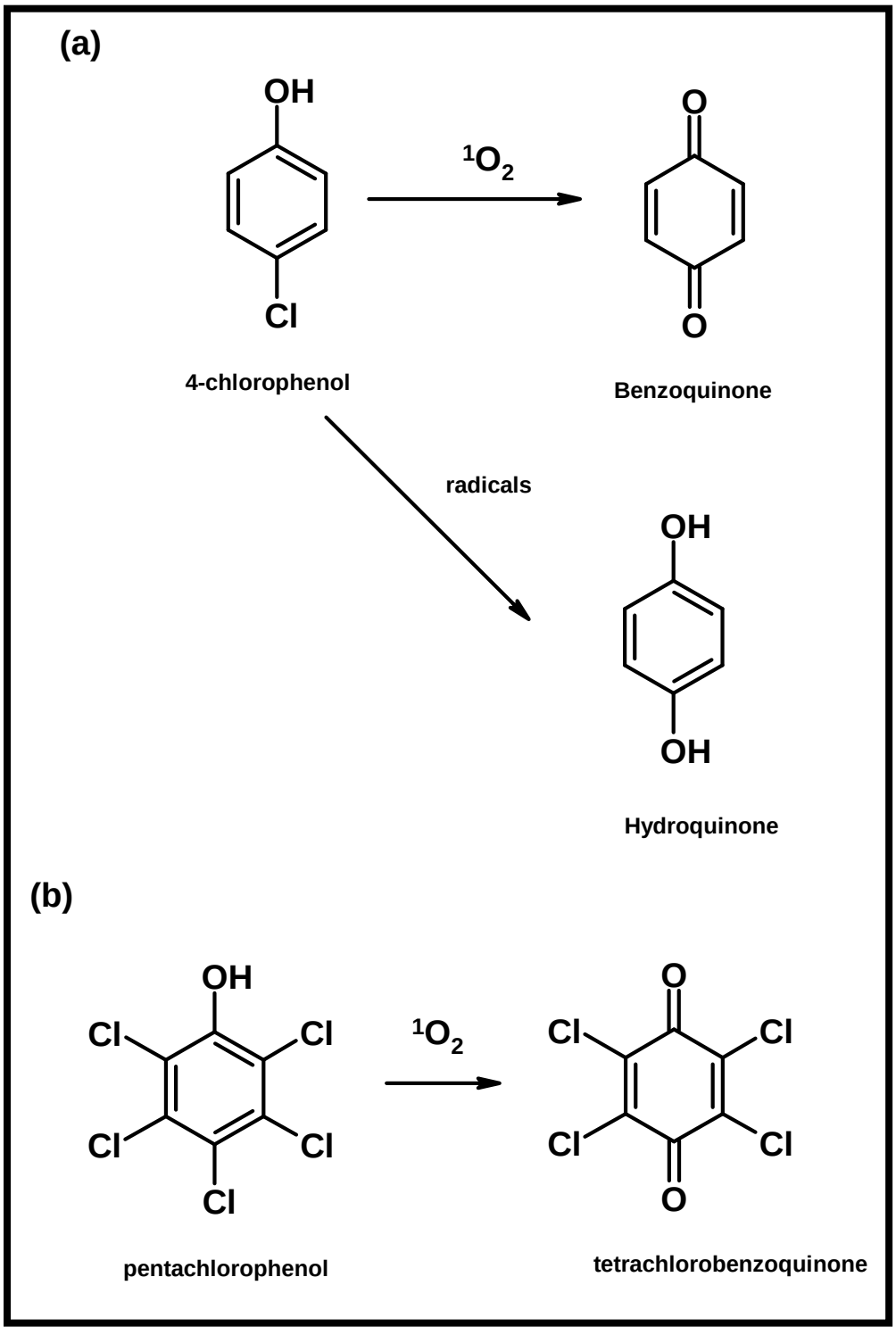

Scheme 5.2: Proposed mechanism for the phototransformation of (a) 4-CP (b) PCP on ads-17c-SWCNT-COOH.

Chapter 6

Conclusion and Future Perspective

6.1. Conclusion

Syntheses and spectroscopic characterization of various octasubstituted phthalocyanine ligands (Pcs) and their open-shell metallated derivatives (MPcs) were successfully carried out. The effects of these metals and substituents on the spectroscopic, photophysical and photochemical properties of the Pcs were investigated. The MPcs with good potential as sensitisers were also investigated for photosensitization of oxidation reactions. Substitution at the non peripheral position led to red shift of the Q band compared to the peripheral substitution and the large red shift led to an unsplit Q band for the unmetalated thio-derivatised Pcs.

The insertion of the metals into the cavity of the Pcs introduced interesting dimension on their optical properties especially with the thio-derivatised phthalocyanines showing trend that was dependent on the length of the alkyl chain. The Pd(II) octakis(pentylthio)phthalocyanine showed a loss of symmetry due to dome-type distortion while the same effect on the optical property of its Ni(II) derivative was due ring deformation. Symmetry was restored with longer alkyl chain. The large platinum metal also caused an extra peak associated with solvent dependent demetallation on the spectrum of benzyloxyphenoxy derivative of PtPc. The α and β substituted metal-free octakis(pentylthio)phthalocyanine and Pd(II) were successfully investigated for metal-binding studies for the formation of PdPc multinuclear complexes. Various products with various number of palladium metals at different position were isolated from this process.

Palladium and platinum improved the triplet quantum yield but reduced the lifetime of the complexes. In spite reduced lifetime the Pd(II)Pc and Pt(II)Pc complexes showed improved singlet oxygen generation capacity than the ligands while Ni(II) insertion resulted in complexes with reduced singlet oxygen quantum yields compared to the ligands. The multinuclear complexes from the metal binding studies gave no triplet peak due to low triplet lifetime. Insertion of the metals led to reduction in the

fluorescence quantum yield due to intersystem crossing and d-π interaction. The non-peripherally substituted derivatives gave fluorescence and excitation spectra that were too weak to interpret.

The high singlet oxygen quantum yield of the Pd(II)Pc and Pt(II)Pc analogues led to their use in homogenous and heterogeneous photosensitization investigation using 4-nitrophenol as model pollutant. All the MPcs gave good performance in homogenous reaction while only PdPcs were immobilized on functionalized single wall carbon nanotubes (SWCNT-COOH) that was used as support in the heterogeneous reaction.

All the PdPcs displayed good photosensitization properties under heterogeneous condition. Successful phototransformation of 4-chlorophenol and pentachlorophenol were also conducted using Pd(II) octakis(dodecylthio)phthalocyanine under homogenous and heterogeneous condition. Investigation of the mechanisms and products of all the reactions confirmed that singlet oxygen played a prominent role in the phototransfromation reactions. This confirms that in spite d-π interaction that reduce the lifetime of the excited states of their complexes these metals (Pd(II) and Pt(II)) are still capable of forming photosensitisers that catalyse oxidation reactions through singlet oxygen mediated pathways

6.2. Future Perspectives

Investigation of the reason why metal-free phthalocyanines derivatives gave high triplet quantum yield and triplet lifetime but low singlet oxygen quantum yield has to be carried out. Also aryloxo-derivatised Ni(II) phthalocyanines and multinuclear palladium phthalocyanines showed no triplet absorption peak probably because of short triplet lifetime. This makes them potential candidate for investigation in photothermal therapy (PTT) of cancer and phosphorescence based sensing.

References

1. A. Braun, J. Tscherniac. 1907, ***Chem. Ber.***, 40, 2709.

2. H. De Diesbach, E. von der Weid. 1927, ***Helv. Chem. Acta*** , 10, 886.

3. A. G. Dandridge, H. A. Drescher, J. Thomas. ***GB patent*** *322169* 1928.

4. R. P. Linstead. 1934, ***J. Chem. Soc.***, 1022.

5. C. E. Dent, R. P. Linstead, A. R. Lowe. 1934***, J. Chem. Soc.,*** 1033.

6. J. M. Robertson,. 1935, ***J. Chem. Soc.*** , 615.

7. J. M. Robertson and R. P. Linstead, C. E. Dent. 1935, ***Nature*** , 135, 506.

8. J. M. Robertson. 1936, ***J. Chem. Soc.***, 1195.

9. J. M. Robertson, I. Woodard. 1937, ***J. Chem. Soc.***, 219.

10. J. M. Robertson, I. Woodard. 1940, ***J. Chem. Soc.***, 36.

11. F. H. Moser, A. L. Thomas. ***The Phthalocyanines.*** Boca Raton : CRC Press, 1983. Vol. 1 and 2.

12. P. Gregory. 2000, ***J. Porphyrins Phthalocyanines***, 4, 432.

13. O. Kaliya, E. A. Luk'yanets, G. N. Vorozhtso. 1999, ***J. Porphyrins Phthalocyanines*** , 3, 592.

14. N. B. McKeown. ***Chem. Industry***. 1999. 92.

15. R. J. Salazar. [ed.] R. A. Meyers. ***Handbook of Petroleum Refining Processes.*** Weinheim : VCH, 1986, 6, p. 571.

16. C. G. Claessens, W. J. Blau, M. Cook, M. Hannack, R. J. M. Nolte, T. Torres, D. Worhle. 2001, ***Monatsh. Chem.*** , 132, 3.

17. M. Bandin, E. Bertounesque, V. Plinchon, J. Simon, V. Ahsen, O. Bekaroglu. 1989, ***J. Electroanal. Chem.***, 271, 173.

18. P. Gregory. 1999, ***J. Porphyrins Phthalocyanines***, 3, 468.

19. K. Davidson, R. Jones, S. Mcdonald. 2001, ***Synth. Met.*** , 121, 1399.

20. Lier, J. E. Van. In ***Photodynamic Therapy of Neoplastic Diseases.*** [ed.] D. Kessel. Boca Raton : CRC Press, 1990. p. 279. Vol. 1.

21. I. Rosenthal. In ***Phthalocyanines: Properties and Applications.*** [ed.] A. B. P. Lever C. C. Leznoff. Weinheim : VCH, 1996. p. 481. Vol. 4.

22. H. S. Nalwa, J. S. Shirk. In ***Phthalocyanines: Properties and Applications.*** [ed.] , A. B. P. Lever C. C. Leznoff. s.l. : VCH: Weinheim,, 1996. p. 79. Vol. 4.

23. G. De la Torre, T. Torres, F. Agullo-Lopez. 1997, ***Adv. Mater.***, 9, 265.

24. I. Booysen, F. Matemadombo, M. Durmus, T. Nyokong. 2011**,** ***Dyes Pigm.***, 89, 111.

25. N. Masilela, T. Nyokong. 2010, ***Dyes Pigm.***, 84, 242.

26. N. Nombona, T. Nyokong. 2009, ***Dyes Pigm.***, 80, 130.

27. D. K. Modibane, T. Nyokong. 2009, ***Polyhedron,*** 28, 1475.

28. D.S. Lawrence, D.G. Whitten. 1996, ***Photochem. Photobiol***, 64 , 923.

29. P. S. Vincett, E. M. Voigt, K. E. Rieckhoff. 1971, ***J. Chem. Phys.*** , 55 , 4131.

30. P. G. Seybold, M. Gouterman. 1969, ***J. Mol. Spec.***, 31, 1.

31. N. Kobayashi, Y. Higashi, T. Osa. 1994, ***Chem. Lett***, 1813.

32., K Teuchner, A. Pfarrherr, H. Stiel, W. Freyer, D. Leupold, . 1993, ***Photochem. Photobiol. 57, 465***.

33. H. Ohtani, T. Kobayashi, T. Ohno, S. Kato, T. Tanno, A. Yamada. 1984, ***J. Phys. Chem.***, 88, 4431.

34. J. H. Brannon, D. J. Magde. 1980, ***J. Am. Chem. Soc.***, 62, 102.

35. W. Freyer, K. Teuchner. 1988, ***J. Photochem. Photobiol. A***, 45, 117.

36. A. Beeby, A. W. Parker, M. S. C. Simpson, D. Philips. 1992, ***J. Photochem. Photobiol. B***, 16, 73.

37. K. Ishii, Y. Hirose, M. Fujitsuka, O. Ito, N. Kobayashi. 2001, ***J. Am. Chem. Soc.***, 123, 702.

38. G. Knor. 1996, ***Inorg. Chem.***, 35, 7916.

39. B. D. Rihter, M. E. Kenney, W. E. Ford, M. A. J. Rogers. 1990, ***J. Am. Chem. Soc.***, 112, 8064.

40. J. D. Spikes, J. E. van Lier, J. C. Bommer. 1995, ***J. Photochem. Photobiol. A***, 91, 193.

41. S. L. Gilat, T. W. Ebbesen. 1993, ***J. Phys. Chem.***, 97, 3551.

42. P. A. Firey, W. E. Ford, J. R. Sounik, M. E. Kenney, M. A. J. Rodgers. 1988, ***J. Am. Chem. Soc.***, 110, 7626.

43. B. D. Rihter, M. E. Kenney, W. E. Ford, M. A. J. Rodgers. 1993, ***J. Am. Chem. Soc.***, 115, 8146.

44. B. D. Rey, U. Keller, T. Torres, G. Rojo, F. Agullo-Lopez, S. Nonell, C. Marti, S. Brasselet, I. Ledoux, J. Lyss. 1998, ***J. Am. Chem. Soc.***, 120, 12808.

45. R. H. Campbell, G. A. Heath, G. I. Hefter, R. C. S. McQueen. 1983, ***J. Chem Soc., Chem. Comm.***, 1123.

46. A. Louati, M. El Meray, J. J. Andre, J. Simon, K. M. Kadish, M. Gross, A. Giraudeau. 1985, ***Inorg. Chem.***, 25, 1175.

47. A. Giraudeau, A. Louat, M. Gross, J. J. Andre, J. Simon, C. H. Su, K. M. Kadish. 1983, ***J. Am. Chem. Soc.***, 105, 2917.

48. D. W. Clack, N. S. Hush, I. S. Woolsey. 1976, ***Inorg. Chim. Acta***, 19, 129.

49. A. B. P. Lever, S. Licoccia, K. Magnell, P. C. Minor, B. S. Ramaswamy. 1982, ***Adv. Chem. Ser.,*** 201, 237.

50. P. A. Barret, C. E. Dent, R. P. Linstead. 1936, ***J. Chem. Soc.***, 1719.

51. C. Ercolani, A. M. Paoletti, G. Pennesi, G. Rossi. 1990, ***J. Chem. Soc., Dalton Trans***., 1971.

52. A. Capobianchi, C. Ercolani, A. M. Paoletti, G. Pennesi, G. Rossi, A. Chiesi-Villa, C. Rizzoli. 1993, ***Inorg. Chem.***, 32, 4605.

53. T. Nyokong. 1995, ***S. Afr. J. Chem.***, 48, 23.

54. E. Marais, R. Klein, E. Antunes, T. Nyokong. 2007, ***J. Mol. Catal. A: Chem.***, 261, 36.

55. E. Marais, R. Klein, E. Antunes, T. Nyokong. 2008, ***J. Coord. Chem.*** , 61, 3727.

56. K. Ozoemena, N. Kuznetsova, T. Nyokong. 2001, ***J. Photochem. Photobiol. A***, 139, 217.

57. K. Ozoemena, N. Kuznetsova, T. Nyokong. 2001, ***J. Mol. Catal. A: Chem.*** , 176, 29.

58. B. Agboola, K. I. Ozoemena, T. Nyokong. 2006, ***J. Mol. Cat. A: Chem.*** , 248, 84.

59. M. Hu, Y. Xu, Z. Xiong. 2004, ***Chem. Lett.***, 33, 1092.

60. X. Xue, Y. Xu. 2007, ***J. Mol. Catal. A,*** 276, 80.

61. A. Sun, Z. Xiong, Y. Xu. 2008, ***J. Haz. mater.***, 152, 191.

62. R. R. Millard, B. I. Greene. 1985, ***J. Phys. Chem.*** , 89, 2976.

63. B. I. Khansov, J. Rivera De La Rosa, O. V. Kharissova, J. L. Almaraz Garza, J. R. Alamguer Rodriguez, L. I. Puente, U. O. Mendez, A. K. Ibarra Arvivu. 2007, ***J. Coord. Chem.*** , 60, 355.

64. E. R. Menzel, K. E. Rieckhoff, E. -M. Voigt. 1973, ***J. Chem. Phys.,*** 58, 5726.

65. W, -H. Chen, K. E. Rieckhoff, E. -M. Voigt. 1986, ***Mol. Phys.***, 59, 355.

66. A. V. Nikolaitchik, M. A. J. Rodgers. 1999, ***J. Phys. Chem. A***, 103, 7597.

67. Z. Xiong, Y. Xu. 2007, ***Chem. Mater***, 19, 1452.

68. M. K. Şener, A. Koca, A. Gül, M. B. Koçak. 2007, ***Polyhedron***, 26, 1070.

69. B. D. Berezin. ***Coordination Compounds of Porphyrins and Phthalocyanines.*** new York : John Wiley and Sons Ltd , 1981.

70. A. G. Gürek, O. Bekaroğlu. 1994, ***J Chem. So.c Dalton Tran*** , 1419.

71. K . Ban, K . Nishizawa, K . Ohta, H. Shirai. 2000, ***J. Mater. Chem.***, 10, 1083.

72. G. Mbambisa, P. Tau, E. Antunes, T. Nyokong. 2007, ***Polyhedron***, 26, 5355.

73. D. Wöhrle, M. Eskes, K. Shigehara, A. Yamada. 1993, ***Synthesis*** , 94.

74. I. Gürol, V. A hsen, Ö. Bekaroglu. 1994, ***J. Chem. Soc., Dalton Trans.*** , 497.

75. C. G. Claessens, T. Torres. 2000, ***Eur. J. Org. Chem.***, 1603.

76. M. Hannack, G. Schmid, , M. Sommerauer. 1993, ***Angew. Chem. Int. ed. Engl.*** , 32, 1442.

77. M. Sommerauer, C. Rager, M. Hannack. 1996, ***J. Am. Chem. Soc.***, 118, 10085.

78. A. W. Snow, , N. L. Jarvis. 1984, ***J. Am. Chem. Soc.*** , 106, 4706.

79. J. G. Young, , W. Onyebuagu. 1990, ***J. org. Chem.*** , 55, 2155.

80. I. G. Abramov, V. V. Plakhtinskii, M. B. Abramova, A. V. Smirnov, G. G. Krasovskaya. 1999, ***Chem. Hetero. Comp.*** , 35, 1342.

81. S. Öztürk, S. Isik, H. –K. Fun, E. Kendi, E. Agar, S. Sasmaz, A. R. Ibrahim,. 1999, ***Acta Cryst.*** , C55, 395.

82. C. Dent. 1938, ***J. Chem. Soc.*** , 1.

83. I. Owen, M. Kenney. 1962, ***Inorg. Chem***., 1, 331 .

84. S. Gaspard, P. Maillard. 1987, ***Tetrahedron*** , 43, 1083.

85. T. J. Hurley, M.A. Robinson, S, I.Trotz. 1967, ***Inorg. Chem.*** , 6, 389.

86. C. C. Leznoff. In ***Phthalocyanines: properties and applications.*** [ed.] A. B. P. Lever C. C. Leznoff. Weinheim : VCH, 1989. p. 1. Vol. 1.

87. N. M. Bigelow, M. A. Perkins. In ***Phthalocyanine Pigments.*** [ed.] H. A. Lubs. New York : Reinhold Press, 1955. p. 577.

88. W. S. Struve. In ***Phthalocyanine Pigments.*** [ed.] H. A. Lubs. New York : Reinhold Press, 1955. p. 606.

89. G. Booth. In ***The Chemistry of synthetic Dyes.*** [ed.] K. Venkataraman. New York : Academic Press, 1971. p. 241.

90. S. Y. Al-Raqa. 2008, ***Dyes Pigm.,*** 77, 259.

91. W, -F. Law, R.C.W. Liu, J. Jang, D. K. P. Ng. 1997, ***Inorg. Chim Acta***, 256, 147.

92. T. Fukuda, T. Ishiguro, N. Kobayashi. 2005, ***Tetrahedron Lett.***, 46, 2907.

93. N. B. R. Vittar, C. G. Pucca, C. Strassert, J. Awruch, V. A. Rivarola. 2008, ***Int. J. Biochem. Cell Bio.***, 40, 2102.

94. X, -F. Zhang, Y. Wang, L. Niu. 2010, ***J. Photochem. Photobiol***., 209, 232.

95. Y. Arslanoglu, A. Koca, E. Hamuryudan. 2007, ***Polyhedro***n, 26, 891.

96. N.Y. Meryem, M. Kandaz, A. Koca, B. Salih. 2006, ***J. Porphyrins Phthalocyanines***, 10, 1022.

97. M. Kandaz, H. S. Cetin, A. Koca, A.R. Ozkaya. 2007, ***Dyes Pigm***, 74, 298.

98. A. Bilgin, A. Mendi, U. Yildiz. 2006, ***Polymer***, 47, 8462.

99. K. Walzer, M. Hietschold. 2001, ***Surface Science***, 471, 1.

100. P. N. Day, Z. Wang, R. J. Pachter. 1998, ***J. Mol. Struc. (THEO-Chem),*** 455, 33.

101. M.J. Stillman, T. Nyokong. In ***Phthalocyanines: Properties and Properties.*** [ed.] C. C. Leznoff A. B. . PLever. New York : VCH Publications, 1989. pp. 133, 139. Vol. 1.

102. M. Gouterman. ***Part A. Physical Chemistry.*** [ed.] D. Dolphin. In The Porphyrins. New York : Academic Press, 1978, Vol. 3, p. 1.

103. A. J. McHugh, M. Gouterman, C. Weiss. 1987, ***Theoret. Chim. Acta.*** , 24 , 246.

104. A. M. Schaffer, M. Gouterman,E. R. Davidson. 1973, ***Theoret. Chim Acta.*** , 30, 9.

105. L. K. Lee, N. H. Sabelli, P. R. LeBreton. 1982, ***J. Phys. Chem.***, 86, 3926.

106. A. J. McHugh, M. Gouterman, C. Weiss. 1972, ***Theoret. Chim. Acta***, 24 , 346.

107. T. H. Huang, K. E. Reickhoff, E. M. Voight. 1982, ***J. Chem. Phys.*** , 77 , 3424.

108. T. H. Huang, K. E. Reickhoff, E. M. Voight. 1981, ***J. Chem. Phys.*** , 85 , 3322.

109. M.J. Stillman. In ***Phthalocyanines: Principles and Properties.*** [ed.] C. C. Leznoff A. B. P. Lever. New York : VCH Publications, 1993. p. 227.

110. J. Mark, M. J. Stillman. 1994, ***J. Am. Chem. Soc.*** , 116, 1292.

111. M. Konami, M. Hatano, A. Tajiri. 1990, ***Chem. Phys. Lett.***, 166 , 605.

112. N. Kobayashi, H. ogata, N. Nonaka, E. A. Luk'yanets,. 2003, ***Chem. Eur. J.*** , 9, 5123.

113. N. B. McKeown. ***Phthalocyanine materials: Synthesis, Strucrure and Function.*** Cambridge : Cambridge University Press, 1998.

114. J. Sleven, C. Gorller-Walrand, K. Binnemans. 2001, ***Journal of Material Science and Engineering C***, 18, 229.

115. A. Jablonski. 1935, ***Z. Phys.***, 94, 38.

116. P. W. Atkins. [ed.] P. W. Atkins. In ***Physical Chemistry. 6th. Oxford*** : Oxford University Press, 1998, 17.

117. K. Ishii, N. Kobayashi. [ed.] R. Guilard K. M. Smith. In ***The Porphyrin handbook***. New York : Elsevier Science, 2003, Vol. 16, p. 102.

118. G. Jori, S.B. Brown. 2004, ***Photochem. Photobiol. Sci.*** , 3 , 403.

119. A. Villanueva, R. Vidania, J.C. Stockert, M. Canete, A. Juarrans. Photodynamic Effects on Cultured Tumor Cells, Cytoskeleton Alterations and cell death mechanisms. [ed.] H. S. Nalwa. ***Handbook of photochemistry and photobiology.*** Valencia : American Scientific Publisher, 2002, Vol. 4, 3, p. 79.

120. A. Ogunsipe, J.-Y. Chen, T. Nyokong. 2004, ***New J. Chem.,*** 28, 822.

121. D.J. Ball, S.R. Wood, D.I. Vernon, J. Griffiths, T.M.A.R. Dubbelman, S.B. Brown. 1998, ***J. Photochem. Photobiol***, B 45, 28.

122. V. Mantareva, V. Kussovski, I. Angelov, E. Borisova, L. Avramov, G. Schnurpfeil, D. Wohrle. 2007, ***Bioorg. Med. Chem.*** , 15 , 4829.

123. D.M. Guldi, T.D. Mody, N.N. Gerasimchuk, D. Magda, J.L. Sessler,. 2000, ***J. Am. Chem. Soc.***, 122, 8289.

124. V. Chauke, A. Ogunsipe, M. Durmus, T. Nyokong. 2007, ***Polyhedron*** , 26 , 2663.

125. M. Idowu, T. Nyokong. 2008, ***J. Photochem. Photobiol. A.,*** 200, 396.

126. M. Idowu, T. Nyokong. 2008***, J. Photochem. Photobiol. A,*** 199, 282.

127. A. Erdogmus, A. Ogunsipe, T. Nyokong. 2009, ***J. Photochem. Photobiol. A***, 205, 12.

128. A. Ogunsipe, T. Nyokong. 2004***, J. Mol. Struct.*** , 689, 89.

129. S. Garpard. 1989, ***J. Chem. Soc. Perkin Trasn,*** , 2, 383.

130. N. Kobayashi, N. Sasaki, Y. Higashi, T. Osa. 1995, ***J. Inorg. Chem.*** , 34 , 1636.

131. T. Shen, Z. –L. Yuan, H, -J. Xu. 1989, ***Dyes Pigm.***, 11, 77.

132. J. Kossanyi, D. Chahraoui. 2000, ***Int. J. Photoenergy*** , 2, 9.

133. N. Masilela, T. Nyokong. 2010, ***Dyes & Pigm.,*** 84, 242.

134. X. –F. Zhang, H. –J. Xu. 1993, ***J. Chem. Soc. Faraday Trans.,*** 89, 3347.

135. S. Fery-Forgues, D. Lavabre. 1999, ***J. Chem. Educ.*** , 76 , 1260.

136. J. Fu, X. Y. Li, D. K. P. Ng, C. Wu. 2002, ***Langmuir*** , 18, 3843.

137. W. Chidawanyika, A. Ogunsipe, T. Nyokong. 2007, ***New J. Chem.,*** 31, 377.

138. M. Durmus, T. Nyokong. 2007, ***Polyhedron***, 26, 3323.

139. P. Kubat, J. Mosinger. 1993, ***J. Photochem. Photobiol. A*** , 96 ,93.

140. I. J. MacDonald, T. J. Dougherty. 2001, ***J. Porphyrins Phthalocyanines***, 5, 105.

141. A. Gilbert, J. Baggott. ***Photo-oxidation reactions, Essentials of Molecular Photochemistry.*** Boca Raton : CRC Press, 1991. pp. 501-525.

142. M. C. DeRosa, R. J. Crutchley. 2001, ***Coord. Chem. Rev.***, 233-234, 351.

143. I. Rosenthal. 1991, ***Photochem. Photobiol.***, 53, 859.

144. J. D. Spikes. 1990**, *Photochem. Photobiol. B***, 6, 259.

145. W. Spiller, H. Kliesch, D. Worhle, S. Hackbarth, B. Roder G. Schnurpfield. 1998, ***J. Porphyrins Phthalocyanines***, 2, 145.

146. C.S. Foote. In ***Singlet Oxygen***. [ed.] R. W. Murray H. H. Wasserman. New York, San Fransisco, London : Academic Press, 1979. p. 139.

147. A. K. Sobbi, D. Wöhrle, D. Schlettwein. 1993**, *J. Chem. Soc. Perkin Trans***, 2, 481.

148. M. J. Cook, I. Chambrier, S. J. Cracknell, D. A. Mayes, D. A. Russell. 1995, ***Photochem. Photobiol***, 62, 542.

149. D. Wöhrle, O. Suvorova, R. Gerdes, O. Bartels, L. Lapok, N. Baziakina, S. Makarov, A. Slodek. 2004, ***J. Porphyrins Phthalocyanines***, 8 , 1020.

150. S. E. Maree, T. Nyokong. 2001, ***J. Porphyrins Phthalocyanines***, 5 , 117.

151. H. Xu, T. Shen, O. Zhou, S. Shen, J. Liu, L. Li, S. Zhou, X. Zhang, Q. Yu, Z. Bi, X. Xias. 1992**, *J. Photochem. Photobiol. A***, 65, 267.

152. M. D. Maree, D. Phillips, T. Nyokong. 2001, ***J. Photochem. Photobiol. A*** , 140 , 117.

153. J. Grodkowski, J. H. Chambers Jr. P. Neta. 1984, ***J. Phys. Chem.*** , 88, 5332.

154. N. A. Kuznetsova, V. V. Okunchikov, V. M. Derkacheva, O. L. Kaliya, E. A. Luk'yanets. 2005**, *J. Porphyrins Phthalocyanines*** , 9 , 393.

155. J. D. Spikes. 1992, ***Photochem Photobiol***, 55, 797.

156. P. Tau, A. O. Ogunsipe, S. Maree, M. D. Maree, T. Nyokong. 2003, ***J. Porphyrin. Phthalocyanine***,, 7 , 439.

157. J. R. Darwent, P. Douglas, A. Harriman, G. Poter, M. C. Richoux. 1982, ***Coord. Chem. Rev.*** , 44 , 83.

158. G. Winter, H. Hechmann, P. Haisch, W. Eberhardt, M. Hanack,, L. Luer, H.-J. Egelhaaf, D. Oelkrug, 1998, ***J. Am. Chem. Soc***., 120, 11663.

159. A.W. Snow. [ed.] K.M. Smith, R. Gilard K.M. Kadish. In ***The Porphyrin Handbook.*** New York : Elsevier Science, 2003, Vol. 17, p. 109.

160. A. R. Monahan, J. A. Brado, F. A. DeLuca. 1972, ***J. Phys. Chem.*** , 76 , 446.

161. W. A. Nevin, W. Liu, S. Greenberg, M. R. Hempstead, S. M. Maruccio, M. M. Melnik, C. C. Leznoff, A. B. P. Lever. 1987, ***Inorg. Chem.*** , 26, 291.

162. E. Schnabel, H. NÖther, H. Kuhn. In ***Chemitsry of Natural and Synthetic Colouring Matters.*** [ed.] B. S. Joshi, S. V. Sunthankar, B. D. Tilak T. S. Gore. New York : Academic Press, 1962. p. 561.

163. K. Bernauer, S. Fallab. 1962***, Fasciculus*** , VII XLV, 2487.

164. A. Skorobogaty, T. D. Smith, G. Dougherty, J. R. Pilbrow. 1985, ***J. Chem. Soc***., 651.

165. M. Kasha. 1963, ***Radiation. Res.*** , 20, 55.

166. M. Kasha, H. R. Rawls, M. Ashraf El-Bayoumi. 1965, ***Pure Appl. Chem.***, 11, 371.

167. Z.A. Schelly, D. J. Howard, P. Hemmes, E. M. Eyring. 1970, ***J. Phys. Chem.***, 74 , 3040.

168. H. Abramczyk, I. Szymczyk, G, Waliszewska, A. Lebioda. 2004, ***J. Phys. Chem.***, 108 , 264.

169. Z. A. Schelly, R. D. Farina, E. M. Eyring. 1974, ***J. Phys. Chem.*** , 74, 617.

170. M. Durmus, T. Nyokong. 2008, ***Spectrochim. Acta,*** 69, 1170.

171. W. Chidawanyika, E. Antunes, T. Nyokong. 2008***, J. Photochem. Photobiol. A***, 195 , 183.

172. D.K. Modibane, T. Nyokong. 2008, ***Polyhedron*** , 27 , 1102.

173. V. Chauke, M. Durmas, T. Nyokong. 2007, ***J. Photochem. Photobiol. A***, 192, 179.

174. P. Tau, T. Nyokong. 2007, ***Electrochim. Acta***, 52, 3641.

175. H. Ogata, R. Higashi, N. kobayashi. 2003, ***J. Porphyrins Phthalocyanines*** , 7, 551.

176. R. D. George, A. W. Snow, J. S. Shirk, W. R. Barger. 1998, ***J. Porphyrins Phthalocyanines*** , 2, 1.

177. M.K. Dosanjh, D.A.J. Wase. 1987, ***Water Res.,*** 21, 205.

178. K. Hayward. Drinking water contaminant hit-list for US EPA. ***Water***. September-October 4, 1998, Vol. 21.

179. L.H. Keith, W.A. Telliard. 1979, ***Environ. Sci. Technol.***, 13, 416.

180. K. I. Abe, K. Tanaka. 1997, ***Chemosphere***, 35, 2837.

181. J. Folke, J. Birklund. 1986, ***Chemosphere***, 15, 895.

182. J. Paasivirta, J. Sarkka, T. Leskijarvi, A. Roos. 1980, ***Chemosphere***, 9, 441.

183. H.K. Veschueren. ***Handbook of Environmental Data on Organic Chemicals***. New York : VNR, 1983.

184. R.C.C. Wegman, H.H. Van den Broek. 1983, ***Water Res.,*** 17, 227.

185. W.F. Jardim, S.G. Moraes, M.M.K. Takiyama. 1997, ***Water Res.,*** 31, 1728.

186. A. Di Paola, V. Augugliaro, L. Palmisano, G. Pantaleo, E. Savinov. 2003, ***J. Photochem. Photobiol. A***, 155, 207.

187. T.G. Danis, T.A. Albanis, D.E. Petrakis, P.J. Promonis. 1998, ***Water Res.***, 32, 295.

188. M. Pera-Titus, V. García-Molina, M. A. Baňos, J. Giménez, S. Esplugas. 2004, ***Appl. Cat. B***, 47, 219.

189. B.N. Lee, J.C. Lou, P.C. Yen. 2002 , ***Water Environ. Res.: A Res. Publ. Water Environ. Fed.***, 74 ,28.

190. L. Li, C. Peishi, F.G. Earnest. 1991, ***AIChE J.*** , 37 , 1687.

191. K.S. Lin, H.P. Wang, M.C. Li. 1998, ***Chemosphere*** , 36 , 2075.

192. Y. Yin, H.E. Allen. In situ chemical treatment, Technology Evaluation Report. Pittsburgh, PA, USA, : ***Ground-water Remediation Technologies Analysis Center***, 1999.

193. F.J. Ben´ıtez, J. Beltrán-Heredia, J.L. Acero, F.J. Rubio. 2000, ***Chemosphere***, 41, 1271.

194. F.J. Benítez, J. Beltrán-Heredia, J.L. Acero, F.J. Rubio. 2000, ***J. Hazard. Mater. B***, 79 , 271.

195. M. Trapido, A. Hivronen, Y. Veressinina, J. Hentunen, R. Munter. 1997, ***Ozone: Sci. Eng.***, 19 , 75.

196. W.S. Kuo. 1999, ***Chemosphere***, 39, 1853.

197. R. Sauleda, E. Brillas. 2001, ***Appl. Catal. B***, 29 , 135.

198. T.M. Hashem, M. Zirlewagen, A.M. Braun. 1997, ***Water Sci. Technol.***, 35 , 41.

199. O. Comninellis. 1994, Stud. ***Environ. Sci.*** , 59, 77.

200. Electrochemical oxidation of phenolic compounds from dilute aqueous solutions. C.P. Huang, C.S. Chu. 1992. Proceedings of the ***First International Symposium on Chemical Oxidation.*** p. 239.

201. J.D. Rodgers, W. Jedral, N.J. Bunce. 1999, ***Environ. Sci. Technol.*** , 33, 1453.

202. W.H. Glaze, J.W. Kang, D.H. Chapin. 1987, ***Ozone: Sci. Eng,*** 9 , 335.

203. W.H. Glaze. 1994, ***Chem. Oxid.*** , 2, 44.

204. R. Andreozzi, V. Caprio, A. Insola, R. Martota. 1999, ***Catal. Today***, 53 , 51.

205. F.J. Benitez, J. Beltrán-Heredia, J.L. Acero, M.L. Pinilla. 1997, ***Ind. Eng. Chem. Res.,*** 36, 638.

206. F.J. Benitez, J. Beltrán-Heredia, T. González, F. Real. 1995, ***Ind. Eng. Chem. Res.,*** 34, 4099.

207. I. Casero, D. Sicilia, S. Rubio, D. Perez-Bendito. 1997, ***Water Res.,*** 31, 1985.

208. S. Guittoneau, J. De Laat, M. Dore, J.P. Duguet, C. Bonnel. 1988, ***Environ. Technol. Lett.***, 9, 1115.

209. J. Hoigné, H. Bader. 1983, ***Water Res.,*** 17 , 173.

210. J. Hoigné, H. Bader. 1983, ***Water Res.,*** 17, 185.

211. O. Legrini, E. Oliveros, A.M. Braun. 1993, ***Chem. Rev.,*** 93, 671.

212. S.J. Masten, S.H. Davies. 1994, ***Environ. Sci. Technol.,*** 28, 180.

213. B. Meunier, A. Sorokin. 1997, ***Acc. Chem. Res.*** , 30, 470.

214. R.M. Miller, G.M. Singer, J.D. Rosen, R. Bartha. 1988, ***Environ. Sci. Technol.***, 22, 1215.

215. G.R. Peyton, F.Y. Huang, J.L. Burleson, W.H. Glaze. 1982, ***Environ. Sci. Technol***. , 16, 449.

216. F.J. Benitez, J. Beltrán-Heredia, J.L. Acero, F.J. Rubio. 2001, ***J. Chem. Technol. Biotechnol.***, 76, 312.

217. J. Yoon, S. Kim, D.S. Lee, J. Huh. 2000, ***Water Sci. Technol.*** , 42 , 219.

218. R. Bauer, G. Waldner, H. Fallmann, S. Hager, M. Klare, T. Krutzler, S. Malato, P. Maletzky. 1999, ***Catal. Today*** , 53, 131.

219. J.M. Herrmann, Ch. Guillard, J. Disdier, C. Lehaut, S. Malato, J. Blanco. 2002, ***Appl. Catal. B***, 35, 281.

220. T. Mawhinney. 1983, ***J. Chromatogr.,*** 257, 37.

221. N. Nensala, T. Nyokong. 2000, ***J. Mol. Catal. A,*** 164, 69.

222. A. Mylonas, E. Papaconstantinou. 1996**, *J. Photochem. Photobiol. A,*** 94, 77.

223. H. Al-Ekabi, N. Serpone. 1988, ***J. Phys. Chem.,*** 92, 5726.

224. H. De Lassa, B. Serrano, M. Salaices. ***Photocatalytic Reaction Engineering***. New York : Springer, 2005.

225. O. Carp, C. L. Huisman, A. Reller. 2004, ***Prog. Solid State Chem.*** , 32, 33.

226. K. Kabra, R. L. Sawheney. 2004, ***Ind. Eng. Chem. Res.***, 43, 7683.

227. V. Maurino, C. Minero, E. Pelizzetti, P. Piccinini, N. Serpone, H. Hidaka. 1997, ***J. Photochem. Photobiol.,*** 109, 171.

228. F. Lücking, H. Köser, M. Jank. 1998, ***Water Res.*** , 32, 2607.

229. G.B. Shul'pin, M.M. Bochkova, G.V. Nizova, N.B. Kozlova. 1997, ***Appl. Catal. B*** , 12, 1.

230. S. Vollmuth, R. Niesser. 1995, ***Chemosphere*** , 30, 2317.

231. A. M. Volodin. 2000, ***Catal. Today***, 58, 103.

232. E. Chamarro, A. Marco, S. Esplugas. 2001, ***Water. Res.***, 35 ,1047.

233. M. S. Dieckmann, K. A. Gray. 1996, ***Wat. Res.,*** 30, 1169.

234. A. Alif, P. Boule. 1991, ***J. Photochem. Photobiol. A***, 59, 357.

235. K-H. Wang, Y-S. Hsieh, L-J. Chen. 1998, ***J. Hazard. Mater.*** , 59, 251.

236. W.Z. Tang, C.P. Huang. 1996, ***Chemosphere***, 3, 1621.

237. E. Lipczynska-Kochany. 1992, ***Chemosphere***, 24, 1369 .

238. G. Mele, R. Del Sole, G. Vasapollo, E. Garcia-Lopez, L. Palmisano, M. Schiavello. 2003, ***J. Catal***. , 217, 334 .

239. M. Zhou, L. Lei. 2006, ***Chemosphere***, 63, 1032 .

240. J. G. Calvert, J. N. Pitts. ***Photochemistry.*** New York : J. Wiley, 1967. pp. 258,285.

241. R. Bonnett. ***Chemical aspect of Photodynamic Therapy***. s.l. : Gordon and Breach, London, 2000. p. 70.

242. R. Gerdes, D. Wohrle, W. Spiller, G. Schneider, G. Schulz-Ekloff. 1997, ***J. photochem. Photobiol. A***, 111, 65.

243. A. Gilbert, J.E. Baggott. ***Essentials of Molecular Photochemistry.*** Oxford : Blackwell Scientific,, 1991. pp. 8, 32, 100.

244. K.J. Laider, J.H. Meiser. B.C. Sanctuary ***Physical Chemistry***. fourth . Boston : Houghton Mifflin Company, 2003. p. 933.

245. Al-Ekabi, N. Serpone. 1988, ***J. Phys. Chem.*** , 92 , 5726.

246. D.D. Dionysiou, A.P. Khodadoust, A.M. Kern, M.T. Suidan, I. Baudin, J.-M Laîné. 2000, ***Appl. Catal. B***, 24 , 139.

247. D. Gryglik, J. S. Miller, S. Ledakowicz. 2007, ***J. Hazard. Mat.*** , 146, 502.

248. Z. Xiong, Y. Xu, L. Zhu, J. Zhao. 2005, ***Langmuir***, 21, 10602.

249. L. Wu, A. Li, G. Gao, Z. Fei, S. Xu, Q. Zhang. 2007, ***J. Mol. Cat. A***, 269, 183.

250. P. Kluson, M. Drobek, A. Zsigmond, J. Baranyi, P. Bata, S. Zarubova, A. Kalaji. 2009, ***App. Cat. B***, 91, 605.

251. Z. Xiong, Y. Xu, L. Zhu, J. Zhao. 2005, ***Environ. Sci. Technol.***, 39, 651.

252. M. A. Zanjanchi, A. Ebrahimian, M. Arvand. 2010, ***J. Haz. Mater.***, 175, 992.

253. R. F. Curl, R. E. Smalley. 1988, ***Science***, , 242, 1017.

254. R. F. Krot. 1992, ***Angew. Chem., Int. Ed. Eng.***, , 31, 111.

255. M. S. Dresselhaus, G. Dresselhaus. 1995, **Annu. Rev. mater. Sci.** , 25, 487.

256. C. W. Jones, W. J. Koros. 1994, ***Carbon***, 32, 1419.

257. M. B. Rao, S. Sircas. 1993, ***Gas Seperation and Purification***, 7,279.

258. L. Ji, F. Liu, Z. Xu, S. Zheng, D. Zhu. 2009, ***Environm. Science Techn.*** , 43, 7870.

259. L. Ji, Y. Shao, Z. Xu, S. Zheng, D. Zhu. 2010, ***Environm. Science Techn.*** , 44, 6429.

260. J. Hu, L. S. Li, W. Yang, L. Manna, W. Wang, A. P. Alivisatos. 2001, ***Science*** , 292 , 2060.

261. W. U. Huynh, J. J. Dittmer, A. P. Alivisatos. 2002, ***Science*** , 295, 2425.

262. K. J. Vahala, P. C. Sercel. 1990, ***Phys. Rev. Lett.***, 65, 239.

263. D. J. Norris, A. Sacra, C. B. Murray, M. G. Bawendi. 1994, ***Phys. Rev. Lett.***, 72, 2612.

264. D. J. Norris, M. G. Bawendi. 1996, ***Phys. Rev. B*** , 53, 16338.

265. D. Bertram, O. I. Micic, A. J. Nozik. 1998, ***Phys. Rev. B*** , 57, R4265.

266. U. Banin, J. C. Lee, A. A. Guzelian,A. V. Kadavanich, A. P. Alivisatos. 1998, ***J. Chem. Phys.*** ,109, 2306.

267. A. P. Alivisatos, K. P. Johnson, X. Peng, T. E. Wilson, C. J. Loweth. 1996, ***Nature*** , 382, 609.

268. I. Chorkendorff, J.W. Niemantsverdriet. ***Concepts of Modern Catalysis and Kinetics.*** Weinheim : WILEY-VCH Verlag GmbH & Co. KGaA, 2003. pp. 129, 131,195.

269. S. Amelinckx, D. van Dyck, J. van Landuyt, G. van Tendeloo. ***Handbook of Microscopy.*** Weinheim : VCH, 1997.

270. M. C. DeRossa, R. J. Crutchley. 2002, ***Coord. Chem. Rev.***, 233 – 234,351.

271. H. Ali, J. E. Van Lier. 1999, ***Chemical reviews***, 99, 2379.

272. D.D. Perrin, W. L. F. Armarego. ***Purification of Laboratory Chemicals*** . 2nd. Oxford : Pegamon Press, 1989.

273. S. Wolfang, K. Holger, W. Dieter, H. Steffen, R. Beate, S. Gunter. 1998***, J. Porphyrins Phthalocyanines***, 2, 145.

274. J. Liu, A. G. Rinzler, H. Dai, J. H. Hafner, R. K. Bradley, P. J. Boul, A. Lu, T. Iverson, K. Shelimov, C. B. Huffman, F. Rodriguez-Macias, T. Y-S. Shon, R. Lee, D. T. Colbert and R. E. Smalley. 1998, ***Science***, 280 , 1253.

275 P. Tau, T. . Nyokong, 2007, ***Electrochim. Acta***, 52 , 3641.

276. M. J. Cook, I. Chambrier, S. J. Cracknell, D. A. Mayes, D. A. Russell. 1995, ***Photochem. Photobiol***, 62, 542.

277. H. M. Annula, C. J. Berlin, H. Wu, Y. S. Li, X. Peng, M. E. Kenny. 2006, ***J. Phys. Chem.***, 5215, 110.

278. S. Khene, A. N. Cammidge, M. J. Cook, T. Nyokong. 2007, ***J. Porphyrins Phthalocyanines***, 11, 761.

279. S. FitzGerald, C. Farren, C. F. Stanley, A. Beeby, M. R. Bryce. 2002, ***Photochem. Photobiol. Sci***., 1, 581.

280. T. Nyokong, H. Isago. 2004, ***J. Porphyrins Phthalocyanines***, 8, 1083.

281. N. Kobayashi, H. Konami. ***Phthalocyanines: Properties and Applications***. [ed.] A. B. P. Lever C. C. Leznoff. New York : VCH, 1999, Vol. 4, 9.

282. A. Ogunsipe, D. Maree, T. Nyokong. 2003, ***J. Mol. Stuct***., 650, 131.

283. N. Y. Meryem, M. Kandaz, A. Koca, B. Salih. 2006, ***J. Porphyrins Phthalocyanines***, 10, 1022.

284. B.B. Koleva, T Kolev, M. S. Zareva, Lamshöft, M. Spiteller. 2008, ***Trans. Met. Chem***. , 33, 911.

285. B.B. Ivanova, M.G. Arnaudov, H. Mayer-Figge. 2005, ***Polyhedron***, 24, 1624.

286. B.B.Koleva, Ts. Kolev, S.Y. Zareva, M. Spiteller. 2007 , ***J. Mol. Struct***., 831, 165.

287. W. Freyer, S. Mueller, K. Teuchner. 2004, ***J. Photochem Photobiol. A***, 163,231.

288. M.O. Senge. 2006, ***Chem. Commun***., 243.

289. G. Ricciardi, A.V. Soldatova, A. Rosa. 2008, ***J. Inorg. Biochem***., 102, 406.

290. A. P. Terzyk, M. Wsniewski, P. Gauden, G. Rychlicki, S. Furmaniak. 2008, ***J. Colloid Interface. Sci***., 20, 40.

291. F. Wilkinson, J. G. Brummer. 1981, ***J. Phys. Chem. Ref. Data***, 10, 825.

292. E. Sibva, M. M. Pereira, H. D. Burrows, M. E. Azenha, M. Sarakha, M. Bolte. 2004, ***Photochem. Photobiol. Sci***., 3, 200.

293. M. Terrones, W. K. Hsu, A. Schwoerer, K. Prassides, H. W. Kroto and D. R. Walton. 1998, ***Appl. Phys. A***, 66, 307.

294. Y. Zhang, X. Sun, L. Pan, H. Li, Z. Sun, C. Sun and B. K. Tay. 2009***, J. Alloys and Compounds***, 480, L17.

295. B. K. Price, J. M. Tour. 2006 , ***J. Am. Chem. Soc***., 128 , 12899.

296. J. Jiang, R. Saito, A. Grüneis, S. G. Chou, Ge. G. Samsonidze, A. Jorio, G. Dresselhaus, and M. S. Dresselhaus. 2005, ***Phys. Rev. B*** , 71 , 045417/25.

297. M. D. Ellison, P. J. Gasda. 2008, ***J. Phys. Chem. C***, 112 , 738.

298. M. Barbeni, E. Pramauro, E. Pelizzeti. 1985, ***Chemosphere*** , 14 , 195.